Self-assembly and anion recognition with binuclear lanthanide complexes

James Andrew Thom

Balliol College

University of Oxford

A thesis submitted in partial fulfilment of the requirements for the degree of *Doctor of Philosophy*.

Trinity Term 2014

Table of Contents

Abstract

'Self-assembly and anion recognition with binuclear lanthanide complexes'

James Thom, Balliol College, University of Oxford

DPhil. Trinity Term 2014.

This work describes an investigation into the solution-phase binding of anionic guests by bimacrocyclic lanthanide complexes. It outlines the preparation of different classes of complexes bearing two metallic domains, and the effects of association on both the complex and the guest.

Chapter one provides a cursory introduction to the fundamental properties of the lanthanides with a focus on luminescence. A brief literature review is given on the use of emissive lanthanide probes for the sensing of analytes.

Chapter two concerns the preparation and properties of a series of binuclear complexes in which the two centres are linked with a short spacer group, with the aim of selectively sequestering small anions such as the halides in solution. The concept of luminescence titration will be introduced and then used to assess the binding parameters of a selection of guests.

Chapter three describes a related class of ditopic lanthanide complexes in which the two metal centres are separated by a semi-rigid butyne linking group. Luminescence studies are again used to evaluate the binding constants of homologous series of dianions to ascertain how the size, geometry and functionalization of the anionic guest impacts on binding.

Chapter four explores the coordination of phosphate species and assesses the ability to bind biologically significant phosphates of some of the complexes from Chapter 3.

Chapter five details an investigation into the effects on guest-selectivity of further lengthening the linking unit which separates the two macrocyclic binding domains.

Chapter six summarises the work done throughout the thesis and draws some overarching conclusions, as well as highlighting areas for further study.

Chapter seven describes the experimental procedures.

Acknowledgments

First and foremost I would like to thank Steve Faulkner for giving me the opportunity to be part of the group, not once but twice. Thank you for the infinite patience, the optimism and for never failing to show me that things weren't as bad as I'd thought. I couldn't have asked for a better and more understanding mentor.

I am very grateful to all the staff at the Chemistry Research Laboratory for the analytical services provided and the support. In particular I would like to thank Dr Nick Rees for help with the NMR facilities. Thanks too must go to the mass spectrometry service for help in recording the MALDI spectra of the metal complexes. Thanks to Dr. Alan Kenwright of the University of Durham for measuring some of the paramagnetic NMR spectra of the lanthanide complexes and for advice on pulse sequences and parameters.

There has also been a wide variety of assistance from outside the building which should be acknowledged. Thanks to Dr. David Staunton of Biophysics for his guidance and advice on CPL, CD, ITC and various other acronym-heavy measurement techniques. I am grateful to Dr. Robert Pal at the University of Durham for his help with CPL measurements. Last but by no means least in this category, thanks to Dr. Thomas Sørensen of the University of Copenhagen for his assistance and suggestions with the molecular models.

To the Faulkner big guns, Mike, Manuel and Octavia. I said in my ICL Graduate Symposium talk that you have taught me everything I know, but not, as you remind me daily, everything you know. It is a testament to your expertise that this remains as true today as it was then. More than this though, it has been your enthusiasm and encouragement to push on and try new approaches that has really made the difference and helped me through a lot of the last four years.

The ensemble cast of the Faulkner group has made the last five years here a huge amount of fun. Becky Snr, Queen's Hill, Jack, Wendy, Aaron and innumerable Part IIs - you made the lab a happy place to be, albeit at the cost of questionable music taste.

Finally on the lab-front, thanks should go to my summer project students - Alice and Anna. Under normal circumstances, babysitting undergrads is the last thing one wants to do over the summer and yet you two were both capable and hard-working and rather than take up time and patience, you ended up helping with some of my chemistry and taking my own research in new directions.

Outside the lab, the list of friends who have put up with me and helped me through my eight years in Oxford is long and tedious, but special mention should go to the fellow residents (inmates?) of the Manor Farm High Performance Centre, human or otherwise.

Rather than name everyone individually, I will thank *en masse* the men and women of the MCBC and OULRC, with whom I've shared some of the highest highs and lowest lows of my time in Oxford and from whom I've learnt a lot about myself.

The folks back home have always been a huge source of support and never more so than this year. The steady stream of calming influence, sound advice, food parcels and the odd financial bailout has really kept me going when things have been tough. Thanks to Mum, Dad, Susie and Chris for being there.

Thanks must also go to the extended family - Martin, Audrey, Robin, Sarah and the other trustees of the Wood-Buxton Educational Trust, who have been exceptionally supportive to both me and my family and whose generosity made the fourth year of this project possible.

Finally, coming in to land, Rachel. You found me outside Camera when I was hungry and miserable and you've made me happy. Thank you.

Abbreviations

a.u.	arbitrary units
ADP	adenosine 5’-diphosphate
AMP	adenosine 5’-monophosphate
ATP	adenosine 5’-triphosphate
ATR	attenuated total reflectance
BET	back energy transfer
br	broad
CT	charge transfer
cyclen	1,4,7,10-tetraazacyclododecane
d	doublet
dd	doublet of doublets
DO3A	1,4,7,10-tetraazacyclododecane-1,4,7-triacetic acid
DOTA	1,4,7,10-tetraazacyclododecane-1,4,7,10-tetraacetic acid
DTPA	diethylene triamine pentaacetic acid
ESMS	electrospray mass spectrometry
ET	energy transfer
HRMS	high resolution mass spectrometry
IC	internal conversion
IR	infrared
ISC	inter-system crossing
LMCT	ligand to metal charge
LRMS	low resolution mass spectrometry
m	multiplet
MALDI	matrix-assisted laser desorption and ionisation

MLCT	metal to ligand charge transfer
MWCO	molecular weight cut-off
NIR	near infrared
PET	positron emission tomography
s	singlet
SAP	square anti-prism
t	triplet
T	triplet state
TBA	tetrabutylammonium
TFA	trifluoroacetic acid
TOF	time of flight
TRES	time resolved emission spectrum
TSAP	twisted square anti-prism

1 Introduction

1.1 Introduction

For many years the lanthanides have been researched because of their interesting and unique photophysical and magnetic properties. Early research focused on the metal salts and their use as solid phosphors in cathode ray tube screens. They found another use as a dopant for glasses and crystals with the advent of lasers such as the Nd:YAG. Recently however, the focus has shifted to their solution phase complexes and their use in magnetic resonance imaging,[1] targeted radiotherapy[2] and luminescent assay.[3] This thesis describes an exploration of the interactions between binuclear lanthanide complexes and a range of anionic guests. In such systems, displacement of inner sphere solvent molecules by anions mirrors the chelate effect, exploiting multiple interactions between host and guest together with size and shape complementarity. If we are to understand these interactions, it is necessary to begin by understanding the nature of the lanthanides and their coordination chemistry. In this chapter, key aspects of such chemistry are discussed and combined with a detailed review of current knowledge of the anion coordination chemistry of kinetically stable lanthanide complexes.

1.2 General Chemistry of the Lanthanides

The unique and characteristic physicochemical properties of the lanthanides derive from their electronic configuration and in particular, the partially filled 4*f* sub-shell. Since the 4*f* orbitals are radially contracted and highly penetrating, they are shielded from the local environment by the 5*s* and 5*p* electrons and thus their interactions with ligand orbitals are negligible. This results in very small ligand-field effects and consequently, the bonding in lanthanide complexes is dominated by electrostatic interactions between the trivalent metal cation and a nucleophilic ligand scaffold. By contrast with *d*-block complexes, where orbital anisotropies must be accounted for, the

coordination geometries of lanthanide complexes are determined primarily by the conformational preferences of, and steric repulsions between the ligands. Furthermore, simple monodentate ligands invariably form labile complexes with the lanthanides.

1.3 Lanthanide Complexes

The luminescent and magnetic properties of the lanthanide metals have seen them pressed into service as probes for many different imaging modalities, both *in vivo* and *in vitro*. Caution must however be used, as the free lanthanide ions all exhibit significant toxicity.[4] This derives from their similar ionic radii to common endogenous cations such as Zn^{2+} and Ca^{2+}, meaning that displacement by the lanthanide can occur. Furthermore, the increased charge density on the lanthanide can result in significantly lower solubility of lanthanide salts with endogenous anions such as phosphate. In such circumstances precipitation of lanthanide colloids can occur and such factors have been strongly implicated in the development of diseases such as nephrogenic systemic fibrosis (NSF).[5] Endogenous free Ln(III) has also been shown to disrupt calcium and zinc mediated signalling processes, such as at the sarcoplasmic reticulum, as well as to permanently displace calcium from the hydroxyapatite structure of bone.[6-8] Any lanthanide based agents to be used *in vivo* must therefore be delivered in such a form that the free metal cation is not released into the body; namely, as a stable complex. The high charge density of the trivalent metal cations means that the Ln(III) ions are hard Lewis acids, and as such bind preferentially with anionic ligands that contain hard donor atoms such as nitrogen and oxygen.

1.3.1 Thermodynamic Stability

Electrostatic attractions between the highly electropositive lanthanide and the electron-rich ligand donor groups mean that the formation of solution-phase complexes is highly favourable in enthalpic terms. As already mentioned, the trivalent lanthanides are hard cations, preferring harder ligand donors such as nitrogen and oxygen and it is thus unsurprising that polyamino-carboxylate ligands, both open-chain and macrocyclic, have been shown to form

thermodynamically stable complexes. Shown in figure 1-1 are four polyamino-carbonyl ligand systems, all of which form thermodynamically favourable complexes with lanthanide cations. For the first three (EDTA, DTPA and DOTA), complexation to the metal cation occurs with the anionic form of the ligand in which all of the carboxylic acid groups are deprotonated. The formal negative charges of the carboxylate groups ensure strong electrostatic attraction to the hard *f*-block metal cations. The fourth ligand scaffold shown is DOTAM, a tetraamide. That this ligand system, which coordinates through a charge neutral N_8-donor set, forms stable complexes with the lanthanides is partially due to the hard donor properties of the amide nitrogen atoms, but largely a consequence of the preorganisation of the macrocyclic framework which minimises the entropy loss suffered upon adoption of the binding conformer.

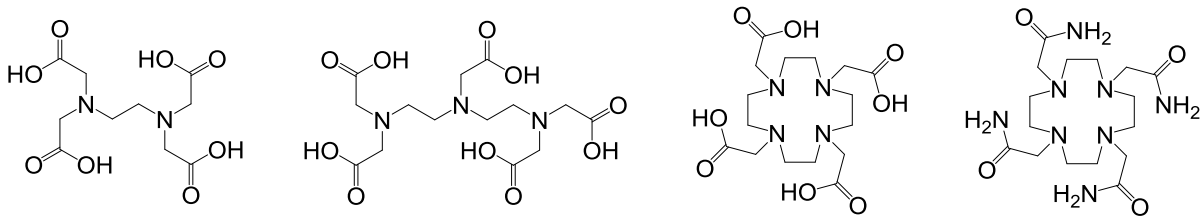

Figure 1-1. Molecular structures of some of the polyaza ligands discussed in this chapter.

In addition to favourable enthalpic contributions, arising from the donor-acceptor interactions, there is also a significant entropic drive to be considered. This stems from the decrease in hydration of both the ligand and the metal upon complexation. In the solution phase, lanthanide metal coordination numbers are typically in the range of nine to twelve and the displacement of large numbers of bound and ordered solvent molecules by one polydentate ligand results in a large gain in entropy.[9-11]

1.3.2 Kinetic Stability

Despite their very high stability constants, there have been several recorded instances of lanthanide chelates releasing substantial fractions of the supposedly bound metal under physiological conditions, leading to a range of health problems. Indeed, gadolinium complexes of acyclic ligands such as Omniscan are now the subject of a Food & Drug Administration warning in

the USA, due to their implication in the onset of the potentially fatal nephrogenic systemic fibrosis. In more 'real-world' systems, competing processes such as precipitation are likely to sequester any lanthanide ions which manage to slip the shackles of their complexing ligand(s). Thus the kinetic inertness of a complex, more than its thermodynamic stability, is a truer predictor of its safety for application *in vivo*. Furthermore, it is clear that immobilising the lanthanide in a complex is the only way of outcompeting the kinetic trap of precipitation. Possibly the most effective metric used to quantify this is the rate constant of dissociation. The complexes of gadolinium have been extensively studied due to their application as MRI contrast agents and it has been found that there is a direct correlation between the rigidity of the ligand and the kinetics of formation and dissociation of the daughter complexes. This work is of tangential relevance to this thesis and has been reviewed extensively elsewhere. The discussion here will therefore be brief.

The complexation of lanthanide ions by ligands such as EDTA and DTPA is a fast process; following an initial association step, the pendant donor groups are capable of independent rotation and rearrangement to coordinate to the metal centre and give the final product.[12] By contrast, formation of lanthanide-DOTA complexes displays very different kinetic characteristics. In this case, the complexation has been postulated to proceed via a three step mechanism, with each step involving multiple donor groups. In the first stage, the metal ion is bound by the flexible pendant carboxylate arms, outside the macrocyclic cavity. This is followed by transfer to inside the cavity and coordination of two of the ring nitrogen atoms. Finally, the last two nitrogen atoms associate with the metal in another concerted step. That each of the individual stages involves cooperative binding of multiple donors is a consequence of the highly rigid nature of the macrocyclic framework.[13]

In considering the kinetic inertness of metal polyamino-caboxylate complexes, the two main processes which lead to decomposition are proton-assisted dissociation and transmetallation, in which another metal ion attacks directly to displace the resident cation. By comparing the

quantities of lanthanide ion released over time in the presence of acid, as well as competing metal cations, it has been determined that for DTPA-based complexes, transmetallation dominates, but for EDTA derivatives, acid-catalysed decomplexation is the main process. It is postulated that this difference derives from the extra negative charge born by DTPA complexes of trivalent metal ions, making them more electrostatically attractive targets for electrophilic attack.[14]

As in the case of EDTA, the dissociation of $[Ln(DOTA)]^-$ complexes has been found to proceed via a proton-assisted mechanism, although even at low pH, the kinetics are much slower than for the analogous DTPA species. Indeed at pH 7, acid-catalysed decomplexation makes a negligible contribution to the release of gadolinium from its DOTA complex.[15] Nor does the presence of competing metal cations, probably due to the lack of space inside the macrocyclic cavity. For $[Gd(DOTA)]^-$, no release of gadolinium was observed, even when the complex was kept for many days in the presence of 2.5 mM aqueous zinc chloride.[16] A recent study into the dissociation kinetics of gadolinium complexes of various macrocyclic and open-chain polyamino-carboxylates also investigated the effect of common physiological ligands such as citrate, phosphate and hydrogen carbonate on the exchange processes between gadolinium contrast agents and the common endogenous Cu(II) cation. In all the open chain, DTPA-derived systems, transmetallation with copper was shown to be accelerated by the presence of such physiological ligands. In the macrocyclic complexes by contrast, dissociation kinetics were found to be entirely independent of the local concentration of both endogenous ligands and the copper cation.[17]

1.3.3 The Macrocyclic Effect

The macrocyclic effect describes the increased stability of a metal complex formed with a cyclic ligand, compared with its acyclic analogue and is predominantly an entropic effect, deriving from the preorganisation of the ligand.[18-20] In acyclic chelate systems, the freely flexible ligand must adopt a single, rigid conformer upon binding to the metal centre and thus it experiences a significant drop in entropy. By its very nature, the cyclic ligand has available to it far fewer degrees

of flexibility, and thus the entropic loss upon binding is significantly reduced. There is also an enthalpic consideration, in that the cyclic ligand, too inflexible to orient itself to maximise solvent interactions, is generally less well hydrated than its acyclic counterpart. Thus upon binding, desolvation of the cyclic system is less energetically expensive, and hence more favoured. This effect is observed on comparing the stability constants of Ln^{3+} complexes of cyclic and acyclic ligand systems.

Metal Ion	log(K) / $mol^{-1}dm^3$		
	DOTA[9]	EDTA[10]	DTPA[10]
Eu^{3+}	28.2	17.3	22.4
Tb^{3+}	28.6	17.9	22.7
Lu^{3+}	29.2	19.8	22.4

Table 1-1. 1:1 Stability constants log(K_s) of Ln^{3+} complexes. (293 K, 1.0 M NaCl, H_2O)

It can be seen that for a given metal, the complexes of DOTA are approximately six orders of magnitude more stable than those of DTPA, and ten orders of magnitude more stable than their EDTA analogues.[21] As one moves across the *f*-block, the stability constants increase in the cases of DOTA and EDTA. This is due to the increasing charge density on the metal centre, resulting in stronger electrostatic attractions between the metal and ligand donors. In the case of DTPA, this increased enthalpic gain is counteracted by the more rigid skeleton and larger binding pocket, meaning the ligand is less able to effectively wrap around the smaller metals found as one approaches the end of the series.

1.3.4 Polynuclear Complexes

Complexes containing more than one lanthanide are advantageous for biomedical imaging as there is a greater content of Ln(III) per mole of complex. Even when bound as stable complexes, cells have a limited tolerance of such imaging agents so it is favourable to administer as little as possible of the molecule to produce a viable image. It is also the case that the relaxivity of monometallic contrast agents is not sufficient for some forms of MRI. Additionally, if one is able to

prepare heterometallic multinuclear complexes, there is the possibility of incorporating more than one reporting modality in the same imaging agent. For polynuclear complexes to have clearly defined properties, the solution-phase speciation must be controlled such that each metal ion resides in its own binding pocket with minimal dissociation between metal and ligand. If this requirement is not satisfied and labile ligands are used, rapid dissociation and recomplexation in solution can result in fast transmetallation, affording statistical mixtures of species. This has been found to occur in the complexes of β-diketonates.[22] Polynuclear complexes should therefore ideally be based on linked macrocyclic domains.

1.4 Lanthanide Luminescence

Transitions between microstates within the *f*-orbital manifold result in the majority of the lanthanides displaying luminescence, spanning from the ultraviolet (Gd^{3+}), across the visible (Eu^{3+} and Tb^{3+}) and into the near infrared (Yb^{3+} and Er^{3+}) regions of the electromagnetic spectrum.[23] Despite the wide range of emission wavelengths, the emission spectra of lanthanide ions are all characterised by sharp lines, whose position and form are largely independent of the local environment at the metal centre, again a consequence of the minimal involvement of the 4*f*-orbitals in bonding.[24]

1.4.1 Sensitised Emission and the Antenna Effect

Population of the emissive lanthanide excited state via direct excitation is inherently inefficient, as both the initial and final states are within the *f*-manifold and hence have the same symmetry with respect to inversion. Such transitions therefore have a $\Delta\ell=0$ and are Laporte forbidden, resulting in very low molar absorption coefficients. That these transitions are allowed at all is due to partial admixture of configurations of the opposite sign (such as the $4f^{n-1}$, $5d^1$) and vibronic coupling to the ligand and solvent sphere, allowing relaxation of the local symmetry.[25, 26]

A more efficient strategy for the production of lanthanide luminescence is that of sensitised emission, in which a nearby chromophore is excited and the energy transferred downhill to

the local metal centre. This process of using a neighbouring group to stimulate metal-based emission is commonly referred to as the 'antenna effect', with the light-harvesting moiety known as the antenna.[27, 28]

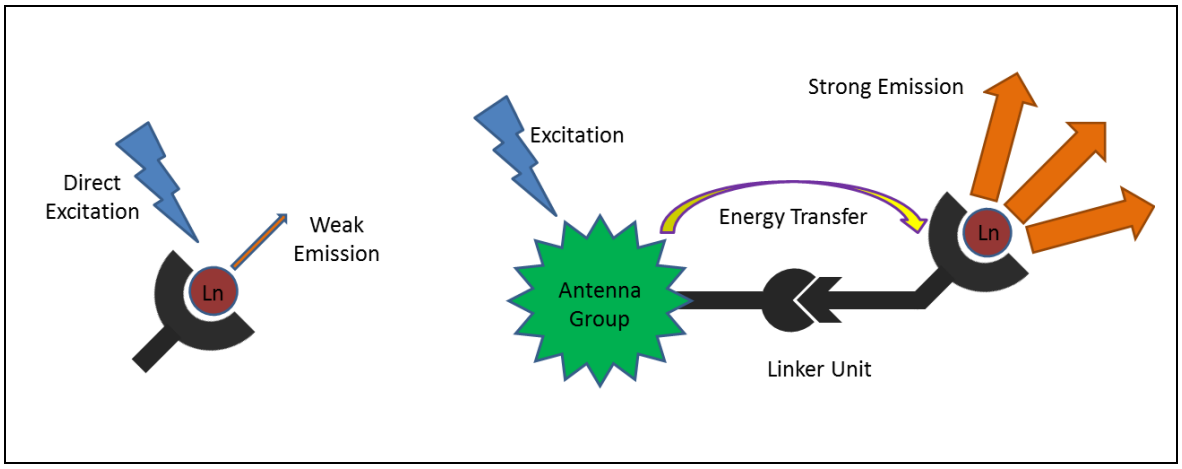

Figure 1-2. Schematic of a lanthanide complex-antenna assembly showing a possible mechanism of sensitised luminescence.

Once the lanthanide excited state has been populated, emission-induced relaxation back down to the ground state is long lived, again a consequence of the Laporte-forbidden nature of the transitions within the *f*-manifold. It is also significantly red-shifted relative to the excitation wavelength, due to significant differences in energy between the donor state of the chromophore and the emissive state of the lanthanide. These properties make lanthanide complexes useful as imaging probes, since time-gating techniques can be used to filter out any short-lived scattered light or extraneous fluorescence from the background and excellent signal-to-noise ratios can be obtained.[29, 30]

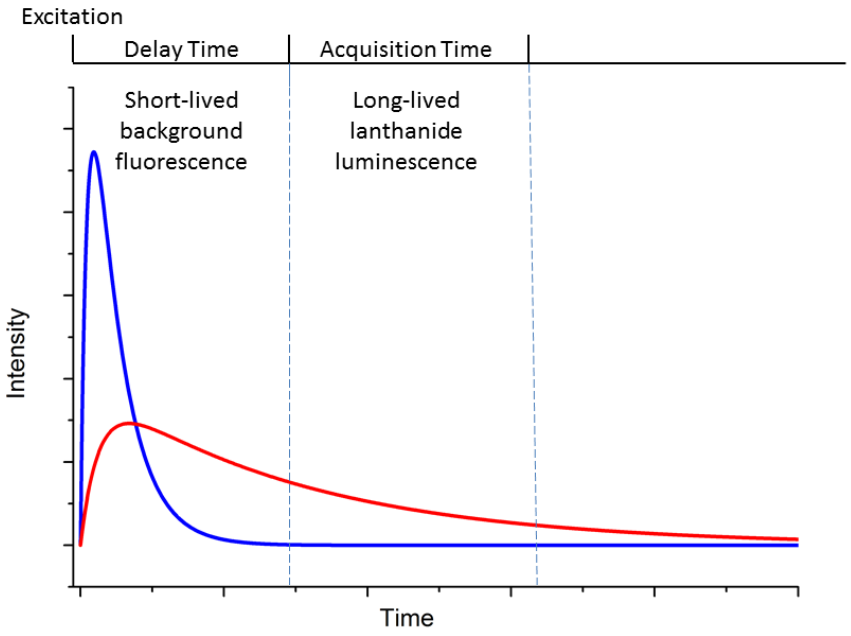

Figure 1-3. Time-gated detection of a luminescent signal. A delay time is applied after the excitation pulse during which the detector is switched off. This allows the short-lived processes to decay away, meaning only long-lived luminescence is detected during the acquisition time.

The large Stokes shift of the luminescence, combined with the sharp line-width means that a single excitation wavelength can stimulate emission from multiple different metal centres, allowing for ratiometric detection.[31]

1.4.2 Energy Transfer Pathways

Figure 1-4 depicts some of the various pathways by which excitation of an antenna chromophore can lead to lanthanide-centred luminescence.

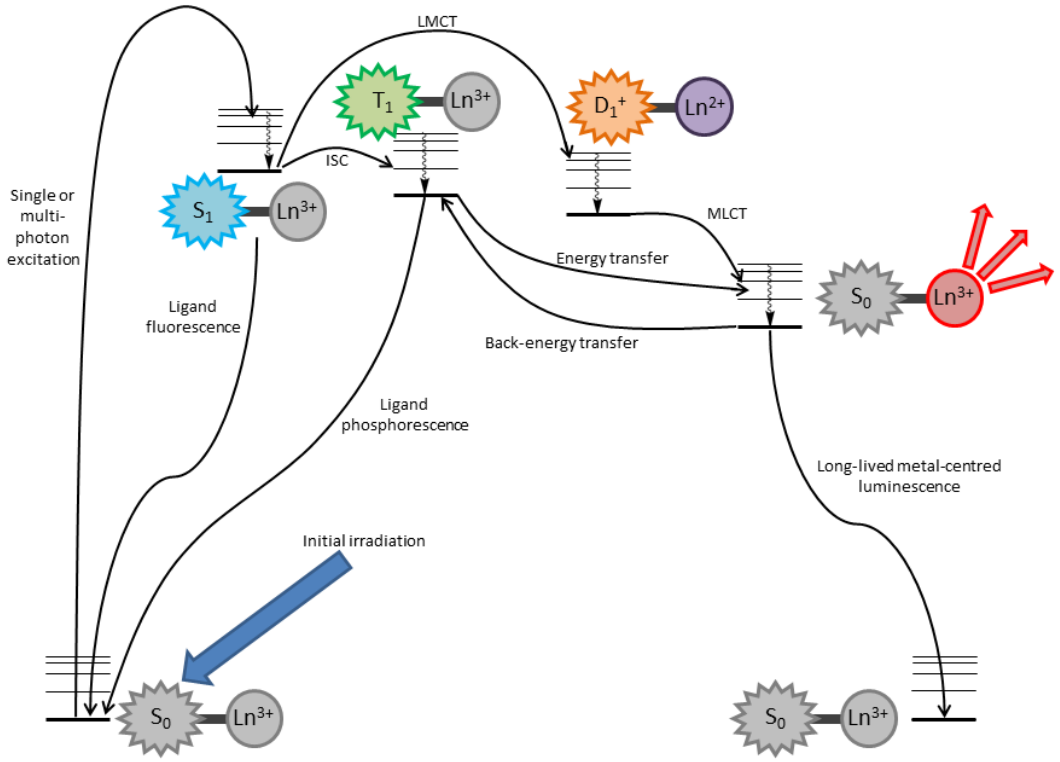

Figure 1-4. A simplified Jablonski diagram showing the main energy transfer pathways leading to emission from a lanthanide ion.

The first stage involves single- or multi-photon absorption by the ground state of the antenna group, leading to the population of the singlet excited state, S_1. Intersystem crossing within the antenna manifold leads to population of the chromophore excited triplet state, T_1. Energy transfer can then occur, from the antenna T_1 to the lanthanide excited state. For optimal energy transfer efficiency, it has been demonstrated that the chromophore T_1 should lie around 2000 cm^{-1} above the emissive metal state, as this minimises thermally-activated back energy transfer, whilst still allowing for a good donor-acceptor energy overlap. To marry this demand with the long-wavelength excitation required to safely penetrate tissue for biomedical imaging, sensitisation of the higher energy lanthanides such as Eu(III) and Tb(III) necessitates the use of chromophores with small energy gaps between the singlet and triplet states. Examples from the literature include the use of benzophenones,[32] acridones,[33] azaxanthones[34] and phenanthridines.[35]

An additional pathway exists for cases where an electron-rich chromophore is paired with a metal possessing a thermodynamically accessible 2+ oxidation state, such as ytterbium. This alternative

route proceeds via a double electron transfer mechanism. First ligand-to-metal charge transfer occurs, from the excited triplet state of the antenna unit to the metal centre, reducing it. This LMCT state is then able to populate the emissive excited state of the lanthanide. Such a pathway explains why sensitisation of ytterbium can still be very efficient, even when the spectral overlap between the antenna donor and ytterbium $^2F_{5/2}$ acceptor states is negligible.[36] In the case of europium (III), LMCT from the chromophore excited state gives rise to a low energy charge-separated state which is unable to populate the emissive $^5D_0$ state and thus gives rise to a reduction in luminescence quantum yield.

Traditionally the light-harvesting group has been an aromatic or poly-conjugated organic moiety, but whilst this is still the case for the higher energy lanthanides such as europium and terbium, transition metal-based chromophores are increasingly finding employment as antennae in the sensitisation of the near IR emitting lanthanides.[28] Compared with their organic counterparts, they offer a higher photostability, with lower risk of photobleaching over time (provided the triplet state is not sufficiently long-lived to be quenched photochemically), as well as a wide and tunable range of absorptions.[37-39] In addition, the MLCT transition which typically leads to the formation of the triplet state in such species has a much higher quantum yield than the analogous ISC process in organic systems and thus energy transfer to, and sensitisation of the lanthanide centre is often much more efficient.

Energy transfer between the donor and acceptor states can proceed via two different mechanisms, as described by Dexter[40] and Förster.[41] Dexter transfer involves an electron exchange mechanism propagated through bonds, requiring overlap between the orbitals of the donor and acceptor groups.[40] This interaction has a distance dependence of e^{-r} and is thus only effective at short range. It is most probably the dominant mechanism of energy transfer when the donor group is directly coordinated to the lanthanide ion. There are however examples of Dexter-like exchange taking place over longer distances, mostly in systems where a d-block metal is used to sensitize a lanthanide ion via an extended fully conjugated ligand

connecting the two metal centres.[42,38] Förster exchange by contrast, is a through-space interaction where a dipole in the donor state induces a complementary dipole in the acceptor state.[41] It is a coulombic interaction and thus decays with distance as r^{-6}. For Förster energy transfer to be efficient, there needs to be a good overlap integral between the emission of the donor state and the absorption band of the emissive state. This is rarely true of lanthanide complexes, where broad emission bands from aryl chromophore states overlap ineffectively with lanthanide absorption bands. However, Förster energy transfer is frequently the only available pathway when Dexter exchange or super-exchange is not feasible.

1.4.3 Quenching

One of the major pathways competing with luminescence to depopulate the lanthanide excited state is energy transfer to the high energy vibrational modes of the surrounding solvent. The quenching properties of many different groups have been studied extensively, and it has been shown that O-H oscillators are amongst the most effective at depopulating the lanthanide excited states.[43, 44] Harmonic overtones from other groups such as N-H, C-H and C=O still need to be taken into account but are significantly less efficient. The extent to which luminescence is quenched by OH oscillators is inversely proportional to the energy separation between the emissive state and the ground-state of the lanthanide ion in question, as the larger the energy gap, the higher the vibrational state of the oscillator and hence the lower the Franck-Condon overlap.[45] Thus the lanthanide ions which possess the largest energy gaps, such as Tb^{3+} and Eu^{3+} are less vulnerable to deactivation by solvent oscillators, whereas those with smaller separations between emissive and ground states, such as Nd^{3+} and Er^{3+} are much more effectively quenched. A consequence of this is that the observed luminescent lifetimes of solution-phase Eu^{3+} and Tb^{3+} complexes are of the order of milliseconds,[46,47] whereas those of the analogous complexes of Nd^{3+} and Er^{3+} are in the nano- to microsecond range.[48,49] In deuterated solvents by contrast, the lower stretching frequencies of the corresponding XD

oscillators lead to a lower Franck-Condon integral and thus less efficient depopulation of the lanthanide excited states.[50] Consequently, observed luminescent lifetimes are longer in deuterated solvents than in the comparable protonated media.[51]

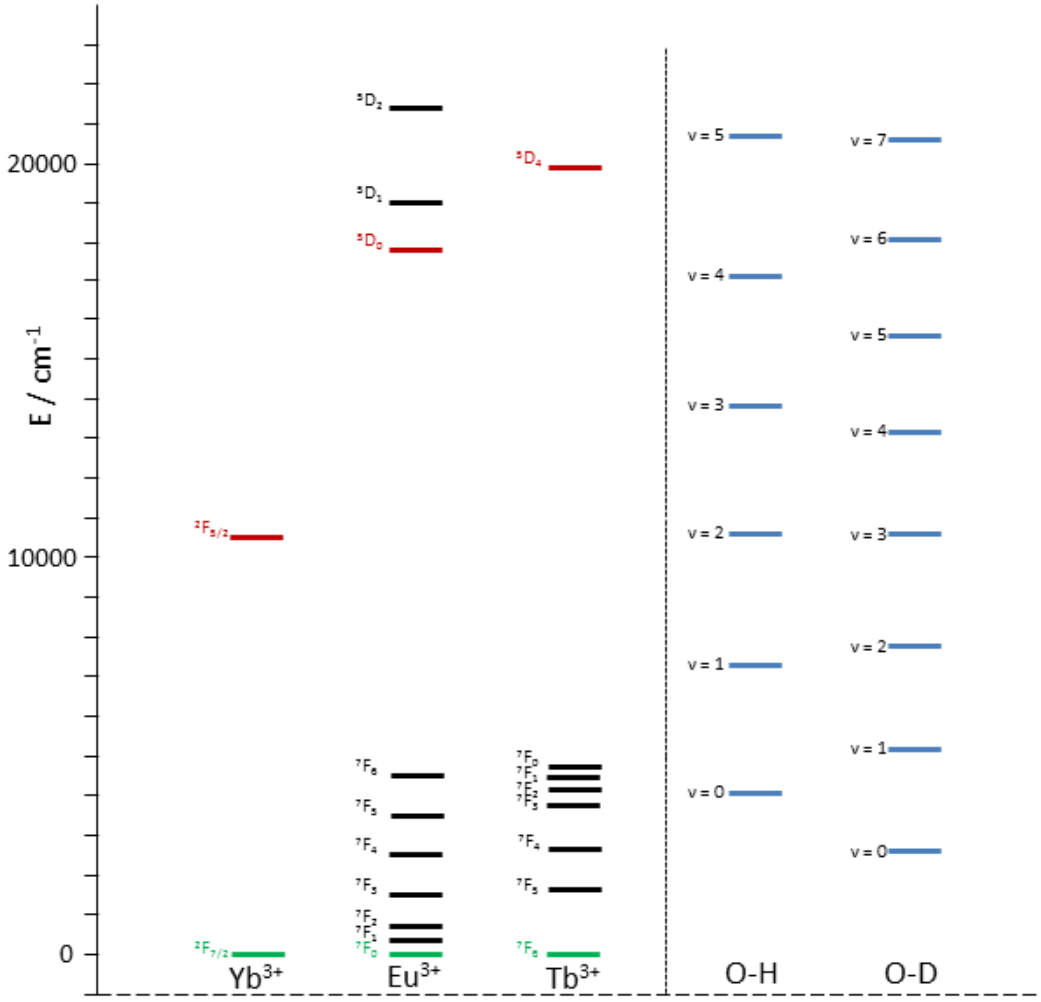

Figure 1-5. A simplified energy level diagram showing the ground and excited states of a selection of the lanthanides used in this study. The vibrational modes of the quenching O-H and O-D oscillators are shown in blue.

The rate of deactivation by OH or OD oscillators is directly proportional to the number of such groups within the lanthanide's coordination sphere and this can be used as a handle by which to calculate the number of bound solvent molecules at a metal centre. By comparing the observed luminescence decay constants (k_{obs}) in protonated and deuterated media, and assuming that other than solvent quenching, all other processes contributing to the observed rate constant remain the same, a modified version of the Horrocks' equation (1.1) may be

used to estimate the number of solvent molecules bound at the metal centre, commonly designated q.[51]

$$q = A\left(k_{H_2O} - k_{D_2O} - B\right) \quad \textbf{(1.1)}$$

In this equation, *A* is an empirically derived constant, specific to the metal ion under study.[52] *B* is a corrective term to account for the slight quenching contributions made by closely diffusing solvent molecules within the complex's extended hydration sphere.[53] The values of *A* and *B* for the more commonly used lanthanide metals in water are shown in table 1-2.

Metal Ion	A	B
Tb^{3+}	5 ms^{-1}	0.06 ms^{-1}
Eu^{3+}	1.2 ms^{-1}	0.25 ms^{-1}
Yb^{3+}	1.0 μs^{-1}	0.1 μs^{-1}

Table 1-2. Values for the A and B constants for selected Ln(III) ions in aqueous solution.

For those lanthanides with smaller separations between their emissive and ground states, the lower frequency C-H/D and N-H/D oscillators from within the ligand scaffold provide a good energy match and thus compete with the solvent harmonics in depopulating the excited states. The result of this is that calculation of q values for Nd^{3+} and Er^{3+} is notoriously unreliable.[54] It should be noted that changing the pH of a solution can result in a change in the q-value observed. Deprotonation of bound water molecules results in a reduction in the average number of O-H oscillators per coordinated solvent, resulting in a lower apparent value of q.

1.4.4 Europium Luminescence

There are several facets of europium luminescence which make this metal ion particularly suited for applications in optical imaging. Following initial excitation, rapid non-radiative decay populates the $^5D_0$ excited state, which then emits down into the ^7F_J levels.[24] The transitions down to the different J-microstates within this manifold have different mechanisms and properties, and thus respond differently to changes in the metal environment.

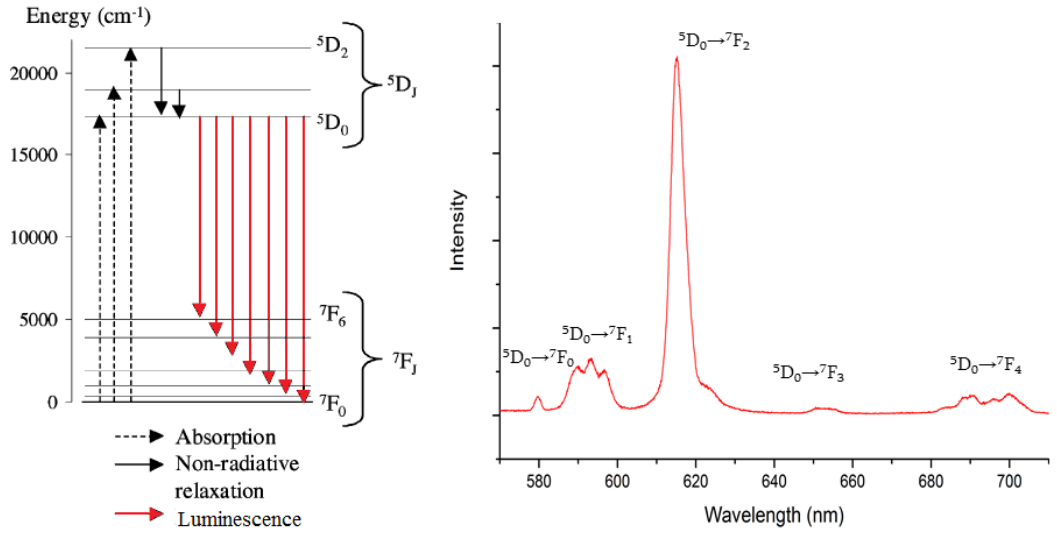

Figure 1-6. Partial energy-level diagram (left) and emission spectrum (right) of the europium (III) cation. Data taken from the emission spectrum of complex [3.c] in methanol.

The Δ*J* = 1 peak, coming at approximately 590 nm, is allowed by a magnetic dipole mechanism. As such, its intensity is largely unaffected by changes in the coordination environment of the metal. By contrast, the Δ*J* = 2 peak, occurring at 616 nm, is a quadrupole-mediated transition and is thus hypersensitive to any perturbations in local symmetry, particularly the nature of the axial donor group. By comparing the ratio of the intensities of these two peaks, rather than the absolute intensities themselves, one has an observable parameter which is independent of the concentration of the probe, and which provides direct information about the local environment at the lanthanide centre.[55] The comparatively large energy gap between the europium emissive and ground states means that spontaneous emission is a relatively slow process, even by lanthanide standards. The result of this is that europium luminescence usually displays lifetimes in the millisecond range, meaning that it can readily be deconvoluted from scattered light and background fluorescence with commonly available, inexpensive apparatus.

In solution-phase complexes the non-spherical distribution of the ligand donor set gives rise to electric field gradients in the macrocyclic binding cavity which lift the degeneracies of the different *J*-states. The extent to which these degeneracies are lifted depends on the symmetry at the metal centre. Each *J*-state is (2*J* + 1)-fold degenerate and thus in an anisotropic electric field can be split

into a maximum of (2*J* + 1) Stark levels, each of which is characterised by its own symmetry label.[56, 57] Thus seemingly simple transitions may in fact be found to consist of many different Stark components, with different relative intensities due to their different transition selection rules. In the case of europium, the situation is simplified by the fact that the $^5D_0$ emissive state is only singly degenerate, making the observed splitting patterns easier to rationalise. Since the splitting of the different Stark levels depends on the local ligand field environment, it stands to reason that perturbing the coordination set results in a change in the energies and weightings of these components and thus changes in the overall spectral form potentially provide a useful handle for monitoring perturbations in the local metal environment.[58]

1.5 Luminescence and Chirality

In isolation *in vacuo*, the electronically excited lanthanide cations are isotropic spherical emitters of luminescence. However in cases where chirality is imposed about the metal centre via electronic interactions with a ligand system possessing chiral or helical geometry, techniques such as circularly polarised luminescence (CPL) and circular dichroism (CD) spectroscopy can be used to probe this induced anisotropy.[59,60] Circular dichroism measures the differential absorption of left and right circularly polarised light. It is not generally appropriate for the analysis of lanthanide complexes due to the low molar extinction coefficients of the forbidden *f-f* transitions, although it can be used to probe chirality in the organic scaffold bearing the metal ion.[61] CPL spectroscopy on the other hand measures the differential emission of left and right circularly polarised light from an excited species.[62] The difference in emission intensity between the two polarisations is expressed by the emission dissymmetry factor, g_{em} , which is formulated in equation 1.2.

$$g_{em} = \frac{2(I_L - I_R)}{I_L + I_R} \qquad \textbf{(1.2)}$$

In the above equation I_L and I_R denote the intensities of left and right polarised light respectively. A non-zero g_{em} value indicates that one chiral species is emitting with a greater total intensity than its enantiomeric partner, most likely because there is more of that enantiomer present. The

emission dissymmetry factor varies directly with the rotatory strength and inversely with the electric dipole strength of the transition in question.[63] For the *f-f* transitions of the lanthanide ions, the rotatory strength of a transition is related to the size and relative orientation of the magnetic and electric dipole moments of the transition, and the angle between them. The majority of transitions with the *f*-manifold are predominantly allowed by an electric dipole mechanism and thus any transitions with a magnetic dipole component will display greater values of g_{em} than those around them. One such example is the $^5D_0 \rightarrow {}^7F_1$ transition in the emission spectrum of europium (III), which is mediated by a pure magnetic dipole mechanism. Though the contribution may be slight, that many *f-f* transitions have at least some magnetic dipole character means that g_{em} values for lanthanide complexes are typically an order of magnitude greater than those observed with chiral organic luminophores, the transitions of which tend to be largely electric dipole in nature. CPL and the dissymmetry factor clearly depend directly on the local environment at the emissive moiety and thus provide useful tools for probing the structure at the metal centre. CPL has been used extensively in the resolution of the solution-phase conformations of luminescent molecules, and especially those which contain helices.[64] Europium and terbium complexes bound by polydentate ligands have been explored by CPL to decipher the overall chirality, both when the ligand itself has a chiral centre,[65-67] and when the chirality is imparted by the cooperative helical twist of the ligating arms of said ligands.[68] As has been discussed in section **1.7**, the rapid ring inversion and arm rotation processes in polyaza-carboxylate ligands such as DOTA mean that the enantiomers are capable of rapid interconversion and hence all samples exist as racemates with no overall dissymmetry in emission from the metal centre. In contrast to the 12N4 DOTA-type systems, complexes based on the smaller 9N3 macrocycle have been shown to be incapable of ring-inversion and by exchanging the arm donor groups from carboxylates to bulky phosphinates, the arm rotation can also be severely retarded.[69] Thus in complexes such as the one shown in figure 1-7, racemisation is slow and the enantiomers can be separated by chiral HPLC, allowing CPL spectra to be recorded for each isomer in isolation.[70]

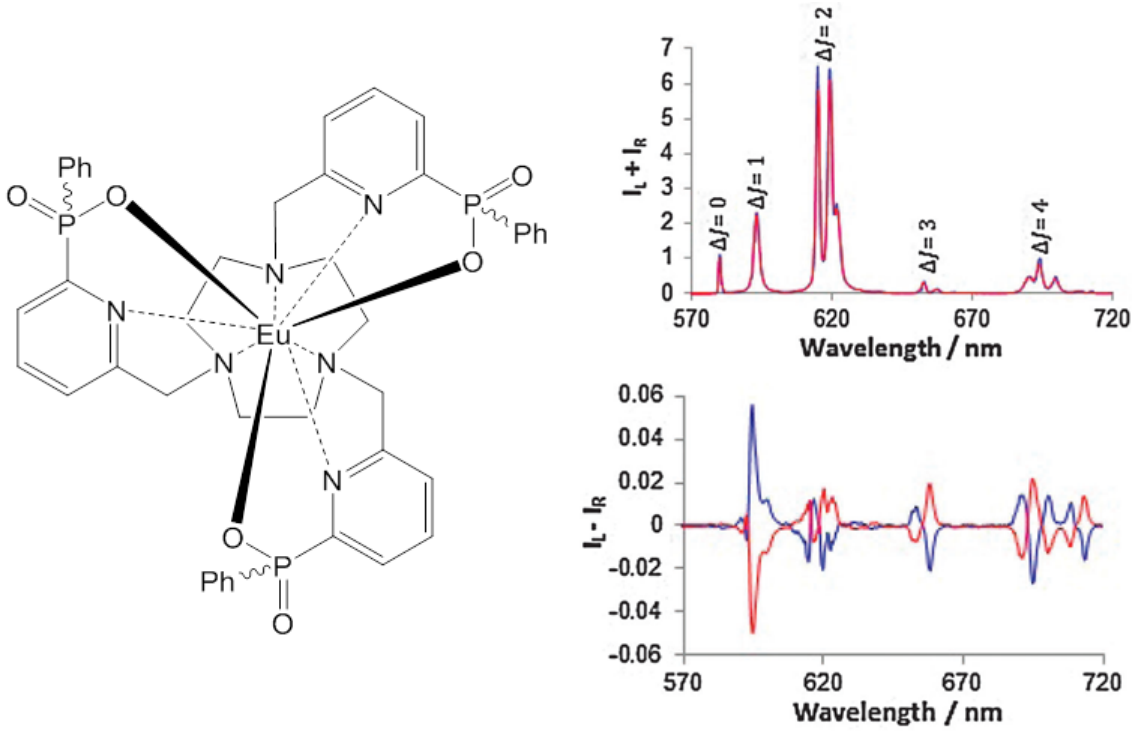

Figure 1-7. The structure of the enantiomerically-locked europium complex shown alongside the total emission (top) and CPL (bottom) spectra of the Δ (blue) and Λ (red) enantiomers. Adapted from reference70.

In addition to merely probing static chirality at a metal centre, CPL may be used to draw inferences about changes in the local environment upon binding. In chiral complexes based on enantiopure ligand systems, association with a guest species can lead to a change in the primary coordination environment which in turn leads to a response in the CPL signal.[71, 72] This can be due to the displacement of a weakly coordinating ligand donor or solvent molecule, or a perturbation to the crystal field, leading to a change in the rotatory strength.[73]

This process can be reversed and extended to systems where in isolation, the complex is dynamically racemic in helicity, with no innate preference for one enantiomeric form and hence no emission dissymmetry. Upon binding of a chiral guest species however, one helical arrangement is favoured over the others and this induces an enantiomeric excess, giving rise to a non-zero g_{em} value. This particular approach is far less common than those previously discussed. In one of the very few documented cases, Carr and co-workers exploited this methodology to develop a sensor for the human serum acute phase protein α_1-AGP. In the absence of this

inflammation biomarker, the europium complex shown in figure 1-8 existed as a dynamic racemate, interconverting freely between its enantiomers and thus displaying no emission dissymmetry. In the presence of added protein however, a large change was observed in the total emission spectral form, accompanied by a significant emission dissymmetry.[74] Investigations into the structure of the ternary adduct revealed that upon binding, both the apical water molecule and one of the azaxanthone nitrogen atoms were displaced from the metal centre by the binding group of the incoming protein. The large lobe of the protein was then oriented such that one helicity of the other three pendant arms was strongly favoured.

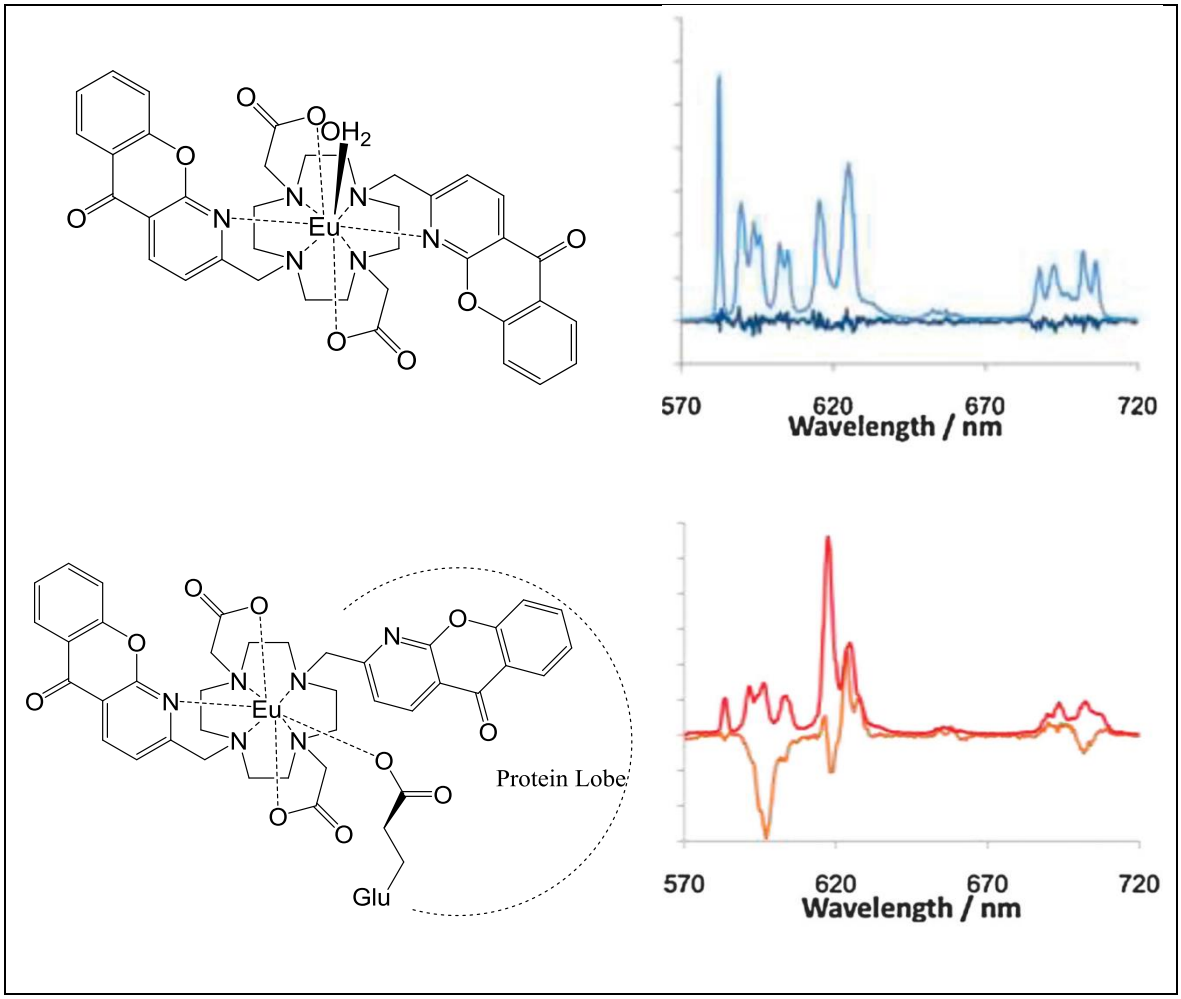

Figure 1-8. Left - the conformational structures adopted by the europium complex in the absence (top) and presence (bottom) of protein α_1-AGP. Right - The corresponding total emission (light blue & red) and CPL (dark blue and orange) spectra for each structure. Adapted from reference 74.

1.6 Magnetic Properties of the Lanthanides

The presence of unpaired electron spins in the 4*f* orbitals imbue the lanthanides with a variety of magnetic properties which have been put to use in the fields such as single molecule magnets, NMR shift agents and MRI contrast agents. The large spin-orbit coupling terms from the ground state result in large magnetic moments μ_{eff} which can be expressed as;

$$\mu_{eff} = g_J\sqrt{J(J+1)} \qquad \textbf{(1.3)}$$

$$g_J = {}^3/_2 + \frac{S(S+1) - L(L+1)}{2(J+1)} \qquad \textbf{(1.4)}$$

In the above equations g_J is the Landé g-factor and is a term representing the total magnetic moment of an electron resulting from the coupling of the spin and orbital angular momentum contributions. For the majority of the lanthanides, calculations performed using the equations shown above give magnetic moment values which display good agreement with those obtained experimentally. For europium (III), the ground state is $^7F_0$ and thus with *J* = 0, application of these formulae would predict a μ_{eff} value of zero. This is however found not to be the case and when measured experimentally, europium complexes often show magnetic moments ranging between 3.3 and 3.5 μ_B. The reason for this behaviour is the thermal population of the low-lying $^7F_1$ and $^7F_2$ states, coming at 330 cm^{-1} and 860 cm^{-1} above the $^7F_0$ ground state respectively. If the Boltzmann population of these states at the temperature of the experiment is taken into account, the Landé formula stated above returns values which match closely those measured by experiment.

1.7 NMR of Lanthanide Complexes

The presence of a paramagnetic lanthanide ion within an organic ligand system induces a profound frequency shift in the resonances of the NMR-active nuclei of the ligand. This shift, Δ can be broken down into contributions from effects happening due to direct through-bond contact between the lanthanide unpaired electron spins and the nucleus under investigation, and from

through-space contributions arising from dipolar coupling of these two magnetic moments. The former is known as Fermi, or contact shift (Δ_c), whilst the latter is called pseudocontact shift (Δ_{pc}). The final component of the lanthanide induced shift is a conventional diamagnetic contribution (Δ_d) from the presence of the highly electropositive cation. The total lanthanide induced shift can therefore be formulated;

$$\Delta_{total} = \Delta_c + \Delta_{pc} + \Delta_d \qquad \textbf{(1.5)}$$

The contact shift contribution is a consequence of through-bond spin coupling, between the orbitals bearing the unpaired spins on the metal ion, and the orbitals centred on the nucleus under investigation. For complexes of paramagnetic lanthanide ions the contact shift component may be expressed;

$$\Delta_c = -\frac{A \cdot \langle S \rangle}{h \cdot \gamma \cdot B_0} \qquad \textbf{(1.6)}$$

In this expression, A is the hyperfine coupling constant, γ is the gyromagnetic ratio of the nucleus in question, B_0 is the strength of the applied field, lifting the degeneracy of the *J*-states and $\langle S \rangle$ is the total spin expectation value. In the case of lanthanide complexes, the unpaired spins are housed in the 4*f* shell on the metal and since these orbitals play a minimal role in bonding with the ligand sphere, one would expect the contact shift due to the metal paramagnet to be slight. Indeed this has been shown to be the case, with the contact contribution to the lanthanide-induced shift found to be all but negligible unless the nucleus under investigation is a σ-donor to the metal centre.

The pseudocontact interaction, by contrast, is a through-space phenomenon and derives from coupling between the nuclear and electronic dipole moments. This effect therefore depends on the magnitude of these dipoles, as well as their relative orientations and separations in space. The expression for the pseudocontact shift in paramagnetic lanthanide complexes was first postulated by Bleaney[75] and is formulated as follows;

$$\Delta_{pc} = \frac{2\beta^2 D}{60k^2T^2}\left(\frac{\langle r^2\rangle A_2^0(3cos^2\theta - 1) + \langle r^2\rangle A_2^2(sin^2\theta cos2\varphi)}{r^3}\right) \quad \textbf{(1.7)}$$

In complexes which display rotational symmetry about the magnetic axis, the second angular term tends to zero and the overall expression can be simplified.

$$\Delta_{pc} = \frac{2\beta^2 D}{60k^2T^2}\left(\frac{\langle r^2\rangle A_2^0(3cos^2\theta - 1)}{r^3}\right) \quad \textbf{(1.8)}$$

In the above expressions the $\langle r^2\rangle A_2^0$ and $\langle r^2\rangle A_2^2$ terms are crystal field parameters and D is a constant specific to the metal ion in question and pertains to the magnetic susceptibility. r, θ and φ are the polar coordinates to describe the position of the nucleus under study, relative to the paramagnetic metal ion, which is defined as the origin of the coordinate space.

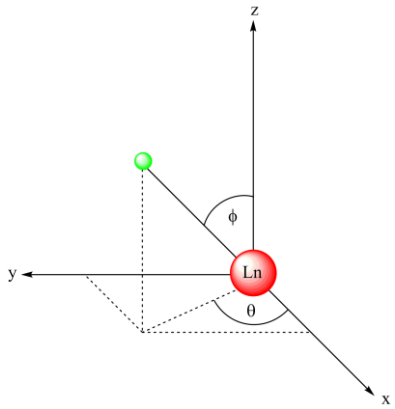

Figure 1-9. Coordinate system used to describe the relative positions of a paramagnetic centre at the origin and the resonant nucleus under investigation.

Since the pseudocontact shift operates via a through-space coupling, the non-bonding nature of the 4*f* orbitals does not hamper it. Indeed, it has been shown that in the case of ^{1}H-NMR studies of lanthanide complexes, the pseudocontact interaction is wholly responsible for the observed lanthanide induced shift.[76,77] The results of this physical effect are immediately apparent upon inspection of the ^{1}H-NMR spectra of complexes bearing paramagnetic lanthanide ions as they display large chemical shift ranges for the proton resonances. The magnitude of the shift observed with a given metal ion is related to its effective magnetic moment μ_{eff}, which is included in the D term of Bleaney's equations. Coupling between the electrons of the *f*-metal and the nuclear

dipoles of the resonant nuclei also leads to an increase in the T_1 relaxation time and again this increases with μ_{eff}. Therefore complexes of lanthanides with small magnetic moments such as Nd^{III} (μ_{eff} = 3.62) display spectra with relatively small range of chemical shifts (typically 50 > $\delta(^1H$ ppm) > -50 ppm) with sharp resonances, whereas those such as Tb^{III} (μ_{eff} = 9.72) show large induced chemical shifts (400 > $\delta(^1H$ ppm) > -400 ppm) and broad lines.[78] In the cases of lanthanum and lutetium, which have an empty and full 4*f*-shell respectively the only shift effects are dipolar in nature and thus complexes of these metals are useful diamagnetic analogues for structural studies.

1.7.1 NMR studies of DOTA derivatives

Since one can measure the magnitude of the lanthanide induced shift, it is possible to calculate coordinates for the resonating nucleus relative to the metal centre and thus extract structural information which can be correlated with data obtained by single crystal X-ray diffraction. The majority of the studies performed have centred on mono-nuclear complexes with axial symmetry, due to the reduced complexity of the calculations involved. One such system which has been studied extensively are the lanthanide complexes of the C_4-symmetric ligand 1,4,7,10-tetraazacyclododecyl-tetraacetic acid, more commonly abbreviated to DOTA.[77] DOTA is an octadentate ligand, coordinating through the four tertiary amine nitrogens of the ring, which sit below the lanthanide ion, and through the oxygens of the four pendant carboxylate arms, sitting above. The ninth, apical coordination site caps the face formed by the four carboxylate arms and is most usually occupied by a solvent molecule.

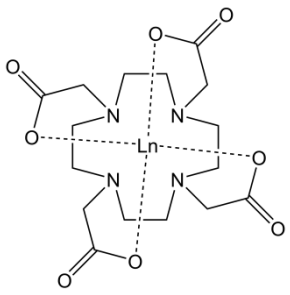

Figure 1-10. Molecular structure of $[Ln^{III}.DOTA]^-$.

The C_4-symmetric complex exists as four isomeric species in solution, defined by their N-C-CO (Δ/Λ) and N-C-C-N (δ/λ) helicities.[79] Thus for LnDOTA complexes there exist two diastereomeric pairs of enantiomers: the pair of Δ/λλλλ and Λ/δδδδ adopt a regular square antiprismatic geometry (termed SAP) with an N_4/O_4 twist angle of 40°, and the pair Λ/δδδδ and Δ/λλλλ are twisted square antiprisms (TSAP) with a 29° twist angle.[80] Interconversion between the two isomers may occur either by cooperative arm rotation (Δ→Λ) or by ring inversion (δ→λ).[81]

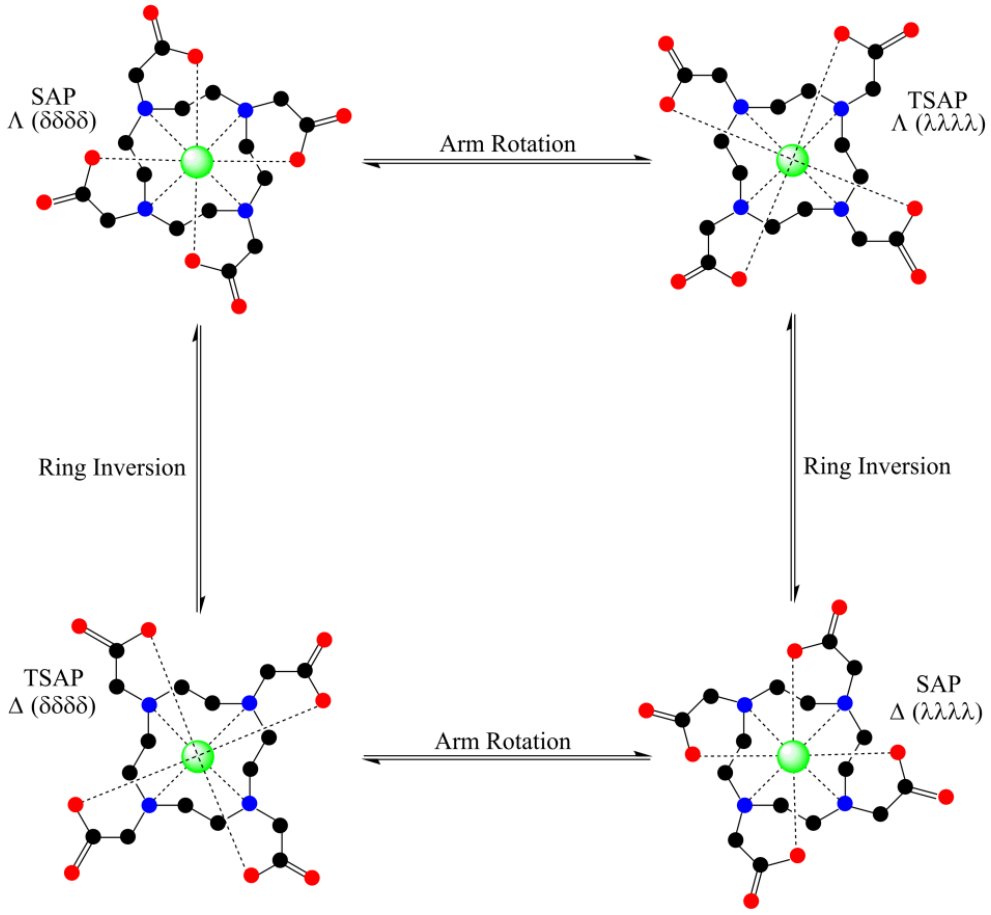

Figure 1-11. Schematic of the isomers of lanthanide DOTA complexes and the processes by which they interconvert. Adapted from reference 81.

The former process is substantially faster and at ambient temperatures leads to line broadening, whilst the latter is slow and gives rise to sharp peaks for each isomer. Investigations into the position of the TSAP/SAP equilibrium have shown that the SAP isomer is more compact with a lower overall hydration state and thus is favoured in solution for all but the largest lanthanide ions.[82] As a direct consequence of this, solvent exchange at the axial

ninth coordination site is significantly faster for the TSAP isomer; by a factor of approximately 50 in the case of water.[83]

Ring inversion leads to exchange between the methylene protons on the cyclen backbone. These pseudo-equatorial and pseudo-axial protons have very different positions in space relative to the local field of the lanthanide ion. They will therefore have drastically different pseudocontact interactions and thus very different chemical shifts.

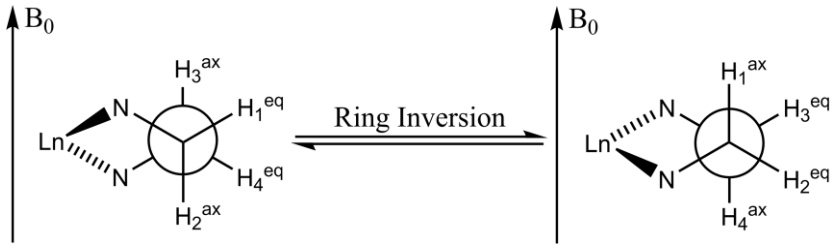

Figure 1-12. Newman projection illustrating the interconversion of axial and equatorial proton environments on the cyclen ring.

There are two other peaks in the proton NMR spectrum which are due to the protons on the acetate arms. These protons are magnetically inequivalent as one is pointing into the ring towards the magnetic axis of the lanthanide ion whilst the other is pointing out and away. If the temperature is increased, the arm rotation becomes sufficiently fast to cause the two peaks to coalesce.[84]

In assigning the spectra, calculations have shown that the most shifted peak corresponds with the resonance of the axial proton of the cyclen unit and indeed this is found to be the case. Table 1-3 shows the shifts and assignments for some of the proton resonances found in the spectrum of $[Yb.DOTA]^-$.[85] In this table, the H_n^{ac} are the resonances of the two methylene protons of the pendant acetate arms.

Proton	δ_H (ppm) in SAP Isomer	δ_H (ppm) in TSAP Isomer
H_1^{ax}	153.7	86.3
H_2^{eq}	21.1	9.9
H_3^{eq}	25.6	11.2
H_4^{ax}	-56.0	-38.3
H_1^{ac}	-47.9	-61.9
H_2^{ac}	-101.5	-33.9

Table 1-3. The shifts of selected resonances in $[Yb.DOTA]^-$ in D_2O. Adapted from reference 85.

1.7.2 Kinetics of exchange processes

NMR studies in which the temperature and pressure of the samples were varied (and the subsequent van't Hoff analyses) have allowed the rate constants and thermodynamic parameters of both the isomerisation and bound water exchange processes to be calculated for DOTA-tetraamide (DOTAM) complexes.[82] Like the aforementioned DOTA species, these complexes were found to exist in solution as a pair of diastereomers with TSAP and SAP geometries and once again, interconversion between the two was via cooperative rotation of the acetamide arms and inversion of the 12N4 ring. In each of the two diastereomers the 9th, apical coordination site could either be occupied by a water molecule or left vacant in the nonhydrated form of the complex. ^{17}O- and ^{1}H-NMR has been used to determine the exchange rates and activation energies for the two isomers and it was found that water exchange was approximately 50 to 100 times faster in the less favoured TSAP conformation.[86, 87] Thus, even though the TSAP conformer only represented a small fraction of total complex concentration, it made an overwhelming contribution to the overall exchange rate. This consequence of solution phase speciation is of particular importance in the case of gadolinium, as the relaxivity of a metal centre depends on the kinetics of water exchange.

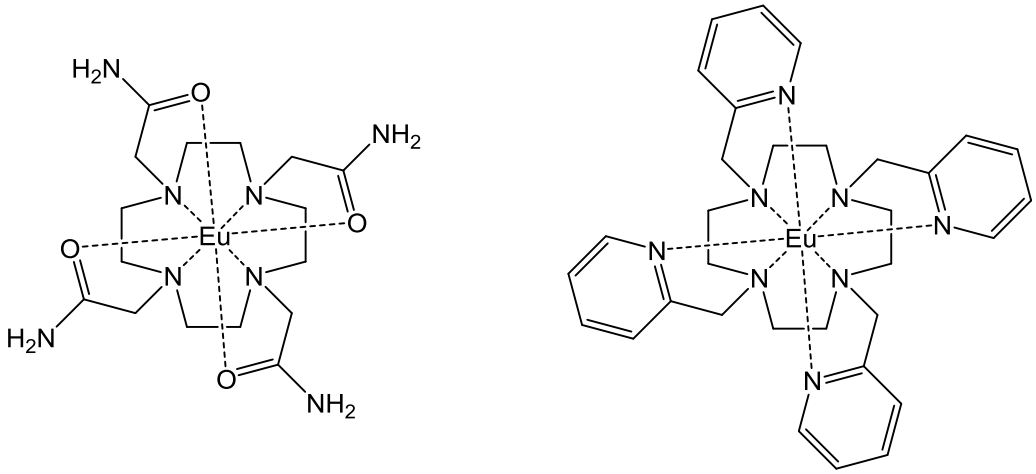

Figure 1-13. Molecular structures of the europium complexes of DOTAM (left) and tetrapicolyl-cyclen (right).

Natrajan *et al.* investigated the energetics of the exchange processes in a related family of tetrapicolyl-cyclen complexes. In addition to variable-temperature NMR, they used DFT calculations to probe the mechanisms by which the TSAP and SAP isomers could interconvert. They found that in this system, the added bulk of the picolyl arms meant that a direct conversion from one isomer to the other via synchronous inversion of all four arms was energetically impossible because of the associated activation energy, which was in excess of 200 $kJmol^{-1}$. Instead, the isomerisation path was found to be a sequence of four single joint inversions, each with an apparent free energy activation of approximately 50 $kJmol^{-1}$.[88]

1.7.3 Effect of the apical donor

In C_4-symmetric octadentate complexes such as those discussed so far, the identity and nature of the donor atom occupying the ninth, apical coordination site has been found to have a profound effect on the shifts of the proton resonances with the ligand scaffold.[79] This occurs by perturbation of the magnetic susceptibility anisotropy and specifically, the second order crystal field coefficient B_0^2 which is one of the components included in the D term of Bleaney's equation (Equation 1.7). In the example shown below, the shift of the most shifted H_1^{ax} proton was measured in a variety of coordinating solvents.

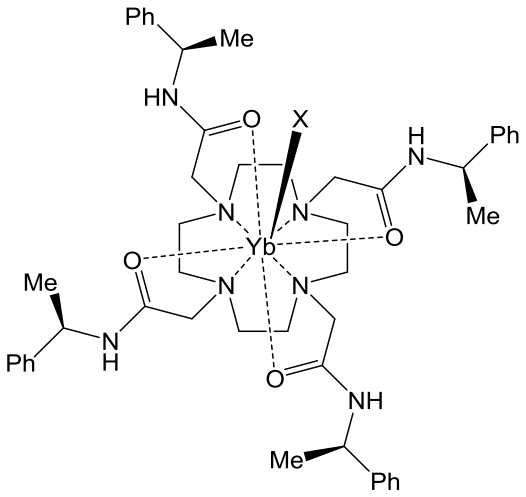

Apical Donor X	$\delta(H_1^{ax})$ / ppm
HMPA	50.0
DMSO	71.1
DMF	88.1
MeOH	112.0

Figure 1-14. The shifts of the axial proton resonances of complex n with different axial donor ligands.[89]

It was found that the less polarisable the apical donor, the smaller the lanthanide-induced shift of the axial protons and the lower the affinity of the coordinated solvent molecule.[89]

1.7.4 Descent in Symmetry

All of the systems synthesised and studied in this work are based on the heptadentate DO3A motif, in which only three of the cyclen nitrogen atoms bear pendant acetate arms, with the fourth used for further functionalisation. The axial symmetry of the molecule is broken and the NMR spectra are much more complex. This is a result of the magnetic axis of the molecule no longer being so readily defined. Indeed, in the multinuclear systems described later, this problem is compounded by the fact that the magnetic axes of the two metal cores are not necessarily aligned. Nevertheless, conclusions regarding the geometry at the metal centre and the TSAP/SAP isomer ratio may be drawn by analogy.

1.8 Responsive Agents

For a probe to report on some aspect of its local environment it must interact with the guest selectively under ambient conditions, so as to modulate an observable parameter, such as a luminescent or magnetic response. To be of practical application, the change must be readily, rapidly and reproducibly measurable, independent of probe concentration and easily calibrated

over the range of physiological conditions. In addition, for use in a clinical setting, the measurements should offer good spatial and temporal resolution and the modulated response must display high signal-to-noise ratio to minimise the dose of probe administered. Two main imaging modalities are able to satisfy this stringent list of requirements; NMR/MRI and luminescence imaging. Lanthanide-based probes have been devised which exploit these two techniques to report on various aspects of the local environment. Due to their relevance in the diagnosis and analysis of tumours, pH and concentration of oxygen have received special attention in this field.

In MRI contrast agents the relaxivity of a metal centre is influenced by the number of water molecules bound at the metal, the residence time and exchange kinetics of those water molecules with the bulk, and the rate of molecular tumbling of the scaffold bearing the metal ion.[90] Simply changing the ambient pH results in a change in relaxivity due to the number of O-H and N-H oscillators per solvent species, as well as the increased residence time due to increased electrostatic interaction. It is also possible to alter the rotational correlation time in response to changing pH. In work by Nwe *et al.* an amine-functionalised polysaccharide chitosan backbone was appended with macrocyclic gadolinium cores.[91] At physiological pH, the amine groups remained neutral and the molecule was uncharged, rotating freely in solution. Upon a decrease of pH, as might occur in hypoxic tumour tissue, the amine groups were protonated, resulting in the molecule bearing an overall positive charge. This caused the probe to be attracted to the negatively charged head units of the phospholipids of the cell membrane and thus be bound at the membrane interface. The resulting immobilisation dramatically increased the rotational correlation time of the molecule as a whole and this was observed to give rise to a sharp increase in the relaxivity per metal centre. Such approaches have one significant flaw, in that they require the concentration of the probe to be known before the change occurs, as otherwise it is difficult to assess the response with certainty.

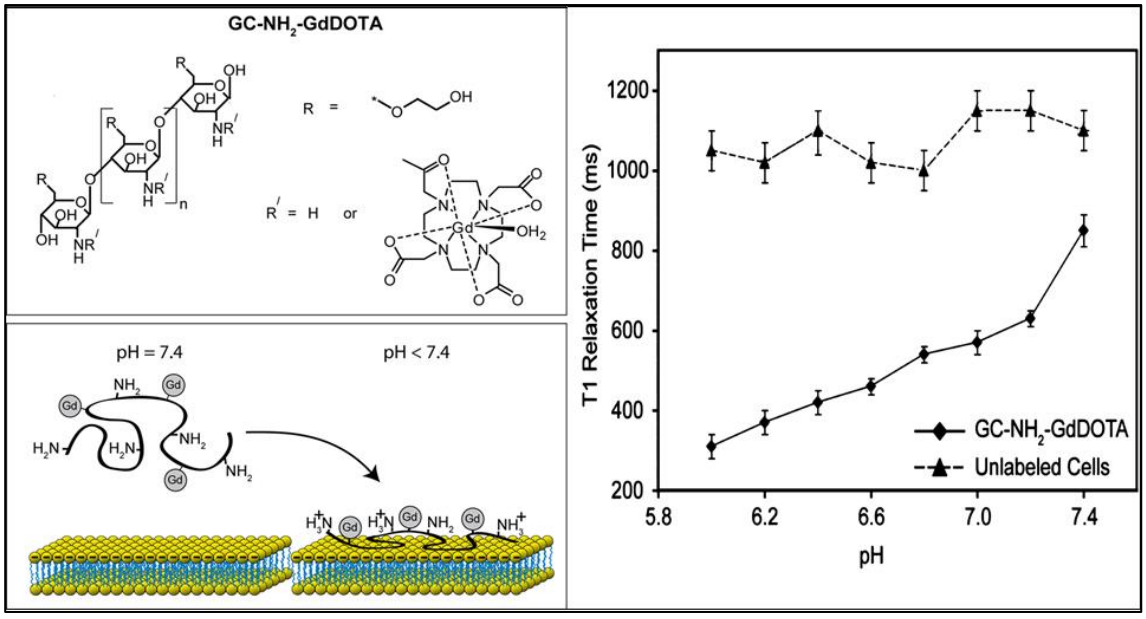

Figure 1-15. Top left - molecular structure of Gd.DOTA-appended chitosan probe. Bottom left - schematic of the pH-mediated mechanism of associated with the phospholipid membrane. Right - pH-dependence of relaxivity. Adapted from reference 91.

Probes reporting via sensitised luminescence can be used to assess local oxygen concentration. Molecular oxygen has a triplet ground state, meaning it can interact with the triplet manifold of the aryl antenna unit. This interaction results in triplet annihilation and depopulates the sensitiser excited state, resulting in a decrease in the quantum yield of luminescence. pO_2-sensitive probes have been developed from near-IR luminescent complexes containing metals such as neodymium, erbium and ytterbium, sensitised by an integral organic chromophore such as eosin or fluorescein. However the greatest opportunity for a lanthanide-based oxygen-sensor involves sensitised emission from terbium. The long-lived emissive $^5D_4$ state of terbium lies at 20,400 cm^{-1}, within range of many common aryl triplet states. This allows for thermally activated back energy transfer to the chromophore triplet manifold, establishing a dynamic equilibrium between this state and the terbium $^5D_4$ level.

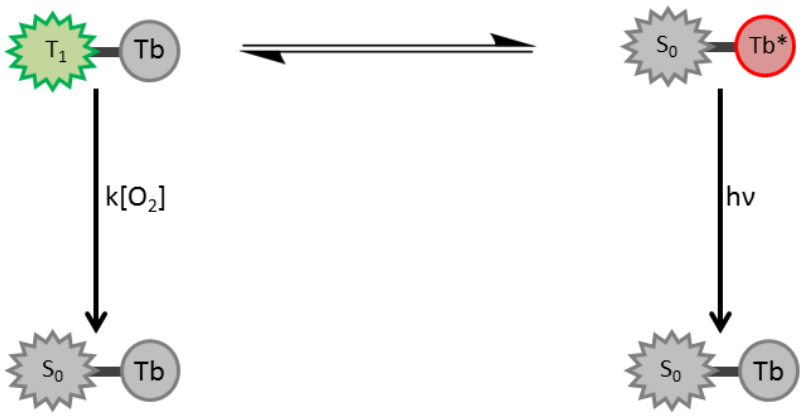

Figure 1-16. Pre-equilibrium of sensitiser and terbium excited states allowing lifetime-based assessments of local pO_2.

As there is now a different process depopulating each state in the equilibrium (collisional quenching with molecular oxygen in the case of the chromophore triplet and luminescence for the terbium excited state), a change in the local concentration of oxygen will result not only in a change in emission intensity from the terbium centre, but also in a change in luminescent lifetime. Unlike the intensity, the lifetime is independent of probe concentration and is therefore potentially of use as a ratiometric measure of O_2 partial pressure. Examples of such systems include terbium chelates appended with coumarin, naphthalene and pyrene antenna units.[92-95] It should be noted that although this approach has been primarily used with complexes of terbium, it is in fact more generally applicable and can be employed for any metal, as long as a chromophore can be found with a triplet state lying sufficiently close in energy.[92]

1.8.1 Cation Detection

The ratiometric detection of endogenous cations such as Zn^{2+} and Ca^{2+} has also been reported. One of the most common methods for the detection of metal ions is to append a stable lanthanide-bearing macrocyclic core with a second binding domain, tuned to suit the metal under study. In work by Mishra *et al.* in 2011, they describe a variety of systems involving an amide group which is capable of acting as a donor in both binding domains.[96] In the absence of the metal to be detected (in this case calcium), the second binding domain, an eight-coordinate EGTA

derivative, is vacant and free to orient itself so as to maximise solvation. The linking amide group is coordinated to the lanthanide centre via the carbonyl oxygen. When calcium is added, the appended binding pocket is organised around the new metal ion and the amide group is abstracted from the lanthanide coordination sphere.

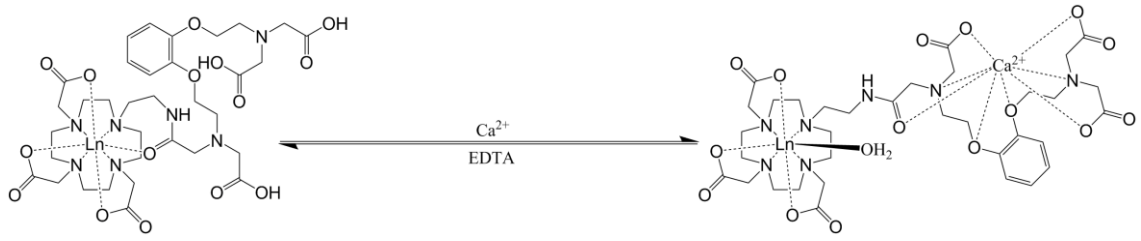

Figure 1-17. The change in coordination environment upon addition of the Ca^{2+} cation.

This leaves a coordination vacancy at the lanthanide-metal centre which can be occupied by a closely-bound solvent molecule. Thus upon addition of calcium, the q-value for the complex as a whole rises from 0 to 1. This is observable by an increase in the water proton relaxivity in the case of the gadolinium species, and a change in the luminescence of the europium complex. This approach can be extended by carefully tuning the size and donor set of the appended binding domain to select for a desired metal. By changing to a six-coordinate pyro-EGTA derivative for example, it was possible to selectively sense for zinc (II). To select for softer cations such as copper, Que and coworkers reported a similar system in which a gadolinium complex was furnished with an amino-thioether unit, capable of adopting a near-tetrahedral geometry. Treatment of the complex with one molar equivalent of aqueous copper resulted in the q-value of the gadolinium centre rising from 0 to 1 and this was accompanied by a 350% increase in relaxivity.[97]

1.8.2 Anion binding

Anion recognition and binding in nature is achieved via a specifically tailored cavity within a protein scaffold, with hydrogen bond acceptors and donors positioned and orientated to interact with complementary regions of charge density on the target anion. In aqueous conditions,

hydrogen bonds would not normally be strong enough to displace water molecules from the solvation sphere of the anion and the guest, but this problem is circumvented by the hydrophobic nature of the interior of the protein structure, which minimises the free energy loss of desolvation. For synthetic systems which lack this hydrophobic scaffold, the hydrogen bonding interactions are too weak to overcome the receptor hydration, and thus such systems are usually relegated to organic aprotic solvent systems. This limitation all but nullifies their utility as bio-imaging agents. By contrast, the electrostatic attraction between an anion and a trivalent lanthanide cation is easily strong enough to overcome receptor desolvation and thus lanthanide complexes have found widespread use in the field of anion-responsive probes for use in aqueous and biological media.

In designing an anion-responsive probe, the most commonly employed and synthetically facile approach is to use metal complexes where coordination of the anion displaces either bound solvent molecules or a weakly coordinating donor from the ligand, forming a ternary adduct in solution. Examples of water displacement abound, but those in which a ligand donor is substituted are fewer and farther between. One example is shown below, in which addition of a bicarbonate anion displaces one of the coordinated azaxanthone nitrogen atoms and is indicated by a 200% increase in emission intensity in the ΔJ=2 peak of the europium at 616 nm.[74]

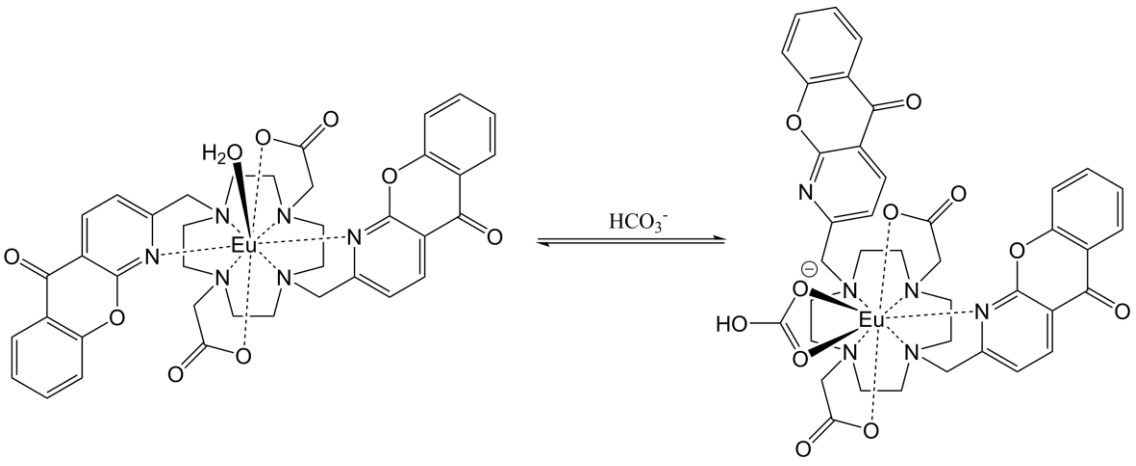

Figure 1-18. Mechanism of action for a europium-based sensor for carbonate. Adapted from reference74.

The binding of an anion can be used to switch on luminescence, if the anion has a chromophore capable of acting as an antenna to sensitise the metal centre. An example of this approach is the sensing of the aromatic salicylate anion via coordination to $[Tb.EDTA(H_2O)_2]^+$, a complex which in isolation, lacks a sensitising chromophore.

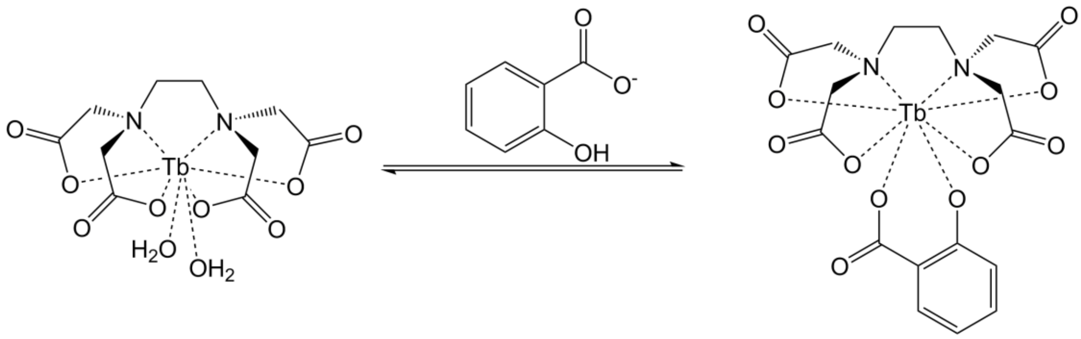

Figure 1-19. Binding of salicylate by $[Tb.EDTA]^-$ results in sensitisation of emission from the metal centre.

In the absence of salicylate, irradiation of the solution at 300 nm does not lead to terbium-based emission, as neither the metal itself, nor the ligand orbitals are capable of absorbing efficiently at that wavelength. Upon coordination however, the aryl chromophore acts as a sensitiser and luminescence from the metal is observed.[98] A similar example is presented by Esplin *et al*, who reported the ratiometric determination of the aspirin metabolite, salicylurate in urine by coordination of the phenoxide group to the macrocyclic $[Tb.DO2A(H_2O)_2]^+$.[99]

The effect the binding of an anion has on the luminescent response of a complex depends on the properties of the guest in question and the way in which it is bound to the host species. Most commonly, the anion directly displaces a bound solvent molecule from the metal centre. This can change both the intensity of emission, by removing quenching oscillators from the immediate coordination sphere, and the spectral form, by perturbing the local symmetry at the metal. This is best documented in the case of europium, where the differences in evolution between the hypersensitive $\Delta J = 2$ peak and other peaks of the emission spectrum can allow for ratiometric analysis, independent of probe concentration.[100] Alternatively, the anion can bind to and thus modify the antenna group in the complex and this can alter the luminescent response in one of several ways. First, the absorption cross-section of the chromophore can change, resulting in a

greater or lesser amount of the incident light being harvested by the complex. Interactions of this nature can be detected by correlating a change in the emissive output of the complex under irradiation, with a change in the absorption spectrum of the receptor. Second, interaction with the guest species can alter in energy the electronic states of the antenna unit so as to alter the energy cascade which populates the lanthanide excited state. An example of this is shown in figure 1-20, where a terbium macrocyclic core was functionalised with a phenanthridine chromophore.

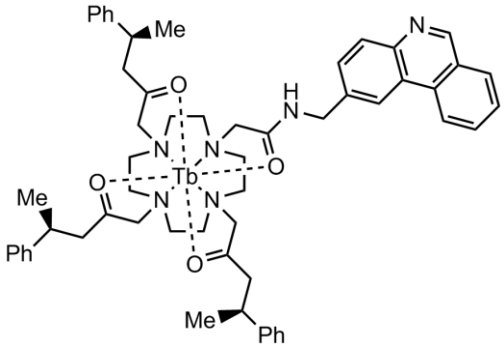

Figure 1-20. Structure of a pH sensitive terbium probe with a phenanthridine antenna group.

At high pH, the phenanthridine nitrogen is unprotonated and the triplet energy of the aryl group measured to be 22,000 cm^{-1}. Under these conditions energy transfer to the terbium centre is efficient, and metal-centred luminescence had a comparatively high quantum yield. Upon protonation to the phenanthridinium species however, the triplet energy of the aryl manifold is reduced to 21,300 cm^{-1}. This change, although small in absolute terms, brings it sufficiently close in energy to the emissive $^5D_4$ state of the terbium to allow thermal back energy transfer from the metal into the sensitiser group. Thus at lower pH, both the lifetime and the intensity of the terbium centred emission was reduced.[101]

Finally, there are instances where the excited state of the antenna group forms an exciplex with an electron-rich anionic guest, resulting in deactivation of the sensitiser via electron transfer and thus reducing both the intensity and the lifetime of the luminescence. This process is analogous to the deactivation of aryl-sensitiser triplet states by molecular oxygen. It is a dynamic quenching

process and is observed to follow simple Stern-Volmer type kinetics. Complexes have been synthesised which are selectively quenched by urate and ascorbate via this mechanism.[102-104]

1.9 Self-assembly

The self-assembly of *d*-block metal-bearing systems to form thermodynamically stable, geometrically defined supramolecular structures in solution has been extensively studied over the last few decades. Supramolecular assemblies containing *f*-elements are a more recent development, but there have been several different classes reported. Polynuclear helicates templated by the high charge density on the lanthanide metal have been studied in detail and the thermodynamic control governing their formation has been thoroughly investigated.[105-109] Coordinatively unsaturated complexes which associate with anions in solution are used as analytical probes and in selective sensing. The solution-phase binding of carboxylates by *f*-metal complexes has been used as a sensitive and high-throughput method to screen chromophores to act as potential sensitisers for lanthanide luminescence.[110, 111] Lanthanide complexes bearing carboxylate functionality have also been shown to undergo pH-sensitive self-assembly. In an early example by Burton-Pye *et al.*, a benzoate-appended DO3A core was found to exist as a distinct monomer at lower pH, but underwent dimerization at higher pH as the benzoate group was deprotonated. This change was observed by an increase in luminescence lifetime and intensity, resulting from the displacement of quenching solvent molecules from the metal centre, as well as decreased separation between the metal and the aryl sensitiser, allowing for more efficient energy transfer.[112]

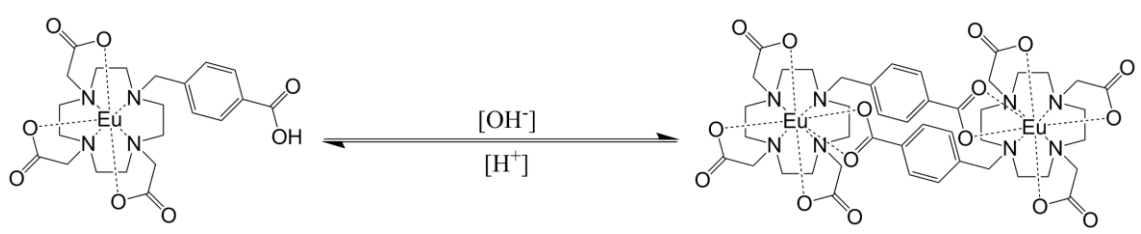

Figure 1-21. pH-dependent self-assembly of a europium complex appended with a benzoate group. Adapted from reference 112.

More recently, bis-carboxylate anions have been shown to selectively bind with binuclear complexes, forming 1:1 bridged adducts in solution. The selectivity of the complex for a particular bis-carboxylate could be tuned by changing the separation between the two metal centres. It was found that the *m*-xylyl-bridged complex shown in figure 1-22 was highly selective for aryl-1,3 dicarboxylic acids over the 1,2 and 1,4 isomers.[113] Benzoate was used as a control as it is only capable of binding to one metal centre.

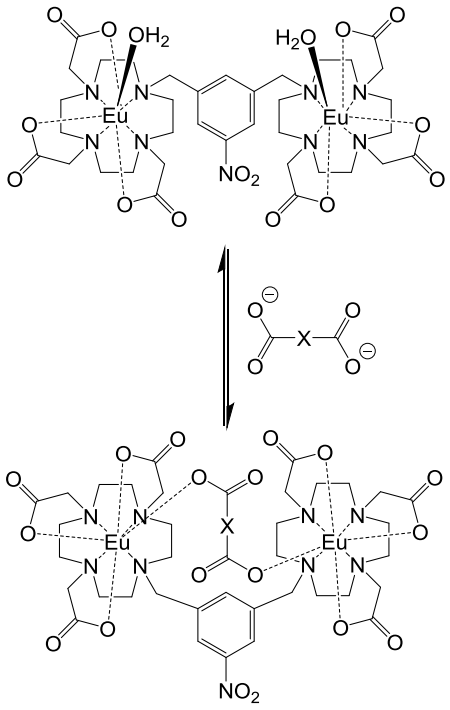

X	K (M^{-1})
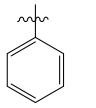	12110
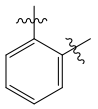	30000
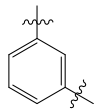	>2.0 x 10^7
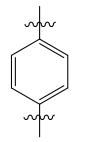	1.9 x 10^6

Figure 1-22. Left - The proposed mechanism of self-assembly between *m*-xylyl-bridged europium complex and different aryl-carboxylates. Right - A table of binding affinities (in 3:1 methanol:water) calculated for different guest species. Adapted from reference 113.

When moving from methanol to an aqueous medium, the insolubility of the phthalates meant that measurements could not be made but when the water-soluble pyridine-diacids were used instead, the same trend was observed with dinicotinate (pyridine-3,5-dicarboxylate) showing by far the highest binding constant.[114]

This strong and selective binding has been exploited by using functionalised aryl-1,3-diacids to gain access to large, polynuclear arrays. Tilney *et al.* used this approach to prepare mixed-

lanthanide heterometallic assemblies in solution, with each lanthanide ion encapsulated in a distinct binding domain.[113, 115]

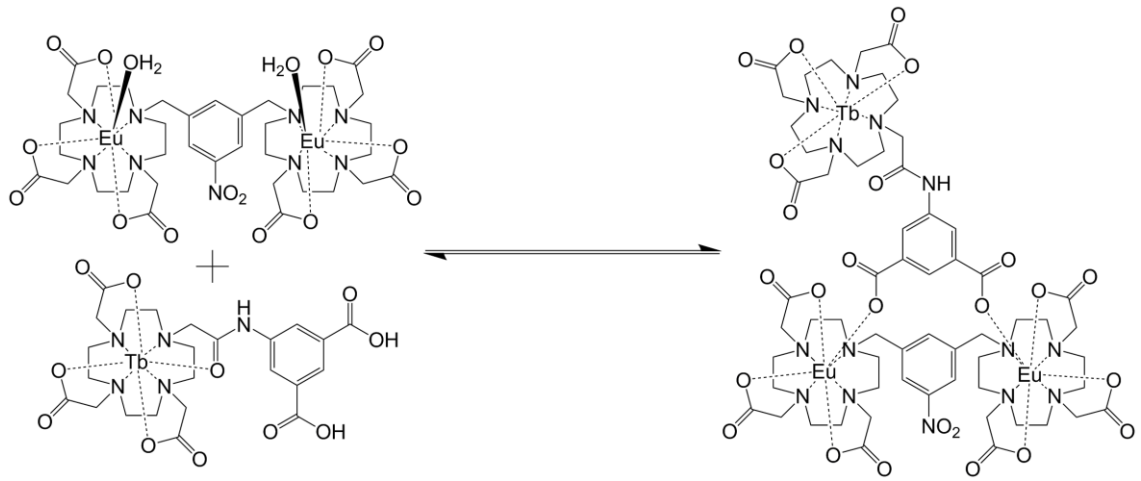

Figure 1-23. Assembly of a tri-nuclear bimetallic array via self-assembly in solution.

The binding was observed by a non-linear rise in the intensity of terbium-centred emission upon titration of the terbium complex. This methodology was extended in work by Hill, in which two dinicotinate anions, orthogonally coordinated to a central rhenium tri-carbonyl moiety, were used to bind two *m*-xylyl-bridged bis-europium complexes, forming the first example of a pentanuclear *d-f* hybrid in solution.[116]

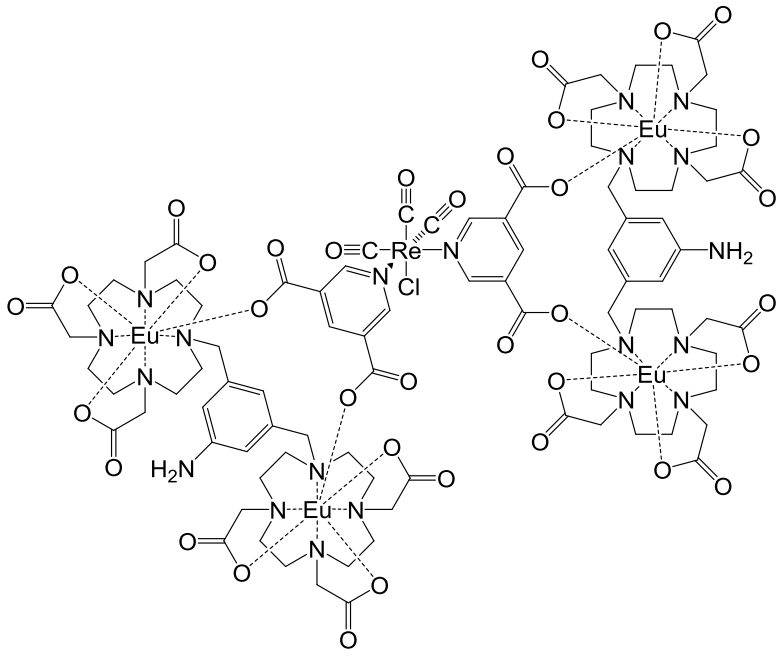

Figure 1-24. Molecular structure of a pentanuclear *d-f* hybrid prepared by Hill by self-assembly in solution.[116]

1.10 Remote Substituent Effects

Recent studies into the solution-phase self-assembly of lanthanide complexes with ditopic anions have focussed on the effects of remote substituents. Building on the previously cited study by Hill, Tropiano *et. al* showed that peripheral modifications to a binuclear lanthanide complex can have a profound influence on anion binding by controlling the global structure of the complex through their demands on conformational space. They demonstrated that association with dianions (in this case, isophthalate) occurred through a well-defined 'binding conformer' of the parent complex.[117]

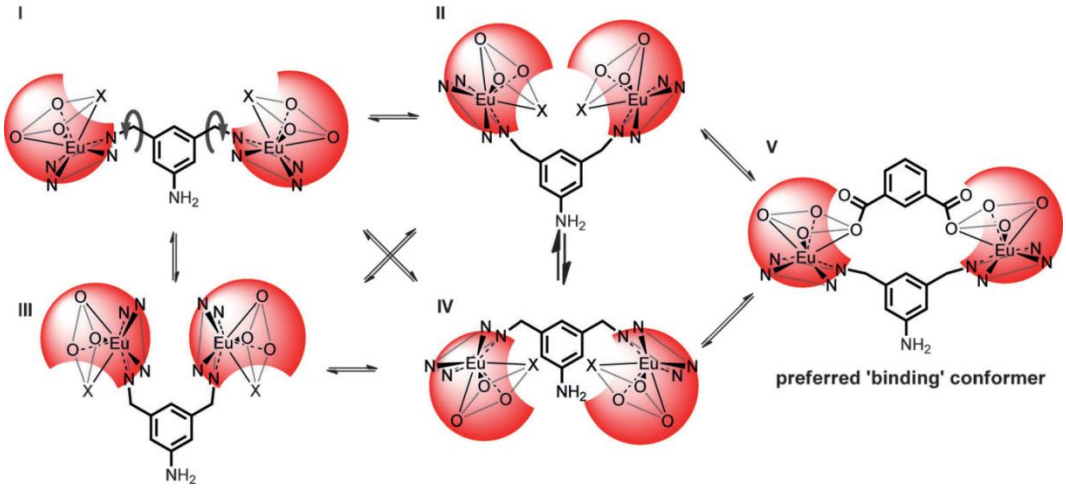

Figure 1-25. Illustration that of the wide variety of conformations available to *m*-xylyl bridged bis-DO3A complexes, only a small range are capable of binding effectively to an isophthalate guest.[117]

This restriction of conformational freedom resulted in a loss of entropy on the part of the complex upon binding. The addition of steric bulk to a site on the complex remote from the binding cavity limited the conformational flexibility, resulting in preorganisation of the parent complex and thus an increase in binding constant on entropic grounds. Larger remote substituents gave rise to larger binding constants as the host preorganisation increased. There came a point however, where the steric bulk of the peripheral group was so large as to prevent adoption of the preferred binding conformer. Beyond this point no affinity for the isophthalate anion was detected.

1.11 Aims

This work describes the preparation of a variety of kinetically stable lanthanide complexes based on the DO3A binding domain to investigate a range of factors affecting anion binding in solution, exploring the prospects for using different spacer groups to control selectivity for different guests. The parameters to be investigated include the number of metal cores in the complex, the separations and relative positions in space of the different metal centres, the conformational freedom available to both host and guest and the solvent and buffer system in which the interactions take place.

The intention from the outset was to explore by physical techniques including multi-nuclear NMR, luminescence, calorimetry and chiral methods such as CD and CPL, and identify how the complexes under study respond to external stimuli.

Chapter 2 concerns the preparation and properties of a series of binuclear complexes with the aim of selectively sequestering small anions such as the halides in solution. The concept of luminescence titration will be introduced and then used to assess the binding parameters of a selection of guests.

Chapter 3 describes a related class of ditopic lanthanide complexes in which the two metal centres are separated by a semi-rigid butyne linking group. Luminescence studies will again be used to evaluate the binding constants of homologous series of dianions to ascertain how the size of the anionic guest impacts on binding. NMR and molecular modelling will be used to attempt to correlate the formation of a host:guest adduct with conformational changes in the complex.

Chapter 4 explores the coordination of phosphate species and assesses the ability to bind biologically significant phosphates of some of the complexes from Chapter 3.

Chapter 5 will detail an investigation into the effects on binding of further lengthening the linking unit which separates the two macrocyclic binding domains.

At the beginning of the project, it was intended to explore the role of intermetallic communication in binuclear complexes. In particular, energy transfer between lanthanides has been shown to be

commonplace in solid phases, while lanthanide-lanthanide energy transfer has previously been demonstrated in bimetallic complexes. We intended to explore the use of thulium in upconverting molecular complexes that rely on using real intermediate states to generate high energy emissive states. This aspect of the work began very well, in that thulium emission was observed in solution from a number of excited states (see figure 1-26).

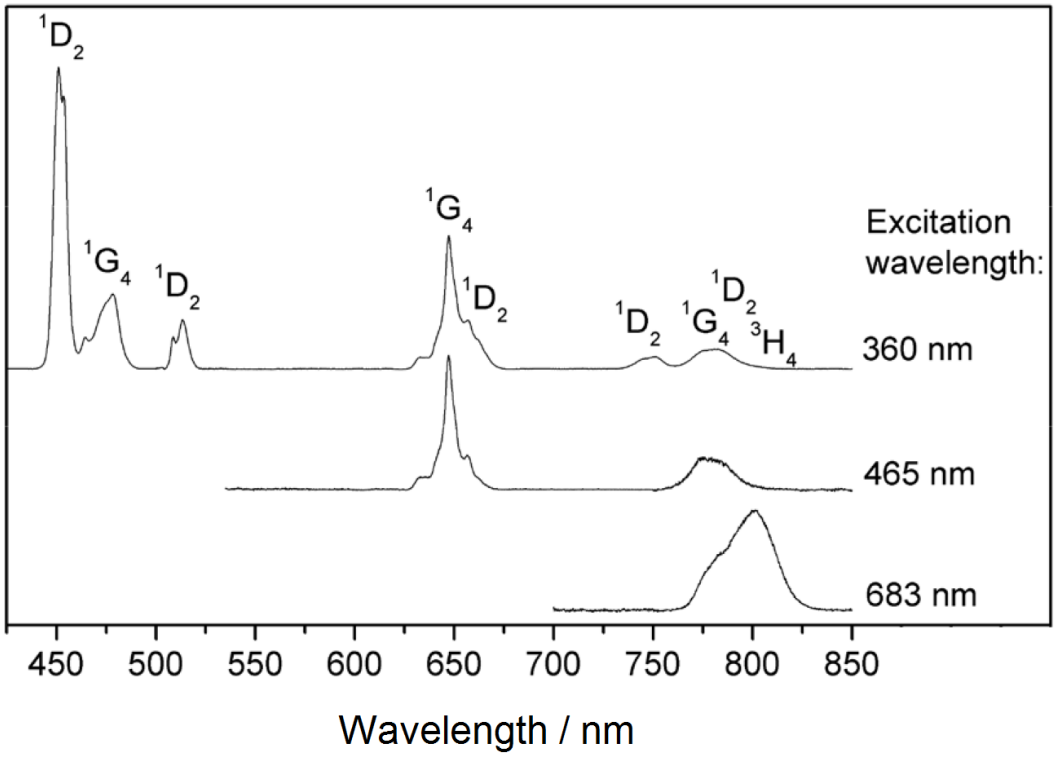

Figure 1-26. Emission spectra of $Tm(OSO_2CF_3)_3$ in d_6-DMSO exciting at 360, 465 and 683 nm. (The signal has been multiplied by 20 at 500 – 700 nm and by 50 at 700 – 850 nm with 360 nm excitation; by 5 at 750 – 850 nm with 465 nm excitation.)

Furthermore, NIR excitation of simple thulium complexes at 784 nm gave rise to upconversion within the thulium manifold through a sequence of transitions involving absorption from the ground state ($^3H_6$ - $^3H_4$), relaxation within the 4*f* manifold ($^3H_4$ - $^3H_5$) and a second absorption event ($^3H_5$ -$^1G_4$), before relaxation of the from the $^1G_4$ state through luminescence in the visible part of the spectrum.

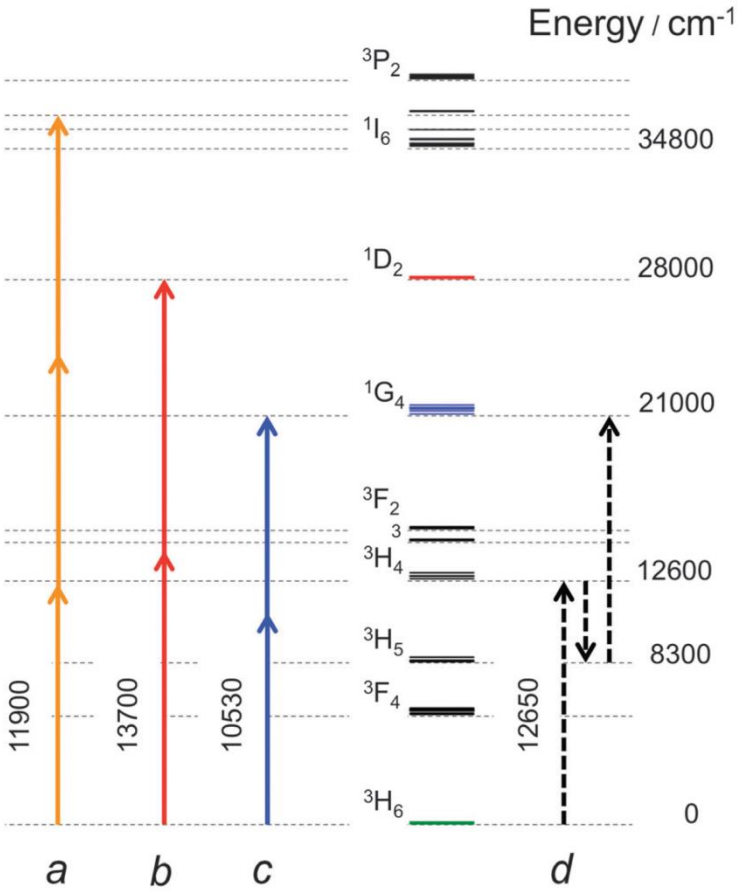

Figure 1-27. Accounting for the observed transitions in the multi-photon excitation spectrum. All processes are reflected in the emission from the $^1G_4$ state, while only a and b result in observed emission from the $^1D_2$ state.

Such observations were unprecedented in solution, and formed the basis of a paper published in PCCP. However, the study also revealed that upconversion processes such as those just described are not observed in complexes bearing even simple aryl chromophores: instead, the excitation spectra of such species are dominated by two- and three- photon excitation of the ligand skeleton. In the light of these observations, it was resolved not to pursue upconversion further in multimetallic systems. The manuscript on thulium luminescence is reproduced in this thesis as Appendix B, but thulium complexes will not be discussed in further detail in the body of this work.

1.12 References

1. S. Aime, M. Fasano and E. Terreno, *Chemical Society Reviews*, 1998, **27**, 19-29.
2. D. Parker, *Comprehensive Supramolecular Chemistry*, Pergamon, 1996.
3. S. Faulkner and R. Aarons, *Imaging and Targeting, The Encyclopedia of Supramolecular Chemistry*, Dekker, 2004.
4. A. Spencer, S. Wilson and E. Harpur, *Human & Experimental Toxicology*, 1998, **17**, 633-637.
5. M. Taupitz, N. Stolzenburg, M. Ebert, J. Schnorr, R. Hauptmann, H. Kratz, B. Hamm and S. Wagner, *Contrast Media Mol Imaging*, 2013, **8**, 108-116.
6. F. N. Franano, W. B. Edwards, M. J. Welch, M. W. Brechbiel, O. A. Gansow and J. R. Duncan, *Magnetic Resonance Imaging*, 1995, **13**, 201-214.
7. P. Wedeking and M. Tweedle, *International Journal of Radiation Applications and Instrumentation. Part B. Nuclear Medicine and Biology*, 1988, **15**, 395-402.
8. P. Wedeking, K. Kumar and M. F. Tweedle, *Nuclear Medicine and Biology*, 1993, **20**, 679-691.
9. W. P. Cacheris, S. K. Nickle and A. D. Sherry, *Inorganic Chemistry*, 1987, **26**, 958-960.
10. R. M. Smith and A. E. Martell, *Science of The Total Environment*, 1987, **64**, 125-147.
11. K. Kumar, C. A. Chang and M. F. Tweedle, *Inorganic Chemistry*, 1993, **32**, 587-593.
12. E. Balogh, R. Tripier, P. Fouskova, F. Reviriego, H. Handel and E. Toth, *Dalton Transactions*, 2007, 3572-3581.
13. J. Moreau, E. Guillon, J.-C. Pierrard, J. Rimbault, M. Port and M. Aplincourt, *Chemistry – A European Journal*, 2004, **10**, 5218-5232.
14. L. Sarka, L. Burai and E. Brücher, *Chemistry – A European Journal*, 2000, **6**, 719-724.
15. E. Toth, E. Brucher, I. Lazar and I. Toth, *Inorganic Chemistry*, 1994, **33**, 4070-4076.
16. S. Laurent, L. V. Elst and R. N. Muller, *Contrast Media & Molecular Imaging*, 2006, **1**, 128-137.
17. Z. Baranyai, Z. Pálinkás, F. Uggeri, A. Maiocchi, S. Aime and E. Brücher, *Chemistry – A European Journal*, 2012, **18**, 16426-16435.
18. F. P. Hinz and D. W. Margerum, *Journal of the American Chemical Society*, 1974, **96**, 4993-4994.
19. D. K. Cabbiness and D. W. Margerum, *Journal of the American Chemical Society*, 1969, **91**, 6540-6541.
20. K. F. Purcell and J. C. Kotz, *Inorganic Chemistry*, International Edition edn., 1977.
21. M. F. Loncin, J. F. Desreux and E. Merciny, *Inorganic Chemistry*, 1986, **25**, 2646-2648.
22. K. Binnemans, in *Handbook on the Physics and Chemistry of Rare Earths*, ed. J.-C. G. B. a. V. K. P. Karl A. Gschneidner, Elsevier, Editon edn., 2005, vol. Volume 35, pp. 107-272.
23. W. T. Carnall, P. R. Fields and K. Rajnak, *The Journal of Chemical Physics*, 1968, **49**, 4412.
24. *Lanthanide Luminescence: Photophysical, Analytical and Biological Aspects*, Springer, 2011.
25. J. H. V. Vleck, *The Journal of Physical Chemistry*, 1937, **41**, 67-80.
26. P. Porcher and P. Caro, *Journal of Luminescence*, 1980, **21**, 207-216.
27. D. Parker, R. S. Dickins, H. Puschmann, C. Crossland and J. A. K. Howard, *Chemical Reviews*, 2002, **102**, 1977-2010.
28. N. M. Shavaleev, L. P. Moorcraft, S. J. A. Pope, Z. R. Bell, S. Faulkner and M. D. Ward, *Chemistry – A European Journal*, 2003, **9**, 5283-5291.
29. A. Beeby, S. W. Botchway, I. M. Clarkson, S. Faulkner, A. W. Parker, D. Parker and J. A. G. Williams, *Journal of Photochemistry and Photobiology B: Biology*, 2000, **57**, 83-89.
30. H. L. Handl and R. J. Gillies, *Life Sciences*, 2005, **77**, 361-371.
31. J.-C. G. Bünzli, *Chemical Reviews*, 2010, **110**, 2729-2755.
32. A. Beeby, L. M. Bushby, D. Maffeo and J. A. G. Williams, *Journal of the Chemical Society, Perkin Transactions 2*, 2000, 1281-1283.

33. A. Dadabhoy, S. Faulkner and P. G. Sammes, *Journal of the Chemical Society, Perkin Transactions 2*, 2000, 2359-2360.
34. P. Atkinson, K. S. Findlay, F. Kielar, R. Pal, D. Parker, R. A. Poole, H. Puschmann, S. L. Richardson, P. A. Stenson, A. L. Thompson and J. Yu, *Organic & Biomolecular Chemistry*, 2006, **4**, 1707-1722.
35. D. Parker, K. Senanayake and J. A. Gareth Williams, *Chemical Communications*, 1997, 1777-1778.
36. W. D. Horrocks, J. P. Bolender, W. D. Smith and R. M. Supkowski, *Journal of the American Chemical Society*, 1997, **119**, 5972-5973.
37. S. I. Klink, H. Keizer and F. C. J. M. van Veggel, *Angewandte Chemie International Edition*, 2000, **39**, 4319-4321.
38. S. Faulkner, L. S. Natrajan, W. S. Perry and D. Sykes, *Dalton Transactions*, 2009, 3890-3899.
39. W. S. Perry, S. J. A. Pope, C. Allain, B. J. Coe, A. M. Kenwright and S. Faulkner, *Dalton Transactions*, 2010, **39**, 10974-10983.
40. D. L. Dexter, *The Journal of Chemical Physics*, 1953, **21**, 836-850.
41. T. Forster, *Discussions of the Faraday Society*, 1959, **27**, 7-17.
42. T. Lazarides, D. Sykes, S. Faulkner, A. Barbieri and M. D. Ward, *Chemistry – A European Journal*, 2008, **14**, 9389-9399.
43. D. Parker and J. A. G. Williams, *Journal of the Chemical Society, Dalton Transactions*, 1996, 3613-3628.
44. Y. Haas and G. Stein, *The Journal of Physical Chemistry*, 1972, **76**, 1093-1104.
45. G. Stein and E. Würzberg, *The Journal of Chemical Physics*, 1975, **62**, 208.
46. D. G. Smith, G.-l. Law, B. S. Murray, R. Pal, D. Parker and K.-L. Wong, *Chemical Communications*, 2011, **47**, 7347-7349.
47. M. P. Placidi, A. J. L. Villaraza, L. S. Natrajan, D. Sykes, A. M. Kenwright and S. Faulkner, *Journal of the American Chemical Society*, 2009, **131**, 9916-9917.
48. T. J. Sorensen, M. Tropiano, O. A. Blackburn, J. A. Tilney, A. M. Kenwright and S. Faulkner, *Chemical Communications*, 2013, **49**, 783-785.
49. C. Song, Z. Ye, G. Wang, J. Yuan and Y. Guan, *Chemistry – A European Journal*, 2010, **16**, 6464-6472.
50. C. M. Andolina, R. A. Mathews and J. R. Morrow, *Helvetica Chimica Acta*, 2009, **92**, 2330-2348.
51. A. Beeby, I. M. Clarkson, R. S. Dickins, S. Faulkner, D. Parker, L. Royle, A. S. de Sousa, J. A. Gareth Williams and M. Woods, *Journal of the Chemical Society, Perkin Transactions 2*, 1999, 493-504.
52. W. D. Horrocks and D. R. Sudnick, *Journal of the American Chemical Society*, 1979, **101**, 334-340.
53. S. Faulkner, S. J. A. Pope and B. P. Burton-Pye, *Applied Spectroscopy Reviews*, 2005, **40**, 1-31.
54. A. Beeby, B. P. Burton-Pye, S. Faulkner, G. R. Motson, J. C. Jeffery, J. A. McCleverty and M. D. Ward, *Journal of the Chemical Society, Dalton Transactions*, 2002, 1923-1928.
55. M. H. V. Werts, R. T. F. Jukes and J. W. Verhoeven, *Physical Chemistry Chemical Physics*, 2002, **4**, 1542-1548.
56. B. R. Judd, *Physical Review*, 1962, **127**, 750-761.
57. G. S. Ofelt, *The Journal of Chemical Physics*, 1962, **37**, 511.
58. *Handbook on the Physics and Chemistry of Rare Earths*, Elsevier, Amsterdam, 1998.
59. G. Muller, *Dalton Transactions*, 2009, 9692-9707.
60. J. I. Bruce, D. Parker, S. Lopinski and R. D. Peacock, *Chirality*, 2002, **14**, 562-567.
61. R. S. Dickins, J. A. K. Howard, C. L. Maupin, J. M. Moloney, D. Parker, J. P. Riehl, G. Siligardi and J. A. G. Williams, *Chemistry – A European Journal*, 1999, **5**, 1095-1105.
62. J. P. Riehl and F. S. Richardson, *Chemical Reviews*, 1986, **86**, 1-16.

63. F. S. Richardson, *Inorganic Chemistry*, 1980, **19**, 2806-2812.
64. F. Stomeo, C. Lincheneau, J. P. Leonard, J. E. O'Brien, R. D. Peacock, C. P. McCoy and T. Gunnlaugsson, *Journal of the American Chemical Society*, 2009, **131**, 9636-9637.
65. J. P. Leonard, P. Jensen, T. McCabe, J. E. O'Brien, R. D. Peacock, P. E. Kruger and T. Gunnlaugsson, *Journal of the American Chemical Society*, 2007, **129**, 10986-10987.
66. M. Seitz, E. G. Moore, A. J. Ingram, G. Muller and K. N. Raymond, *Journal of the American Chemical Society*, 2007, **129**, 15468-15470.
67. G. Muller, James P. Riehl, Kurt J. Schenk, G. Hopfgartner, C. Piguet and J.-Claude G. Bünzli, *European Journal of Inorganic Chemistry*, 2002, **2002**, 3101-3110.
68. J. L. Lunkley, D. Shirotani, K. Yamanari, S. Kaizaki and G. Muller, *Journal of the American Chemical Society*, 2008, **130**, 13814-13815.
69. C. Gateau, M. Mazzanti, J. Pecaut, F. A. Dunand and L. Helm, *Dalton Transactions*, 2003, 2428-2433.
70. J. W. Walton, R. Carr, N. H. Evans, A. M. Funk, A. M. Kenwright, D. Parker, D. S. Yufit, M. Botta, S. De Pinto and K.-L. Wong, *Inorganic Chemistry*, 2012, **51**, 8042-8056.
71. J. I. Bruce, R. S. Dickins, L. J. Govenlock, T. Gunnlaugsson, S. Lopinski, M. P. Lowe, D. Parker, R. D. Peacock, J. J. B. Perry, S. Aime and M. Botta, *Journal of the American Chemical Society*, 2000, **122**, 9674-9684.
72. D. G. Smith, R. Pal and D. Parker, *Chemistry – A European Journal*, 2012, **18**, 11604-11613.
73. R. S. Dickins, S. Aime, A. S. Batsanov, A. Beeby, M. Botta, J. I. Bruce, J. A. K. Howard, C. S. Love, D. Parker, R. D. Peacock and H. Puschmann, *Journal of the American Chemical Society*, 2002, **124**, 12697-12705.
74. R. Carr, L. Di Bari, S. Lo Piano, D. Parker, R. D. Peacock and J. M. Sanderson, *Dalton Transactions*, 2012, **41**, 13154-13158.
75. B. Bleaney, *Journal of Magnetic Resonance (1969)*, 1972, **8**, 91-100.
76. C. C. Bryden, C. N. Reilley and J. F. Desreux, *Analytical Chemistry*, 1981, **53**, 1418-1425.
77. S. Aime, M. Botta and G. Ermondi, *Inorganic Chemistry*, 1992, **31**, 4291-4299.
78. A. F. Cockerill, G. L. O. Davies, R. C. Harden and D. M. Rackham, *Chemical Reviews*, 1973, **73**, 553-588.
79. D. Parker, *Chemical Society Reviews*, 2004, **33**, 156-165.
80. M. l. Purgel, Z. Baranyai, A. s. de Blas, T. Rodríguez-Blas, I. n. Bányai, C. Platas-Iglesias and I. Tóth, *Inorganic Chemistry*, 2010, **49**, 4370-4382.
81. M. Polášek, J. Kotek, P. Hermann, I. Císařová, K. Binnemans and I. Lukeš, *Inorganic Chemistry*, 2008, **48**, 466-475.
82. S. Aime, M. Botta, M. Fasano, M. P. M. Marques, C. F. G. C. Geraldes, D. Pubanz and A. E. Merbach, *Inorganic Chemistry*, 1997, **36**, 2059-2068.
83. S. Aime, A. Barge, M. Botta, A. S. De Sousa and D. Parker, *Angewandte Chemie International Edition*, 1998, **37**, 2673-2675.
84. J. F. Desreux, *Inorganic Chemistry*, 1980, **19**, 1319-1324.
85. M. P. M. Marques, C. F. G. C. Geraldes, A. D. Sherry, A. E. Merbach, H. Powell, D. Pubanz, S. Aime and M. Botta, *Journal of Alloys and Compounds*, 1995, **225**, 303-307.
86. S. Zhang, Z. Kovacs, S. Burgess, S. Aime, E. Terreno and A. D. Sherry, *Chemistry – A European Journal*, 2001, **7**, 288-296.
87. M. Woods, M. Botta, S. Avedano, J. Wang and A. D. Sherry, *Dalton Transactions*, 2005, 3829-3837.
88. L. S. Natrajan, N. M. Khoabane, B. L. Dadds, C. A. Muryn, R. G. Pritchard, S. L. Heath, A. M. Kenwright, I. Kuprov and S. Faulkner, *Inorganic Chemistry*, 2010, **49**, 7700-7709.
89. R. S. Dickins, D. Parker, J. I. Bruce and D. J. Tozer, *Dalton Transactions*, 2003, 1264-1271.
90. E. J. Werner, A. Datta, C. J. Jocher and K. N. Raymond, *Angewandte Chemie International Edition*, 2008, **47**, 8568-8580.

91. K. Nwe, C.-H. Huang and A. Tsourkas, *Journal of Medicinal Chemistry*, 2013, **56**, 7862-7869.
92. R. Hueting, M. Tropiano and S. Faulkner, *RSC Advances*, 2014, **4**, 44162-44165.
93. A. Beeby, R. S. Dickins, S. FitzGerald, L. J. Govenlock, C. L. Maupin, D. Parker, J. P. Riehl, G. Siligardi and J. A. G. Williams, *Chemical Communications*, 2000, 1183-1184.
94. A. Beeby, D. Parker and J. A. G. Williams, *Journal of the Chemical Society, Perkin Transactions 2*, 1996, 1565-1579.
95. D. Parker, *Coordination Chemistry Reviews*, 2000, **205**, 109-130.
96. A. Mishra, N. K. Logothetis and D. Parker, *Chemistry – A European Journal*, 2011, **17**, 1529-1537.
97. E. L. Que, E. Gianolio, S. L. Baker, S. Aime and C. J. Chang, *Dalton Transactions*, 2010, **39**, 469-476.
98. M. P. Bailey, B. F. Rocks and C. Riley, *Analytica Chimica Acta*, 1987, **201**, 335-338.
99. T. L. Esplin, M. L. Cable, H. B. Gray and A. Ponce, *Inorganic Chemistry*, 2010, **49**, 4643-4647.
100. Y. Bretonniere, M. J. Cann, D. Parker and R. Slater, *Organic & Biomolecular Chemistry*, 2004, **2**, 1624-1632.
101. D. Parker, P. Kanthi Senanayake and J. A. Gareth Williams, *Journal of the Chemical Society, Perkin Transactions 2*, 1998, 2129-2140.
102. R. A. Poole, C. P. Montgomery, E. J. New, A. Congreve, D. Parker and M. Botta, *Organic & Biomolecular Chemistry*, 2007, **5**, 2055-2062.
103. F. Kielar, C. P. Montgomery, E. J. New, D. Parker, R. A. Poole, S. L. Richardson and P. A. Stenson, *Organic & Biomolecular Chemistry*, 2007, **5**, 2975-2982.
104. G.-L. Law, D. Parker, S. L. Richardson and K.-L. Wong, *Dalton Transactions*, 2009, 8481-8484.
105. M. Elhabiri, R. Scopelliti, J.-C. G. Bünzli and C. Piguet, *Journal of the American Chemical Society*, 1999, **121**, 10747-10762.
106. J.-C. G. Bünzli and C. Piguet, *Chemical Reviews*, 2002, **102**, 1897-1928.
107. X.-Y. Chen, Y. Bretonnière, J. Pécaut, D. Imbert, J.-C. Bünzli and M. Mazzanti, *Inorganic Chemistry*, 2006, **46**, 625-637.
108. C. M. G. dos Santos, A. J. Harte, S. J. Quinn and T. Gunnlaugsson, *Coordination Chemistry Reviews*, 2008, **252**, 2512-2527.
109. C. Piguet, M. Borkovec, J. Hamacek and K. Zeckert, *Coordination Chemistry Reviews*, 2005, **249**, 705-726.
110. S. Faulkner, B. P. Burton-Pye, T. Khan, L. R. Martin, S. D. Wray and P. J. Skabara, *Chemical Communications*, 2002, 1668-1669.
111. S. J. A. Pope, B. P. Burton-Pye, R. Berridge, T. Khan, P. J. Skabara and S. Faulkner, *Dalton Transactions*, 2006, 2907-2912.
112. S. Faulkner and B. P. Burton-Pye, *Chemical Communications*, 2005, 259-261.
113. J. A. Tilney, T. J. Sorensen, B. P. Burton-Pye and S. Faulkner, *Dalton Transactions*, 2011, **40**, 12063-12066.
114. L. R. Hill, T. J. Sorensen, O. A. Blackburn, A. Brown, P. D. Beer and S. Faulkner, *Dalton Transactions*, 2013, **42**, 67-70.
115. T. J. Sørensen, L. R. Hill, J. A. Tilney, O. A. Blackburn, M. W. Jones, M. Tropiano and S. Faulkner, *European Journal of Inorganic Chemistry*, 2014, **2014**, 2520-2528.
116. L. R. Hill, O. A. Blackburn, M. W. Jones, M. Tropiano, T. J. Sorensen and S. Faulkner, *Dalton Transactions*, 2013, **42**, 16255-16258.
117. M. Tropiano, O. A. Blackburn, J. A. Tilney, L. R. Hill, M. P. Placidi, R. J. Aarons, D. Sykes, M. W. Jones, A. M. Kenwright, J. S. Snaith, T. J. Sørensen and S. Faulkner, *Chemistry – A European Journal*, 2013, **19**, 16566-16571.

2 A Propyl-linked bis(DO3Ayl) System

2.1 Introduction

To investigate the possibility of binding of small anions such as the halides from aqueous solutions, a system was conceived whereby two lanthanides were held in close proximity. It was supposed that having two electropositive binding domains close together would afford several advantages in this regard. First the coordination of two highly charged cations to one bridging anion would be enthalpically very favourable, hopefully overcoming the significant solvation associated with small anions which has often thwarted past attempts to sequester the halides in water. Second, the short tether between the macrocyclic cores would lead to steric strain, limiting the conformational freedom exhibited by the organic ligand scaffold and thus reducing the entropy loss upon binding.

The design of this particular ligand system was inspired by a similar framework described by Moore *et al*. In their work of 2012 they described the preparation and properties of a system in which two DO3A-type macrocyclic binding domains were linked by a three-carbon chain bearing an alcohol group on the middle carbon.[1]

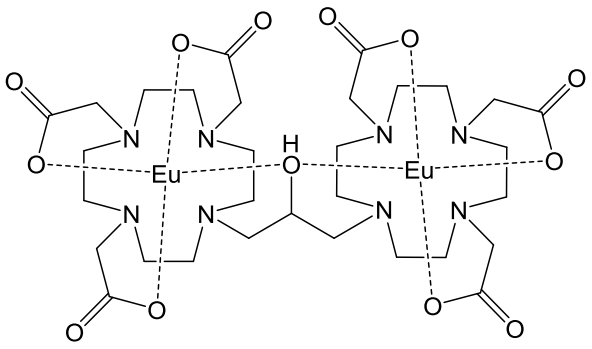

Figure 2-1. Structure of binuclear europium complex from reference 1.

In this complex, theoretical and spectroscopic data indicated that both metal centres were coordinated to the oxygen of the central hydroxyl group, creating two fused five-membered rings. The highly electropositive trivalent metal centres polarised the OH bond, drastically increasing the

acidity of the alcohol, bringing the pK_a into the physiologically relevant region of 4-8. This in turn resulted in the lifetime of the lanthanide luminescence displaying a dependence on the ambient pH. When the surrounding medium was more acidic, the hydroxyl group was protonated, increasing the number of quenching O-H groups coordinated to the metal centre and causing a drop in the luminescent lifetime. Conversely, under basic conditions, deprotonation of the alcohol to give the alkoxide gave rise to longer-lived luminescence as the quenching oscillator was removed from the metal's coordination sphere. Molecular modelling of the system as a whole suggested that there was also assistance from two acetate arms bridging between the two binding domains.

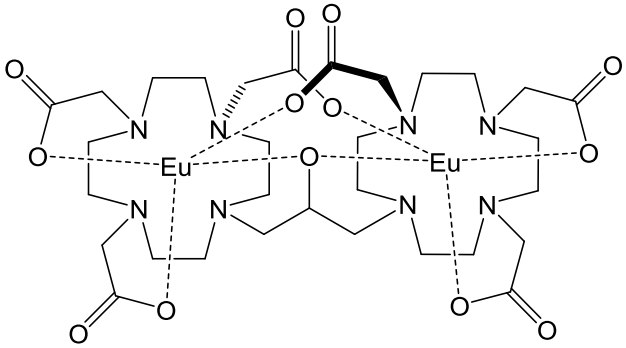

Figure 2-2. Proposed mechanism by which the two macrocyclic domains are linked.

Rather than sense a change in local pH, it was our intention to design a system in which the response was generated by the presence of a specific anion. It was speculated that removal of the alcohol group from the propyl bridge linking the macrocycles could give a complex with the ability to bind small anions such as hydroxide or the halides via self-assembly in solution.

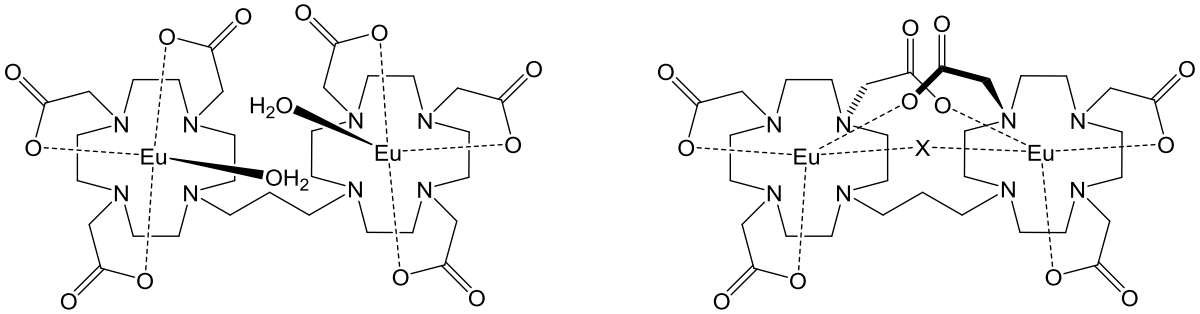

Figure 2-3. Proposed solution-phase structures of complex [2.d] in the absence (left) and presence (right) of an anionic guest.

As shown in figure 2-3, in the absence of an appropriate anionic guest, the two *f*-block cores would effectively be separate, each with a bound solvent molecule capping the empty face of the DO3A cavity. If however, a suitably sized, negatively charged species were present, it would be hoped that the anion would be sequestered between the two metal centres and the acetate arms would further link the two lanthanide ions together, expelling the bound solvent during the process. This would result in a large change in symmetry and electrostatics at the metal centre which would modulate the magnetic and luminescent properties of the complex as a whole. As with the systems described earlier, this complex would also be expected to be sufficiently flexible to accommodate a variety of different guests.

2.2 Synthesis & Characterisation

A synthetic route was designed based on linking pre-protected DO3A binding domains together and the homometallic binuclear complexes were prepared according to the scheme shown in scheme 2-1.

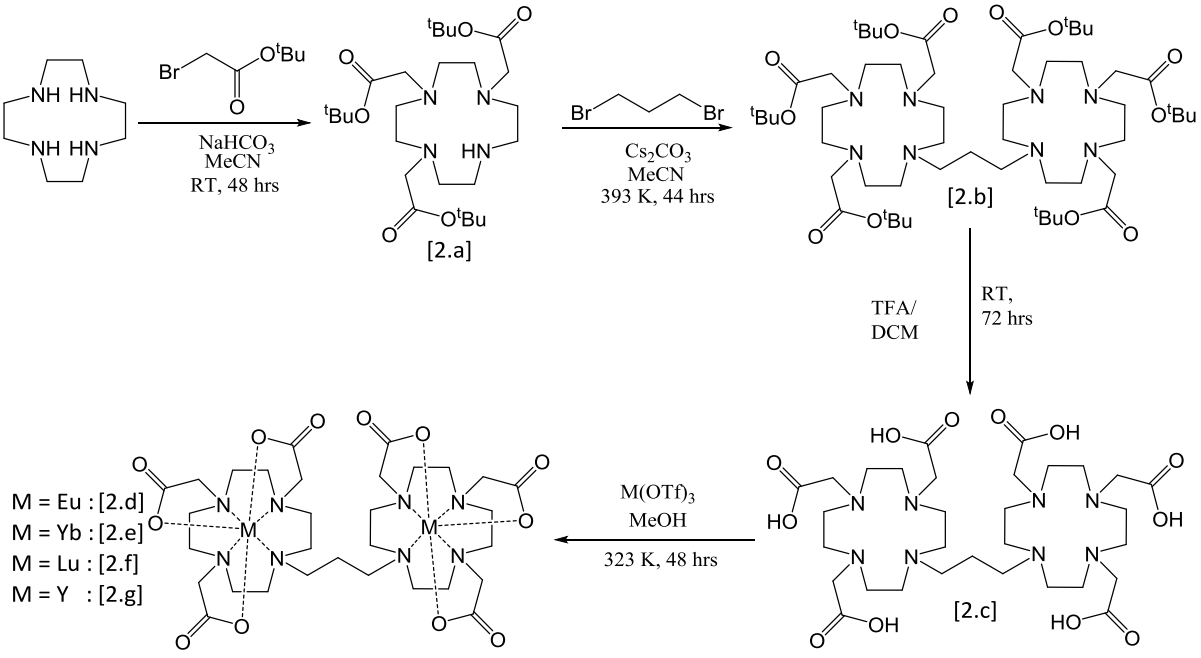

Scheme 2-1. Synthetic strategy for the preparation of propyl-linked bi(DO3A)-yl complexes.

The 12N4 macrocycle was first triply alkylated with a slight excess of *tert*-butyl bromoacetate in acetonitrile under basic conditions, in a slight modification of the well-known literature procedure

to yield the triester [2.a].[2-4] Any traces of the tetra-substituted side-product were removed by recrystallisation from hot toluene. The product was identified and purity assessed initially by electrospray mass spectrometry, with a peak observed at *m/z* = 514 corresponding to the desired tri-alkylated species and one at *m/z* = 651 arising from the tetra-substituted side product coordinated to a sodium cation. ^{1}H-NMR was used to confirm the identity of the target species. The *tert*-butyl protons were found to give rise to two resonances in a 2:1 ratio, corresponding to the ester groups protecting the carboxylate arms adjacent and opposite to the vacant ring nitrogen.

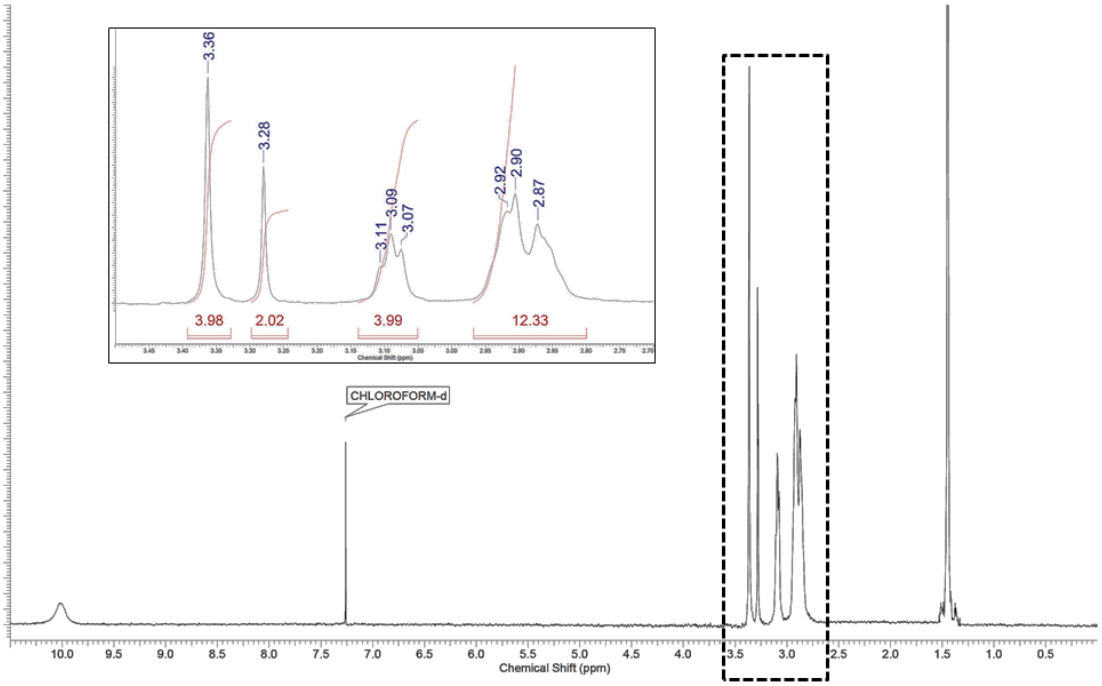

Figure 2-4. ^{1}H-NMR of the triester [2.a]. Magnified inset shows the region of the spectrum corresponding to the cyclen ring and acetate arm methylene protons. Recorded in $CDCl_3$ at 298 K.

Once protected, two of these binding domains were subsequently linked via substitution at the fourth ring nitrogen with 1,3-dibromopropane, carrying out this ligating double-alkylation in dry acetonitrile with caesium carbonate acting as the base. Purification was achieved by column chromatography on neutral alumina, eluting with a dichloromethane-methanol mixture (49:1) to yield the bi-macrocyclic product [2.b], initially as a viscous yellow oil. Trituration in hexane was

used to remove the last traces of methanol and this afforded the target compound as an off-white powder. The ^{1}H-NMR spectrum of the hexaester product showed broader peaks attributed to the cyclen ring and acetate arm methylene protons, and sharper resonances corresponding to the two inequivalent *tert*-butyl protons. The diagnostic peak in this instance was the broad pseudo-singlet observed at 1.64 ppm which was assigned to the methylene protons at the C_2 position on the propyl bridge. Overall the proton spectrum of the propyl-linked species was somewhat sharper than those typically observed for the previously studied bis-DO3A systems. It was hypothesised that the close proximity of the two binding domains reduced the conformational possibilities available and hindered conversion between the available range of diastereoisomers.

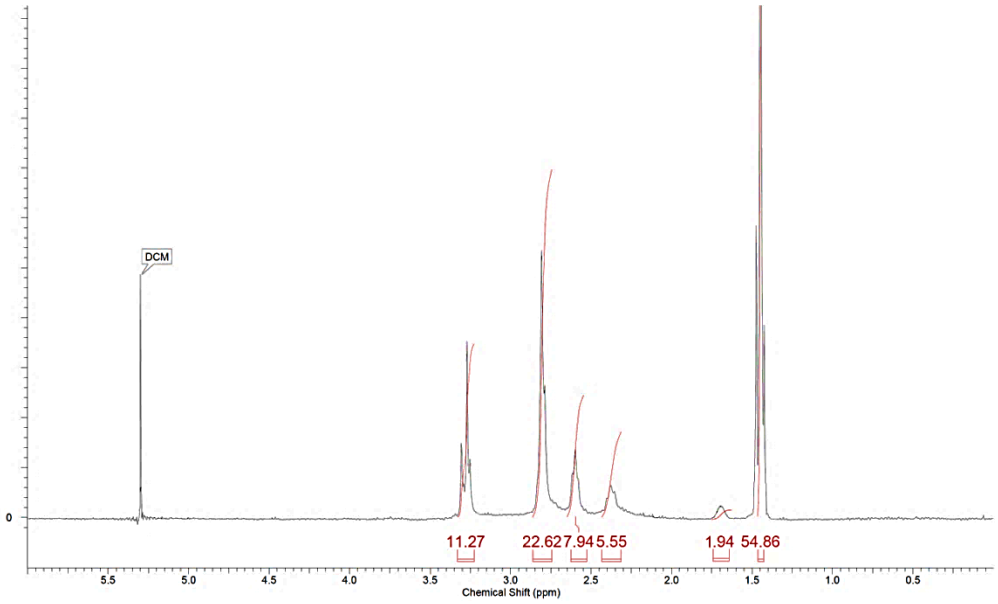

Figure 2-5. ^{1}H-NMR of pro-ligand [2.b], recorded at 298 K in CD_2Cl_2.

Due its amine-rich structure and ease of protonation, it was hardly surprising to find that the hexaester product was doubly ionised under mass spectrometry conditions, giving rise to a peak at *m/z* = 535. Signals observed at *m/z* = 357 and 268 were found to correspond to the triply and quadruply charged species respectively. It was confirmed that these peaks were due to multiply ionised product species rather than decomposition or fragmentation by inspection of the isotope splitting patterns, which were found to be separated by half, third or quarter mass units respectively.

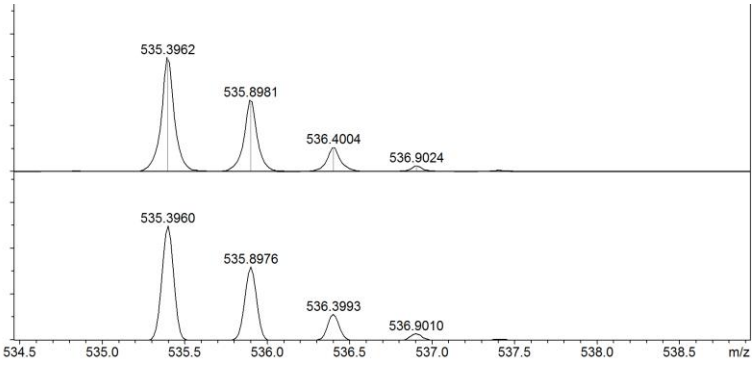

Figure 2-6. Theoretical (top) and experimental (bottom) high resolution electrospray mass spectra of hexaester [2.b] as the $[M]^{2+}$ species.

The *tert*-butyl esters were cleaved by acid hydrolysis, reacting with trifluoroacetic acid in dichloromethane to expose the deprotected ligand. The product was generated as a dark yellow oil which was again converted to an off-white powder upon trituration with diethyl ether. The progress of the reaction was monitored by ^{1}H-NMR spectroscopy, as the peaks around 1.40 ppm corresponding to the *tert*-butyl protons disappeared upon deprotection. The resonances arising from the cyclen ring and acetate arm methylene protons were observed to undergo broadening upon cleavage, most likely due to the reduction in the steric bulk of the arms resulting in increased rates for the ring-inversion and arm rotation processes. ES^{+}MS confirmed the removal of all six of the protecting ester groups, with the molecular ion of the hexaacid product observed at *m/z* = 733.

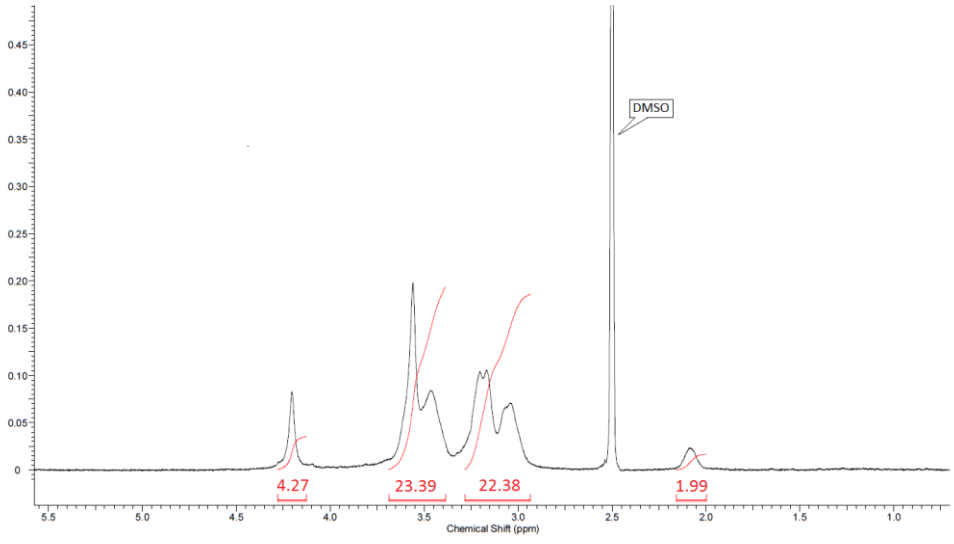

Figure 2-7. ^{1}H-NMR of the hexaacid free-ligand [2.c]. Recorded in d_6-DMSO at 298 K.

Complexation was carried out in methanol with an excess of the appropriate metal triflate, and the surplus metal was precipitated as the insoluble hydroxide by raising the pH of the solution once the reaction had reached completion. The complexes were purified by dialysis in water, to ensure that no uncomplexed metal remained. Removal of the water under reduced pressure afforded the complexes as finely-divided off-white powders. MALDI-MS was used to confirm the presence of metal ions in each binding domain, as the large numbers of isotopes of the various lanthanides lead to highly distinctive isotope splitting patterns for the binuclear species.

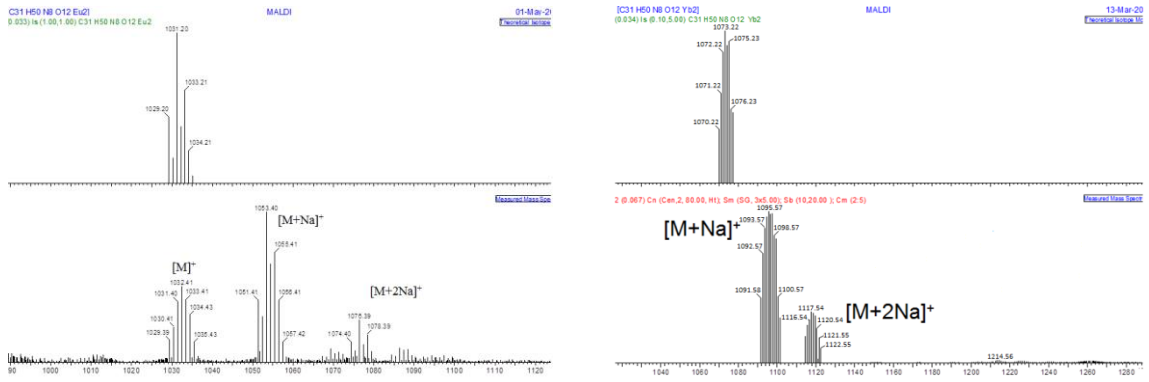

Figure 2-8. Theoretical (top) and experimental (bottom) MALDI-MS reports showing the characteristic isotope patterns for the bis europium [2.d] (left) and bis-ytterbium [2.e] (right) complexes.

The two paramagnetic metal ions in such close proximity greatly shifted and broadened the resonances of the nuclei of the ligand scaffold and thus made the NMR spectra difficult to interpret. Examination of the most shifted resonances (assigned to the pseudo-axial ring protons) in the neutral (pD = 7) spectrum of the bis-europium species indicated that the major isomer present was SAP-like in geometry, whilst the broad nature of the lines indicated that the two were in slow exchange. The (relatively) simple mixture of diastereomers observed would indicate that the conformation at one binding centre was influencing the other, limiting the total conformational space accessible to the molecule as a whole.

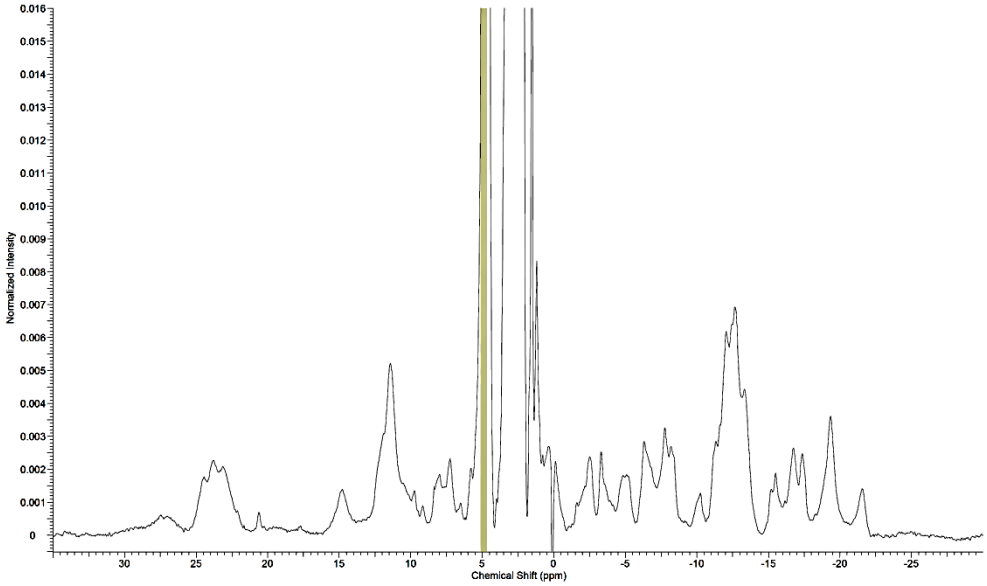

Figure 2-9. ^{1}H-NMR of bis-europium complex [2.d], recorded at 298 K in D2O, pD 7.

Raising the pD of the sample was found to sharpen the peaks somewhat but not nearly as much as was observed with some of the binuclear complexes separated by longer, more rigid spacer units studied later in this work. It should also be noted that in this instance, raising the pD merely sharpens the existing peaks and does not give rise to any new resonances (as seen later), indicating that the ratio of isomers is independent of local acidity and that the SAP form is dominant across the pH range.

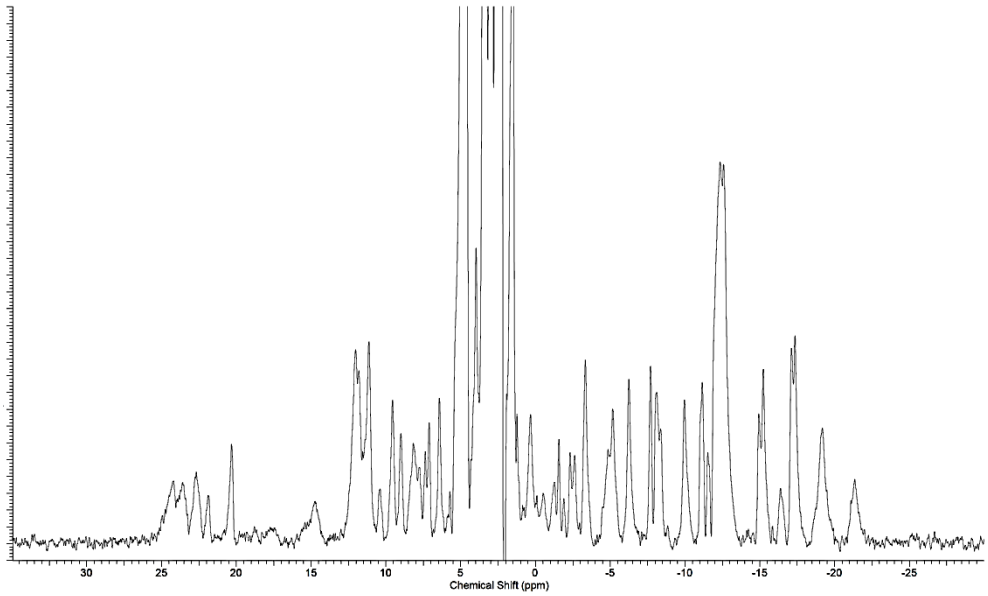

Figure 2-10. ^{1}H-NMR of bis-europium complex [2.d], recorded at 298 K in D_2O, pD 13.

The ytterbium complex was also studied, as it was hoped that the greater shifts range associated with ytterbium complexes would make the spectra easier to interpret. In this instance even at neutral pD the resonances observed were sharper, indicating slower isomer exchange around the smaller metal centre. It is clear that the speciation in these systems is complicated, comprising a mixture of SAP and TSAP geometry at the lanthanide. Furthermore, there may be differences between the donor sets at the metal centres: as well as responding to orientation and separation, the observed chemical shift can also depend upon changes to the second order crystal field parameter B_0^2 as a consequence of changes in the ligand donor set.[5, 6] In this case, such changes, conceivably as a consequence of bridging donors linking the metal centres, may explain some of the more unusual chemical shifts observed in figure 2-10 (such as those around 70 ppm). Detailed analyses of these shifts are complicated by the presence of two paramagnetic centres, with each potentially making a contribution to the observed shift of any given nucleus.

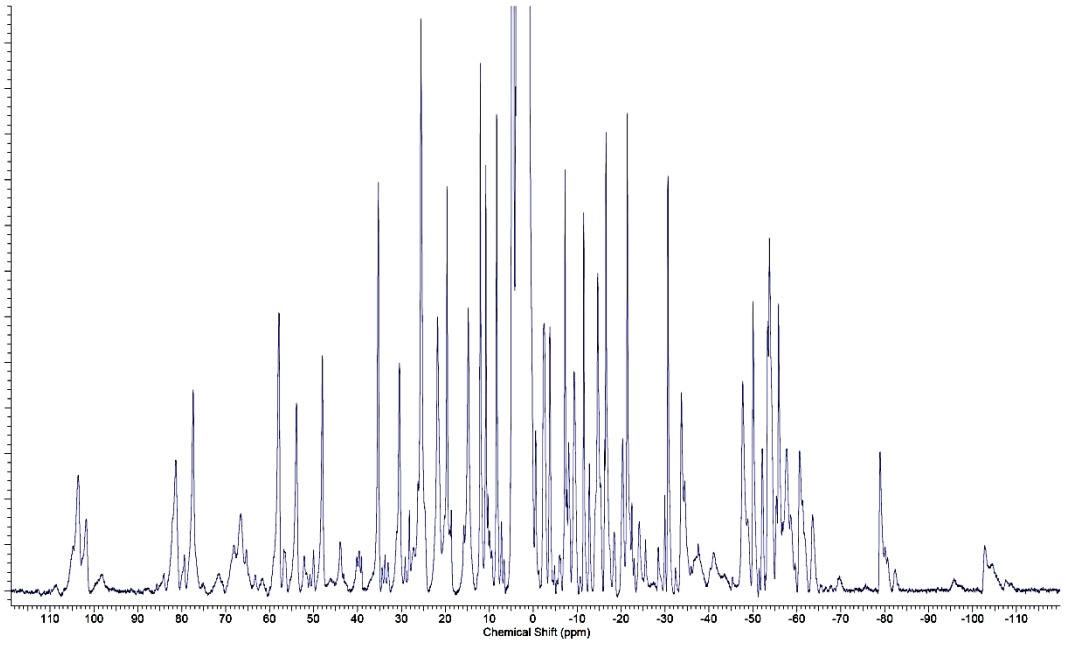

Figure 2-11. ^{1}H-NMR of bis-ytterbium complex [2.e]. Recorded at 298 K in D_2O, pD 8.

The bis-yttrium species was also prepared. The trivalent yttrium cation has a similar ionic radius to lanthanides from the middle of the 4*f*-series (102 pm for 8-coordinate Y^{3+}) but has two key advantages for NMR studies. First, it is a closed shell cation with no unpaired electrons and thus

has no paramagnetic moment. Any effects exerted by the metal on neighbouring resonant nuclei will therefore be solely dipolar in nature and hence far more predictable. The ^{1}H-NMR of the bis-yttrium species was found to be sharper than that of the free ligand, with more peaks observed, indicating slower exchange between isomers when the metal is present. The resonances were not shifted outside the scope of a typical proton experiment, as was the case with the paramagnetic europium and ytterbium species. Despite its lack of luminescent or magnetic utility, yttrium does display one property to warrant the synthesis of its complexes. The sole naturally occurring isotope of yttrium ^{89}Y has a nuclear spin of ½, meaning any resonant nuclei bonded directly to the metal centre will have their NMR signal split. This property can and has been used by the group and others to detect fluoride bound to the metal centre by a splitting in the fluoride signal, as well as to estimate the exchange rate of bound anions with the bulk and proximity of the bound anion to the metal centre.

2.3 Anion Binding

2.3.1 Introduction

The complexes prepared were used in luminescence titrations against a variety of different anions including the halides. As has already been seen, the solution-phase structure of the complexes is highly dependent on ambient pH. The same can also be said for the speciation of any carboxylate anion guests and so it was resolved to control this variable by buffering the solutions. This had the additional advantage that the pH could be selected to reflect physiological conditions, keeping the results obtained relevant in the scope of bio-assay. The two buffers chosen were HEPES and phosphate buffer. HEPES is one of Good's buffers and is commonly used in biochemical applications due to its ability to maintain pH in spite of varying CO_2 partial pressure. It exists predominantly as a zwitterion and does not coordinate to metal centres. Thus in these studies, any incoming anionic guest need only displace bound solvent from the metal centre. By contrast, phosphate buffer was chosen because phosphate species have previously been shown to

associate with coordinatively unsaturated lanthanide complexes in solution.[7, 8] Hence the binding studies under these conditions will require the incoming anionic guest to displace a bound phosphate species and will thus more realistically simulate physiological conditions, where common endogenous ligands such as citrate and lactate will fill any coordination vacancies at the metal centres.

2.3.2 Luminescence Titration Protocol

To probe the binding processes for various anions, successive emission spectra were recorded as the concentration of the anion under study was increased. The integrated areas of the individual peaks in the emission spectra were recorded and these data plotted against the titrant concentration. To ensure that the luminescence intensity was not altered by dilution, the titrant solutions were made using the complex stock solution as the solvent, thereby holding the concentration of the complex constant throughout the experiment. In each instance, the optimal excitation wavelength was determined by measuring the excitation spectrum whilst observing one of the well-defined emission maxima associated with lanthanide-centred emission. Binding constants were calculated using DynaFit® software.[9] The integrated areas under the europium emission peaks were plotted against the concentration of titrant and the resulting curves fitted iteratively by testing the possible binding models against the observed data.[10] The software automatically varies the binding constant(s) from the initial inputted values to minimise the residual squares and chi squared parameters. To guard against false or local minima, the data were tested from different starting points. The calculated binding constants are displayed in table 2-1.

Titrant	Buffer	pH	K (M^{-1})	99% Confidence Interval	Calculated ΔG ($kJmol^{-1}$)
KF	PB	7.4	61190	41500 - 100000	-26.8
	HEPES	7.5	684	658 - 710	-15.9
KCl	PB	7.4	24440	11800 - 71300	-24.6
	HEPES	7.5	9761	4830 - 20800	-22.4
NaCl	PB	7.7	53210	36300 - 70200	-26.5
KBr	PB	7.4	10960	9040 - 13500	-22.7
	HEPES	7.5	2495	1530 - 4180	-19.1
KI	PB	7.6	3926	2400 - 6400	-20.2
	HEPES	7.5	6005	3750 - 10300	-21.2
K_2.oxalate	PB	7.7	1697	1690 - 1710	-18.1
NaN_3	PB	7.7	39814	37500 - 42300	-25.8
Na_3PO_4	HEPES	7.6	646	576 - 723	-15.8

Table 2-1. Binding constants and confidence intervals calculated for complex [2.d] with various anions in HEPES and phosphate buffer systems. ΔG values calculated assuming T = 293 K.

For almost all the halide salts, addition of the titrant resulted in a decrease in integrated luminescence intensity from all bands. Shown in figure 2-12 is an example typical of the results acquired, showing the overlaid successive emission spectra. The inset shows how the integrated intensities of the peaks in the europium emission spectrum varied as a function of bromide concentration. Beneath the spectra are shown examples of the fitted data and confidence intervals generated by the DynaFit® software.

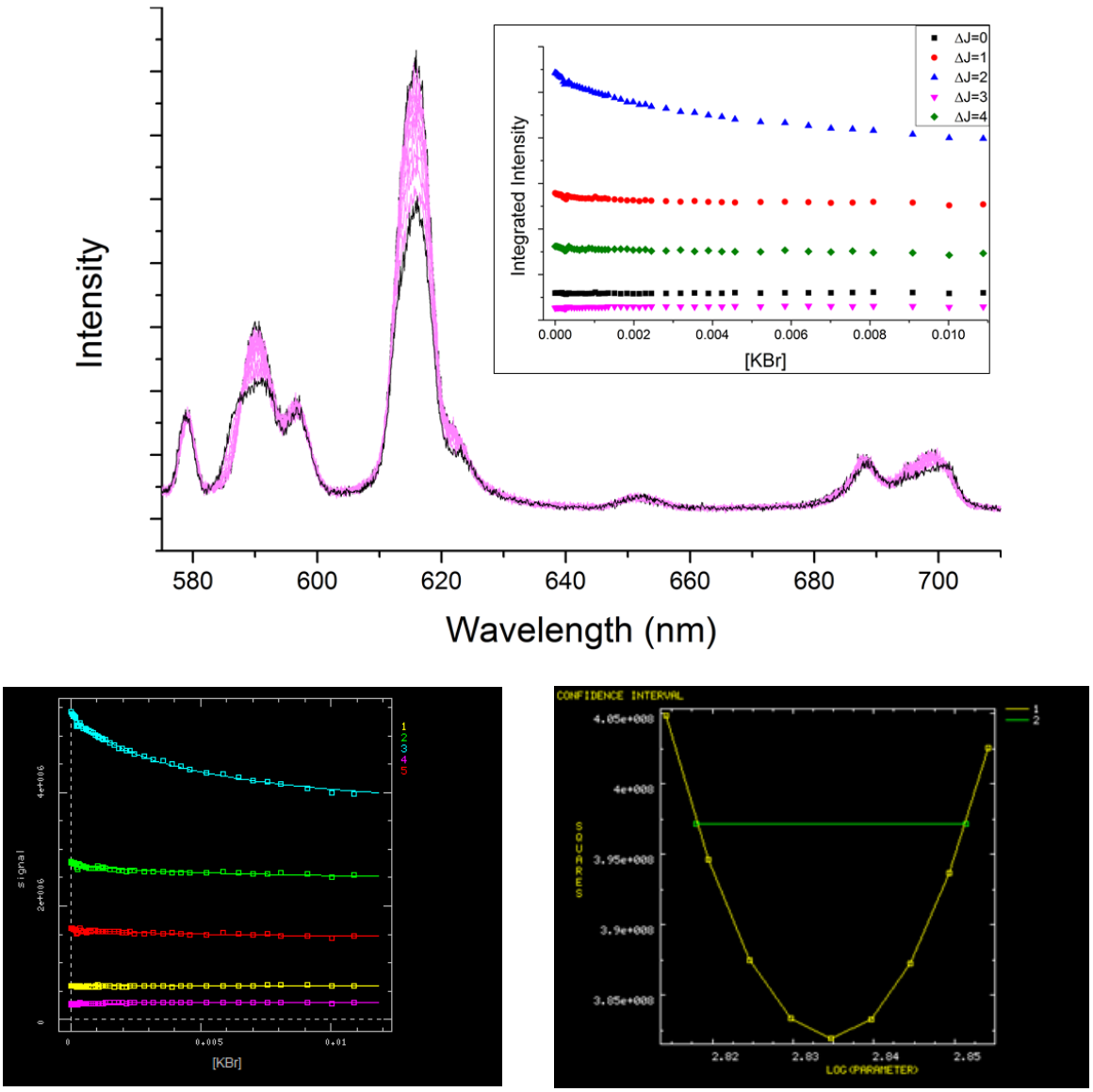

Figure 2-12 Top - Overlaid emission spectra of [2.d] recorded upon addition of KBr. Inset shows the integrated intensities of the different peaks as a function of KBr concentration. Bottom Left - Fitted data curves. Bottom Right - 99% Confidence Intervals calculated with Dynafit.

As the halide guest is displacing a bound water, one would expect that binding would lead to an increase in luminescence intensity. That this was not found to be the case is possibly as a consequence of photo-electron transfer (PET) or ligand to metal charge transfer (LMCT) quenching of the europium excited state by the halide. Alternatively, it could be that the halide is not fully desolvated when bound and thus brings more quenching water molecules close to the metal.

The affinities observed decreased down group VII, with fluoride binding the most strongly and iodide the least. In rationalising this behaviour one must consider the size and charge density of

the anion, as well as the thermodynamics of its desolvation upon association with the metal complex. Table 2-2 shows the ionic radii, hydration enthalpies and approximate hydration sphere sizes of the anionic guests used in this section.

Anion	Ionic Radius (pm)	Number of inner-sphere water molecules	Hydration Enthalpy (ΔG_{hyd} - $kJmol^{-1}$)
F^-	133	2.7	-465
Cl^-	181	2.0	-340
Br^-	196	1.8	-315
I^-	220	1.6	-275
OH^-	133	2.7	-430
N_3^-	195	1.9	-295
HPO_4^{2-}	200	1.8	-465

Table 2-2. Thermodynamic parameters of hydration for some of the anionic guests used in this chapter. References[11-15]

As one descends group VII, the monovalent anions grow larger and thus their charge density decreases, which leads to a reduction in both the enthalpic and entropic components of ΔG_{hyd}. The weaker electrostatic interactions with the solvent reduce the enthalpic gain upon solvation of the halide. However this also makes the larger halides less polarising, meaning a lesser imposition of order in the surrounding solvent sphere and thus a less negative entropic term. That the Gibbs free energy for the whole process gets less negative as the anion increases in size implies that, for the halides at least, the enthalpic interactions dominate the thermodynamics of solvation. The strength of electrostatic interactions between the halide and the metal centres will depend on the polarisability of the anion and the separation between the two charges. Descending the halides, the anions become larger and thus distance to the metals will increase, which should result in decreased attraction between the ion pair. However, the desolvation of the anion must also be considered. As shown in Table 2-2, the lighter the halide, the greater the number of water molecules in its inner-coordination sphere. Upon association with the metal centre, it is presumed

that these bound solvent species will be released to the bulk thus it would be expected that binding of the anion should lead to an increase in the entropy of the system. Both these factors would therefore indicate that binding should be stronger for the smaller halides.

A further consideration is that of cavity size. As demonstrated in the analogous system discussed in section **2.1**, a hydroxyl group is sufficiently large to bridge between the two metal centres due to the participation in bonding of two pendant acetate arms. With an ionic radius of 133 pm, the hydroxyl-group is isoelectronic and isomorphic with the fluoride anion. It could be that the cavity is in fact ideally sized for groups as small as fluoride and hydroxide and that the heavier halides are in fact too large to be optimally accommodated.

It is notable that in almost all cases, weaker binding was observed when HEPES was used in lieu of phosphate buffer. The only exception to this trend was in the case of iodide. At 3926 M^{-1}, the affinity of the binuclear europium complex for the iodide anion in phosphate buffer was just over half that of the same system in HEPES. This is surprising because as previously discussed, phosphates have been shown to be capable of binding to lanthanide centres whereas HEPES is generally thought to be non-coordinating in aqueous environments. One might therefore expect competitive binding in phosphate buffer and thus a reduction in observed affinities for the titrant anions. That this is not the case could imply either, that HEPES is in fact capable of coordinating to metal centres, (and indeed, if this is the case, does so more strongly that phosphate), or that HEPES is in some way capable of aiding the solvation of the anion, reducing the thermodynamic gain upon association with the metal centre. An alternative possibility is that phosphate is too large to sit in the host cavity whilst coordinating readily to both metal sites, and that 1:1 complexation results in binding to only one centre. This is disfavoured due to the steric bulk of the second metal site in close proximity.

In an attempt to separate the effects of cavity size selection from those of simple electrostatics, titrations were carried out with two small molecular anions, oxalate and azide. In both cases, addition of the guest resulted in a rise in luminescent intensity. The addition of oxalate in

particular elicited a dramatic increase in the brightness of all bands by nearly an order of magnitude. It was also noted that the spectral form of the emission spectra changed, particularly at the ΔJ = 1 and 4 bands. The relative weightings of the transitions to the different Stark levels within these bands clearly changed, indicating a change in the local environment, most probably as a consequence of perturbation to the B_0^2 crystal field parameter.

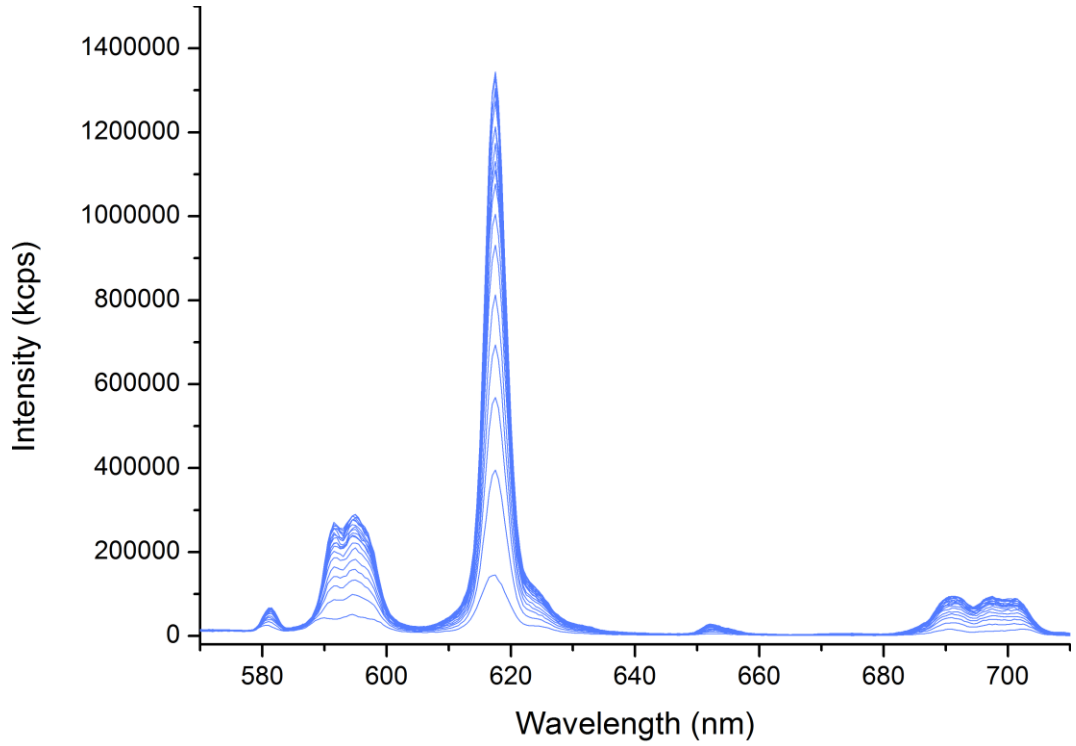

Figure 2-13. Overlaid emission spectra of complex [2.d] upon addition of potassium oxalate, recorded at pH 7.7 in HEPES buffer at 298 K

A change in local symmetry at the metal centre was confirmed by comparison of intensities between the hypersensitive quadrupolar ΔJ = 2 transition and the other less sensitive, electric dipole transitions. As shown in figure 2-14, there was a second region of the binding curve as after reaching a maximum, the luminescence intensity decreased slowly upon further addition of the titrant. This was deduced to be simple Stern-Volmer-type collisional quenching due to the linear dependence on titrant concentration of this part of the curve. That such a decrease was not the result of a second type of binding event was confirmed by the unchanging symmetry at the metal site, as demonstrated by the constant peak ratios.

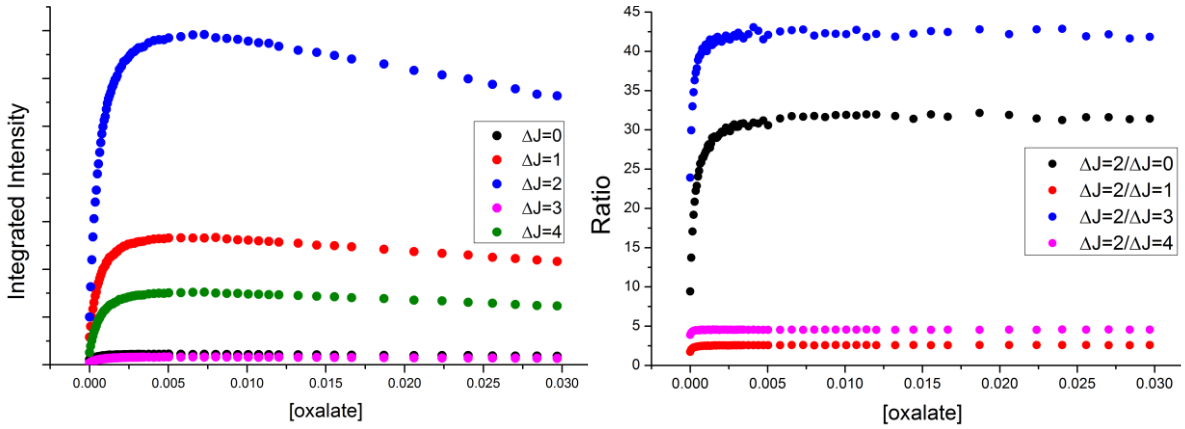

Figure 2-14. Binding curves showing the change in integrated emission intensities (left) and peak ratios (right) of complex [2.d] upon addition of potassium oxalate.

In attempts to ascertain the magnitude and sign of any changes in crystal field parameters, high resolution spectra were recorded, focussing on the ΔJ = 1 and ΔJ = 4 bands both before and after addition of a large excess of the target anion. Shown in figure 2-15 are the spectra recorded for complex [2.d] with sodium azide and potassium oxalate.

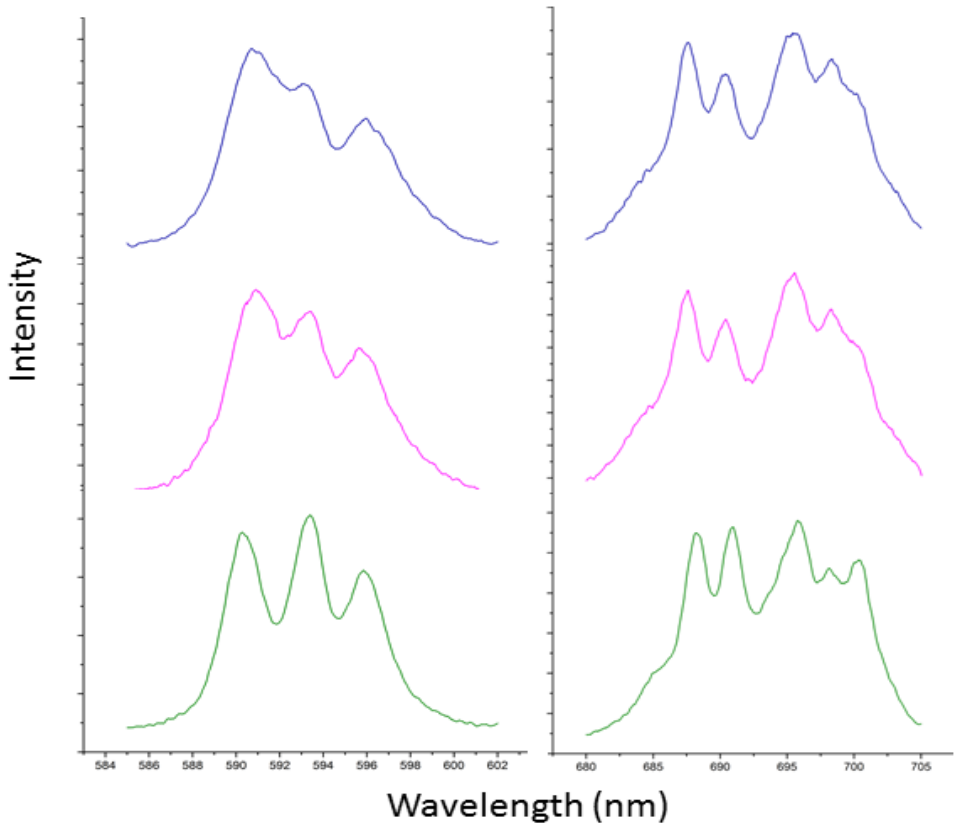

Figure 2-15. High-resolution emission spectra focussing on the ΔJ = 1 (left) and ΔJ = 4 (right) bands of complex [2.d] in isolation (blue trace) and bound with azide (purple trace) and oxalate (green trace). Recorded in HEPES buffer at pH 7.6.

Whilst it is obvious upon inspection that the relative intensities of the different Stark transitions within these bands are changing, a rigorous treatment of these data was precluded by the natural resolution of the spectra. In the emission spectra of lanthanide ions in solids or more rigid ligand scaffolds, it has often been possible to fully separate out the component peaks within the different ΔJ bands. In this instance however, the line-widths of the component peaks are relatively broad, most probably a consequence of flexibility or fluxionality on the part of the ligand.

Despite the lesser magnitude of its effect on the luminescence intensity, the binding of azide was much stronger than that of the other molecular anions, oxalate and phosphate. Indeed, at 39814 M^{-1} it is second only to those observed for fluoride and chloride. It was initially postulated that the order of magnitude difference between azide and oxalate was simply a reflection of the difference in separation between the donor atoms in the two systems, with the small binding cavity in the host complex much more selective for the smaller azide guest. However, given that azide has a similar ionic radius to the bromide anion, this rationalisation did not suffice to explain the behaviour of azide relative to the smaller halides and so another was sought. So far our treatment of the azide anion had been predicated upon the assumption of an α-γ binding arrangement, in which each of the two terminal nitrogen atoms of the azide guest were coordinated to a different metal centre. In light of its similarity to the binding constants calculated for the halides however, another possibility was put forward; that of an α-α' binding mode, in which the azide acted as a pseudo-halide with one of the terminal nitrogen atoms coordinated to both metal centres.

Figure 2-16. Schematic of the two possible binding modes for azide and [2.d]. α-α' (right) and α-γ (left).

This binding mode would drastically reduce the portion of the azide required to fit inside the binding cavity of the host. That azide binds so much more strongly than oxalate would appear to imply that such a coordination model with one carboxylate oxygen bridging the two centres is not available to the longer dicarboxylate. Efforts were made to investigate the nature of azide binding through ^{15}N-NMR, but the results proved inconclusive.

2.3.3 NMR

To correlate the binding of an anion at the metal centre with any changes in coordination geometry or crystal field about the metal centres, NMR studies were performed in instances where solution-phase halide binding had been observed. Whereas the luminescence measurements were made using the europium complex, the majority of the NMR studies were performed with the ytterbium analogue [2.e] due to the greater lanthanide-induced shift range inherent in the Yb^{3+} cation. ^{1}H-NMR spectra were recorded, first of the complex [2.e] in isolation and then in the presence of an excess (10 molar equivalents) of the anion in question.

Perhaps unsurprisingly, the greatest spectral changes were observed in the case of strongest binding, fluoride. Addition of an excess of the anion in the form of its potassium salt resulted in a significant increase in the number of resonances observed. Most significant was the appearance of dramatically more shifted resonances at 122 and 137 ppm. Exchange of the axial water molecule for a more electron rich donor such as F^- has been shown to invert the crystal field parameter B_0^2 in DOTA-tetraamides[16] but in this instance the magnitude of the change and the fact that the original peaks in the spectrum do not completely disappear mean that this is unlikely to be the sole factor at work. Most probable is that there is a fairly major change in geometry taking place between the bound and free forms. That these different forms are distinguishable would imply that they are in relatively slow exchange on the NMR timescale.

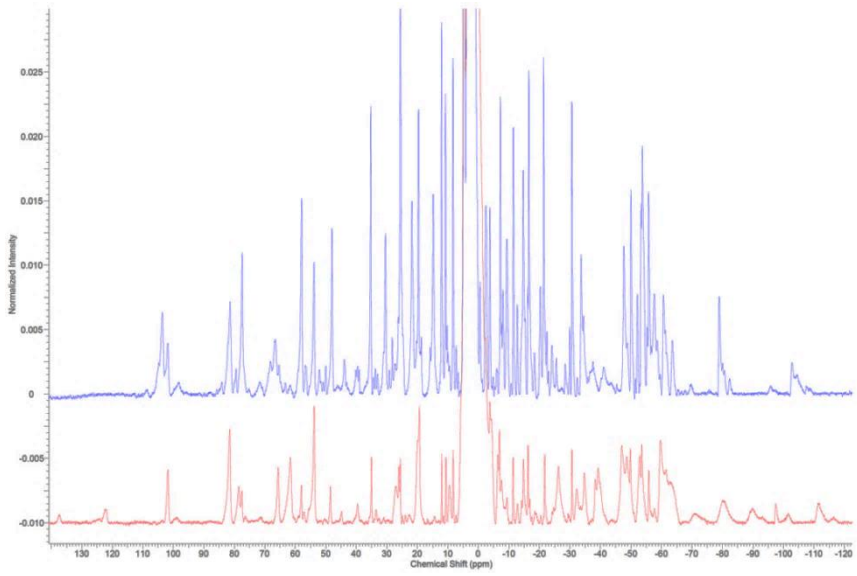

Figure 2-17. ^{1}H-NMR of [2.e] before (blue) and after (red) the addition of 10 molar equivalents of KF. Recorded at 298 K in D_2O, pD7.8.

In the case of chloride, it was found that binding altered not only the relative weightings of the isomers, but also the shifts of the resonances corresponding to each isomer, implying faster exchange and observation of a weighted average shift, given the greater simplicity.

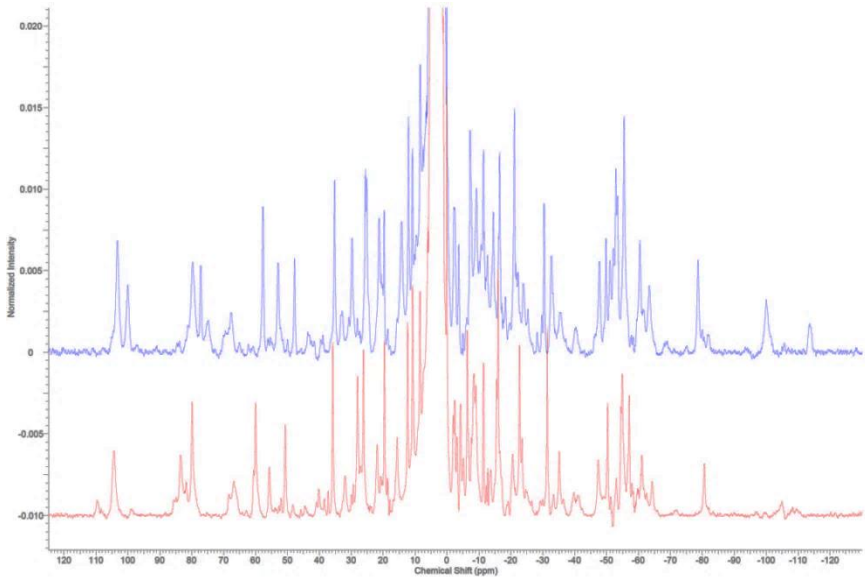

Figure 2-18. ^{1}H-NMR of [2.e] before (blue) and after (red) the addition of 10 molar equivalents of KCl. Recorded at 298 K in D_2O, pD7.4.

The addition of oxalate also precipitated a similarly dramatic change, with peak shifts, splittings and ratios all changing.

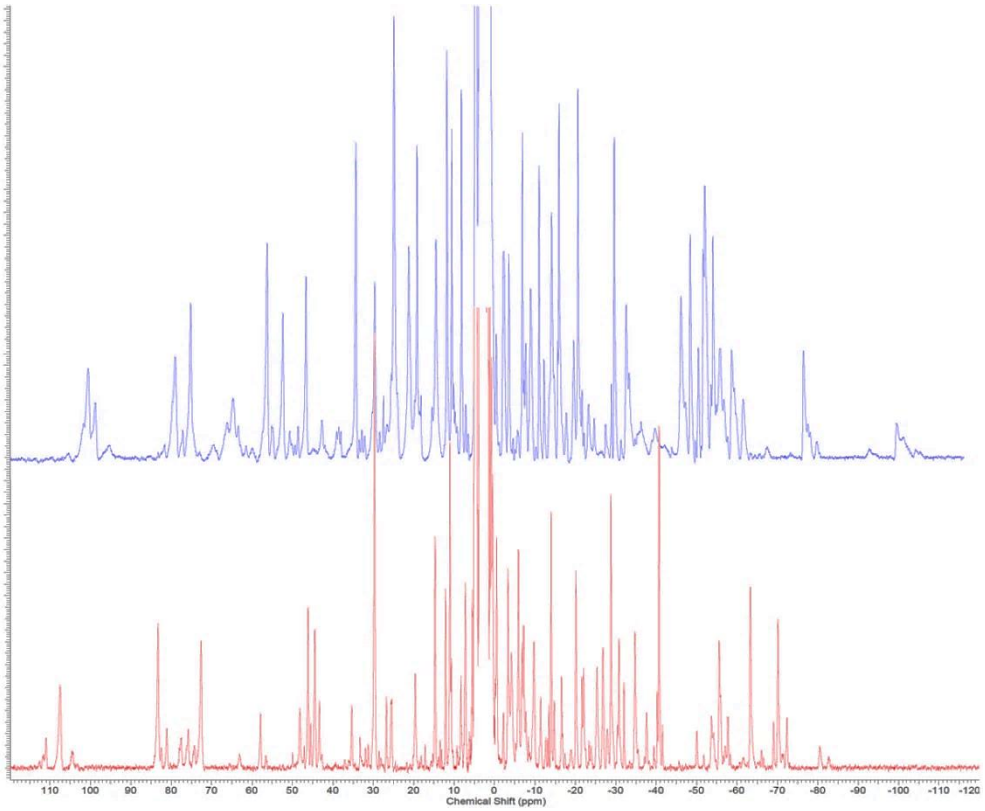

Figure 2-19. ^{1}H-NMR of [2.e] before (blue) and after (red) the addition of 5 molar equivalents of potassium oxalate. Recorded at 298 K in D_2O, pD7.7.

The form the spectra recorded was different in the case of each anion, implying that there may be more than one binding conformer available to the complex or that diastereoisomerism may also be occurring in the ternary assembly as well as in the unbound complex.

2.4 ^{19}F-NMR

Having witnessed a change in both the luminescent response and the ^{1}H-NMR spectra of the metal complexes upon addition of fluoride, ^{19}F-NMR spectra were recorded to detect any lanthanide induced shift in the resonances of fluoride anions bound directly to the metal centre. Initially the bis-europium and bis-ytterbium complexes were used as the paramagnetic moments associated with the partially-filled 4*f* sub-shell. The sole resonance in the sample was observed around -125 ppm, corresponding to unbound aqueous fluoride. No other signals were seen, possibly as a consequence of line-broadening when binding to both lanthanides. Unpublished work within the group by Blackburn *et al* has found that in mononuclear DOTA-tetraamide type

systems, the resonances of bound fluoride are shifted by several hundred ppm upfield, with some examples reaching out to -700 ppm. Sweep widths were duly increased in the search for the bound species but to no avail. It is possible that since the fluoride binding cavity is postulated to be proximal to two paramagnetic lanthanides rather than just one, the peak is shifted even further. It was also found in the DOTA-tetraamide systems that the bound fluoride peaks were significantly broadened due to massively enhanced relaxivity. This then raises the alternative possibility that with two lanthanides, the relaxation is so fast that signal is broadened to the point it is indistinguishable from the baseline.

In a parallel attempt to witness the impact of fluoride binding by NMR, ^{19}F-spectra were measured for the bis-yttrium complex with KF in D_2O. As discussed in section **2.2**, the only naturally occurring isotope, ^{89}Y, has a nuclear spin of ½. One would therefore expect the resonance of a fluoride ion coordinated across two separate yttrium centres to be split into a triplet. Again however, these endeavours proved fruitless. Only a signal thought to arise from unbound aqueous fluoride was seen, with neither significant dipolar shift nor splitting due to the metal in evidence. Once more doubt was cast on the nature of the binding.

In further unpublished work from the group, this time by Botta *et al* the residence times of bound water on lanthanide centres were measured for a class of *para*-xylyl linked binuclear complexes, not structurally dissimilar from those described in this chapter. In this work, it was found that for the ytterbium species, the solvent coordinated directly to the metal centre had a residence time of the order of 6 ns. Neither the yttrium cation nor the fluoride anion were investigated in this particular study, but as they are of very similar radius to that of ytterbium and water respectively, the pairing here would reasonably be expected to display broadly similar behaviour. The negative charge born by fluoride may result in a longer residence time than the neutral water species, but it is unlikely to be dramatically greater. The acquisition time in the pulse sequence of the ^{19}F-NMR experiments is typically measured in milliseconds, meaning that the exchange between bound and bulk fluoride nuclei is much faster than the timescale of the experiment. It therefore stands to

reason that the observed spectrum will be a population-weighted average of the bulk and bound environments, both in term of shift and splitting. As the concentration of unbound bulk fluoride is so much higher than that of the bound anion, it should be expected that the spectra recorded closely resemble that of free aqueous fluoride alone. Attempts to resolve the two different environments by reducing the acquisition time of the experiment ultimately proved unsuccessful and merely resulted in increased signal broadening and a decreased signal to noise ratio.

2.5 Conclusions and Further Work

In this chapter it has been demonstrated that ditopic lanthanide complexes with short separations between the two metallic domains are capable of overcoming significant solvation effects and binding small anions such as the halides in aqueous solution.

Isothermal Titration Calorimetry (ITC) is a technique used to determine the thermodynamic parameters of interactions in solution. It is used extensively in biochemical fields to assess the nature and strength of binding between large macromolecular structures such as proteins and antibodies with smaller guest molecules. The titration is performed automatically in a thermally conducting vessel surrounded by an adiabatic jacket. A heating element holds the whole apparatus at a constant temperature as aliquots of the titrant are added and the power input required to do this indicates whether the association event is exo- or endo-thermic and to what extent. By performing this process at two or more different temperatures, it is possible to calculate the enthalpic and entropic values of the binding, as well as the binding constant and parameters such as the heat capacity of the system, from which can be extracted information regarding the change in hydration of the adduct as a whole upon binding. Such measurements would surely shed further light on the mechanism by which self-assembly occurs in solution.

Furthermore, a thorough computational theoretical treatment that addresses changes in both the crystal field parameter B_0^2 and the structure of the complex is essential if these systems are to be fully understood.

Despite the large affinities observed for the halides, due to the small magnitude of the change in luminescence upon binding of the halides, the binuclear complexes described in this chapter are probably insufficiently sensitive to act as sensors for small anions. The one possible exception is in the case of oxalate, where the increase in luminescence may be sufficiently large to warrant further attention.

2.6 References

1. J. D. Moore, R. L. Lord, G. A. Cisneros and M. J. Allen, *Journal of the American Chemical Society*, 2012, **134**, 17372-17375.
2. S. Aime, A. Barge, M. Botta, J. A. K. Howard, R. Kataky, M. P. Lowe, J. M. Moloney, D. Parker and A. S. de Sousa, *Chemical Communications*, 1999, 1047-1048.
3. A. Dadabhoy, S. Faulkner and P. G. Sammes, *Journal of the Chemical Society, Perkin Transactions 2*, 2002, 348-357.
4. D. D. Dischino, E. J. Delaney, J. E. Emswiler, G. T. Gaughan, J. S. Prasad, S. K. Srivastava and M. F. Tweedle, *Inorganic Chemistry*, 1991, **30**, 1265-1269.
5. D. Parker, *Chemical Society Reviews*, 2004, **33**, 156-165.
6. R. S. Dickins, D. Parker, J. I. Bruce and D. J. Tozer, *Dalton Transactions*, 2003, 1264-1271.
7. P. Atkinson, Y. Bretonnière, D. Parker and G. Muller, *Helvetica Chimica Acta*, 2005, **88**, 391-405.
8. S. J. Butler and D. Parker, *Chemical Society Reviews*, 2013, **42**, 1652-1666.
9. P. Kuzmič, *Analytical Biochemistry*, 1996, **237**, 260-273.
10. T. B. Gasa, J. M. Spruell, W. R. Dichtel, T. J. Sørensen, D. Philp, J. F. Stoddart and P. Kuzmič, *Chemistry – A European Journal*, 2009, **15**, 106-116.
11. M. H. Abraham and Y. Marcus, *Journal of the Chemical Society, Faraday Transactions 1: Physical Chemistry in Condensed Phases*, 1986, **82**, 3255-3274.
12. Y. Marcus, *Journal of the Chemical Society, Faraday Transactions 1: Physical Chemistry in Condensed Phases*, 1986, **82**, 233-242.
13. Y. Marcus, *Journal of the Chemical Society, Faraday Transactions 1: Physical Chemistry in Condensed Phases*, 1987, **83**, 339-349.
14. Y. Marcus, *Journal of the Chemical Society, Faraday Transactions*, 1991, **87**, 2995-2999.
15. G. Hummer, L. R. Pratt and A. E. García, *The Journal of Physical Chemistry*, 1996, **100**, 1206-1215.
16. O. Blackburn and S. Faulkner, Unpublished Results.

3 A Butynyl-linked bis(DO3Ayl) System

3.1 Introduction

In the previous chapter it was seen how two macrocyclic lanthanide domains held in close proximity by a short linking tether are capable of cooperatively accommodating small anionic guests such as halides. To tune the host cavity to selectively bind larger anions, it was rationalised that the separation between the two metal centres would need to be increased. It was desirable that the geometry of the host complex be sufficiently rigid that it should be well defined, but with enough flexibility in the bridge linking the metal cores that the cavity could respond to the presence of a guest to optimise the fit. To that end, it was decided to tie together two binding domains with a 2-butynyl linking unit. The highly rigid triple bond at the centre of such a group limits the conformational flexibility and thus the range of possible distances between the lanthanide centres, while still allowing free rotation about the C1-C2 and C3-C4 axes

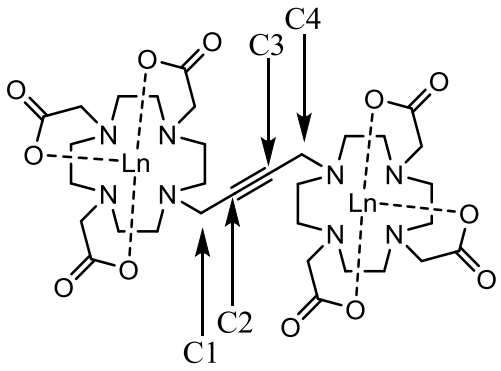

Figure 3-1. Molecular structure of complexes [3.c] - [3.g].

By using approximate bond lengths and angles (drawn from the literature for sterically and electronically similar systems)[1], it was straightforward to estimate the accessible range of intermetallic separations. Figure 3-2 shows the two extreme possibilities (with the N-C1 and N'-C4 bonds either anti to one another or fully eclipsed). The calculated distances between the two amine nitrogens through which the two binding domains were linked are also shown. The

conformational flexibility of each individual macrocyclic domain adds a further level of complexity, as would any steric interactions between the macrocycles which could preclude the adoption of certain whole-molecule arrangements. The simple trigonometric approach used here aims merely to demonstrate the comparatively narrow range of conformational space available and thus does not attempt to take either of these factors into account. A more detailed approach (using molecular modelling software) is undertaken in section **3.7**.

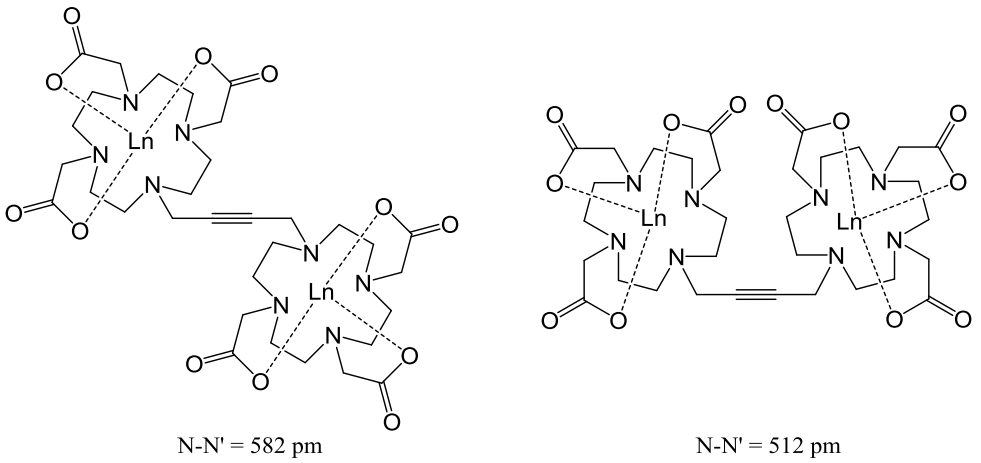

Figure 3-2. Conformations of [3.c] resulting in the longest (left) and shortest (right) intermetallic separations.

3.2 Synthesis & Characterisation

The butyne-bridged bis-DO3A complexes were prepared in an analogous manner to their propyl-ligated counterparts seen in chapter 2. The pre-protected macrocyclic binding domains were linked together by reaction with 1,4-dichloro-but-2-yne in dry acetonitrile in the presence of base, as shown in Scheme 3-1. In this instance, alkylation was performed at room temperature and a shorter reaction time was required to allow the process to go to completion. It can be postulated that this increase in reactivity was due to the proximate alkyne group activating the terminal carbon site to nucleophilic attack. It is thought that hyperconjugation of the alkyne π-system and the C-Cl σ* orbital could stabilise the transition state of the S_N2 reaction pathway, lowering the potential barrier and hastening the rate-determining step. Also thought to play a role was the fact that the linking butyne unit is longer than its propyl counterpart and thus there is reduced steric

hindrance between the DO3A cores in the bicyclic product. Following work-up, the protected pro-ligand [3.a] was purified by column chromatography on neutral alumina, eluting with a 49:1 dichloromethane:methanol mixture and the binding sites were subsequently unmasked by acid cleavage of the *tert*-butyl ester groups. As before, complexation was carried out by treatment of the free-ligand with appropriate metal triflate in methanol, to afford the homometallic complexes in quantitative yield.

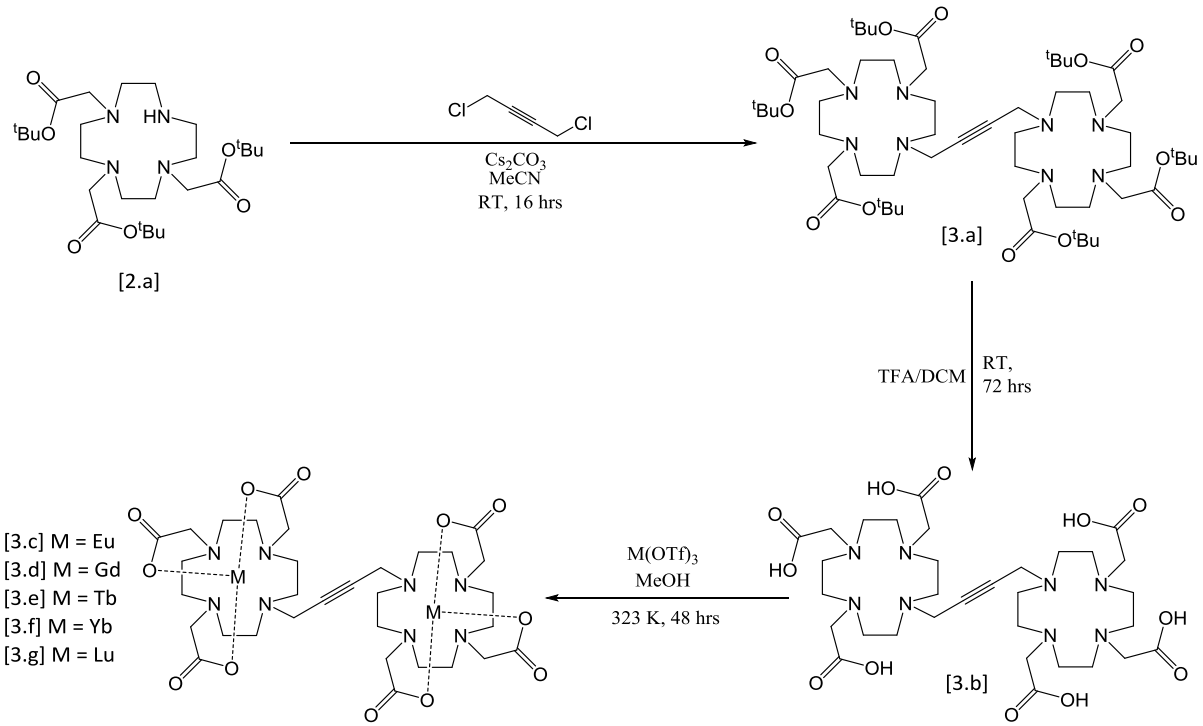

Scheme 3-1. The synthetic strategy used for the preparation of butynyl-linked bis-DO3A complexes.

The formation of the hexaester, [3.a], shown in Scheme 3-1, was monitored by thin layer chromatography and electrospray mass spectrometry, the former watching for depletion of the dichloro-linking unit, the latter for the product $[M+Na]^+$ peak at *m/z* = 1101. In contrast to the case of the propyl-linked system, described in section **2.2**, the ^{1}H-NMR spectrum of the hexaester pro-ligand was difficult to interpret as the differential exchange rates of the different proton environments resulted in a mixture of both sharp and very broad peaks.

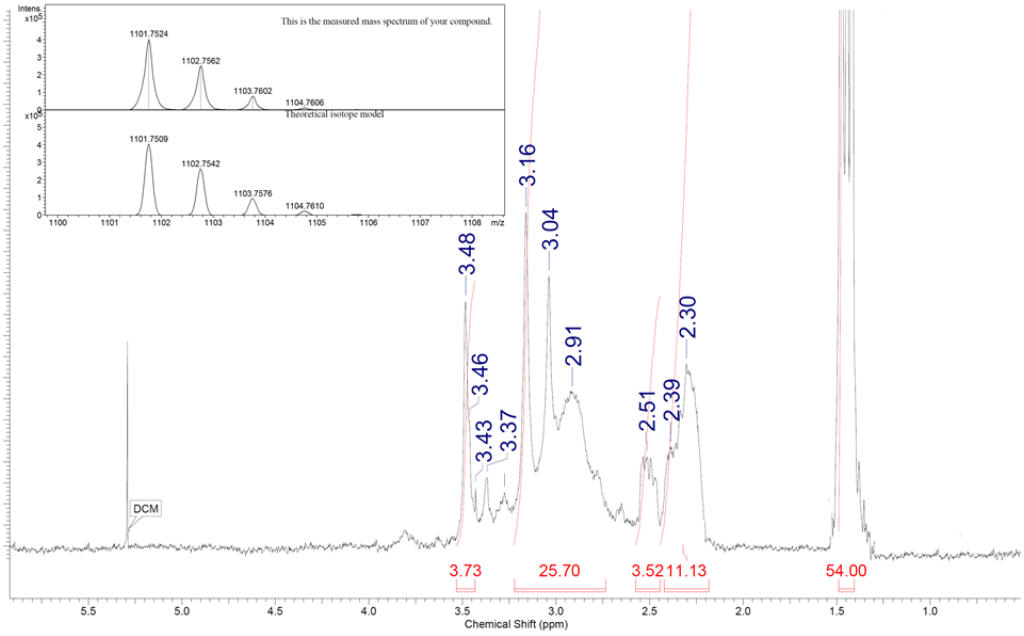

Figure 3-3. ^{1}H-NMR of the hexaester [3.a], recorded at 298 K in CD_2Cl_2. Inset shows the measured (top) and theoretical (bottom) high-resolution electrospray mass spectra.

In the second step, the unmasking of the binding cavities was confirmed by the disappearance of the *tert*-butyl group peaks at 1.45 and 1.42 ppm in the ^{1}H-NMR spectrum. Upon removal of the bulky *t*-butyl groups, the regions of the spectrum corresponding to the cyclen ring and arm methylene protons grew significantly simpler, with the many resonances present in the spectrum of the hexaester coalescing into three broad bands in the hexaacid product. These bands were assigned to the cyclen ring protons, the -CH_2- units of the pendant acetate arms and the methylene groups adjacent to the alkyne functionality.

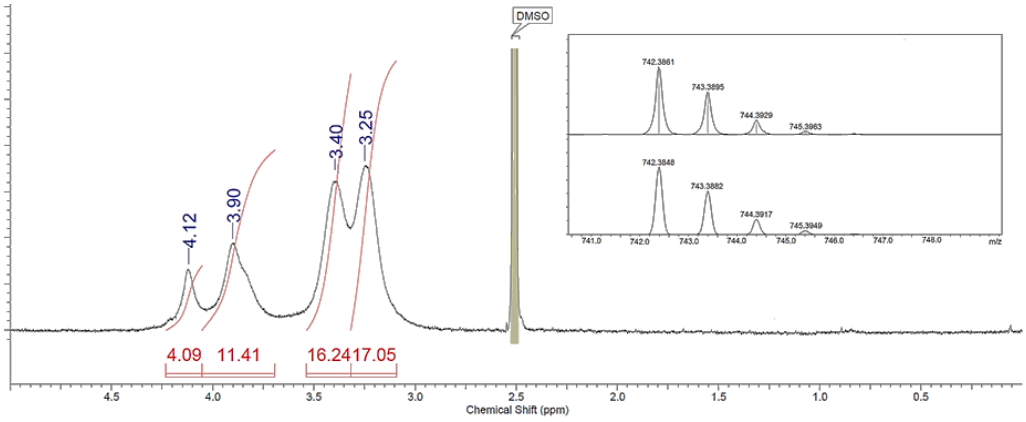

Figure 3-4. ^{1}H-NMR of the hexaacid [3.b], recorded at 298 K in d_6-DMSO. Inset shows the theoretical (bottom) and measured (top) high-resolution electrospray mass spectra.

In the complexation step, the effect on the ^{1}H-NMR spectrum of the introduction of the two lanthanide ions depended on the identity of the metal in question, and the spectra of the open shell complexes are discussed in greater detail below. In the complexes of europium, terbium, ytterbium and dysprosium, the open 4*f* shell and resulting magnetic moments of the metal ions gave rise to highly shifted and broadened signals.

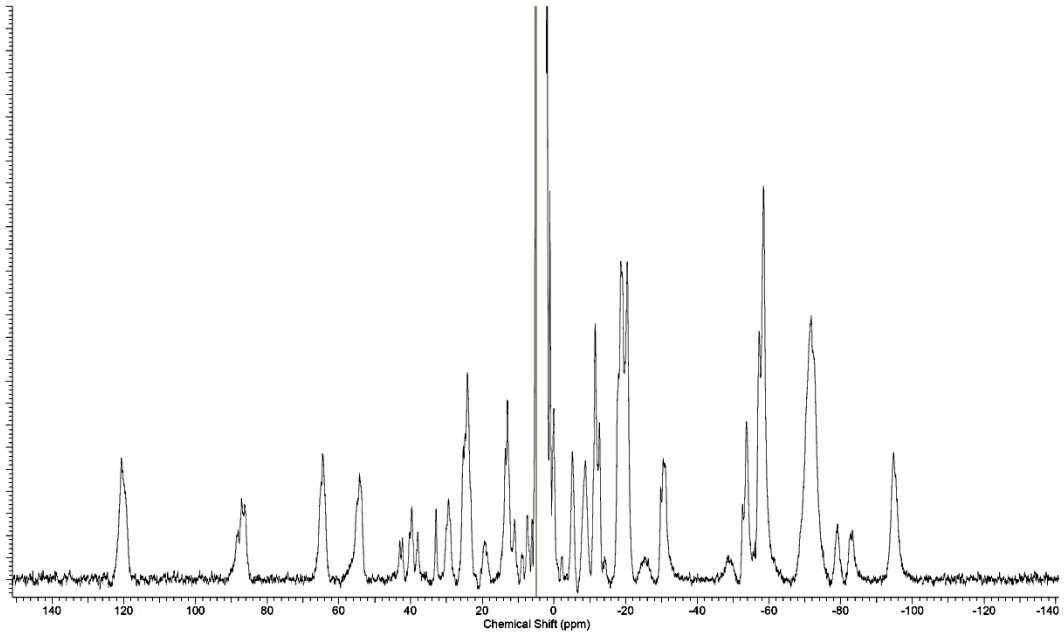

Figure 3-5. Paramagnetic ^{1}H-NMR of the bis-ytterbium complex [3.f], recorded at 298 K in D_2O, pD 10.

The fact that the mixture of diastereomers was comparatively simple would appear to imply that there may be a degree of correlation between the two centres, with the conformation at one influencing that at the other.

In the complexes of the diamagnetic lutetium and yttrium ions, the spectra were found to be very similar to that of the free ligand, except that the peaks were slightly more shifted due to the dipolar shift effects of the highly electropositive coordinated metal. Figure 3-6 shows the spectrum of the lutetium complex. In this it is clear that there is still significant motion within the structure: the coupling between the CH_2 groups on the ring backbone is not resolved.

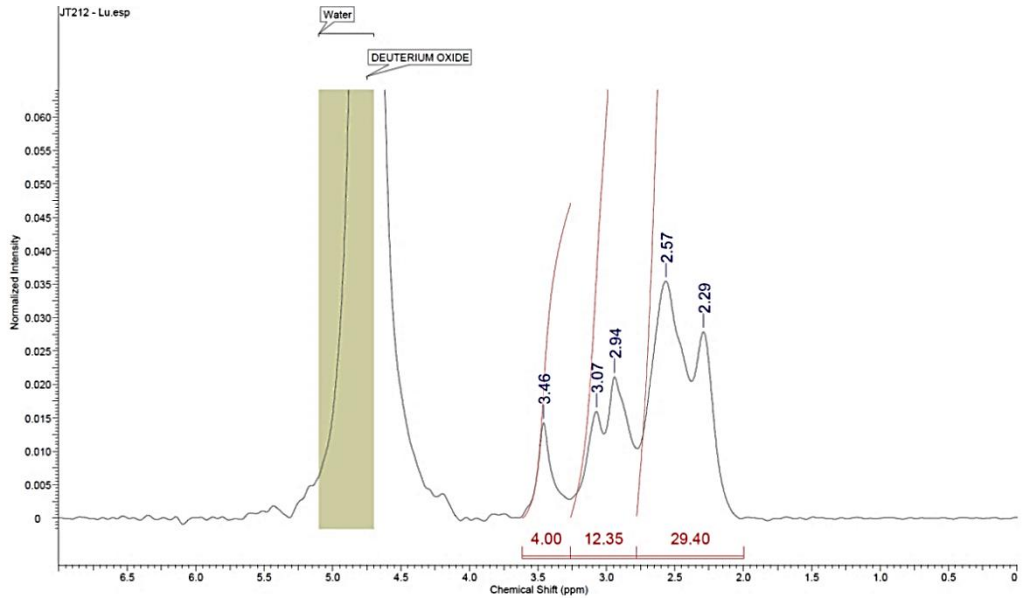

Figure 3-6. ^{1}H-NMR of the bis-lutetium complex [3.g], recorded at 298 K in D_2O, pD 8.

3.3 NMR Studies

The form of the ^{1}H-NMR spectra of the paramagnetic complexes was found to show a strong dependence on local pH/pD. In acidic and neutral environments, the peaks were very broad indicating exchanging ring protons. An examination of the most shifted resonances, ascribed to the axial ring protons on the azamacrocycle ring, determined that the local geometry at each metal centre was approximately square anti-prismatic (SAP).

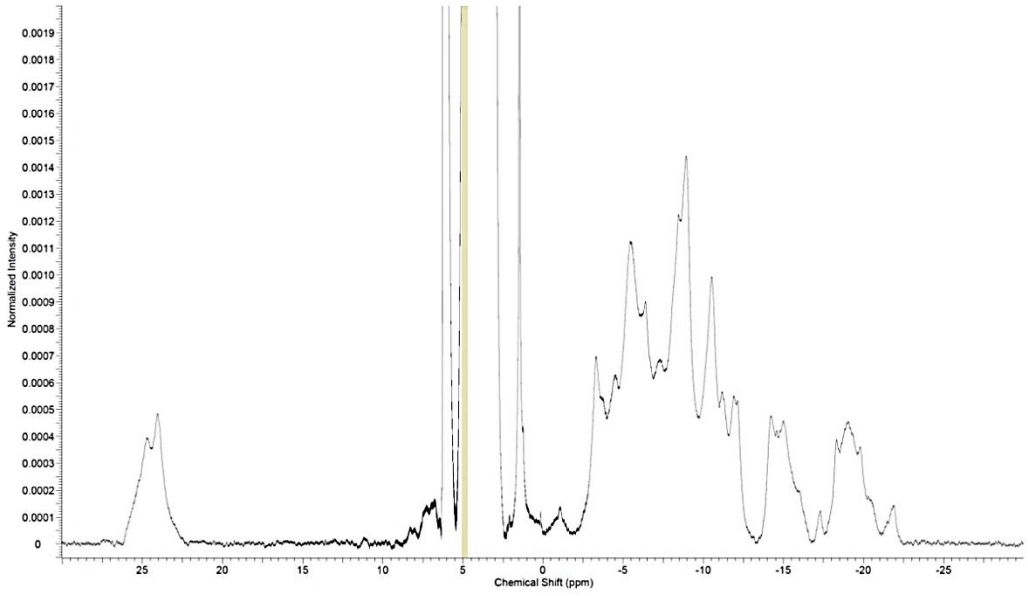

Figure 3-7. Paramagnetic ^{1}H-NMR of the bis-europium complex [3.c], recorded at 298 K in D_2O, pD 5.

At high pH however, the spectra were quite different. First, there were more peaks observed, implying a mixture of SAP and TSAP diastereomers present in slow exchange. From the most shifted protons, it was again determined that the SAP isomer was present, but in this instance, the less shifted peaks (16 -17 ppm in the spectrum of the bis-europium complex shown in figure 3-6) indicated that there was also some twisted square anti-prism present as a minor component. The resonances were also much sharper, indicating that exchange between the isomers had slowed significantly. The fact that the mixture of diastereomers was comparatively simple implied a degree of correlation between the two centres, with the conformation at one ring influencing that at the other.

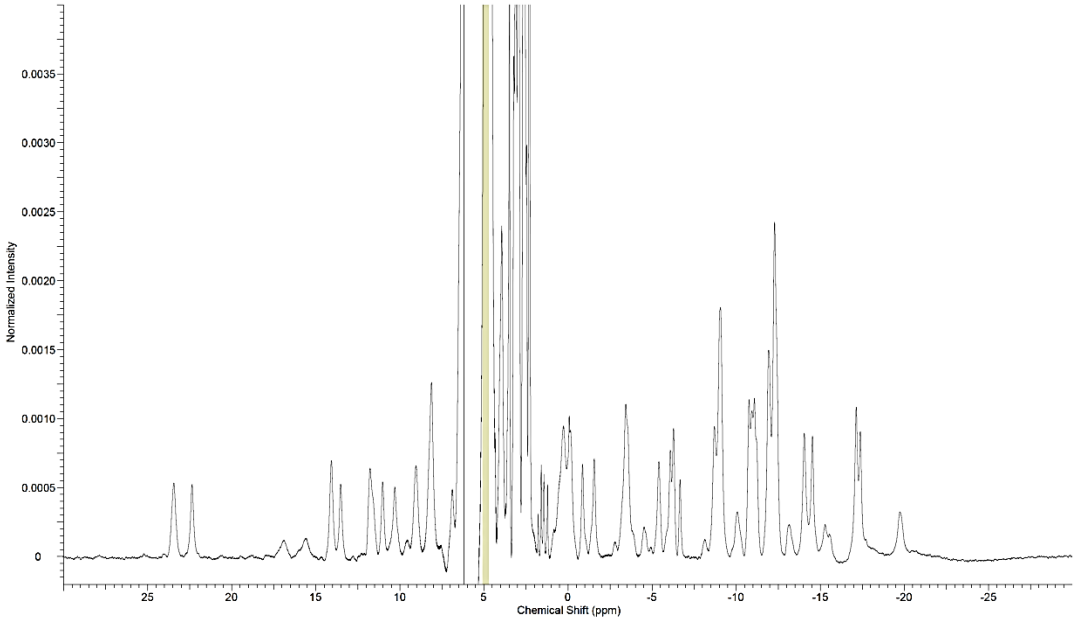

Figure 3-8.Paramagnetic ^{1}H-NMR of the bis-europium complex [3.c], recorded at 298 K in D_2O, pD 11.

The crossover between the two regimes was found to be quite abrupt, occurring just above pD 8 for all the metals studied.

3.4 Anion Binding

To inform the selection of likely anionic guests, the space accessible for binding at the metal centre was examined via calculation of the number of coordinated solvent molecules, using the modified Horrocks' equation as discussed in section **1.4**. Luminescent lifetimes of the different

metal complexes were measured in H_2O and D_2O. It was important that the pH/pD of the protonated and deuterated samples were as close as possible to being the same for two key reasons. First, as has already been shown by NMR, the isomeric structures adopted by complexes of this ligand system display a strong dependence on the pH. By analogy with the DOTA complexes discussed in Section **1.7**, it is reasonable to assume that the TSAP and SAP-like isomers of these bi-DO3A-yl complexes will have markedly different solvent binding and exchange properties and thus this must be accounted for. Secondly, the protonation (or deuteration) state of the bound solvent species will directly affect the number of O-H or O-D oscillators close to the metal centre, potentially influencing the results. As shown in the previous chapter both buffers and the halide and oxo counterions of common acids are more than capable of coordinating to lanthanide centres and so it was resolved to fix the pH by dialysis in H_2O. Once the pH in the chamber had reached neutral, the sample was lyophilised via repeated freeze-pump-thaw cycles and then redissolved in the appropriate solvent.

Complex	$\tau(H_2O)$ / µs	$\tau(D_2O)$ / µs	q
[3.c] (Eu)	620	1650	0.9
[3.e] (Tb)	1130	1510	0.8
[3.f] (Yb)	0.96	3.32	0.6

Table 3-1. The luminescent lifetimes and q-values for the complexes of the butyne-linked bi(DO3A)yl ligand system.

As the DO3A binding domain is only heptadentate, while lanthanide aqua complexes are typically nine-coordinate, one might reasonably expect there to be space within the coordination sphere for one to two bound solvent molecules and indeed such values have been measured for mononuclear complexes based on the DO3A cavity. For all the ions studied, the experimental value was less than one. This most probably arises from the close proximity of the organic scaffolds of the macrocycles, limiting the available space at the metal centre for solvent coordination. The parameter q is necessarily an average of all the species present in solution, weighted by their relative populations. Thus these lower than expected q-values could be a

mixture of values arising from conformers which are significantly less hydrated and those which display q-values closer to what is 'expected'. Alternatively, they could be a result of the reduced space at the metal centre resulting in increased separation between the metal centre and the solvent molecules, leading to reduced overlap and hence less efficient quenching by the OH oscillators.

3.4.1 C_n-diacids

It was decided to assess the effect of anion size on binding using a homologous series of dicarboxylic acid guests, shown in figure 3-9. Using simple alkyl chains as spacers has the advantage of eliminating variables such as the identity of the donor atom as well as any other stereoelectronic effects such as π-stacking which could influence binding. Furthermore, larger spacers imbue the guest with a degree of flexibility. This complements the flexibility of the host that can be inferred from the NMR studies described in the previous section, potentially allowing fit into a binding cavity. It should also be emphasised that the flexibility observed in the structure of the complex might mean that species bind in more than one cavity type. As such, it was resolved at the outset to explore such structural variation using both luminescence and NMR.

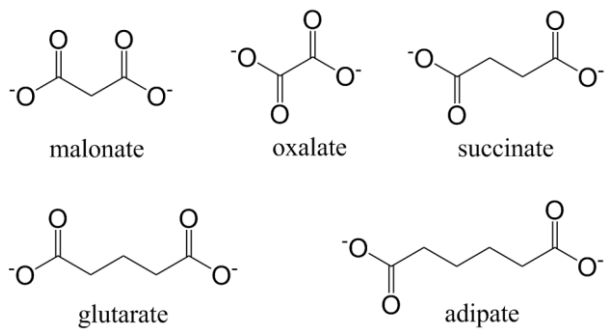

Figure 3-9. The various unsubstituted C_n-dicarboxylate guests studied in this section.

The pK_a values of the acid groups vary slightly with the length of hydrocarbon chain separating them, but in the pH range at which the titrations were performed, the overwhelmingly dominant species present in all cases was the dianion.

The dianions were titrated against the bis-europium complex [3.c], following the protocol for luminescence titrations as laid out in section **2.3**. 0.1 M HEPES buffer was used to hold the pH value constant throughout the titration. The binding constants obtained are shown in table 3-1.

Titrant	pH	K (M^{-1})	99% Confidence Interval	Calculated ΔG ($kJmol^{-1}$)
oxalate	7.7	7813	7550 - 8070	-21.8
malonate	7.7	403	386 - 421	-14.6
succinate	7.7	55	53.0 - 56.5	-9.8
glutarate	7.7	72	71.8 - 73.1	-10.4
adipate	7.7	60	53.6 - 65.9	-10.0

Table 3-2. The binding constants and confidence intervals calculated for the interactions between complex [3.c] and different dicarboxylate guests. ΔG values calculated assuming T = 293 K.

In all cases, following direction excitation of the europium ion at 394 nm, binding of the anion resulted in an increase in the luminescence intensity observed, presumably due to displacement of bound quenching O-H oscillators.

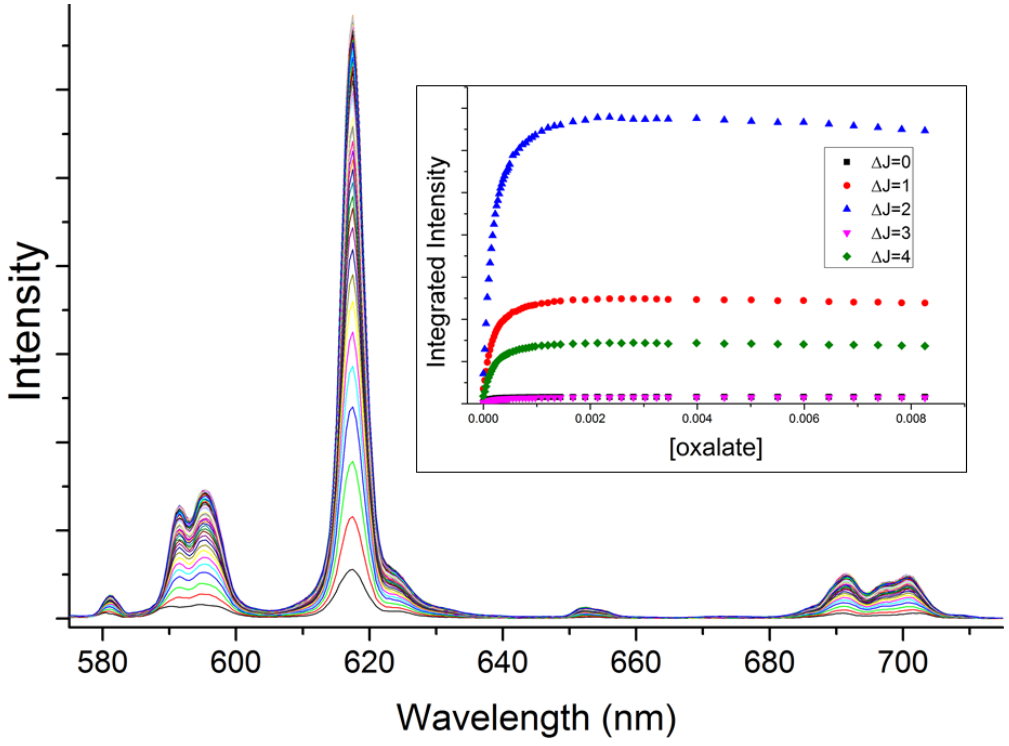

Figure 3-10. Overlaid emission spectra of [3.c] recorded upon addition of potassium oxalate. Inset shows the integrated intensities of the different peaks as a function of oxalate concentration.

This was most pronounced in the case of oxalate, where the addition of one equivalent of anion resulted in a ten-fold increase in integrated luminescence intensity across the different ΔJ bands, with the greatest increase seen in the quadrupolar ΔJ = 2 transition at 616 nm.

The binding of oxalate was also by far the strongest for the dicarboxylates tested, implying a small separation between the metal centres in a binding conformer which is selective for the smaller acids. The fact that the oxalate anion has very limited conformational freedom is also likely to contribute significantly to the observed binding constant, as there will be minimal loss of entropy upon binding across the metal centres.

The next largest binding constant observed was for malonate, the C_3-diacid. This was an order of magnitude lower than that of oxalate, but still significantly larger than those found for the longer chain acids. This would agree with the supposition that the binding conformer of the host complex has a short inter-nuclear separation, thus preferentially binding to smaller anions. That oxalate binds more strongly than malonate is likely because the cavity between the metal centres is slightly too small for the longer malonate anion, precluding optimal coordination of the carboxylate groups to the metal centres. While oxalate and malonate are both highly preorganised, it is undoubtedly significant that the carboxylate groups present very different bite-angles across the metals.

The concept of non-complementarity of size may be extended to the dianions obtained from the larger diacids, succinic, glutaric and adipic acids. It is, however, interesting to note, that rather than a simple decrease in binding as the inter-carboxylate separation increases, we see a very similar value for all three titrants. This may indicate an interplay of multiple factors. As the hydrocarbon skeleton linking the carboxylate head groups grows in length, it gains additional flexibility. This allows the adoption of conformers where the donor groups are positioned to coordinate effectively to the metal centres. However against the enthalpic gain from increased electrostatic interaction must be set the conformational entropy lost by the adoption of the

binding conformer. As the backbone gets longer and more flexible, both of these components increase and thus the observed binding constants remain quite similar.

3.4.2 Backbone Rigidity and Guest Conformation

In the hope of further elucidating the role played by the conformational freedom of the dianion backbone, the binding was probed for the two isomers of 2-butene-1,4-dicarboxylate, maleate and fumarate.

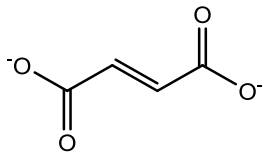

fumarate

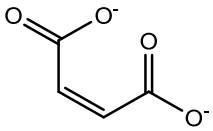

maleate

Figure 3-11. Molecular structures and common names of the isomers of butene-dioic acid.

Both of these species have their respective conformational spaces limited by the lack of rotation about the C_2-C_3 bond enforced by the π-system. In each system there is also a degree of conjugation between the π-system of the central alkene and those of the two planar carboxylate fragments. This overlap is far from total but it does provide a slight barrier to rotation about the C_1-C_2 and C_3-C_4 bonds. In both cases therefore, the range of orientations and positions of the two acid head groups is severely limited. This lack of entropic freedom in the free anion means that upon binding, the loss of entropy should be lower and thus stronger binding may be observed, but only if the increased rigidity does not render the suitable binding conformer inaccessible.

Titrant	pH	K (M^{-1})	99% Confidence Interval	Calculated ΔG ($kJmol^{-1}$)
fumarate	7.7	763	755 - 771	-16.2
maleate	7.7	184	182 - 185	-12.7

Table 3-3. The binding constants and confidence intervals calculated for complex [3.c] and the *cis/trans* isomers of butene-dicarboxylate. ΔG values calculated assuming T = 293 K.

Both maleate and fumarate were found to bind more strongly than succinate (K_a = 54 M^{-1}). From this it may be inferred that the optimal (or at least, most acceptable) binding conformer is still available to the guest in spite of the extra rigidity afforded by the alkene group and that the

reduced drop in entropy in the adoption of this conformer is responsible for the higher binding constants. The fact that *trans* fumarate binds more strongly than its *cis* analogue merely indicates that its configuration of charged head groups allows more efficient coordination to the lanthanide centres. Interestingly, in both cases, addition of the guest resulted in a significant decrease in luminescence intensity, rather than the increase typically observed with the saturated dicarboxylates. As the guest species will still be displacing bound solvent from the metal centre, this would imply that the dicarboxylates with π-systems are more effective at quenching the lanthanide luminescence than the O-H oscillators. It was not clear whether this behaviour was the result of a CT event from the alkene π-system to the metal ion, or merely enhanced quenching of the metal by a mode of the alkene guest fortuitously matched in energy to the emissive state.

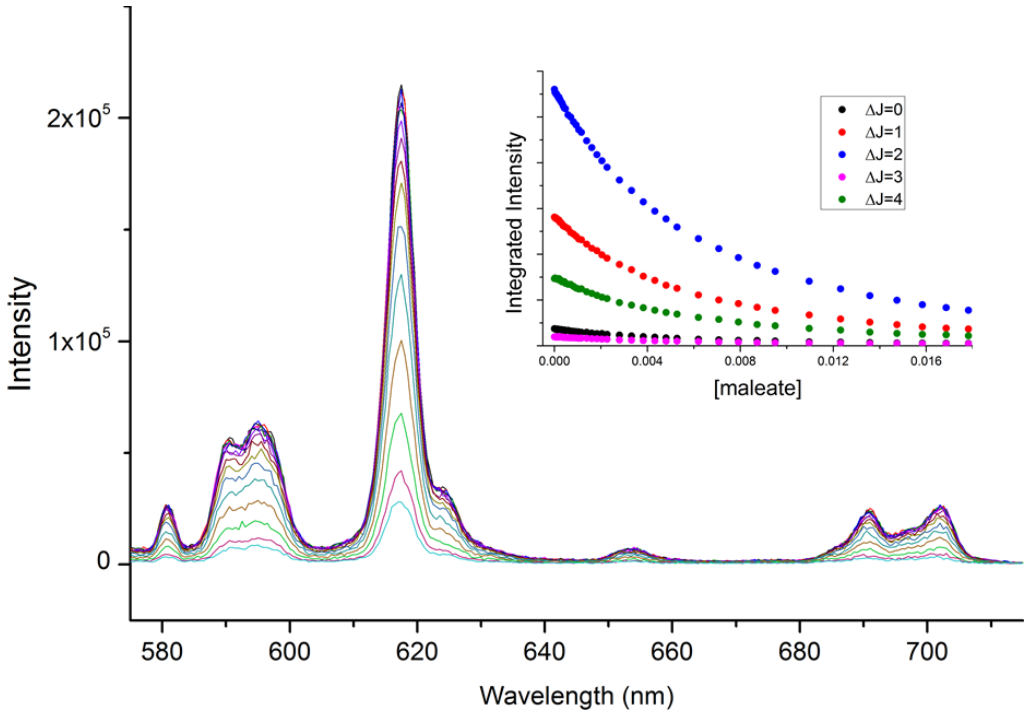

Figure 3-12. Overlaid emission spectra of [3.c] recorded upon titration with potassium maleate. Inset shows the integrated intensities of the different peaks as a function of maleate concentration.

3.4.3 Cyclohexanedicarboxylates

The effect of guest dianion preorganisation on binding was explored further through use of the cyclohexane-dicarboxylates, as once again, their increased rigidity should result in a lower loss of conformational entropy upon binding, when compared with their acyclic analogues.

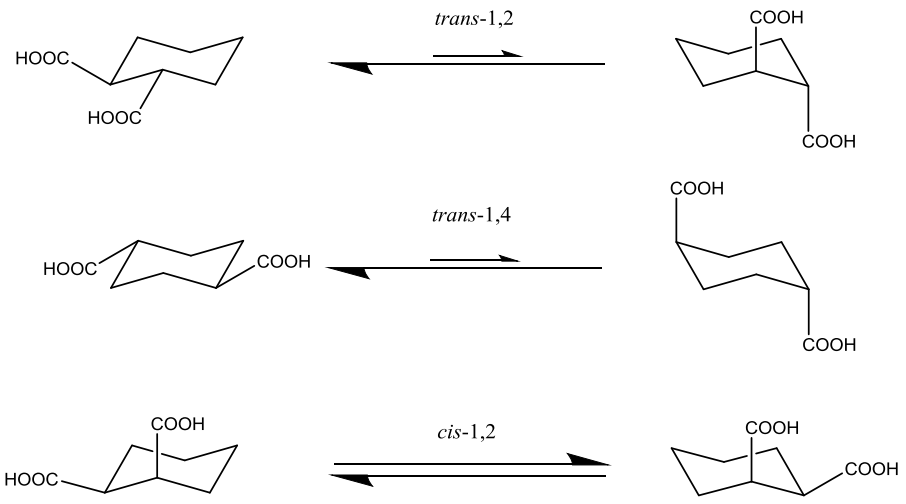

Figure 3-13. Structures and conformational equilibria of the cyclohexyl-dicarboxylates used in this chapter.

The relatively high A-values (1.92) of the carboxylate groups mean that the *trans*-1,2 and *trans*-1,4 isomers will exist almost exclusively as one conformer, with the two carboxylate groups in equatorial positions to avoid 1,3-diaxial steric strain. In the case of the *cis*-1,2 isomer, both of the accessible chair conformers are energetically equivalent, with one carboxylate in an axial position and the other sitting equatorial to the ring, and thus the barrier to ring-flipping is lower than for the *trans* species. Rudimentary molecular modelling was used to estimate the distances between the two donor groups in each of these major conformers.

Isomer	Inter-carboxylate Distance (pm)
cis-1,2-cyclohexane dicarboxylate	318
trans-1,2-cyclohexane dicarboxylate	292
trans-1,4-cyclohexane dicarboxylate	591

Table 3-4. Calculated through-space distances separating the sp^2-carbons of the carboxylate groups for the dominant isomer.

For the two *trans* isomers, the energetic penalties of adopting the diaxial conformer, allied with the high barrier to ring flip due to the comparatively bulky carboxylate groups, mean that the diequatorial form is dominant and thus the calculated distances, whilst far from precise, may be assumed to be reasonably correct. In the case of the *cis*-1,2 dianion however, the reduced barrier means it may adopt boat or twist-boat conformations to bind to the complex, with the decreased

energetic conformational preference of the guest being offset by the increased electrostatic interaction with the metal centres afforded by improved host-guest complementarity. The binding constants for the cyclohexyl-dicarboxylates and their straight-chain counterparts are shown in table 3-5.

Titrant	pH	K (M^{-1})	99% Confidence Interval	Calculated ΔG ($kJmol^{-1}$)
succinate	7.7	55	53.070 - 56.473	-9.8
cis-1,2	7.6	693	676.85 -709.80	-15.9
trans-1,2	7.6	233	229.5 - 235.89	-13.3
adipate	7.7	60	53.649 - 65.939	-10.0
trans-1,4	7.6	137	135.24 - 138.68	-12.0

Table 3-5. The binding constants and confidence intervals calculated for the interactions between complex [3.c] and the cyclohexyl-dicarboxylate guests. The values for the C_4 and C_6 aliphatic dicarboxylates are included for comparison. ΔG values calculated assuming T = 293 K.

As observed previously, the binding was accompanied by an increase in luminescence intensity. In all cases, the cyclic dicarboxylates show a significantly higher affinity for the metal complex than their acyclic analogues, providing further evidence that loss of conformational entropy in the guest may well be an important factor in determining the strength of binding. The cyclic *cis*-1,2-dicarboxylate offers the best fit to the cavity of the host complex as it shows the highest binding constant. This may be a consequence of having the most favourable geometric arrangement of the two anionic head groups, or it could reflect the increased flexibility of the scaffold linking said groups, allowing a better induced fit.

3.4.4 Backbone substituents

Thus far the only parameters to be varied between the different dicarboxylate guests have been the separation between the two acid head groups and the flexibility of the chain linking them. To investigate the influence on binding of substituents on the carbon skeleton of the diacid guests, binding studies were performed using bis-carboxylates which had been additionally functionalised.

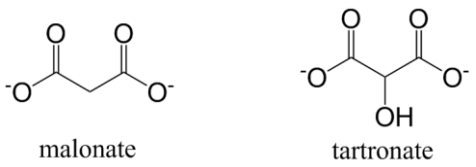

Figure 3-14. Structures of the three-carbon guests.

Initially malonate and tartronate were compared. In both titrations, introduction of the anion resulted in a significant increase in the intensity of luminescence and fitting this rise in intensity gave the binding constants shown in table 3-6.

Titrant	pH	K (M^{-1})	99% Confidence Interval	Emission Lifetime at end-point
malonate	7.70	403	385.92 - 421.47	1.01 ms
tartronate	7.70	2391	2237.3 - 2555.3	0.89 ms

Table 3-6. Comparison of the binding constants calculated for the malonate and tartronate guests.

Hydroxylation of the malonate backbone resulted in a dramatically increased affinity for the dinuclear europium complex, with the binding constant increasing by an order of magnitude.

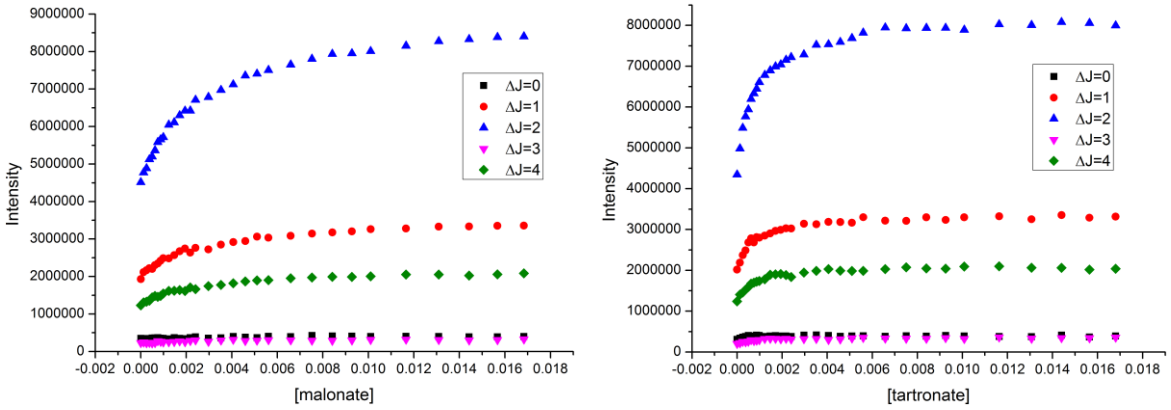

Figure 3-15. The integrated luminescence intensities of complex [3.c], plotted against the concentration of malonate (left) and tartronate (right).

It is interesting to note the change in the luminescent lifetimes of the europium-centred emission. In the absence of any titrant, the emissive lifetime of europium complex [3.c] in HEPES buffer at pH 7.70 was found to be 0.46 ms. Binding of either anion displaces bound solvent from the metal centres, resulting in reduced non-radiative quenching by O-H oscillators and giving rise to an

increased luminescent lifetime. As the binding with tartronate is an order of magnitude larger than with malonate, one might expect this to be reflected in a longer emissive half-life of the [3.c]:tartronate complex, compared to its malonate counterpart. However this is not found to be the case and indeed, at 0.89 ms, the luminescence of the tartonate adduct is shorter-lived than that of the complex with malonate, which was found to be 1.01 ms. It is possible that upon binding, the hydroxyl group on the C_3 skeleton is close enough to the metal centres for the stretching harmonics of the O-H bond to non-radiatively quench the metal centre.

The C_4-skeleton of succinate provides a wealth of opportunities for further functionalised anions with which to probe the role of back-bone substituents in binding. Binding studies were performed with the dicarboxylates shown in figure 3-16.

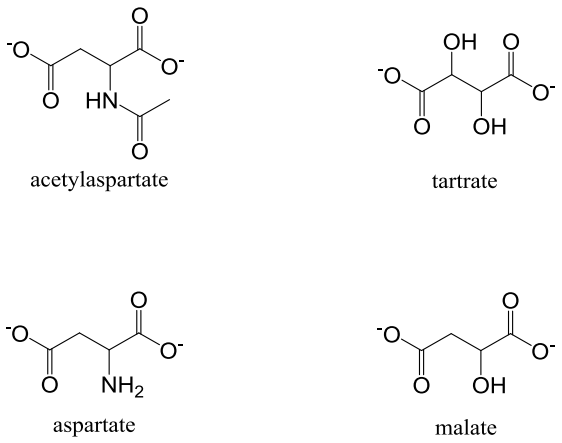

Figure 3-16. Molecular structures of the different functionalised C_4 dicarboxylate guests.

The addition of one hydroxyl group to the 2-position of succinate backbone gives the malate anion. This modification resulted in a roughly five-fold increase in affinity for europium complex [3.c]. An additional substitution at the 3-position afforded the tartrate species and again the trend was continued, with tartrate showing a binding constant an order of magnitude greater again. In all three cases, binding of the anion gave rise to an increase in total luminescence intensity, with the greatest gains being seen in the $\Delta J = 1$ and $\Delta J = 2$ bands. Unlike in the case of malonate and tartronate, the presence of additional hydroxyl groups on the guest backbone did not seem to impact on the emissive lifetimes of the host-guest adduct. By the end point of the titrations with

succinate, malate and tartrate, the emissive lifetime of ΔJ = 2 peak was essentially the same in all cases, with values between 0.79 ms and 0.85 ms. As expected, these lifetimes were longer than those of the complex in isolation, which were measured at 0.57 ms and 0.46 ms in PBS and HEPES respectively. These values were sufficiently close to one another to presume that, unlike in the case of the C_3-acids, the backbone O-H groups were not interacting with the metal centres to quench luminescence. The value of 0.82 ms for the succinate adduct is shorter than that of the complex with malonate, most probably as the weaker binding means that there is a slightly greater fraction of the complex present with a solvent species resident on the metal instead of the carboxylate guest.

Titrant	Buffer	pH	K (M^{-1})	99% Confidence Interval	Emission Lifetime at end-point (ms)
succinate	HEPES	7.7	55	53.070 - 56.473	0.82
	PBS	7.6	*	*	
malate	HEPES	7.7	328	310.72 - 347.39	0.80
	PBS	7.6	241	229.99 - 252.61	0.79
tartrate	HEPES	7.7	1894	1709.8 - 2094.6	0.84
	PBS	7.6	746	698.36 - 796.49	0.85
aspartate	HEPES	7.7	NBD	N/A	-
	PBS	7.6	NBD	N/A	-
N-acetyl aspartate	HEPES	7.7	*	*	0.80
	PBS	7.7	*	*	0.81

Table 3-7. The binding constants and confidence intervals calculated for the interactions in different buffers between complex [3.c] and the substituted C_4 dicarboxylate titrants. NBD = No Binding Detected. * = Binding detected but too weak to be fitted satisfactorily with DynaFit® software.

Hydroxylation of the C_6-backbone of the adipate anion gave rise to the mucate species, which is unique amongst those anions studied so far, in that the alcohol groups at the 3- and 4-positions of the backbone are in γ and δ positions relative to the carboxylate donor groups, opening up the possibility of larger chelate rings to the metal centre.

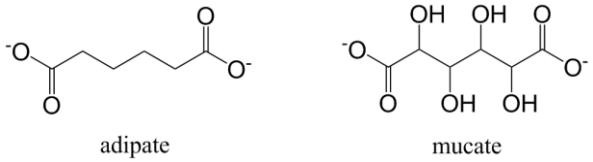

Figure 3-17. Structures of the two C_6-guests.

Titrant	pH	K (M^{-1})	99% Confidence Interval	Emission Lifetime at end-point (ms)
adipate	7.7	60	53.649 - 65.939	0.76
mucate	7.7	3648	3246 - 4106	0.82

Table 3-8. The binding constants and confidence intervals calculated for complex [3.c] and the six carbon guests.

Once again the functionalization of the skeleton linking the two acid groups with polar hydroxyl groups results in a large increase in the binding constant, in this instance by two orders of magnitude. This increase in affinity upon substitution of the anion backbone was a common trend across the different length guests and there were several different postulated rationalisations for this widely observed behaviour. One potential factor was the coordinating role of the proximal hydroxyl group. Alcohol groups alone are not usually sufficiently hard donor groups to displace bound solvent molecules from lanthanide centres. If acting in concert with the charged carboxylate groups however, it is reasonable to suppose that such moieties could coordinate to the metal cation, forming a 5-membered chelate ring, and that this additional electrostatic interaction could contribute favourably to determining the position of the equilibrium, resulting in an increased in observed binding constant.

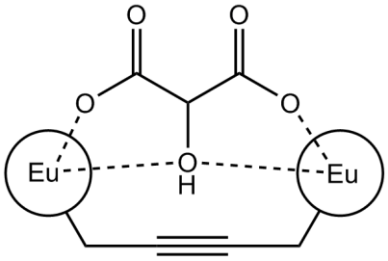

Figure 3-18. Schematic of the proposed chelating binding mechanism for complex [3.c] and dicarboxylate guests incorporating a hydroxyl group in the β-position.

Indeed such behaviour has been observed by the groups of Botta[2] and Parker.[3] In their studies of heptadentate q = 2 complexes they noted that upon binding of carboxylate ligands such as lactate and citrate, both bound water molecules were displaced from the metal centre. A 1:1 complex:guest stoichiometry was confirmed and so they proposed that the second bound solvent was being displaced by the β hydroxy group in the formation of a five-membered chelate ring. Further evidence in support of their hypothesis came from crystallographic data, which showed not only five- but also four-membered chelate rings formed with ligands such as carbonate and acetate.

An alternative hypothesis to that of cooperative coordination is one of backbone solvation. Previous studies on *meta*-xylyl bridged bis-macrocyclic complexes have shown that the host complex must adopt a particular conformer of complementary shape to the anionic guest for binding to occur. It is not unreasonable to extend this logic to the dicarboxylate guest species, especially in the cases where the acid head groups are separated by a long and flexible alkyl chain. In adopting a conformation where the two carboxylate groups are directed in towards the metal cores, the hydrocarbon back-bone of the anion guest needs to fold 'outwards' towards the solvent medium. If the skeleton is a saturated hydrocarbon it will be hydrophobic and thus forcing it out into the aqueous surroundings would lead to unfavourable enthalpic interactions between the guest species and the solvent medium. By contrast, in the cases where the anionic guest has a backbone functionalised with polar side groups, hydrogen bonding with the protic solvent means that there is no enthalpic penalty associated with the adoption of a binding conformer.

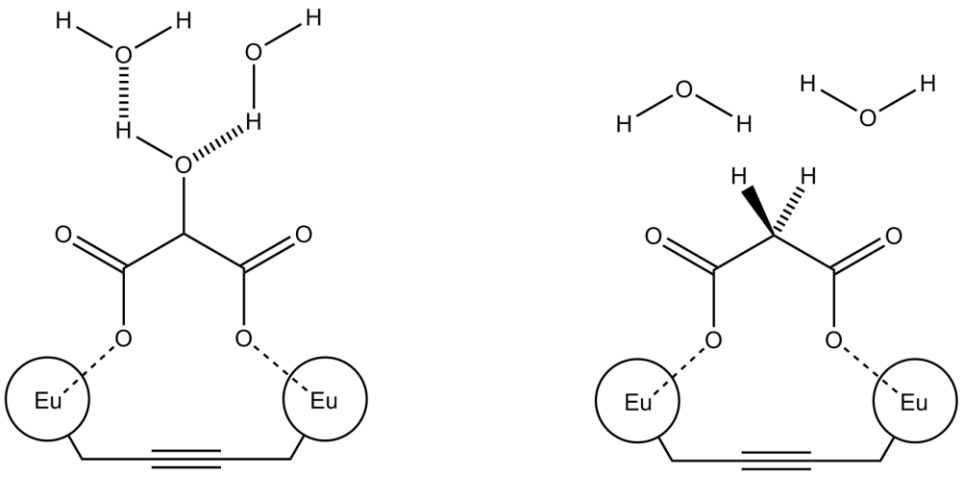

Figure 3-19. Illustration of the potential role played by solvation of the non-binding portion of the guest species.

It is perhaps worthy of note that in the pairing where the greatest difference was observed between the substituted and unsubstituted guests, that of adipate and mucate, the hydroxyl groups in the γ positions relative to the donor head group open the possibility of both of these effects occurring simultaneously. This then could possibly explain difference of two orders of magnitude observed in the affinities.

Finally, it is suggested that increased hydrogen-bonding interactions between the alcohol groups and the aqueous environment means that the hydroxyl-functionalised anionic guests are more solvated when unbound. Binding to a metal host could disrupt this coordination sphere due to steric interaction with the ligand scaffold of the complex, which would result in the release of bound solvent. The entropy increase from this process would likely outweigh the enthalpy of solvation, resulting in a positive contribution to the binding constant.

When comparing the binding constants of the four-carbon diacids, it is perhaps surprising to note that no binding at all was detected in the case of aspartate, which differs from the saturated skeleton species by an amino group in the 2-position. Amines have been shown to be effective donors to lanthanide ions in solution: indeed the poly-aza macrocyclic framework of the complex in question depends on it. Amines are also capable of hydrogen bonding to protic solvents, so one might reasonably predict that aspartate would display an increased affinity with the metal

complex compared to the parent succinate. That this is not found to be the case is most likely due to the speciation of the aspartate at the pH of the experiment. At pH 7.70, the predominant species in solution is the zwitterion, in which both carboxylic acids are dissociated and the amine group is protonated to the ammonium. This extra positive charge on the aspartate guest will most likely lead to repulsions with the highly charged lanthanide ion centre, inhibiting binding. The α-amine group of aspartate has a pK_a of 9.61 and thus at pH values higher than this, will exist not as the alkyl-ammonium species, but as the charge neutral amine. Under these conditions one would expect aspartate to show a greater affinity than succinate for the reasons given above. This is however outside the pH range afforded by the HEPES and PBS buffer systems and thus these experiments were not performed.

This explanation does not hold in the case of N-acetylaspartate, as the pK_a of the side-chain nitrogen is much higher than in the non-esterified amino acid and thus at the pH of the experiment, the dominant species is once again the dianion. In this instance, the most likely rationalisation is one of size, with the steric bulk of the acetate group preventing close approach to the metal binding centre. The amide moiety is also less hydrophilic than the hydroxyl groups of the tartrate

3.5 Probing Chirality

As relatively strong binding had been observed between the europium complex [3.c] and (enantiopure) L-tartrate, it was decided to explore the possibility of tartrate acting as a chiral auxiliary and through coordination to the metal centre, defining the chirality there and giving rise to an observable dissymmetry. Initially circular dichroism (CD) spectroscopy (see Section **1.5**) was used. Being an absorption-based technique, baselines first had to be recorded for the HEPES buffer solution, complex [3.c] in the absence of L-tartrate and L-tartrate in the absence of the complex. Due to the parity-forbidden nature of the *f-f* transition at 394 nm normally used to excite the metal, the absorption coefficient was found to be vanishingly

small. Attempts to utilise the broad carbonyl-based bands around 230 nm were thwarted, both by the absorption of the HEPES sulfonyl groups and by the signal of the unbound fraction of tartrate in solution. Switching to phosphate-buffered saline, which is transparent in the 210-250 nm region, alleviated the first of these problems but the second proved insurmountable. The strong chiral absorption of the L-tartrate swamped the signal arising from the carbonyl groups of the pendant arms of the complex, making it impossible to identify any change at the metal centre.

Circularly Polarised Luminescence experiments were performed in collaboration with Dr. Robert Pal of the University of Durham. Lack of a white light excitation source necessitated the use of a tuned laser array to populate the emissive state of europium. A Photo-elastic Modulator (PEM) was used to control the beam-path to selectively allow left or right circularly polarised light through to the detector. A schematic of the apparatus used is shown in figure 3-20.

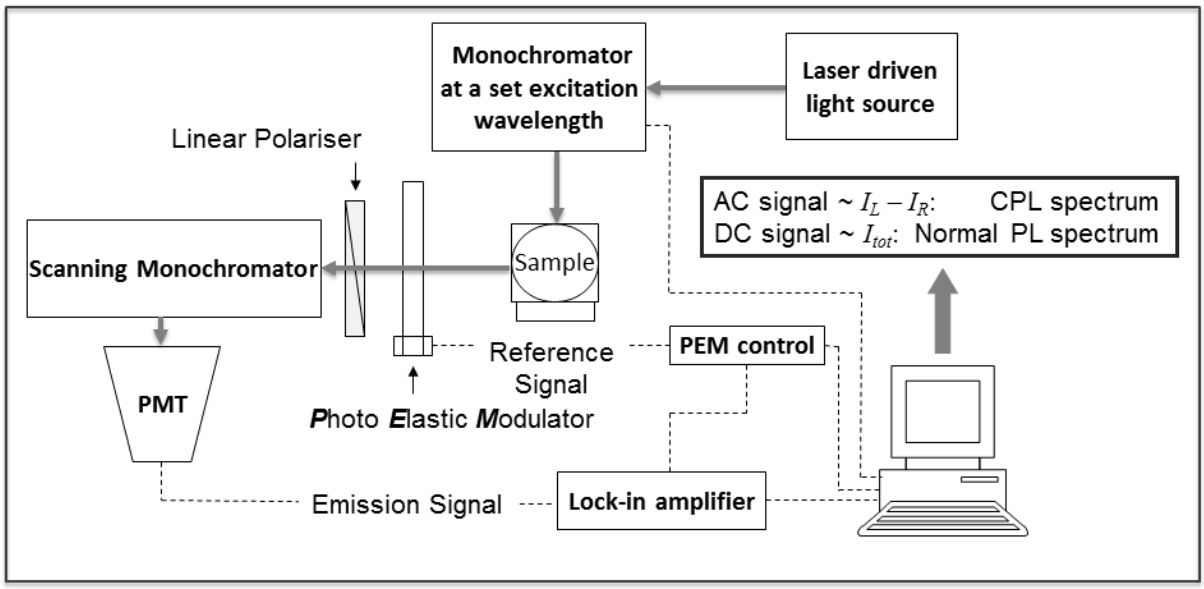

Figure 3-20. Illustration of the apparatus used to measure and record CPL spectra.

Each lanthanide centre can exist as one or other helical enantiomer, as defined by the pendant carboxylate arms. As these two isomers are energetically equivalent, in the absence

of any external factors, the complex should exist as a racemic mixture. Each enantiomer will preferentially emit photons of one helicity but as the relative populations of the enantiomers are equal, prior to binding one would expect zero emission dissymmetry and thus zero signal. Upon binding however, the enantiopure guest should hopefully favour the adoption of one enantiomer over the other, thus creating a population imbalance and leading to greater emission intensity in one circular polarisation. Total emission ($I_L + I_R$) and CPL ($I_L - I_R$) spectra were recorded of the complex in isolation and then in the presence of an excess of L-tartrate. Unlike in the CD experiment, the observed parameter under study originates solely from the chirality at the metal centre and thus the unbound fraction of tartrate in solution does nothing to obscure the signal. There were however other issues and the results obtained using this experimental set-up were found to be less than satisfactory. The *ad hoc* assembly of the laser-driven light source used to excite the complex led to low signal intensities, whilst problems with scattering and stray light passing through the detection system lead to a very unfavourable signal-to-noise ratio. Spectra were nevertheless taken and are shown in figure 3-21.

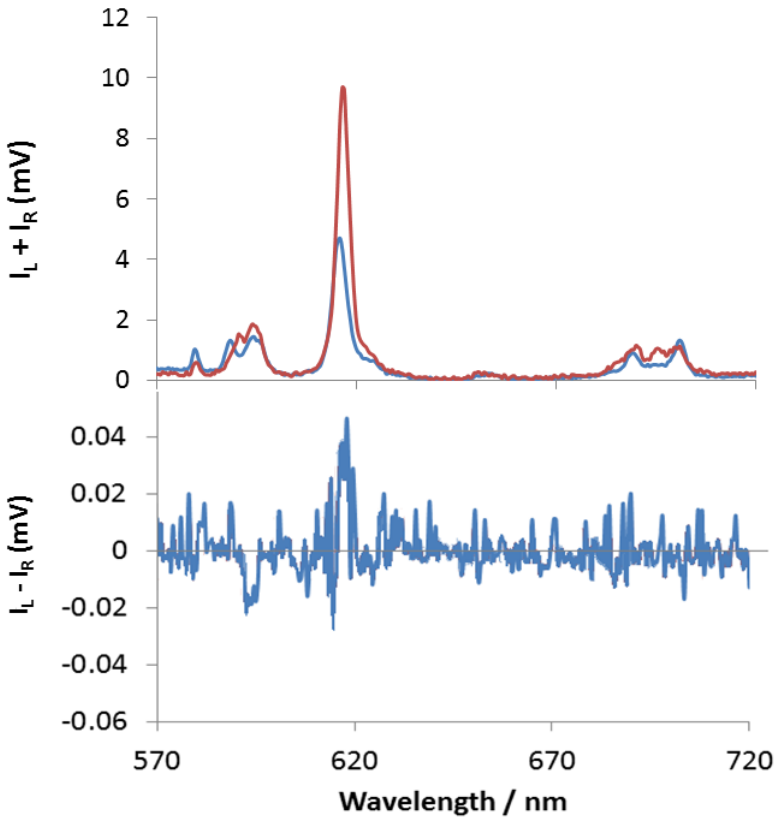

Figure 3-21. Top - Luminescence spectra of complex [3.c] in the absence (red trace) and presence (blue trace) of L-tartrate. Bottom - CPL spectrum of [3.c] with L-tartrate bound.

The decrease in total emission intensity following addition of the L-tartrate guest confirms that the binding behaviour observed earlier is indeed occurring but the CPL spectrum is less conclusive. The noise here makes the discernment of any change more challenging. The ΔJ = 2 peak clearly displays a non-zero response but the noise threshold is such that any attempt to rationalise perceived changes in the regions corresponding to the ΔJ = 1 and ΔJ = 4 peaks may be mere apophenia on the part of the author.

The crucial stumbling block in this particular experiment was a lack of light. The absence of a sensitiser group on either the host scaffold or the tartrate guest meant that direct excitation of the metal needed be used and the pitiful quantum yields associated with this method of generating luminescence conspired to obscure the slight spectral changes arising from this subtle interaction with the local environment. This flaw could be circumvented via the incorporation of a light-harvesting antenna group into either the guest or host complex.

3.6 NMR Studies

In selected instances where reasonably strong binding was observed, studies were performed to see if the binding event observed by luminescence gave rise to a change in the NMR spectrum, either of the complex or of the binding species. Having witnessed the pH-dependence of the solution-phase structure and thus the form of the NMR spectrum, it was decided to perform these experiments in buffered solutions. Phosphate buffer was selected as it does not possess any organic protons of its own which could mask the resonances of the species being studied. The samples were adjusted to pD8 using the appropriate deuterated acids and bases.

Oxalate was selected for study as it had displayed the highest affinity when measured by luminescence. Shown in figure 3-22 are the paramagnetic proton spectra recorded, first in isolation and then in the presence of 10 molar equivalents of dipotassium oxalate.

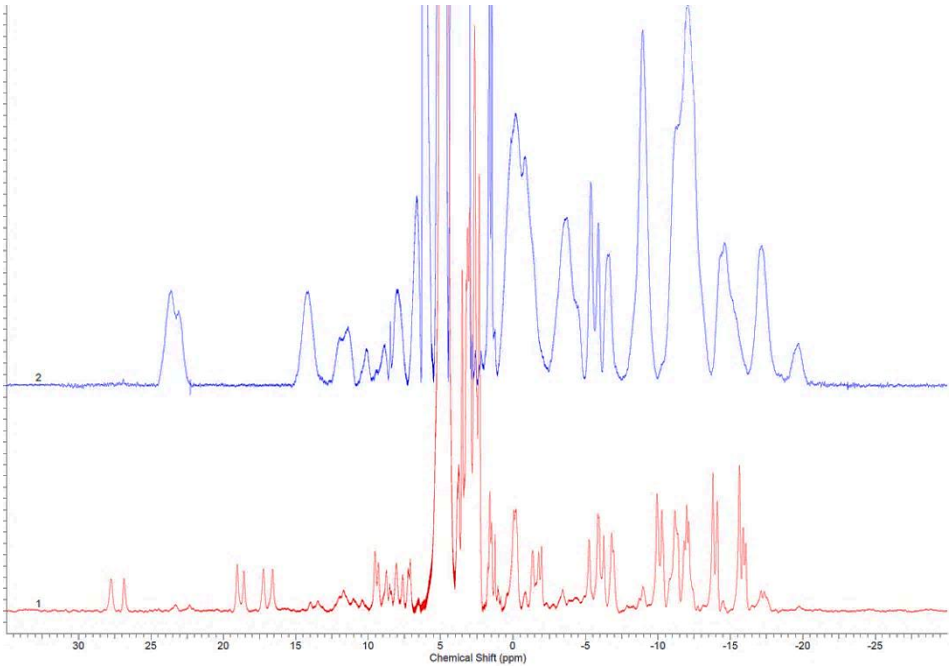

Figure 3-22. Paramagnetic ^{1}H-NMR spectra of complex [3.c] in isolation (blue trace) and in the presence of 10 molar equivalents of potassium oxalate (red trace). Recorded at 298 K in phosphate buffered D_2O, pD8.

Clearly the conformation of the complex has undergone significant changes in the formation of the ternary adduct with the dicarboxylate. At pD 8 and in the absence of the guest, the resonances of the europium complex are broad and ill-defined, indicating exchange between

isomers on the timescale of the experiment. Addition of the oxalate guest results in a significantly sharper spectrum with a greater number of resonances and much narrower line-widths. From this it can be inferred that the structure of the adduct is more rigid than that of the free complex, with slower or reduced exchange between the isomers.

Tartrate was also selected for study by NMR as it too had been observed by luminescence to bind somewhat strongly and was also one of the few chiral guests with potential utility in techniques such as CPL.

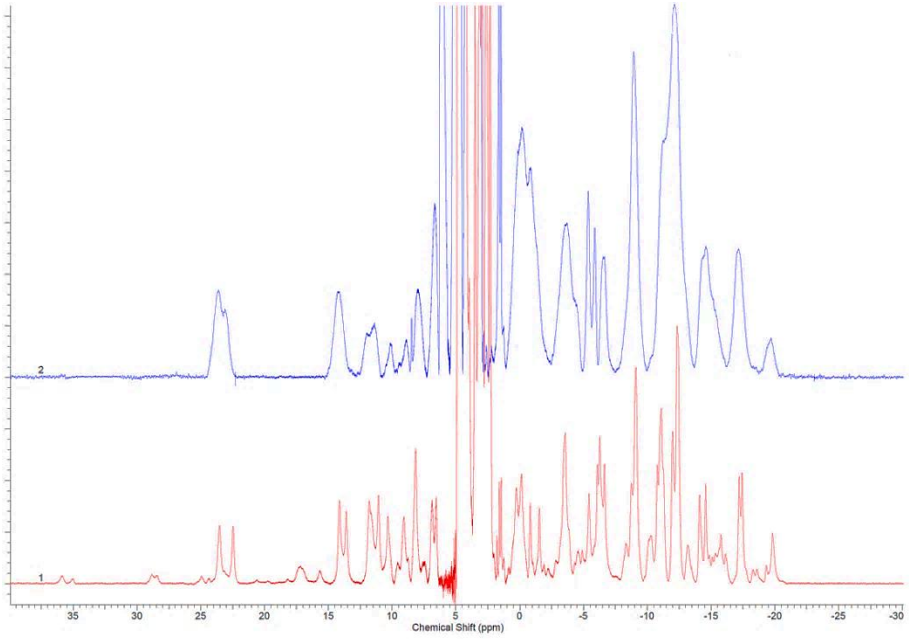

Figure 3-23. Paramagnetic ^{1}H-NMR spectra of complex [3.c] in isolation (blue trace) and in the presence of 10 equivalents of potassium tartrate (red trace). Recorded at 298 K in phosphate buffered D_2O, pD8.

Again it would appear that on formation of the host:guest array with tartrate, the complex gains significant rigidity as the peaks sharpen and increase. Worthy of note is the appearance of three pairs of more shifted minor peaks, coming around 36, 29 and 25 ppm. These could be indicative of there being two different conformations of the complex capable of accommodating the tartrate guest. Alternatively, as resonances such as these are not observed for the oxalate system, it is possible that they are due to the protons of the tartrate guest itself.

Spectra of the assemblies formed with other anionic guests were all found to display narrower line-widths than the free complex, indicating decreased flexibility and hindered isomer exchange.

The final form of the spectra however, was found to vary extensively. This is clear evidence that the host complex is capable of accessing a range of conformers to best accommodate the guest species. It suggests that the lock and key model of binding, often applied to certain biological systems and organic arrays relying on directional hydrogen- or halogen bonds, is in this instance not valid and instead we must consider an induced-fit mechanism, where both host and guest can change their geometries to maximise the favourable binding effects.

3.7 Computational Models

In an effort to rationalise the apparent different conformations adopted by complex [3.c] upon binding of the various anions, selected molecular models were generated in collaboration with Thomas Sørensen of the University of Copenhagen. The models were generated using Spartan 08 modelling software and the geometries optimised using semi-empirical methods, in particular PM3. Whilst models generated in this manner are far from a proof of molecular geometry, they can be useful when taken in context with the body of other experimental obsevations.

First of all, an energy minimisation was carried out on the free complex in solution, devoid of any potential guests other than the solvent. This would provide a baseline against which the various binding conformers could be compared.

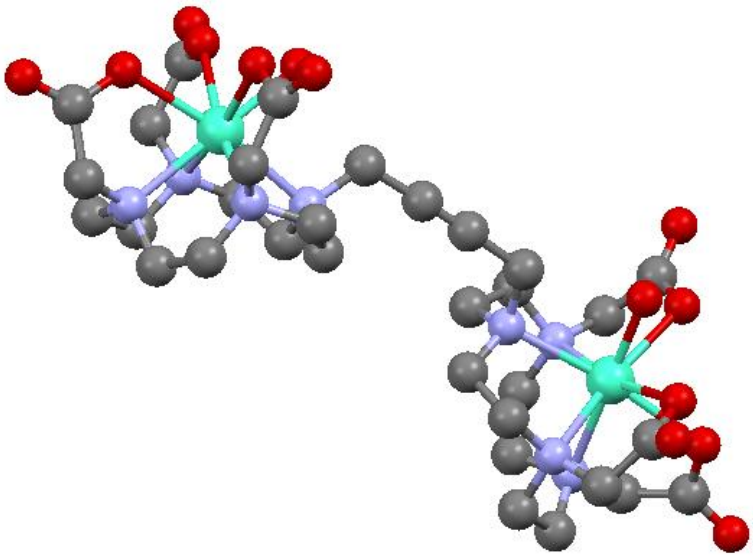

Figure 3-24. Molecular model of complex [3.c]. Hydrogens omitted for clarity.

It is noteworthy that the conformation resulting in the least steric strain between the two macrocyclic cores does not in fact have them in a fully *anti*-configuration across the alkyne linker, but instead has them slightly staggered with a torsion angle of 33°, possibly to allow the greatest distance between the pendant acetate arms of each centre. In this arrangement, there is a separation between the two lanthanide ions of 10.34 angstroms. The distance between the two ring nitrogen atoms through which the complexes are linked was calculated to be 5.45 Å and was well within the range predicted in section **3.1**.

Moving to the smallest of the dianions oxalate, the picture changes dramatically. The torsion angle between the C_1-N and C_4-N' bonds of the alkyne linker has increased from 33° to 162° and the four carbon chain as a whole has undergone a slight deviation from its previously linear arrangement. Crucially, the distance between the two europium ions has decreased hugely, from 10.34 Å to 7.41 Å.

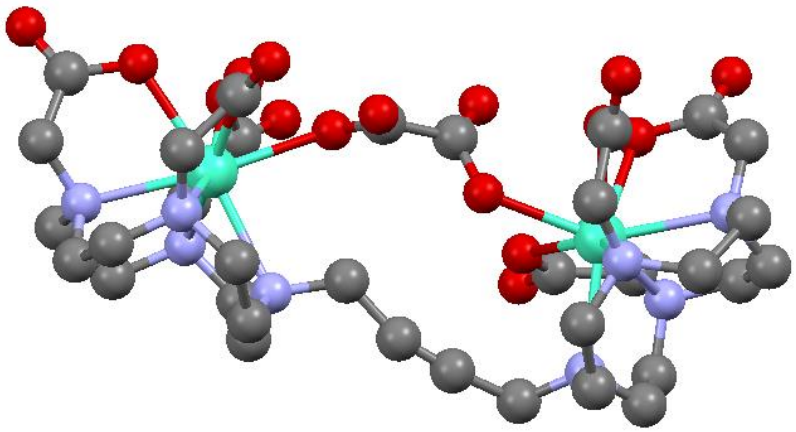

Figure 3-25. Molecular model of the adduct of complex [3.c] with oxalate. Hydrogens omitted for clarity.

The oxalate too has undergone a significant conformational change to bind to both metal centres. Theoretical studies have long held that in solution, the D_{2d} conformer of dianionic oxalate is the most stable, with a twist angle of 90° and the π-systems of the two carboxylate fragments orthogonal to one another. Crystalline hydrates of oxalic acid on the other hand have been shown to adopt a co-planar geometry: it is thought that in the solid state, the ease of stacking of the D_{2h} arrangement outweighs the stereoelectronic preferences which hold sway in solution. In the

ternary adduct shown here, neither of these extremes is observed and instead, there is a torsion of approximately 51° between the two planar carboxylate units. The intermetallic separations and C_1-N/C_4-N' torsions of the alkyne linker for the adducts of complex [3.c] and the different unsubstituted dicarboxylates are tabulated in table 3-9.

Guest	Intermetallic Separation (Å)	C_1-N/C_4-N' Torsion (°)	Binding Constant (M^{-1})
No guest	10.34	33	-
oxalate	7.41	162	7813
malonate	7.33	89	403
succinate	8.79	29	55
adipate	9.52	47	60
fumarate	8.72	41	763
maleate	7.90	94	184

Table 3-9. Calculated geometric parameters and equilibrium constants for selected complex [3.c]:guest adducts.

These data are probably indicative of an induced-fit model of binding, with both the host and guest changing their conformations in the formation of the ternary adduct. It was assumed that the geometry calculated in the absence of a guest is the optimal solution-phase conformer of the complex. It is therefore interesting to note that the strength of binding for a particular guest does not correlate with the deviation from optimal geometry required by the complex for the accommodation of said guest. Oxalate in particular displayed the highest affinity for complex [3.c], and yet the models would indicate that in accommodating the oxalate guest, the complex is required to undergo one of the biggest deviations from its 'preferred' conformational arrangement, with the distance between the two metal ions dropping by almost three angstroms, from 10.34 Å to 7.41 Å. By contrast, in the case of the adduct with the six carbon adipate anion, the intermetallic separation is much closer to its equilibrium value at 9.52 Å and yet the binding constant is much lower. Comparison of the four carbon guests, succinate and fumarate shows that in both cases, the distance between the metal centres is very similar, and yet the binding of

fumarate is more than an order of magnitude stronger than that of succinate. The calculated distances between the C_1 and C_4 carbon atoms of the carboxylate donor groups are also almost the same in each case (3.85 Å for fumarate and 3.71 Å for succinate) and so the only major difference left between the two cases is the extra rigidity imparted to fumarate by the alkene group in its carbon skeleton.

Taken together, these observations would appear to favour a general conclusion that in this particular series of adducts, one of the dominant factors influencing the value of the equilibrium constant is the loss of conformational entropy on the part of the guest species. Oxalate, having available to it a very limited range of conformational freedom, exhibits strong bonding to the complex [3.c], even though the small size of oxalate means that the complex must distort from its optimal arrangement. Malonate similarly has limited conformational entropy in its unbound state and thus the loss on binding is also small. By this logic, upon lengthening the dicarboxylate guest from succinate to adipate, one would reasonably expect the binding constant to further decrease but this is not found to be the case. It is inferred that this is due to the longer adipate dianion allowing the complex host to adopt a binding conformer more closely resembling its preferred geometry. Alternatively, it could be the case that with its extra length and flexibility, the adipate is capable of more efficiently coordinating to the metal centres, resulting in greater electrostatic attractions and a greater enthalpic gain upon binding.

Models were also made in a quest to rationalise the differences in equilibrium constants observed between the substituted and unsubstituted guests. Specifically, we aimed to investigate the feasibility of the formation of chelate rings, with the hydroxyl groups on the guest backbone cooperatively binding at the metal centres. Models were initially made for the hydroxyl-substituted three-carbon guest, tartronate, with the central hydroxyl group coordinating to one, both or neither metal centre.

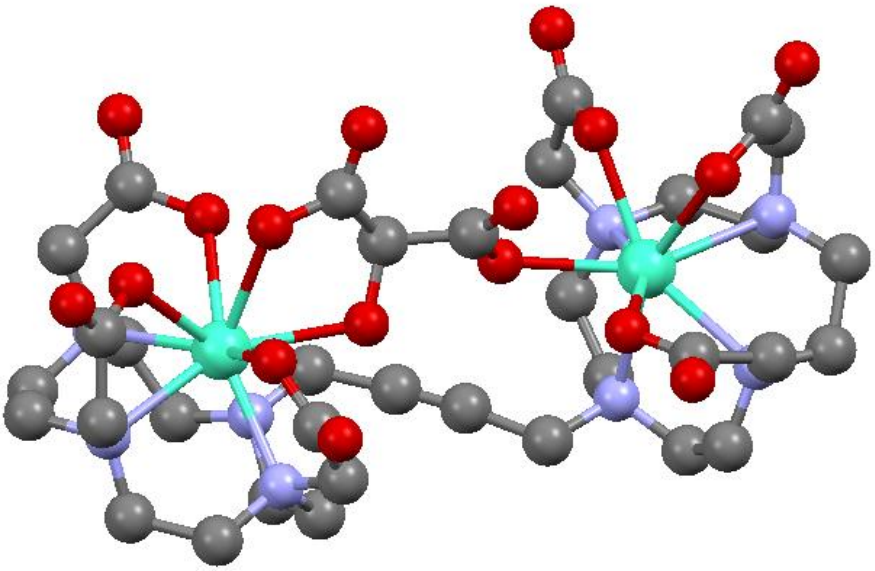

Figure 3-26. Molecular model of the adduct of complex [3.c] with tartronate in which the guest is bidentate at one metal centre and monodentate at the other. Hydrogens omitted for clarity.

It was found that the model in which the guest overall was bidentate at one metal centre and monodentate at the other offered the lowest energy profile. Similar models were generated for the four-carbon dicarboxylate tartrate and again in this case it was found that the best fit was obtained by the model in which the hydroxyl group β to the acid head group coordinated to the metal centre, forming a five-membered chelate ring at each europium ion.

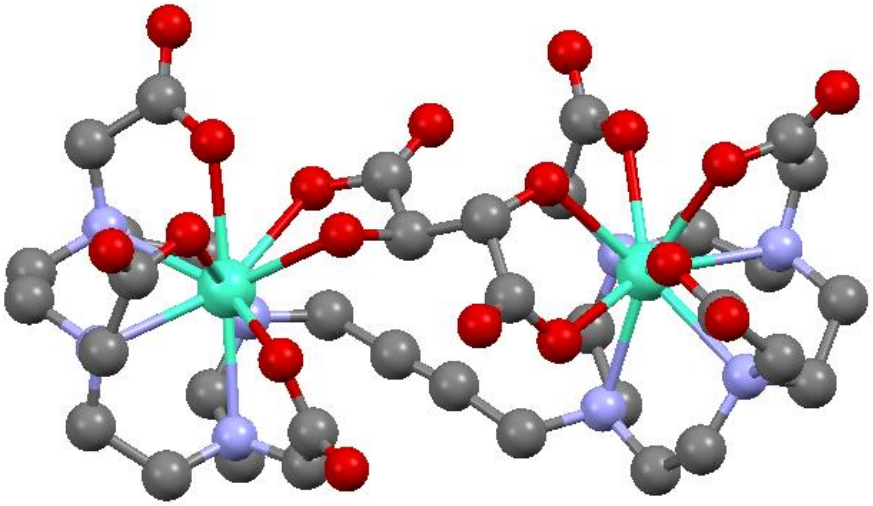

Figure 3-27. Molecular model of the adduct of complex [3.c] with tartrate in which the guest is bidentate at both metal centres. Hydrogens omitted for clarity

It should once again be made absolutely clear that these models do not constitute a proof, either of the overall molecular geometry or of the chelating nature of the hydroxylated guests, but they may provide further insight into the mechanism by which substituents on the guest backbone can influence the binding constant for the guest as a whole.

3.8 Comparisons with p-DO3A

In calculating the binding affinities offered, model-discrimination was used to determine the most likely binding mode and in all cases, a 1:1 stoichiometry was found to produce by far the best fit with the experimental data. Whilst this in itself is not proof of the formation of a ternary adduct in which the dianion bridges the metal centres, it is a reasonable piece of evidence in support of such a hypothesis.

Assuming a 1:1 stoichiometry, the most likely alternative binding mode would entail coordination of one anionic head group to one metal centre, with the carbon backbone directed out away from the complex and the second donor group pendant in the solvent medium. This would leave the second metal centre with a bound solvent species still coordinated to the metal centre. A model discrimination analysis would not be able to distinguish this binding modality from the bridging mechanism proposed. Such a situation would technically result in two inequivalent metal centres; one with an anionic donor filling the apical coordination site and one in which the binding cavity was capped with a bound water molecule. However the rates of exchange between the bound and bulk solvent and anion would be sufficiently high that the different environments would not be resolvable in a luminescence experiment and all that would be seen would be an intractable population-weighted average of the two.

To further assess the possibility of binding to just one metal centre, it was resolved to perform selected binding studies with a mononuclear lanthanide complex which shared similar stereoelectronic properties to the ditopic species [3.c].

The propargyl-appended DO3A species has been used extensively by the group due to its utility as a synthon for copper-catalysed azide-alkyne Huisgen cycloaddition. The europium complex of this ligand system was prepared according to scheme 3-2 following the literature procedure.[4]

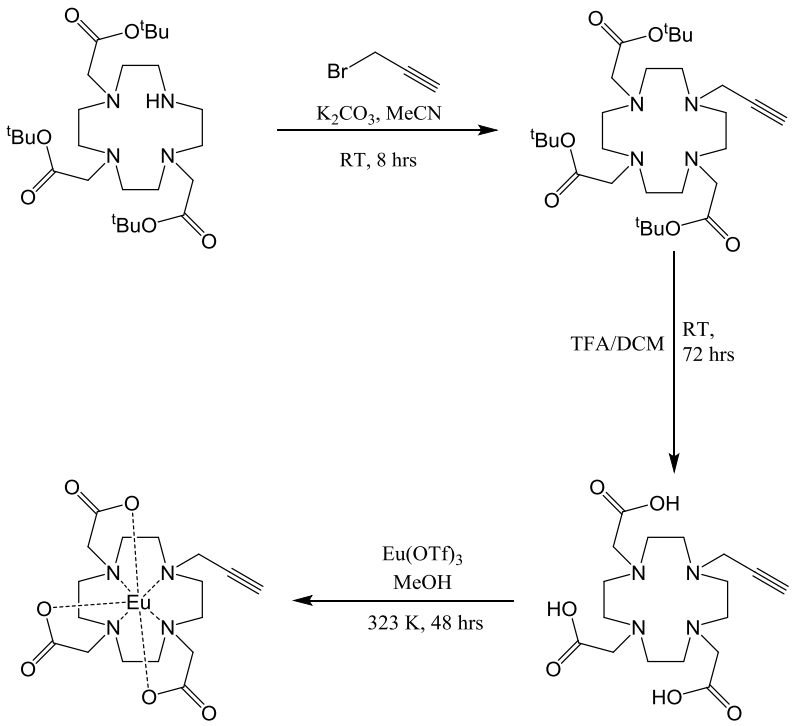

Scheme 3-2. Synthetic strategy used for the preparation of mono-nuclear complex [3.j].

The synthesis of this mononuclear system is well documented elsewhere and so will not be discussed in detail in this work. It is however worth drawing attention to the ^{1}H-NMR spectrum of the final europium complex product [3.j], recorded in D_2O. It is significantly simpler than that of the alkyne-linked dimer and the most shifted resonances indicate that the simple monomeric species exists almost exclusively in the TSAP conformation.

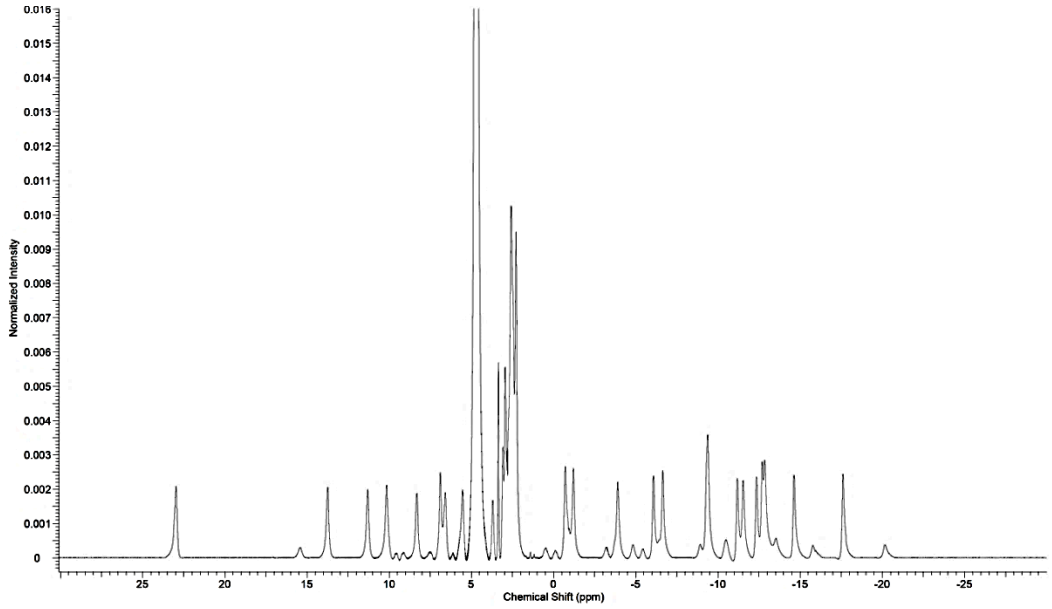

Figure 3-28. ^{1}H-NMR of complex [3.j]. Recorded at 298 K in D_2O, pD 9.

Luminescence binding studies were performed with selected anions in an attempt to resolve the effects of binding across two metal centres.

Complex	Anion	Binding Constant (M^{-1})
[3.c]	acetate	50
[3.c]	oxalate	7813
[3.c]	malonate	403
[3.c]	phosphate	252
[3.j]	acetate	2100
[3.j]	oxalate	100
[3.j]	malonate	807
[3.j]	phosphate	451

Table 3-10. Comparison of binding affinities for the mono- and binuclear europium complexes with a selection of anionic guests. Carried out in HEPES buffer at pH 7.6.

Comparisons of the affinities of different anions for the mono- and binuclear complexes revealed an interesting trend, with a marked difference between the smaller and larger anions. It was noted that the guests thought to be able to bridge across two metal centres, such as oxalate, the binding constants were higher for complex [3.c]. It was assumed that this was due to the ability of

these ditopic ligands to coordinate across both metal centres. Conversely, the affinities calculated for the smaller anions such as acetate and phosphate were higher for the mononuclear complex [3.j]. The result for malonate with mononuclear complex looks at first to be anomalously high. This is clearly not a consequence of bridging across two metal centres and so one must consider the accessible space at the metal centre in the two complexes. As in section **3.4**, this was estimated by calculating the number of bound solvent molecules at the metal centre.

Complex	$\tau(H_2O)$ / μs	$\tau(D_2O)$ / μs	q
[3.c]	620	1650	0.9
[3.j]	410	1560	1.8

Table 3-11. Comparison of luminescent lifetimes and q-values for complexes [3.c].and [3.j].

The increased hydration state of the metal in the pDO3A complex compared to in the dinuclear system is clearly indicative of greater accessible space at the metal centre. Indeed with approximately two water molecules coordinated, there is now perhaps sufficient coordinative vacancy at the metal centre to allow smaller guests such as acetate to act as bidentate donors, forming a four or five membered chelate ring of the type seen in reference 3. This would certainly go some way to explaining the increased binding constants observed for mononuclear pDO3A complex [3.j] with the smaller anions.

3.9 Reduction of the alkyne back-bone

The effects of the rigidity of the anionic guest have been extensively discussed so far in this chapter. Notable by its absence however is an investigation into the impact on self-assembly exerted by the flexibility of the back-bone linking the two binding domains in the metal complex itself. To this end, it was resolved to lift the conformational constraints imposed by the highly rigid back-bone by reducing the alkyne functionality, first to each of the daughter alkene isomers and finally to the fully saturated C_4-alkyl chain.

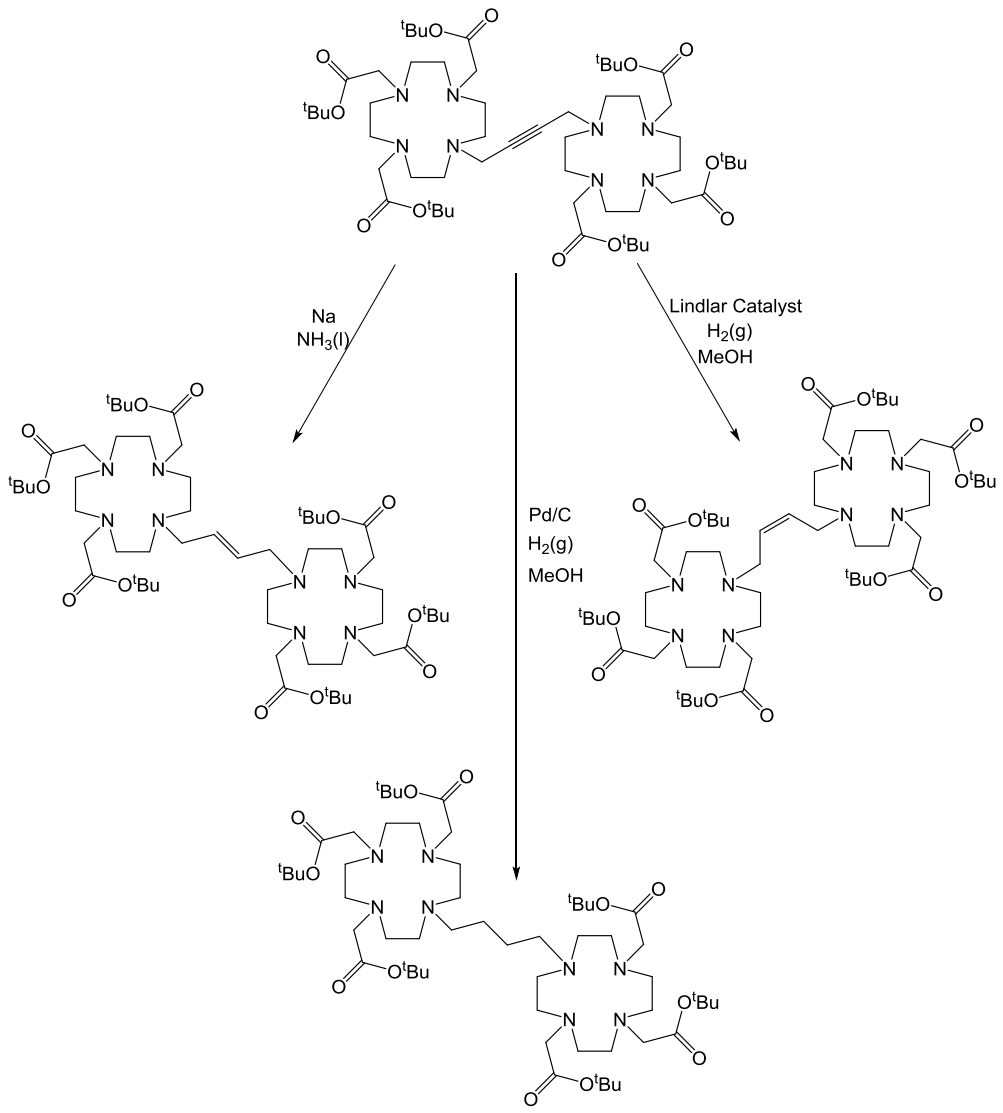

Scheme 3-3. Proposed conditions and reagents for the stereoselective reductions of the backbone of pro-ligand [3.a].

Reduction of the alkyne to the *cis*-alkene was attempted with a heterogeneous transition metal catalyst. To prevent over-reduction to the alkane, a partially poisoned catalyst was chosen. Lindlar's catalyst was suspended in dry methanol and the europium complex added. The resulting suspension was stirred under an atmosphere of hydrogen gas for 8 hours, but no reaction was detected. The peak at 2154 cm^{-1} in the IR spectrum, attributed to the alkyne mode persisted after the reaction and the ^{1}H-NMR spectrum remained unchanged. The process was repeated with both the free ligand and the *tert*-butyl protected pro-ligand but to no avail. Performing the reaction under high pressure in a bomb vessel charged with 4 bar of hydrogen also came to

nought. It was therefore supposed that the catalyst, detuned with surface-bound quinoline and lead to prevent over-reduction, was in fact insufficiently reactive to facilitate adsorption and reduction of the sterically hindered alkyne.

A related series of reactions was attempted using palladium on charcoal. This unpoisoned catalyst should have been significantly more reactive and indeed, in this case a change was observed in the reaction mixture. Due to the absence of lanthanide-induced shifts in the NMR spectra, the pro- and free-ligands were the simplest to study. Following treatment of the ester-protected pro-ligand with the Pd/C catalyst, the ^{1}H-NMR spectrum was similar to that of the starting material with the addition of a broad resonance at 5.61 ppm. This was tentatively ascribed to the presence of two alkene protons, which was surprising as the more active catalyst should, in theory, have fully reduced the alkyne to the alkane species. The identity of the partially reduced species was confirmed by ES^{+}MS with peaks observed at m/z = 1104, 1082, 552 and 541, corresponding to the $[M+Na]^{+}$, $[M]^{+}$, $[M+Na]^{2+}$, and $[M]^{2+}$ species respectively. IR spectroscopy showed the disappearance of the alkyne stretch at 2154 cm^{-1}. Increasing the reaction time, reaction temperature, catalyst loading and hydrogen pressure (individually at first, later together) did not result in further reduction.

Due to the mechanism of heterogeneous catalytic hydrogenation, it was presumed that the product observed was the *cis*-alkene linked species. However as the proton resonances were too broad to extract a coupling constant, it was not possible to confirm this. Furthermore, the recovered yield was very poor, possibly due to the alkene product adsorbing irreversibly to the catalyst surface. For these reasons, it was decided that hydrogenation of the parent alkyne-linked complexes was not a suitable methodology to access the desired targets.

Instead, direct attempts to synthesise the more conformationally flexible species were undertaken, taking advantage of protocols analogous to that used in the preparation of the initial alkyne complex. Two equivalents of the ubiquitous tri-*tert*butyl-protected cyclen core were treated with the appropriate dichloro- or dibromo-species in the presence of base.

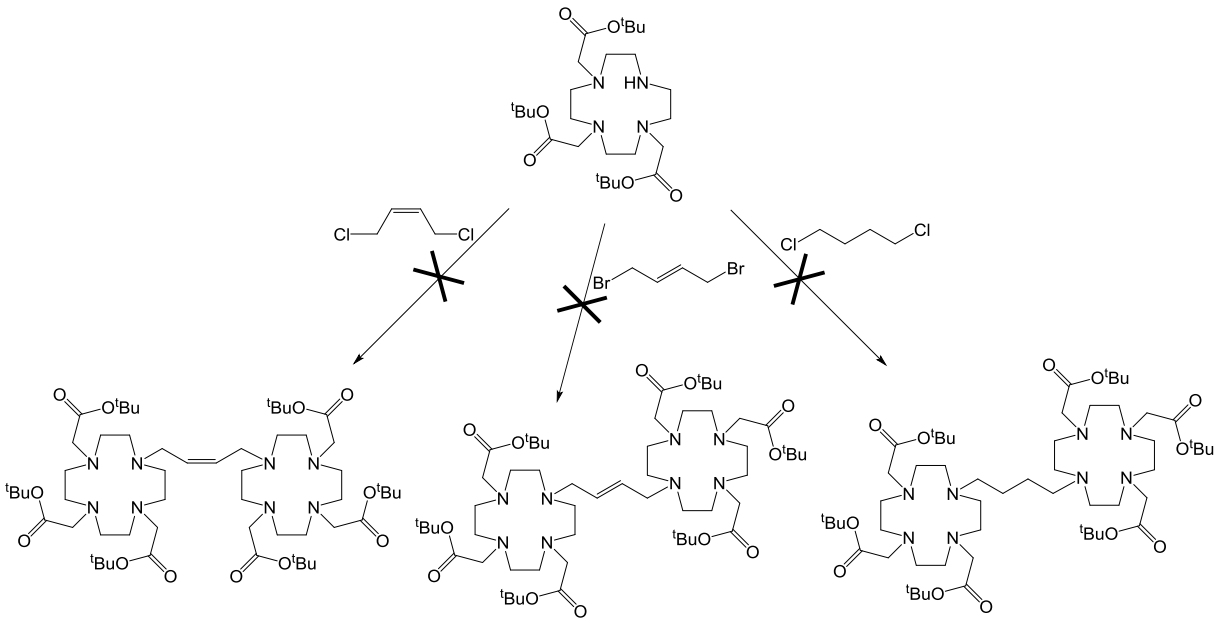

Scheme 3-4. Unsuccessful attempted synthetic attempts to produce the reduced backbone species by direct alkylation.

As perhaps should have been anticipated, in all cases the intramolecular reaction was significantly faster and thus dominated the intermolecular process. In fact it would appear to have been more through luck than judgement that in the examples studied so far, the linking unit has either been too short or too inflexible to allow intramolecular reaction. It was not possible in each case to assign the precise regio-chemistry of the product(s) formed, merely that they were not the desired targets. Based on the available spectroscopic data (and in particular, the fact that the molecules formed all seemed to bear a permanent positive charge), allied with chemical intuition, the following structures were proposed as the identities of the species generated.

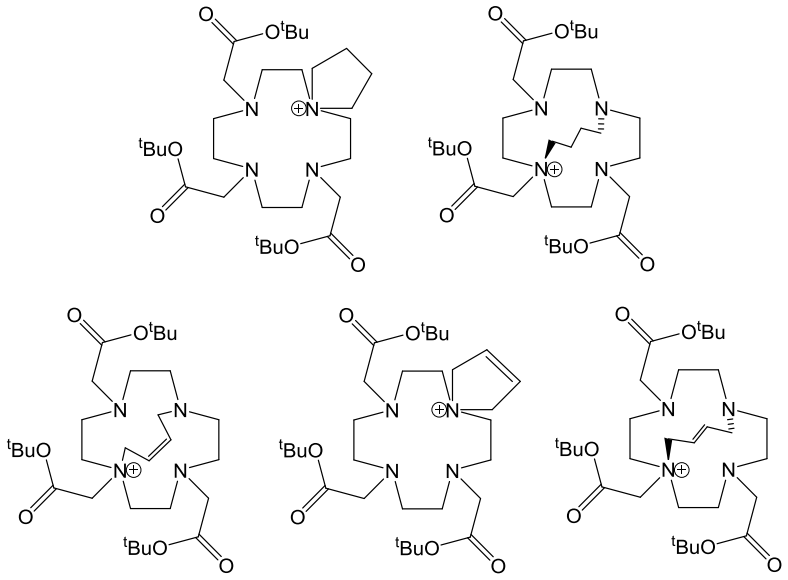

Figure 3-29. Speculated side products of the unsuccessful alkylation reactions.

3.10 Conclusion and Further Work

In this chapter it has been demonstrated that binuclear complexes undergo assembly with dianions in solution and these interactions have been monitored and studied using a variety of physical techniques. The overwhelming picture painted here is that in the solution-phase self-assembly of lanthanide complexes with anionic guests, the classical lock and key hypothesis is invalid and we must instead consider an induced-fit model. It is clear that the selectivity can be influenced and tuned by modifying the length and flexibility of the chain separating the metal cores and the donor groups of the guest, but achieving an absolute selectivity with complexes of this nature is very improbable due to the flexibility of the macrocyclic DO3A binding cavity itself.

It has been shown that the binding of chiral guest species can induce a complementary chirality at the metal centre, although weaknesses in the experimental method prevented a more thorough investigation.

Molecular models have been made and refined using semi-empirical methods in attempts to shed light on the coordination modes and molecular conformations of binding.

3.10.1 Synthetic Endeavours

In this chapter there have been instances where a full elucidation of the situation has been thwarted by the inherent limitations of the physical method or of the equipment. A key example is that of the attempted CPL measurements, in which the poor signal-to-noise ratio inherent to the apparatus made a definitive assessment of the chirality induced at the metal centre problematic. In making the measurements detailed earlier in this chapter, efforts were made to overcome this limitation through fine-tuning of the experimental set-up, from increasing the number of scans performed to cooling the sample. Ultimately however, populating the $^5D_0$ emissive state of the europium ion via excitation of the forbidden *f-f* transition meant that the intensity of luminescence from the sample was too weak to draw definitive conclusions. Thus far all the steps taken to improve the quality of the results centred on the optimisation of the physical methods. As an alternative and complementary line of inquiry, chemical efforts should be made to circumvent the problem of low luminescence output, through incorporation of a chromophore into either the ligand system or the chiral titrant guest. Ligand scaffolds which incorporate antenna units are of course commonplace and as has been seen in section **1.8** (and shall be further demonstrated in section **5.3**) sensitisation of luminescence via self-assembly with a chromophoric guest is also well documented. In this instance coupling of the chiral tartrate to a light-harvesting moiety through one of the hydroxyl groups in the C_2 and C_3 positions would be the most obvious line of enquiry.

Bimetallic complexes could offer a variety of advantages over their homonuclear counterparts due to the presence in a single molecule containing two different lanthanides reporting on different parameters via different physical mechanisms. In the field of theragnostic agents in particular, the potential for dual modality imaging and/or treatment is an attractive prospect indeed. There are however a number of difficulties associated with their preparation which must be overcome. In ligands such as [3.b], which have identical binding sites, the high kinetic stability of the DO3A site, so vital in defining speciation and preventing the release of toxic metals *in vivo*, is in fact a

hindrance when preparing heterometallic molecules. The fact that, once resident in a binding cavity, a lanthanide ion will remain there, means that treatment of the free ligand with a single equivalent each of two different metal salts will result in a statistical mixture of the different homo- and hetero-metallic possibilities. Due to the chemical similarities of the lanthanide elements, the separation of such a mixture, whilst not intractable, would certainly be challenging. Two main synthetic strategies have been used in the past when attempting to generate mixed-metal complexes. The first involves differentiating the binding sites in some way. In 2003, Pope and Faulkner prepared a mixed terbium-ytterbium species using such a strategy. DO3A-type cavities bearing terbium ions were appended to a central vacant DTPA-type binding domain which was then used to complex an ytterbium cation. In this system, intermetallic energy transfer allowed excitation of the terbium ions to sensitise emission from the ytterbium.[5] This is however unsuitable for application in the ligand system described in this chapter, as the metal sites must be equivalent for a true assessment of guest binding. Another way to differentiate the sites is to use orthogonal protecting groups to mask the two binding domains, allowing for selective and sequential deprotection and complexation at each site. Such an approach was utilised by Natrajan *et al*., protecting two DO3A-type cavities as ethyl and *t*-butyl esters which could be exposed under basic and acidic conditions respectively.[6] Whilst superficially elegant, such a strategy requires a long linear synthesis with thorough purification at each step and thus overall yields tend to be very low.

The only alternative remaining would be to make and separate the statistical mixture obtained from the 1:1 addition of ligand and lanthanide salt. The mono-nuclear metal:ligand adduct could then be treated with a second metal, yielding the hetero-metallic system. Preliminary attempts to exploit this methodology using reverse-phase HPLC to separate the statistical mixture have met with mixed success. The separation achieved was found to be reasonably efficient, but the yields recovered were poor and much of the reaction mixture was lost.

3.10.2 Further uses of molecular modelling.

The attempts in section **3.7** to model the binding interactions and conformational preferences of the various host-guest pairings, whilst interesting and instructive in providing a qualitative overview of the problem, told us little that was not already strongly suspected. To put the modelling to a more quantitative use and simultaneously gain more information about the molecular geometries required for binding, the predicted conformers should be correlated with data gathered from NMR studies of binding. As discussed in section **1.7**, the Bleaney equation can be used to predict the shift of a spin-active nucleus based on its position relative to a lanthanide ion. It should therefore be feasible to reverse the process and use the shifts of peaks to calculate spatial coordinates of the resonant nuclei and thus refine the model. The reasons that such an investigation has not already been undertaken are twofold. First, in the case of binuclear species such as complex [3.c], the two paramagnetic lanthanide ions will give rise to two separate magnetic axes. The Bleaney equation defines positions in a spherical coordinate set with the lanthanide at the origin and the magnetic axis aligned with the z-axis ($\phi = 0$).[7] Thus in evaluating the shift of a given nucleus, contributions would have to be considered from interactions with each metal centre. Even this however may not be sufficient, as it is possible that the two magnetic moments, close as they are in space, may couple to one another and thus further complicate proceedings. Second, recent work in the group has shown that changing the axial donor to a DO3A/DOTA-like complex can have a profound and sometimes unpredictable effect on the second order crystal field parameter B_0^2. It would therefore have to be determined whether changes in the shift were due to a movement relative to the metal centre, or due to a crystal-field induced change in the strength or orientation of the magnetic axis. Together these factors would make an analysis of this type conceptually and computationally non trivial and take it outside the scope of this work.

3.11 References

1. F. H. Allen, O. Kennard, D. G. Watson, L. Brammer, A. G. Orpen and R. Taylor, *Journal of the Chemical Society, Perkin Transactions 2*, 1987, S1-S19.
2. R. S. Dickins, S. Aime, A. S. Batsanov, A. Beeby, M. Botta, J. I. Bruce, J. A. K. Howard, C. S. Love, D. Parker, R. D. Peacock and H. Puschmann, *Journal of the American Chemical Society*, 2002, **124**, 12697-12705.
3. S. J. Butler and D. Parker, *Chemical Society Reviews*, 2013, **42**, 1652-1666.
4. M. Jauregui, W. S. Perry, C. Allain, L. R. Vidler, M. C. Willis, A. M. Kenwright, J. S. Snaith, G. J. Stasiuk, M. P. Lowe and S. Faulkner, *Dalton Transactions*, 2009, 6283-6285.
5. S. Faulkner and S. J. A. Pope, *Journal of the American Chemical Society*, 2003, **125**, 10526-10527.
6. L. S. Natrajan, A. J. L. Villaraza, A. M. Kenwright and S. Faulkner, *Chemical Communications*, 2009, 6020-6022.
7. B. Bleaney, *Journal of Magnetic Resonance (1969)*, 1972, **8**, 91-100.

4 Phosphorous Oxyanion Binding

4.1 Introduction

Phosphorylated sugars, nitrogenous bases and amino acids are amongst the most important anions found in nature. They fulfil crucial roles in many different biological systems, including energy sources (ATP), information storage and propagation (nucleosides and DNA) and cell differentiation and development (phosphorylated tyrosine, serine and threonine).[1-4]

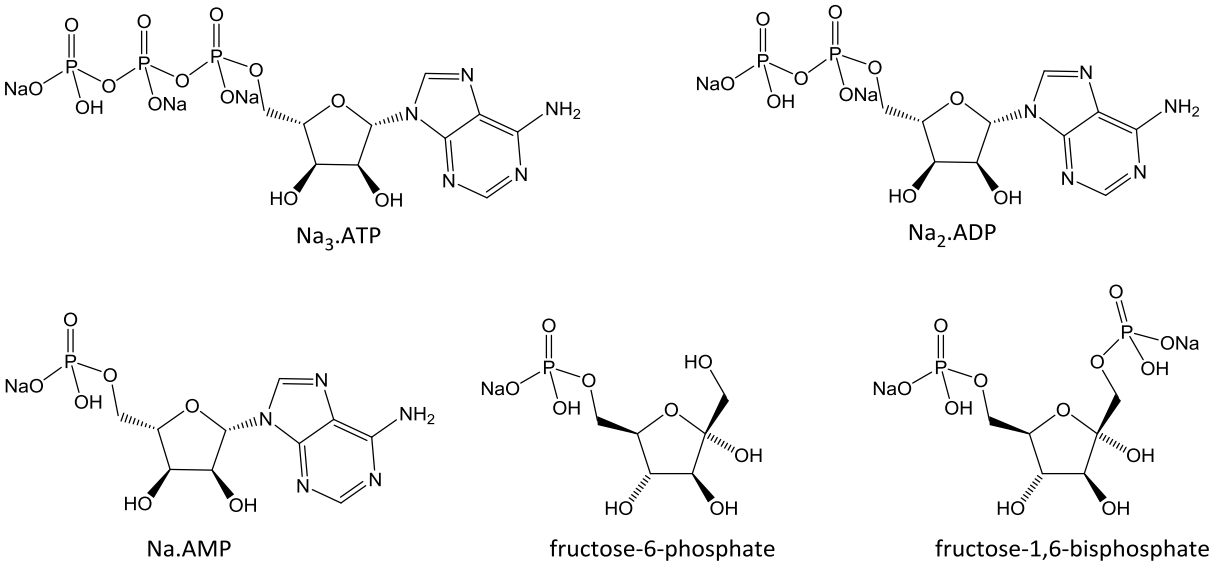

Figure 4-1. Molecular structures of some of the biological phosphate esters used in this chapter.

In biochemical reaction systems, the addition of a phosphate group to a substrate is a common method of increasing its reactivity.[5] ATP, the universal biochemical energy currency, acts in enzymatic processes to convert organic hydroxyl groups to charged phosphate esters, increasing their electronegativity. This has the added result of increasing the polarity of the reactive intermediates, thus ensuring that they cannot escape the reaction site across the phospholipid membranes which divide cellular environments and apparata. A prime example of a crucial pathway mediated by phosphorylated intermediates is glycolysis, in which one of the key intermediates is fructose-1,6-bisphosphate. It is this doubly phosphorylated sugar which is split

into two three-carbon fragments which then isomerise to enter the citric acid cycle and it is therefore a key focus in the study of glucose metabolism. Attempts to image this pathway began with studies of the rate of glucose transport and metabolism using radiolabeled tracers such as FDG,[6] but have been extended to other techniques such as ^{1}H-glucoCEST[7] and ^{31}P-MRS.

Phosphorus magnetic resonance spectroscopy (^{31}P-MRS) has been used to provide a non-invasive clinical method to assess *in vivo* bioenergetic changes, by comparing the intensities and shifts of the resonances corresponding to various phosphorus-bearing species.[8, 9] Of particular interest are the concentrations of the high-energy phosphates, ATP and phosphocreatine and the ratio of these to their lower energy analogues ADP and inorganic phosphate (P_i). Used in conjunction with conventional T_1-MRI, localised ^{31}P-MRS can be used to correlate structural features with metabolic processes, leading to a clearer understanding of the link between cellular biochemistry and the pathology and progression of diseases, without the need for living tissue biopsy. Indeed this technique has been used extensively in the diagnosis and assessment of myocardial infarction, where the concentrations of ATP and phosphocreatine have been found to correlate strongly with the viability of the cardiac tissue.[10] There are two primary disadvantages of ^{31}P-MRS. The first is one of poor spatial volume resolution. At its most sensitive, ^{31}P-MRS can achieve a voxel volume of the order of 1 cm^3, which is approximately equal to that of the more common PET techniques.[11] The second main drawback is that of long acquisition times. In ^{1}H-MRI, an adequate signal to noise ratio can be achieved with short acquisition time due to the massively high abundance of water in biological media. Phosphorus on the other hand is significantly less common, with typical human tissue total concentrations in the region of 10 mM, split between the various phosphate esters and P_i. The situation is compounded by the fact that the phosphate esters all display very similar chemical shifts and thus a high spectral resolution and signal to noise ratio is required to accurately distinguish between them. A search of literature available at this date reveals a distinct paucity of phosphorus contrast or shift agents and the few examples that are present are non-endogenous phosphorus compounds which report on their local environment through changes in

the shift of the phosphorus nuclei. There have been very few successful attempts towards a contrast agent which works by selectively shifting or enhancing the relaxation of the resonances of common endogenous phosphates. Such agents, should they be achieved, would present useful advantages. By moving selected resonances out of the standard range, the number of scans required to discern the different resonances would fall dramatically, reducing the clinical acquisition time. Alternatively, by using the same scanning parameters and longer acquisitions, shifting the resonances would result in a significant enhancement of spatial resolution.[12, 13] Phosphorus oxy-anions have been shown to be capable of coordinating to coordinatively unsaturated lanthanide complexes in solution[14] and so it was therefore decided to investigate whether any of the lanthanide complexes thus far prepared would be capable of acting in this capacity.

4.2 Luminescence Binding Studies

As any modulations in the shift or relaxation of the phosphorus nuclei will occur when they are proximate to the metal centres, the first stage in assessing the ability of a complex to act as a contrast agent, was to ensure that the phosphate molecules did in fact bind to the metal complex. To that end, luminescence screening studies were carried out, titrating the binuclear europium complex [3.c] against a variety of targets as show in figure 4-2.

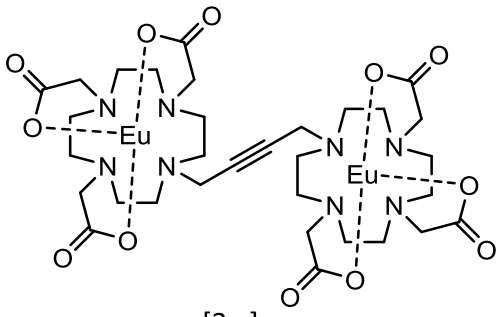

[3.c]

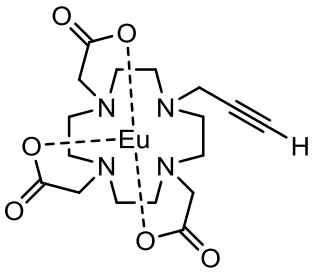

[3.j]

Figure 4-2. Structures of complex [3.c] and [3.j] used in this chapter.

In making these measurements, residual fluorescence from the aromatic titrants was found to be present and to overlap with the metal-based emission, obscuring the desired signal. A longer time

gate was therefore introduced to allow scattered light and short-lived organic autofluorescence to decay before data acquisition began. The binding constants calculated are displayed in table 4-1.

Titrant	Buffer	pH	K (M^{-1})	99% Confidence Interval
Na.AMP	HEPES	7.7	298	290.64 - 305.07
Na_2.ADP	HEPES	7.6	424	408.43 - 440.72
Na_3.ATP	HEPES	7.6	695	647.89 - 746.11
fructose-6-phosphate	PBS	7.6	NBD	-
	HEPES	7.6	NBD	-
fructose-1,6-bisphosphate	PBS	7.7	2848	2619 - 3104
	HEPES	7.7	2521	2243 - 2840
$Na_3.PO_4$	HEPES	7.7	252	223 - 283

Table 4-1. The binding constants and confidence intervals calculated for the interactions between complex [3.c] and different phosphate guests in different buffer systems. NBD : No Binding Detected.

In the cases of the phosphorylated nucleosides (AMP, ADP and ATP), the binding event was observed by a marked increase in luminescence intensity in the ΔJ = 1,2,3,4 peaks and a slight decrease in the ΔJ = 0 peak. Changes in the local symmetry at the metal centre were confirmed by a change in the ratio of the hypersensitive ΔJ = 2 peak to the other transitions. Plots typical of those acquired are shown in figure 4-3.

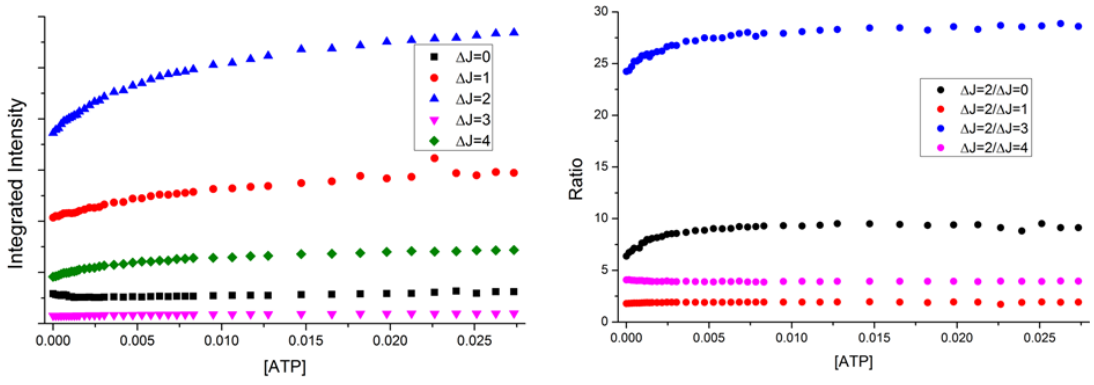

Figure 4-3. The integrated intensities (left) and peak ratios (right) of the luminescence of complex [3.c] as a function of ATP concentration. Recorded in HEPES buffer at pH 7.6.

It was also noted that increasing the length of the phosphate-ester chain appended to the adenosine unit gave increase in the binding affinity with the metal complex. The pK_a of the terminal phosphate group does decrease very slightly with chain length but in all cases, speciation will be similar at the pH of the experiment. It is possible that the longer the chain, the more readily a binding conformation could be adopted, with the terminal phosphate coordinating to one metal centre and the β or γ groups or a donor from the adenylyl group binding to the other.

Modulation of the spectral form of the ΔJ = 1 peak was also observed in all cases, with changes to the relative weightings of the different Stark components of the transition as shown in the inset in figure 4-4. In inorganic ionic solids, analysis of the form of the ΔJ = 1 peak has been used to assign the local symmetry at the metal centre. In aqueous solutions, the fluxionality of the organic ligand, allied with the low symmetry environment make an absolute assignment infeasible, but as explained in section **1.4**, changes in the spectral form of the ΔJ = 1 peak can be qualitatively correlated with a change in local symmetry and more specifically, with the nature of the donor occupying the axial coordination site left vacant by the macrocyclic ligand. In all cases, the nature of the spectral change was the same. In the starting HEPES buffer solution, the ΔJ = 1 band consisted of two resolvable but broad peaks, the first at 590 nm and the second at 596 nm, with the former being more intense than the latter. As binding occurred over the course of the titration, both peaks grew in intensity and both were slightly blue-shifted. The relative changes to these peaks occur to differing degrees, so that by the end point, the higher energy peak had shifted to 589 nm, whilst the lower came at 593 nm and was the more intense of the two.

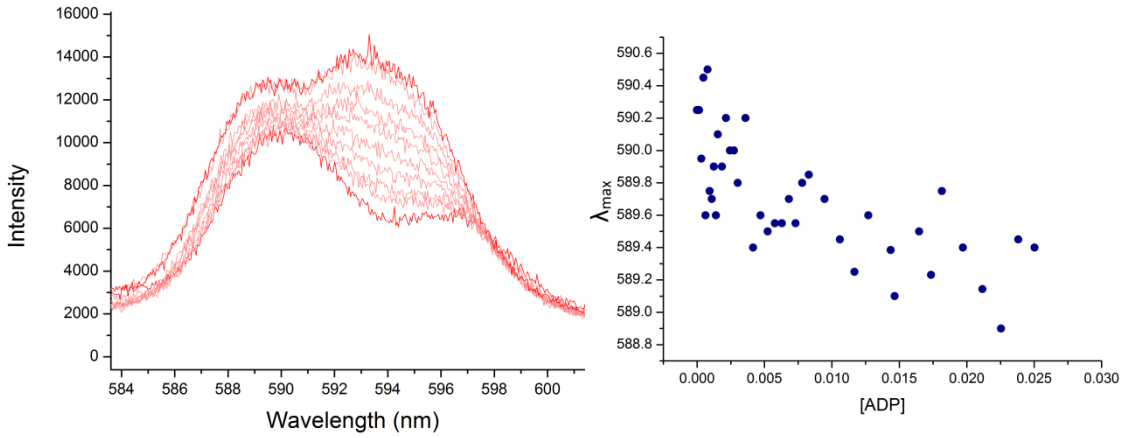

Figure 4-4. Left - the ΔJ = 1 band of successive emission spectra of complex [3.c] recorded with increasing ADP concentration. Right - the wavelength of the ΔJ = 1 emission maximum as a function of ADP concentration.

The ΔJ = 2 peak also underwent a blue-shift over the course of the titration, as shown in figure 4-5.

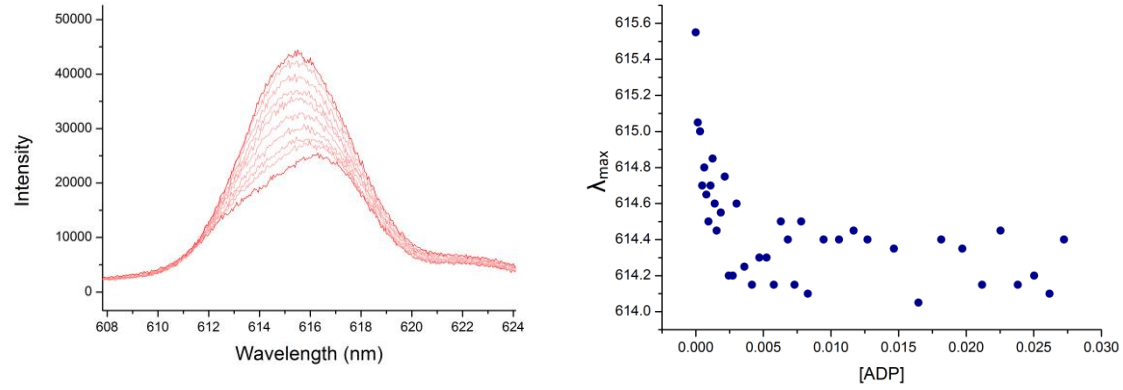

Figure 4-5. Left - the ΔJ = 2 band of successive emission spectra of complex [3.c] recorded with increasing ADP concentration. Right - the wavelength of the ΔJ = 2 emission maximum as a function of ADP concentration.

Finally, it should be noted that the ΔJ = 4 band also evolved upon binding, with both the major component peaks undergoing a red-shift. The higher in energy of the two peaks shifted from around 688 nm to 690 nm by the end point of the experiment, whilst the lower energy of the pair moved from 699 nm to 700 nm.

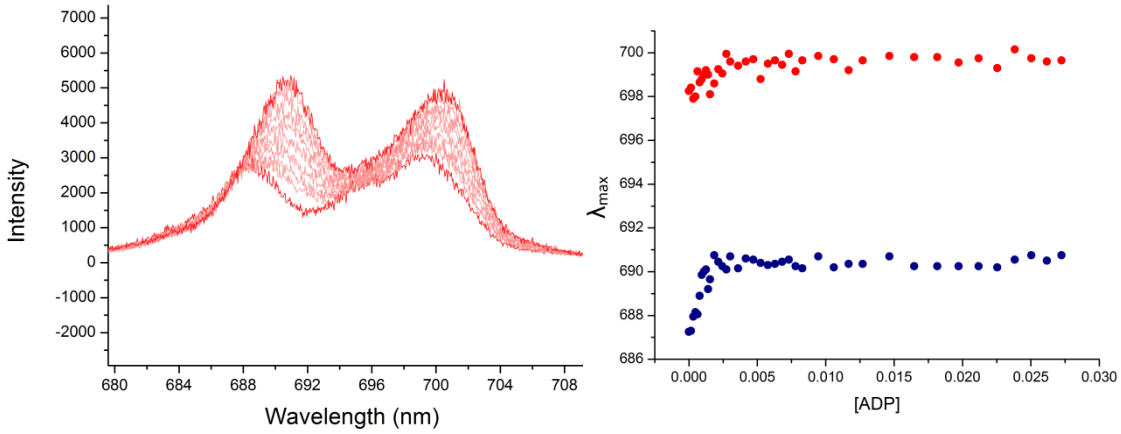

Figure 4-6. Figure 4-7. Left - the ΔJ = 4 band of successive emission spectra of complex [3.c] recorded with increasing ADP concentration. Right - the wavelength of the ΔJ = 4 emission maximum as a function of ADP concentration.

Plotting the wavelengths of the emission maxima of the component peaks of the ΔJ = 1, 2 & 4 bands against the concentration of phosphate titrant provided a further set of curves which could be used to calculate affinity constants. In all cases, the values obtained by this method were in close agreement with those derived from the integrated intensity and peak ratio metrics, despite the low signal-to noise ratio inherent in this particular parameter. These changes are all consistent with a change in the second order crystal field parameter B_0^2 upon changing the axial donor from a water molecule to a phosphate ester group.

In contrast to the nucleosides, binding of fructose bisphosphate to the metal centre resulted in a decrease in the luminescence intensity in all the different ΔJ peaks. As noted previously however, the ΔJ = 1 and ΔJ = 4 bands were found to undergo qualitatively similar changes in their spectral form. This is consistent with the supposition that changes in these peaks are related to the nature of the axial donor. In both cases a bound water molecule is being exchanged for a phosphate group and thus we would expect to see broadly similar changes across all such titrations. The decrease in luminescence intensity upon the binding of fructose bisphosphate could either be a consequence of PET or LMCT deactivation of the europium centre by the sugar guest, or could be a result of increased O-H quenching as the hydroxyl groups on the sugar backbone are brought close to the metal centres upon binding.

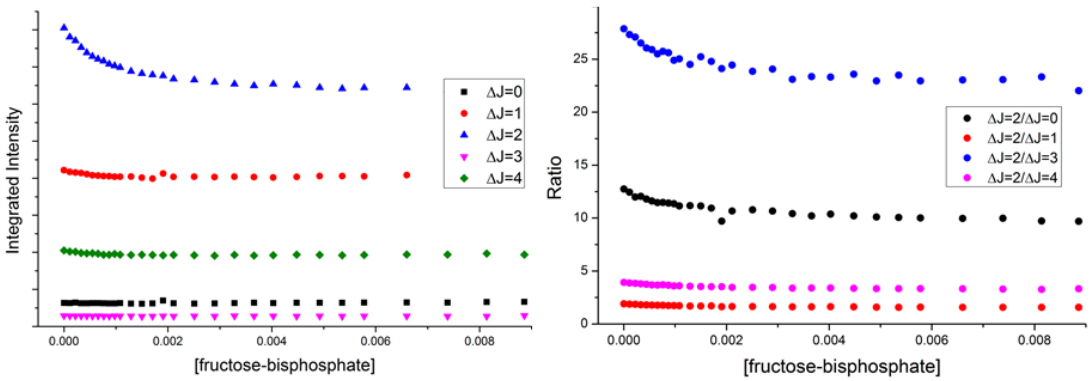

Figure 4-8. The integrated intensities (left) and peak ratios (right) of the luminescence of complex [3.c] as a function of fructose-1,6-bisphosphate concentration. Recorded in HEPES buffer at pH 7.7.

Of all the phosphates tested, by far the greatest affinity was shown by fructose-1,6-bisphosphate. This is most probably due to the spacing between the phosphate groups presenting a good fit to the binding cavity of the host complex. Furthermore, the values obtained for the equilibrium constants in HEPES and PBS were within error of one another.

Fructose phosphate on the other hand, was not found to bind at all to the ditopic europium complex, indicating that, at least in the case of the sugars, coordination to both metal centres is required to overcome desolvation of the guest species. A potential complication arises however, from the speciation of fructose-1,6-bisphosphate in solution. In aqueous conditions at neutral pH, the unsubstituted sugar exists as an equilibrium mixture of structural isomers; namely, the open chain, five-membered furanose and six-membered pyranose structures. For the parent fructose, the mole fractions are typically <5%, 25% and 70% respectively. In the case of the bisphosphate however, the situation is simplified somewhat as the conversion of the hydroxyl groups in the 1 and 6 positions to phosphate esters prevents the intramolecular attack leading to the 6-membered pyranose ring and hence only the straight chain and furanose isomers are available.[15]

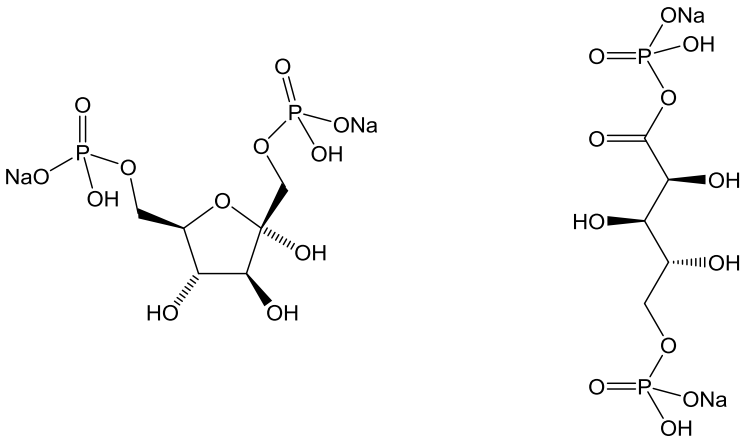

Figure 4-9. Furanose (left) and open ketone (right) isomers of fructose-1,6-bisphosphate.

In an effort to understand the role played by the organic components of the various phosphorylated species, the affinity of the complex for simple inorganic phosphate was probed. Obviously it was only possible to carry out this experiment in HEPES buffer due to the presence of phosphate species in PBS. At the pH of the experiment (7.74), complex [3.c] was found to have a binding constant with Na_3PO_4 of 252 M^{-1}. This is significantly lower than might be expected by chemical intuition, as phosphate is a hard anion with high charge density. Indeed, precipitation of the lanthanide ions as sparingly soluble phosphate salts has been suggested to be one of the key processes causing nephrotoxicity in kinetically labile contrast agents. One likely contributing factor is the high thermodynamic cost of desolvation of an anion so capable of hydrogen bonding with the surrounding environment. More significant however is that upon closer examination of the solution-phase speciation, it is revealed that at pH 7.74, the dominant species present is the HPO_4^{2-} dianion and approximately 15% of the total phosphate exists as $H_2PO_4^-$. This reduction in charge density could partially explain the anomalously low affinities. The third pK_a for PO_4^{3-} is approximately 12.9, meaning that to probe the binding of the trianionic species, the titration would have to be carried out at a pH higher than this. This is well outside the operating range of any of the non-coordinating buffers and indeed is so high that colloid formation and precipitation would most likely render any results meaningless.

In section **2.3**, it was noted that stronger binding was observed when a phosphate anion-based buffer was used in place of the allegedly non-coordinating HEPES, indicating that either HEPES was in fact coordinating to the metal centre (and doing so more strongly than the phosphate species in PBS), or that it was in some way assisting in the solvation of either host or guest and thus making association less favourable. The first of these hypotheses is readily disproved on the basis that titration in HEPES with sodium phosphate lead to a change in luminescence. However, this observation does not help in determining the veracity of the second. To gather further information, ^{1}H-NMR spectra were recorded of the binuclear complex [3.c] in D_2O buffered with HEPES or PBS. As the solution-phase structure has already been shown to display a strong dependence on ambient pH, the pD in each instance was adjusted to 7.5 using NaOD and DCl.

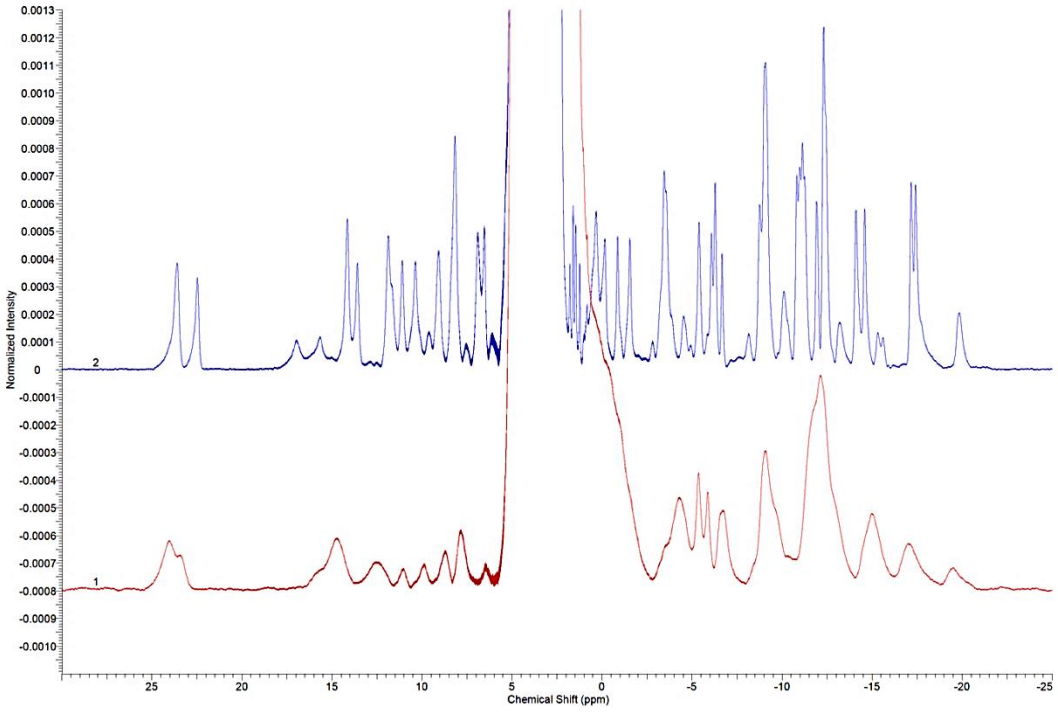

Figure 4-10. Paramagnetic ^{1}H-NMR spectra of complex [3.c] in PBS (blue trace) and HEPES (red trace) in D_2O at pD 7.5.

For the spectra recorded in HEPES, the resonances observed are broad, indicating an intermediate exchange between isomers on the timescale of the measurements. By contrast, in PBS the peaks are more numerous, sharper and much better defined, implying slow exchange between chemical environments. This can be rationalised by the different coordinative properties of the two buffers

and the pathway by which the isomers of the complex interconvert. As has already been shown, the anionic phosphate species which comprise the PBS buffer system are suitable donor groups for the hard lanthanide cations and thus they coordinate to the metal centres in solution. Conversely, HEPES is thought to be a non-coordinating system. Furthermore, as stated in section **1.7**, the most likely energetic route leading to exchange between the isomers of DO3A-type complexes involves decoordination of the axial donor at the metal centre (most commonly solvent), followed by a rearrangement of the ligand and then resolvation. The non-coordinating nature of HEPES means that the apical donor will most probably be water in relatively fast exchange with the bulk solvent. In PBS however, the donor group filling the site left vacant by the ligand is more likely to be a coordinated phosphate group. Being negatively charged, the residence time on the metal centre is likely to be substantially higher and thus the isomer exchange will be slower. This then adds further weight to the supposition that HEPES is non-coordinating, leaving the decreased anion affinities in this buffer unexplained.

Since the phosphates of adenosine all displayed low affinities, close to that of simple inorganic phosphate, it was hypothesised that any binding occurring was taking place through just one of the phosphate groups at a single metal centre. That the binding curves were found to best correspond to a model of 1:1 binding however, would indicate that the metal cores are in sufficiently close proximity that the binding of a guest at one centre effectively blocked the other site, thus stopping the reaction at the bimolecular stage and preventing the formation of a 1:2 adduct. Once again, the mononuclear europium complex of pDO3A [3.j] was used to further probe this supposition. If the theory postulated above were in fact the case, one would reasonably expect the phosphates to show similar interactions with the single-core complex, most probably with increased affinities due to reduced steric crowding around the metal centre. If however the electrostatic attractions of two nucleophilic donor groups to two separate metal centres are required to securely bind the nucleoside to the complex, then switching to a

mononuclear system should result in a dramatic decrease in binding strength. The affinities of [3.j] (europium p-DO3A) for the adenylyl-phosphates are shown in table 4-2.

Titrant	Buffer	pH	K (M^{-1})	99% Confidence Interval
Na_3PO_4	HEPES	7.6	451	442.7 - 460.04
Na_2.ADP	PBS	7.7	984	931.6 - 1036.8
	HEPES	7.6	2307	1989.2 - 2650.7
Na_3ATP	PBS	7.7	1239	859.6 - 1849.0
	HEPES	7.6	2910	2345.1 - 3491.7

Table 4-2. The binding constants and confidence intervals calculated for the interactions between complex [3.j] and selected phosphate guests in different buffer systems.

All binding was once again found to be in best agreement with a model describing the formation of a 1:1 adduct. The binding constants are all markedly higher than those observed with the binuclear complex [3.c], adding credibility to the theory that binding in the ditopic system is occurring at just one of the metal centres through one of the phosphate moieties, most likely the terminal group. One can rationalise the greater binding constants arise from the more open, less hindered metal site, allowing reduced steric repulsions between the incoming phosphate and the ligand. Indeed it is possible that at the more open metal centre of the mononuclear complex, the terminal phosphate group is capable of acting as a bidentate donor, coordinating through two oxygen atoms to form a four membered chelate ring (see section **3.4**).

With this in mind, it was possible to put forward another rationalisation for the increase in binding affinities as the number of phosphate groups is increased; namely, that the longer the flexible polyphosphate ester chain, the greater the ability of the rest of the nucleoside to adopt a conformation which reduces any steric interactions between the nitrogenous base portion of the guest and the rest of the complex, whilst still allowing an unhindered approach for the donor phosphate group, maximising enthalpic gain from the electrostatic interaction.

4.3 NMR Studies

^{1}H-NMR spectra were measured in the absence and presence of the titrant phosphates in an attempt to correlate any binding events with a structure change in the host complex. The pH-dependence of complex [3.c] has already been well documented so in all cases, the samples were buffered. Phosphate buffered saline was selected, as the other buffers used in this work (such as HEPES and TRIS) have protons of their own which could obscure the less shifted parts of the target spectrum. Spectra were recorded of the host complex [3.c] in the presence of a large excess of the guest phosphate (10 molar equivalents). Shown in figure 4-11, for example, is the ^{1}H-NMR spectrum recorded upon addition of the sodium salt of AMP.

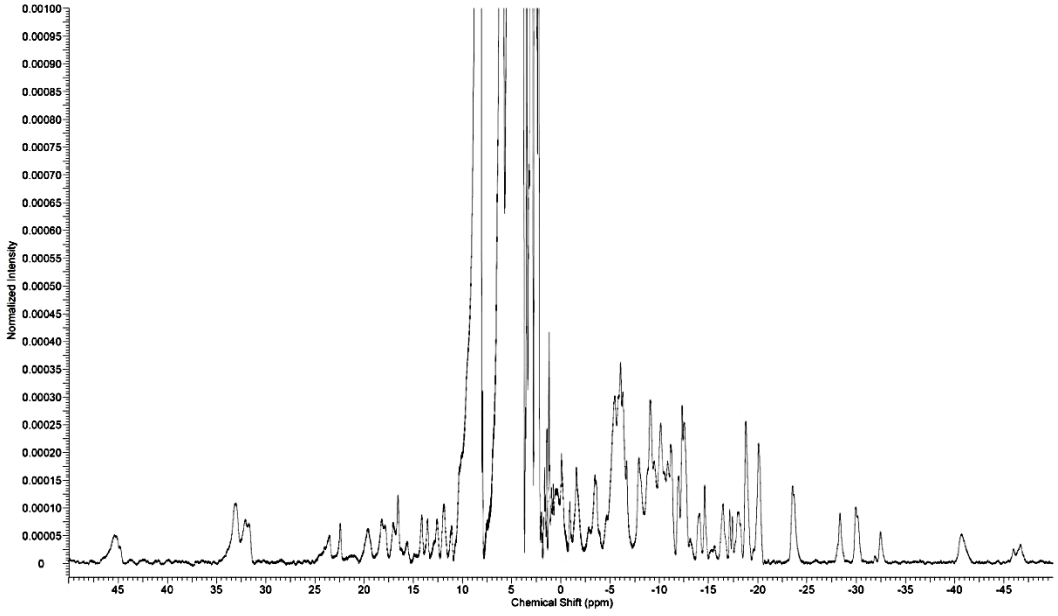

Figure 4-11. Paramagnetic ^{1}H-NMR spectrum of complex [3.c] treated with Na.AMP. Recorded at 298 K in D_2O, pD 8.

It is immediately apparent that binding of the anion results in dramatic spectral changes. First we observe peaks with a far greater shift, out to +/- 45 ppm. This could be due to an increase in the crystal field parameter B_0^2 as a result of exchanging the bound water for a more electron-rich phosphate donor group. The spectra recorded in the presence of the other nucleoside phosphates, ADP and ATP were found to exhibit qualitatively similar effects, with the shift of the most shifted peaks decreasing as the length of the phosphate ester chain increased.

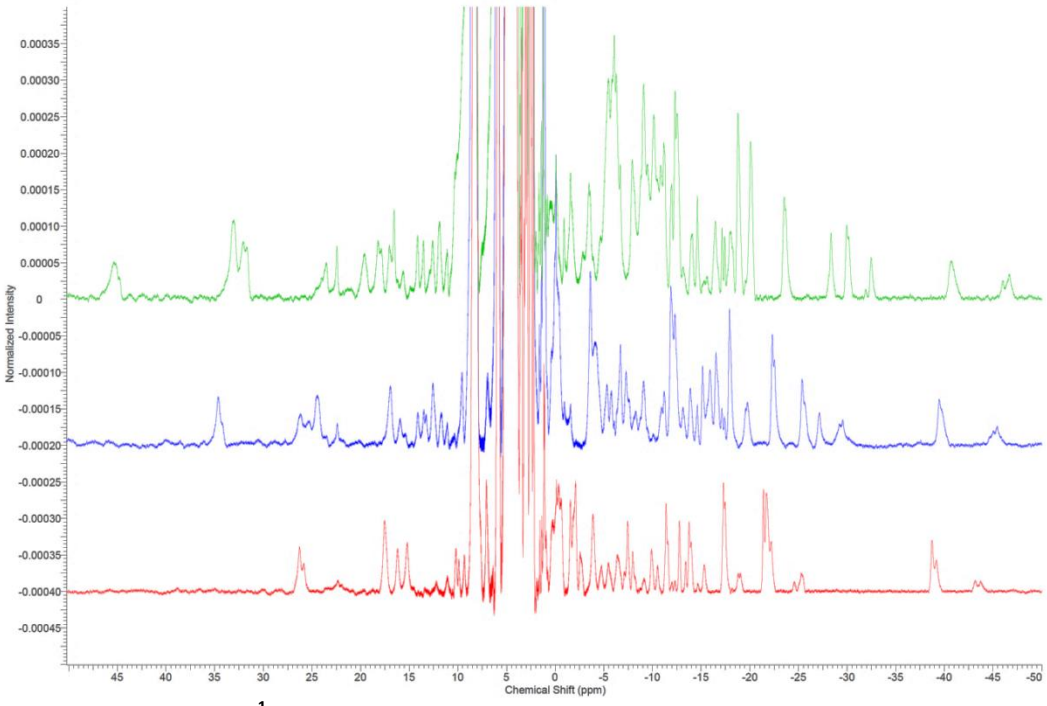

Figure 4-12. Paramagnetic ^{1}H-NMR spectra of complex [3.c] with 10 molar equivalents of AMP (green trace), ADP (blue trace) and ATP (red trace). All recorded at 298 K in D_2O, pD 8.

The extent to which the shifts change between the different nucleoside phosphate esters is too great to be attributed to changes in the crystal field. It is true that the length of ester chain affects the electron density on, and thus the donor capabilities of the terminal phosphate group but such differences are slight. Far more likely is that the binding of the guest enforces a change in the macrocycle geometry, causing the methylene protons of the ring and arms to change in position relative to the paramagnetic axis. The shorter the phosphate ester chain, the closer the bulky adenosine group is to the macrocycle and hence the greater the steric strain, leading to a larger deflection in geometry. This hypothesis would support the earlier observation that affinities increase with the number of phosphate groups in the chain.

It has thus far been assumed that as the protons of any guest species are unlikely to be closer to the paramagnetic metal centre than those of the macrocyclic cage, it is highly doubtful that the most shifted resonances correspond to anything other than the protons of the host. This assumption however was predicated upon the binding of the guest to both metal centres. As has been discussed, there is a weight of evidence that suggests that this is not the case and in fact only one metal is involved in binding to a phosphate group. Such a binding mode could result in

the nitrogenous base portion of the guest molecule being held close in space to the second lanthanide centre. This then raises the possibility that the most shifted resonances do not in fact arise from the protons of the macrocycle but from those of the adenosine unit (either of the purine ring system or the ribose sugar moiety) and are shifted due to their close proximity to the second metal core. The longer the flexible phosphate ester chain, the further the adenosine unit is from the second europium ion and thus the less shifted the resonances of its protons.

The addition of fructose-1,6-bisphosphate elicited a different but similarly marked response in the form of the paramagnetic ^{1}H-NMR spectra. In this instance, the more shifted peaks of the complex are fewer in number and significantly broader than they were in the cases of the adenosine phosphates. This would imply that even though fructose bisphosphate is binding more strongly than the phosphorylated nucleosides, it is still in intermediate exchange with unbound bulk bisphosphate. Alternatively, it may be the case that there is exchange between the isomers of the fructose bis-phosphate whilst it is coordinated, leading to an enforced change in the geometry of the metal complex to match the change in shape of the guest.

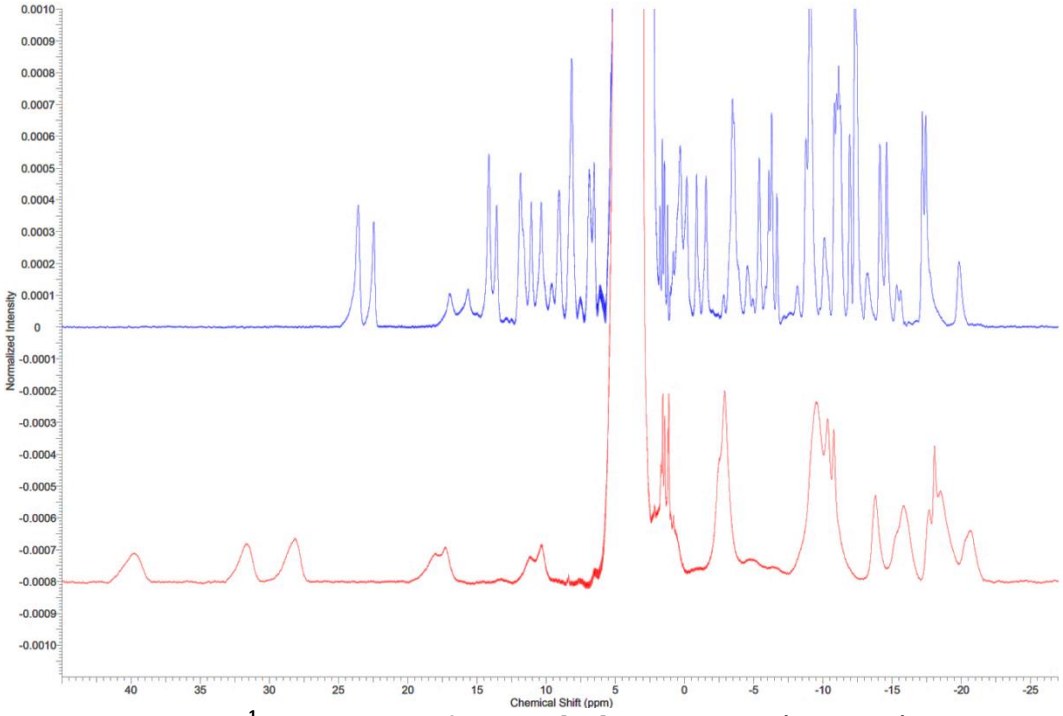

Figure 4-13. Paramagnetic ^{1}H-NMR spectra of complex [3.c] in the absence (blue trace) and presence (red trace) of 10 molar equivalents of fructose-1,6-bisphosphate. Recorded at 298 K in phosphate buffered D_2O, pD 8.

In an attempt to discern the effects of binding upon the guest as well as the host, standard diamagnetic proton NMR spectra were also recorded. Figure 4-14 shows the 'normal' shift region of the spectrum of fructose-1,6-bisphosphate before and after the addition of 5 molar equivalents of [3.c]. Even prior to the addition of the europium-bearing species, it is apparent that the spectrum is too complex and displays more peaks than can be assigned to a single isomer, providing further evidence for complex speciation in solution. Addition of the binuclear europium species [3.c] resulted in a number of spectral changes.

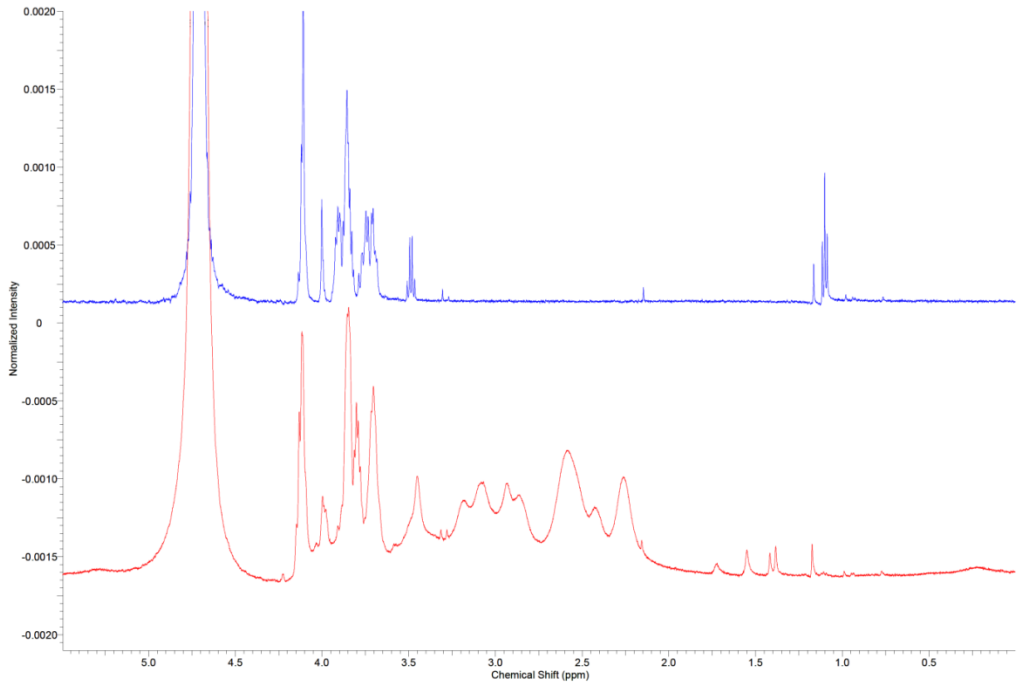

Figure 4-14. Diamagnetic ^{1}H-NMR spectra of fructose-1,6-bisphosphate in isolation (blue trace) and in the presence of complex [3.c] (red trace). Recorded at 298 K in D_2O, pD 8. Obviously, with the addition of new proton environments in close proximity to the paramagnetic centres in the host complex, one would reasonably expect to see new, broadened resonances and indeed this is found to be the case. What is more interesting however is the evolution of the peaks which correlate with those in the spectrum of the pure fructose bisphosphate. All are seen to undergo significant broadening with loss of splitting upon introduction of the europium complex, with slight changes in shift also observed. It is interesting to note that the intensities of the peaks change relative to one another. This may indicate a change in the balance of isomers present, or may simply be a consequence of spectral overlap with signals arising from the protons of the complex.

Up to this point it has been a tacit assumption that due to the high charge density and nucleophilicity of phosphate groups the association of these phosphorylated biomolecules and the ditopic europium species will occur via coordination of these donor groups to the metal centres. It is therefore reasonable to assume that in pairings where binding does occur, the phosphorus nuclei of the bound phosphate groups will be in close proximity to the paramagnetic lanthanide nuclei and will thus experience a lanthanide-induced shift in the ^{31}P-NMR spectrum. As it demonstrated the highest affinity of all the phosphates as measured by luminescence, fructose 1,6-bisphosphate was selected to test if the binding event was observable via ^{31}P-NMR. Spectra were taken of the sugar bisphosphate, first in isolation and then in the presence of complex [3.c].

As discussed in section **4-2**, fructose-like sugars are capable of interconverting between several different isomers in the solution phase. This is evident in the initial spectrum, where four different resonances are observed (shown in figure 4-15), despite there ostensibly only being two different phosphorus environments.

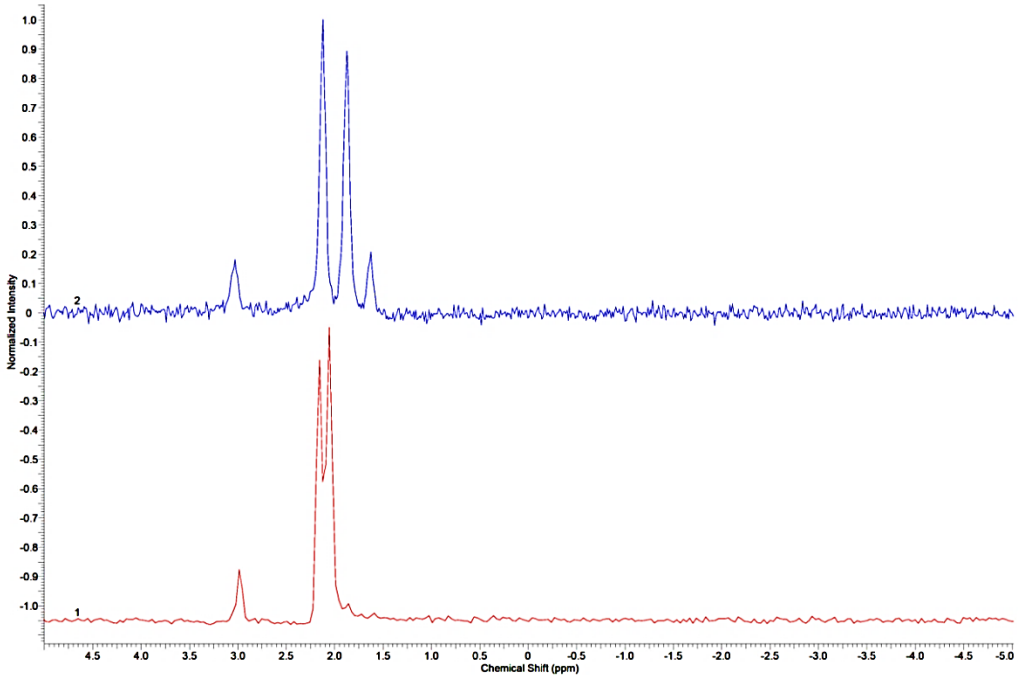

Figure 4-15. ^{31}P-NMR spectra of fructose-1,6-bisphosphate in the absence (blue trace) and presence (red trace) of complex [3.c]. Recorded at 298 K in D_2O.

Addition of complex [3.c] resulted in changes to the spectrum and again, the different peaks evolve differently upon addition of the host complex. This could merely be as a result of

incomplete binding. At 2521 M^{-1}, the binding constant calculated for this particular host-guest pairing means that even with an excess of complex, some of the fructose-bisphosphate will still be present as the unbound form. Since the magnitude of lanthanide-induced shift displays a strong dependence on distance from the lanthanide centre, only the fraction of the population actually bound to a metal centre will display any changes. An alternative rationalisation is that only one of the isomeric forms is capable of binding to the complex. Thus binding would depopulate one side of the isomer exchange equilibrium, pulling the equilibrium point over and hence altering the ratios of the peaks observed.

4.4 Conclusions and Further Work

In this chapter it has been shown that biologically important phosphate esters associate with mono- and binuclear lanthanide complexes in solution. Perhaps unsurprisingly, the binuclear complexes display selectivity for bidentate phosphates that can chelate to both lanthanide centres, such as fructose-1,6-bisphosphate.

In studying the binding of the different phosphate esters of the nucleoside adenosine two different possible explanations were offered to rationalise the behaviour of the shifted resonances in the ^{1}H-NMR spectra. These might be profitably investigated further by performing similar binding studies with the other nucleosides; guanosine, cytidine and methyl-uridine. If it is indeed the case that the most shifted resonances are from the peaks of the nitrogenous base portion of the guest, one would certainly expect to see a marked difference in the form of the spectra. If, on the other hand, the first hypothesis is correct and the change in shift is due to different host binding conformers enforced by steric interactions with the guest, then changing the bulk of the nucleoside by swapping the double-ring purine adenine for a single-ring pyrimidine such as thymine or cytosine should also have an effect.

Another area that merits further investigation is in the study of ^{31}P contrast media, which (as noted earlier in this chapter) is woefully underexplored. These results have shown that the

binding constants of even the most strongly bound species are relatively low, and that all systems are in exchange with bulk on the timescale of the NMR experiment. Dramatic enhancements of the T_1 relaxation time of ^{31}P nuclei could be anticipated as a consequence of phosphates binding to gadolinium complexes and these should translate to enhancements of the observed T_1 for the same phosphate in bulk solution. This would open the possibility of a phosphorus-based imaging methodology, where the method is essentially analogous to that of proton MRI which is so widely used today. Endeavours have therefore already been made within the group to measure the phosphorus relaxivity of complexes such as these. On the basis of these results, others within the Faulkner group have already begun to explore such possibilities, demonstrating that Gd.p-DO3A can enhance the ^{31}P relaxation rate observed in bulk solution by a factor of around 400 $mM(Gd)^{-1}s^{-1}$.[16] It remains to establish whether complexes that are selective for a single species can play a role in deconvoluting the phosphate speciation involved in glycolysis.

4.5 References

1. F. H. Westheimer, in *Phosphorus Chemistry*, American Chemical Society, Editon edn., 1992, vol. 486, pp. 1-17.
2. A. J. Cozzone, *Annual Review of Microbiology*, 1988, **42**, 97-125.
3. J. Berg, J. Tymoczko and L. Stryer, *Biochemistry*, 5 edn., W.H.Freeman & Co Ltd, 2002.
4. D. Voet and J. Voet, *Biochemistry*, 4 edn., John Wiley & Sons, 2011.
5. J. R. Knowles, *Annual Review of Biochemistry*, 1980, **49**, 877-919.
6. A. Zhu, D. Lee and H. Shim, *Seminars in Oncology*, 2011, **38**, 55-69.
7. S. Walker-Samuel, R. Ramasawmy, F. Torrealdea, M. Rega, V. Rajkumar, S. P. Johnson, S. Richardson, M. Goncalves, H. G. Parkes, E. Arstad, D. L. Thomas, R. B. Pedley, M. F. Lythgoe and X. Golay, *Nat Med*, 2013, **19**, 1067-1072.
8. J. Sandstede, *European Radiology*, 2003, **13**, 52-61.
9. D. W. J. Klomp, B. L. van de Bank, A. Raaijmakers, M. A. Korteweg, C. Possanzini, V. O. Boer, C. A. T. van de Berg, M. A. A. J. van de Bosch and P. R. Luijten, *NMR in Biomedicine*, 2011, **24**, 1337-1342.
10. Z. Zhang, J. Li, S. Wu, Y. Liu, Z. Fan, X. Zhou, H. Zhao, D. Li and Y. Huan, *Magnetic Resonance Imaging*, 2010, **28**, 936-942.
11. L. Valkovič, M. Chmelík, I. Just Kukurová, M. Jakubová, M. C. Kipfelsberger, P. Krumpolec, M. Tušek Jelenc, W. Bogner, M. Meyerspeer, J. Ukropec, I. Frollo, B. Ukropcová, S. Trattnig and M. Kršňák, *NMR in Biomedicine*, 2014, n/a-n/a.
12. H. J. Lamb, J. Doornbos, J. A. den Hollander, P. R. Luyten, H. P. Beyerbacht, E. E. van der Wall and A. de Roos, *NMR in Biomedicine*, 1996, **9**, 217-227.
13. L. E. Hudsmith and S. Neubauer, *JACC: Cardiovascular Imaging*, 2009, **2**, 87-96.
14. P. Atkinson, Y. Bretonnière, D. Parker and G. Muller, *Helvetica Chimica Acta*, 2005, **88**, 391-405.
15. C. F. Midelfort, R. K. Gupta and I. A. Rose, *Biochemistry*, 1976, **15**, 2178-2185.
16. S. Faulkner and M. Tropiano, Unpublished results.

5 Extended Systems

5.1 Introduction

To further investigate the effects of the geometry and separation of the two metal centres on their anion binding properties, it was resolved to synthesise and study a series of compounds in which two macrocyclic binding domains are separated by a variety of longer spacer units. Having already established the numerous available conformational possibilities inherent to flexible systems with alkyl spacers, more rigid linking moieties were used such that the relative positions of the two metal centres were better defined whilst still retaining some flexibility close to the lanthanide centres to allow the adoption of an optimal binding conformer to suit the guest in question. Schematic depictions of the target species are shown in figure 5-1.

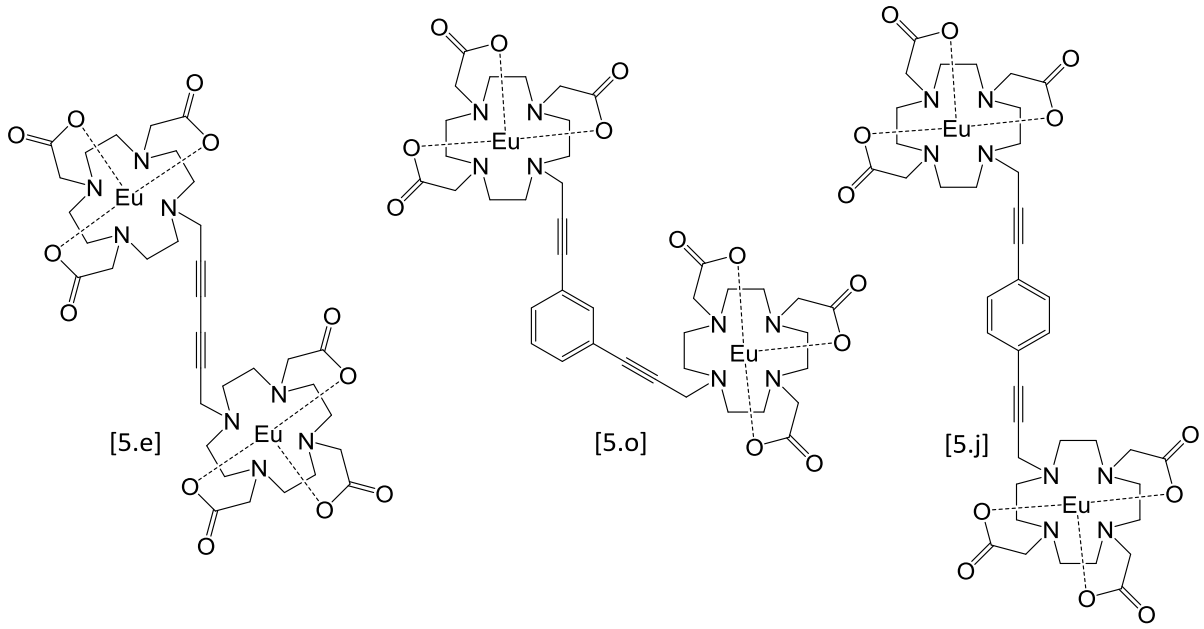

Figure 5-1. Molecular structures of the different synthetic targets for this chapter.

Estimates of the distances between the macrocyclic linking amine nitrogen atoms are tabulated in table 5-1. As in section **3.1**, these estimates were obtained via the application of trigonometry to average bond lengths and angles drawn from the literature for stereochemically analogous moieties. In each instance, the shortest possible separation is assumed to be achieved when the

two C-N and C'-N' bonds are fully eclipsed, whilst the longest is when they are staggered by 180 degrees.

Compound	Smallest N-N' Separation (pm)	Greatest N-N' Separation (pm)
[5.e]	763	813
[5.j]	1192	1224
[5.o]	947	1081

Table 5-1. Calculated range of inter-macrocycle distances for the complexes shown in figure 5-1.

5.2 Synthesis

The bis-macrocyclic complexes seen in figure 5-1 were prepared via syntheses analogous to those shown earlier in this work. Unlike in previous examples however, the linking units were not commercially available; in each case, they had to be prepared before they could be used to ligate two DO3A-type cavities.

5.2.1 Hexadiyne-linked System

The synthetic route to achieve the dichloro-diyne linking unit is shown in scheme 5-1. A modified literature procedure was followed, using a palladium-catalysed homo-coupling to generate the 1,6-dihydroxyhexa-2,4-diyne from two propargyl alcohol moieties.[1-4] After work-up the product was isolated as a pale yellow solid in 27% yield. The ^{1}H-NMR spectrum showed a single resonance at 4.24 ppm, corresponding to the methylene groups proximal to the alkyne unit. The consumption of all propargyl alcohol substrate was confirmed by the absence of the peak at 3.41 ppm which corresponded to the acetylenic proton in the starting material. The ^{13}C-NMR showed the expected three environments with resonances at 78.3, 70.1 and 50.8 ppm.

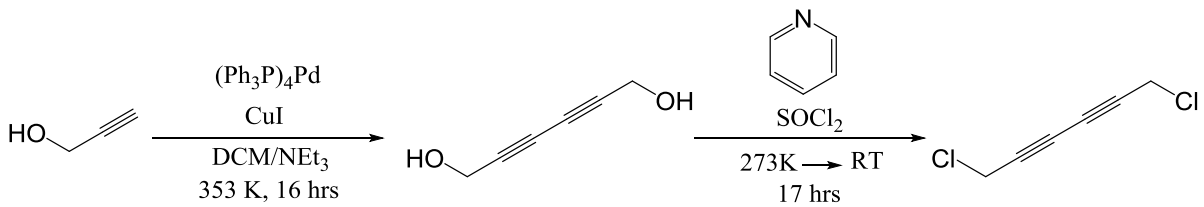

Scheme 5-1. Synthesis followed for the preparation of the 1,6-dichlorohexa-2,4-diynyl linking unit.

The terminal alcohol groups were subsequently converted to chlorides via treatment with thionyl chloride and trace pyridine in a single high-yielding step.[3] Exchanging the alcohol groups for chlorides resulted in a shift in the methylene proton resonance from 4.24 ppm to 4.16 ppm.

Reaction of the 1,6-dichlorohexa-2,4-diyne [5.b] with the triester [2.1] in the presence of caesium carbonate in acetonitrile yielded the bimacrocycle [5.c]. This was purified by column chromatography, using neutral alumina as the stationary phase and eluting with a 49:1 dichloromethane:methanol mixture.

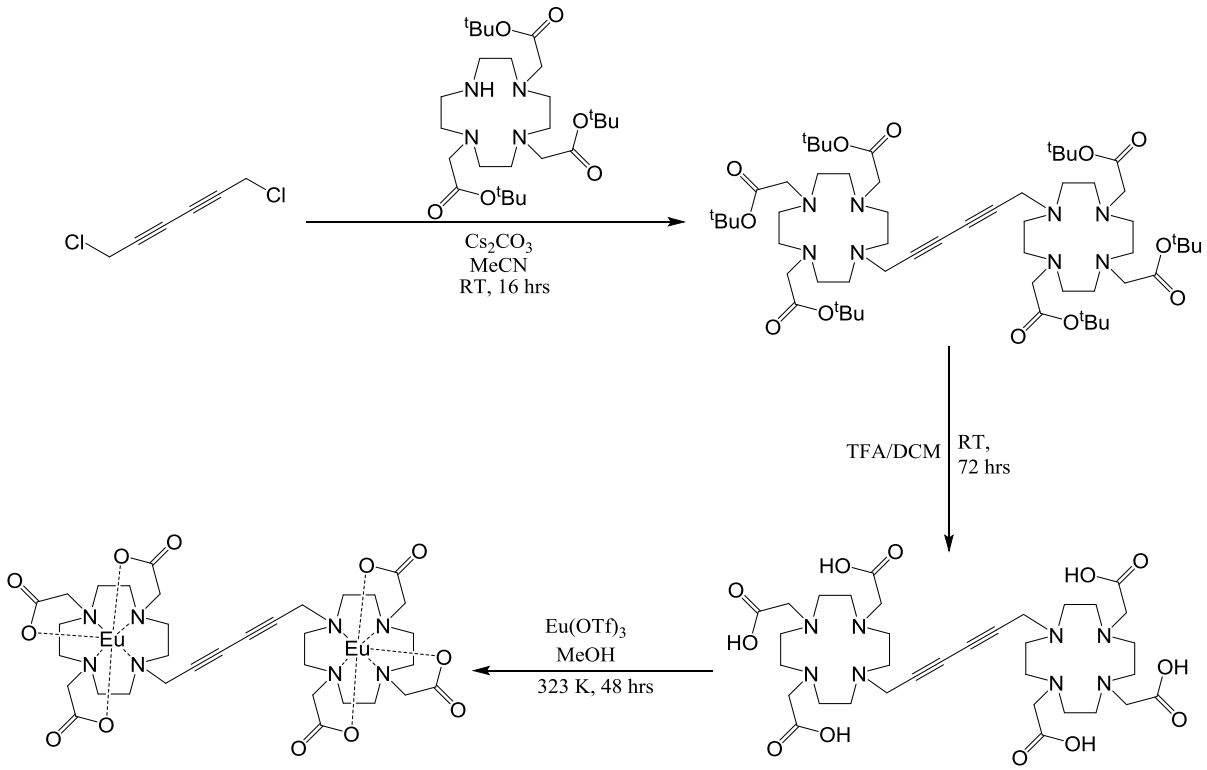

Scheme 5-2. Synthetic procedure used to generate complex [5.e].

Species bearing 1,3-diyne groups have previously been shown to be unstable with respect to photo-induced polymerisation and allene formation.[5] Although such reactivity is rare in solution due to greater intermolecular separation, the first steps of the scheme were performed in the dark to minimise this possibility. It has generally been found that larger, bulkier end groups capping the diyne functionality inhibit photo-reactivity of this nature. Thus once the heavy DO3A-triester groups had been affixed to each end, it was assumed that the species as a whole would be photostable and indeed this was found to be the case.

The ^{1}H-NMR spectrum of the hexaester [5.c] was found to be sharper than those of the other bis-macrocycles described so far in this work (with the exception of the propyl-linked system), with more resonances distinguishable in the cyclen region and narrower line-widths across the spectrum as a whole. It was reasoned that this could be a result of reduced steric interactions between the two cores due to a greater separation between them. This would reduce any conformational correlation between the two binding centres, allowing for a greater number of conformational permutations and increased interconversion between the two forms. As in the cases described earlier in this thesis, high-resolution electrospray mass spectrometry was used to confirm the identity of the bimacrocycle.

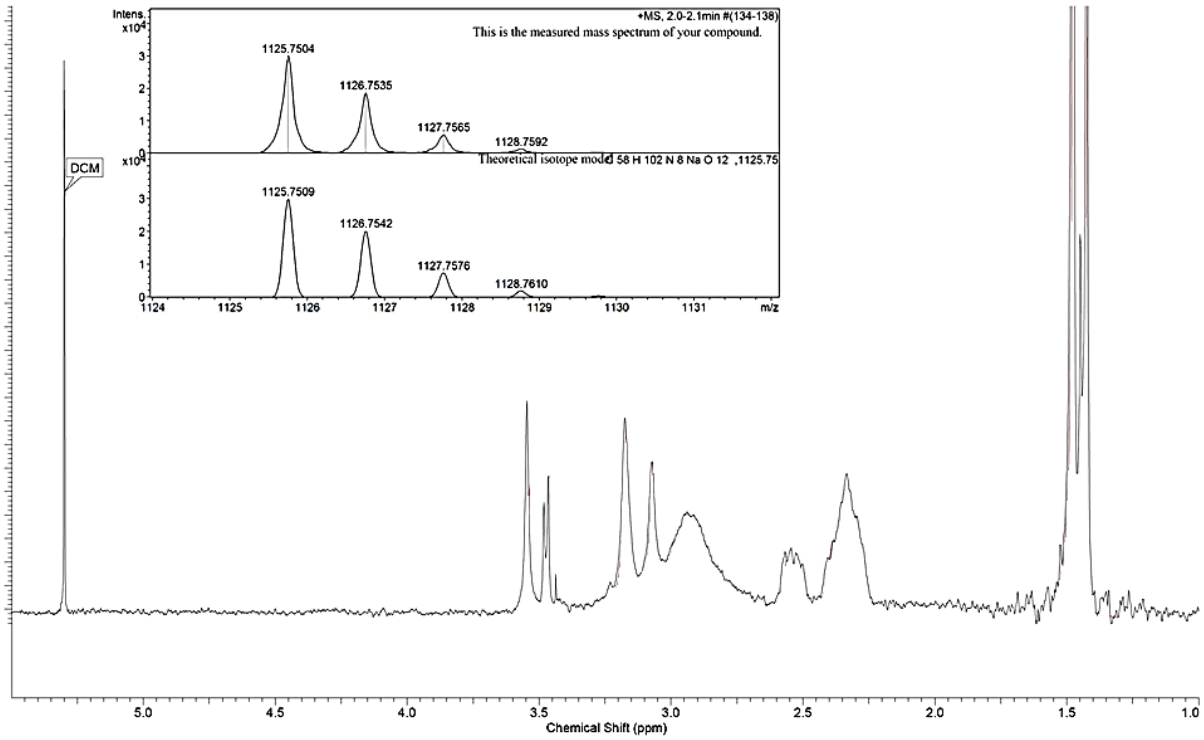

Figure 5-2. ^{1}H-NMR of the hexaester [5.c]. Recorded at 298 K in CD_2Cl_2. Inset shows the theoretical (bottom) and measured (top) high-resolution electrospray mass spectra.

Cleavage of the ester groups by treatment with trifluoroacetic acid resulted in the formation of bis(DO3A)yl-hexa-diyne [5.d]. The ^{1}H-NMR spectrum of the product was far simpler, containing fewer and much broader resonances. This was thought to be a consequence of faster exchange between diastereomers in the protonated pro-ligand. Whether this was due to a reduction in the

barrier to ring inversion upon removal of the bulky *tert*-butyl groups or a consequence of greater interaction with the aqueous environment was unclear.

The spectrum of the bis-europium complex [5.e] displayed more peaks than were observed in the mono-alkyne separated species [3.c], but displayed a simpler spectral form, with far more of the resonances having integrals corresponding to just a single proton. Again it was hypothesised that with the two paramagnetic metal centres further apart, they would have greatly reduced steric interactions. Thus, the conformation at one centre would have far less influence over the arrangement of ring and arms at the other. In effect, a greater separation between the two binding domains meant that each group could act in isolation and thus there were more isomers observed. The greater separation between the two paramagnetic lanthanide ions also made it more likely that the shift observed for any given proton arose primarily due to interactions with just the closer of the metal centres, with any pseudocontact contributions from the more distant metal centre being negligible.

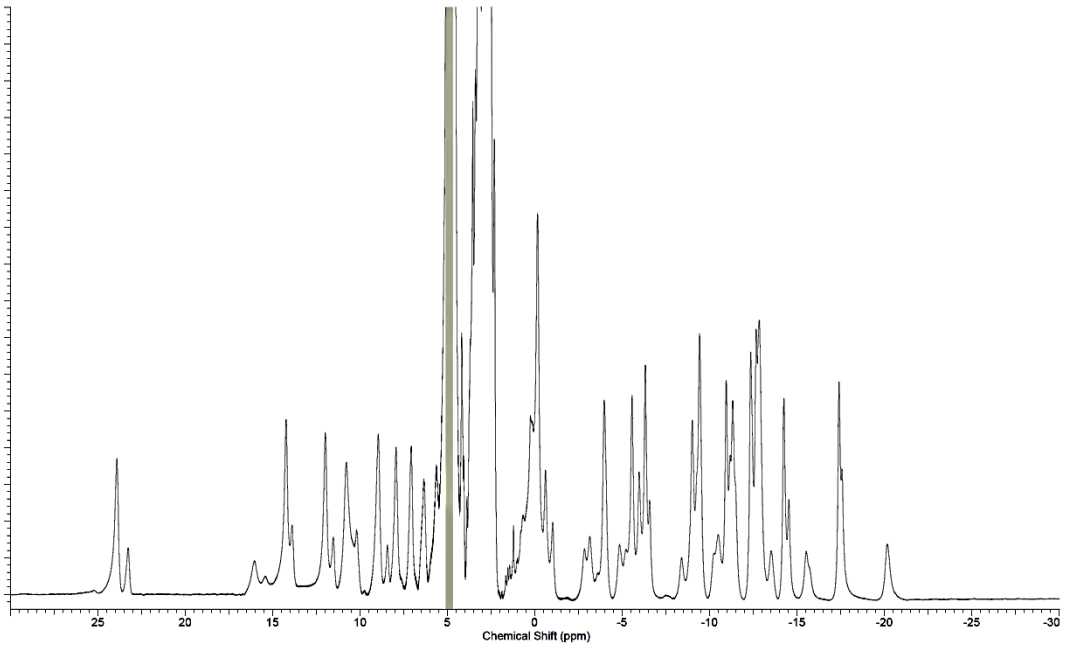

Figure 5-3. Paramagnetic ^{1}H-NMR of complex [5.e]. Recorded at 298K in D_2O, pD 10.

5.2.2 Dialkynylbenzene-linked Systems

The first attempt to synthesise the bis-alkynylbenzene linkers involved a double lithiation of 1,4-diethynyl-benzene at the acetylenic positions, followed by electrophilic attack by formaldehyde. This gave the desired product in a one pot reaction as shown in scheme 5-3.

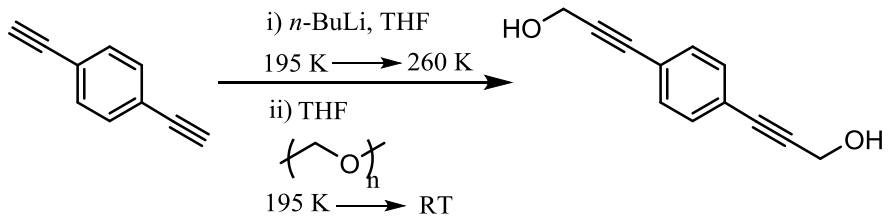

Scheme 5-3. Synthetic protocol followed for the synthesis of the linker precursor [5.f].

The yield (14%), however left something to be desired and the mono-substituted side-product was found to dominate the product mixture following preliminary work-up. This inefficiency, combined with the sensitivity and toxicity of the reagents required, caused an alternative to be sought. Given the success of the palladium:copper homocoupling used in the preparation of the diyne linker, it was decided to extend this methodology to generate the carbon skeleton in the 1,3- and 1,4-dialkynyl-benzene systems, in this case joining two propargyl alcohol groups with a central dibromo- or diiodo-benzene unit.[6, 7]

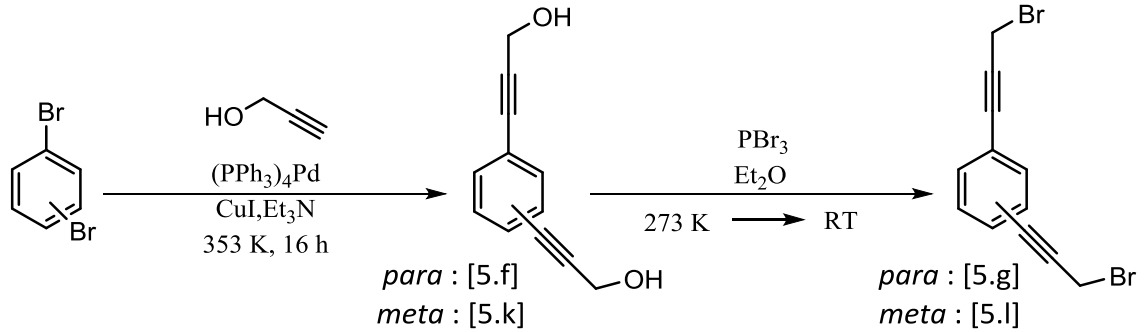

Scheme 5-4. Synthetic method used to prepare the different bis-bromomethyl-diethylbenzene linker groups.

This process was found to be cleaner than the method initially proposed, with a higher yield of the desired target and fewer side-products generated. Additionally, the reagents were less hazardous and more tolerant of varying conditions. It was however found to be imperative to

thoroughly degas the reaction mixture in the initial step, prior to the introduction of the palladium (0) species.

Once the bis propargyl alcohols had been obtained they were converted to their respective dibromo-species via treatment with phosphorus tribromide in diethyl ether as outlined in scheme 5-4.[8] These were then used to alkylate two triester [2.a] cores. Identical conditions were used in the preparation of the final complexes for both the *meta*- and *para*-substituted systems.

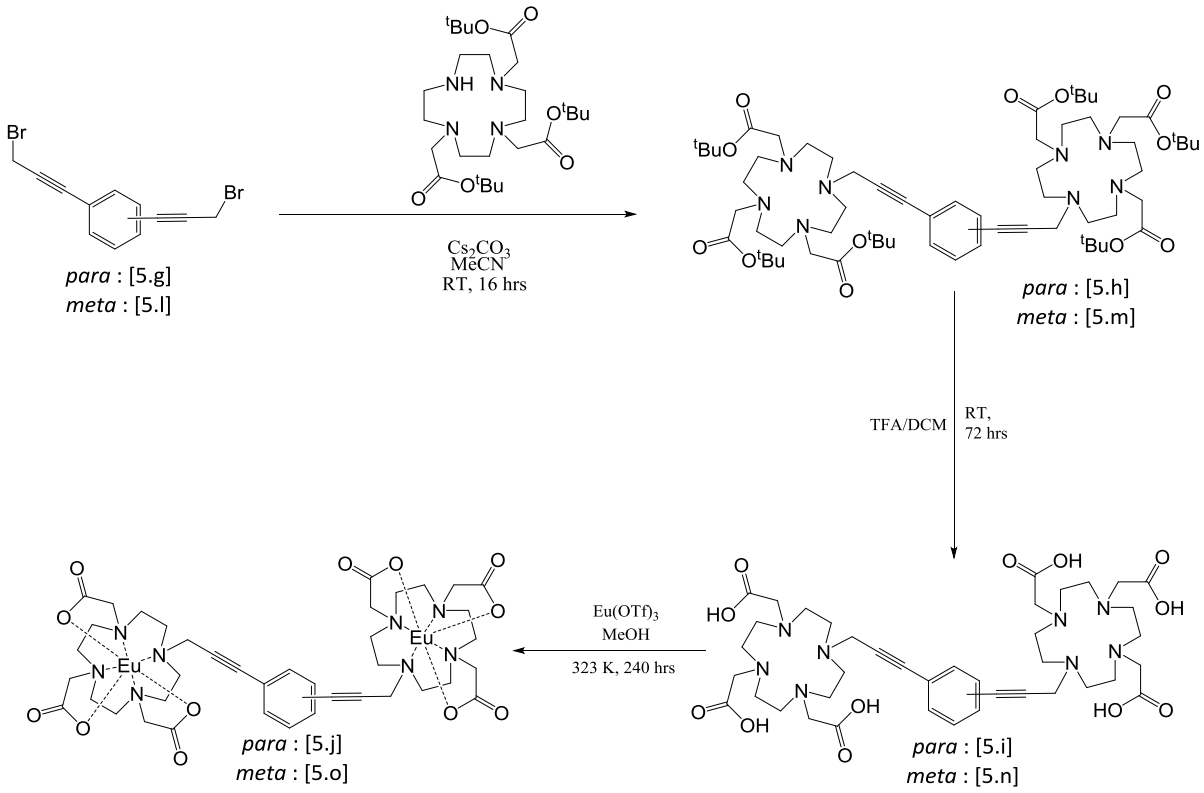

Scheme 5-5. Synthetic procedure followed to prepare complexes [5.j] and [5.o].

As would be expected, the 1,3- and 1,4- species were indistinguishable by mass spectrometry at all points along the reaction scheme. In their respective hexaester forms, both isomers were observed as the $[M+Na]^+$ (*m/z* = 1202) species under electrospray conditions.

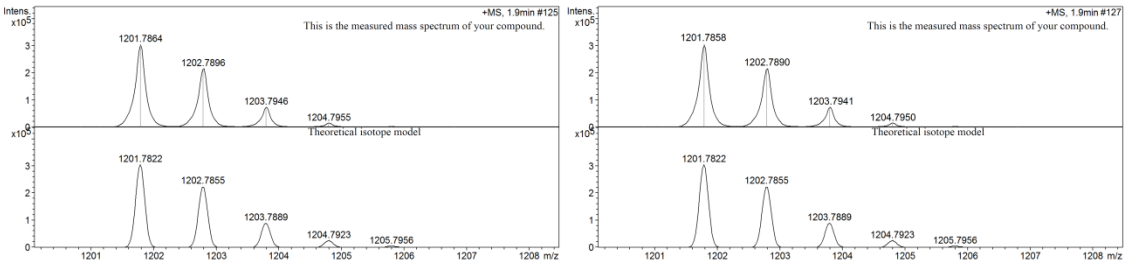

Figure 5-4. Measured (top) and calculated (bottom) high resolution electrospray mass spectra of the dialkynylbenzene-linked hexaesters [5.m] (left) and [5.h] (right).

The ^{1}H-NMR spectra also displayed large similarities, especially in the regions corresponding to the cyclen ring and pendant arm protons. In the hexaester and hexaacid species, the most significant differences were observed in the more shifted parts of the spectrum in the resonances of the aryl-group protons, where the *para*-isomer showed a simple singlet for all four equivalent proton environments. The *meta*-isomer by contrast displayed the expected trio of resonances in the aromatic region, with a pseudo-singlet from the proton in the 2-position and two multiplets from the 4- and 5-positions.

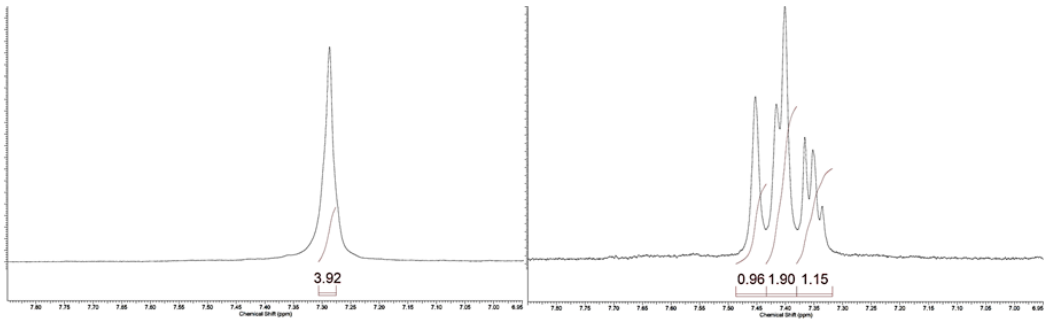

Figure 5-5. The aromatic region of the ^{1}H-NMR spectra of hexaesters [5.h] (left) and [5.m] (right). Both spectra recorded at 298 K in $(CD_3)_2SO$.

In behaviour analogous to that observed in earlier chapters, the removal of the ester groups to expose the binding sites resulted in a simplification of the ^{1}H-NMR spectra, with all the methylene signals coalescing into four broad bands corresponding to the cyclen ring protons (3.35 - 3.21 ppm), the two different acetate arm environments (3.81 ppm and 3.62 ppm) and the -CH_2- groups proximal to the alkyne groups. The spectrum of the *para*-substituted ligand [5.i] is shown in figure 5-6. It was also noted that the peaks in the aromatic region shifted upon deprotection.

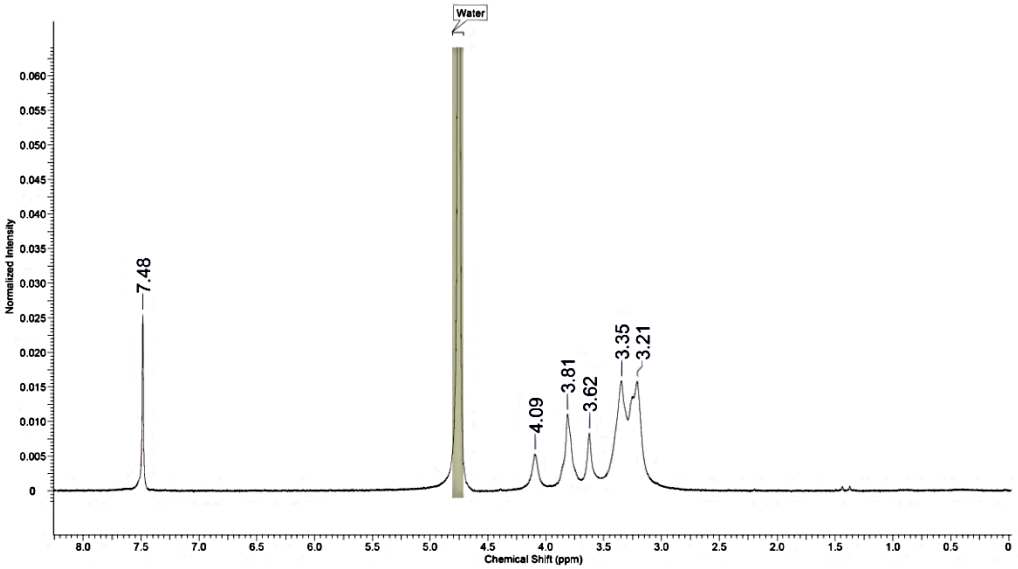

Figure 5-6. ^{1}H-NMR spectrum of hexaacid free ligand [5.i]. Recorded at 298 K in D_2O.

The free ligands [5.i] and [5.n] were found to be significantly less soluble in methanol than the analogous propyl- and butynyl-linked species described earlier in this work. Complexation reactions with europium triflate thus had to be performed at much higher dilutions, and consequently were left for significantly longer to ensure the process ran to completion, and in fact this never occurred for the *meta*-substituted isomer and the reaction was deemed to have failed. Figure 5-7 shows the paramagnetic ^{1}H-NMR recorded for the *para*-isomer of the europium complex [5.j], recorded in D_2O at pD 7. The poor signal to noise ratio was attributed to the exceedingly low solubility of the sample (found to be less than 1 mg / mL).

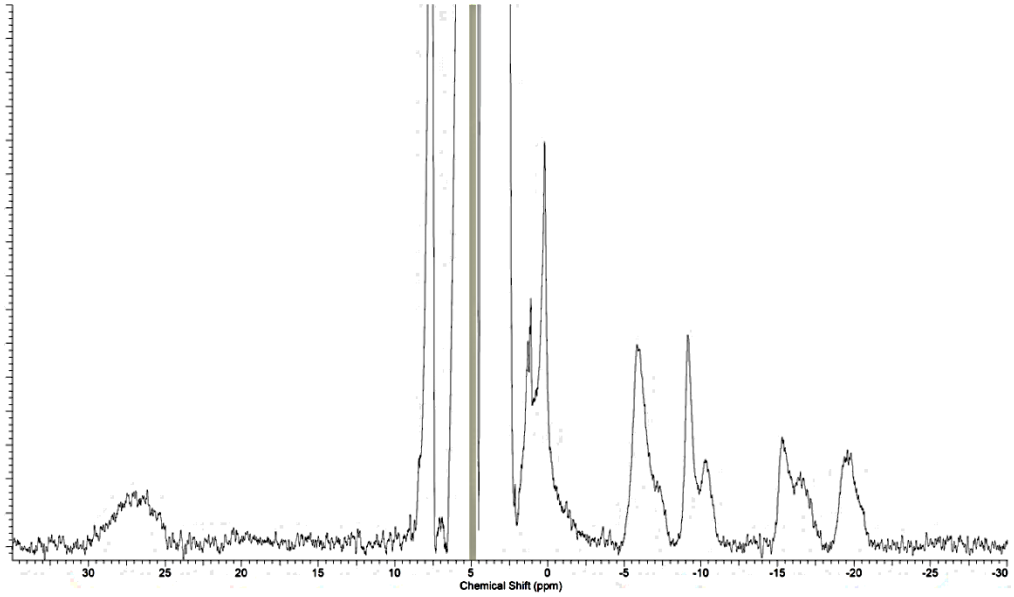

Figure 5-7. Paramagnetic ^{1}H-NMR of complex [5.j]. Recorded at 298 K in D_2O, pD 7.

From the shifts and widths of the resonances it is clear that at this pD, the isomers are in slow exchange. It was assumed that as with all the other complexes studied in this work, the isomer speciation and exchange rates would display a dependence on the local pH. Attempts to investigate this by raising the pD of the sample with NaOD resulted in the complex going from being sparingly soluble, to essentially insoluble. This issue with solubility will become a recurring theme in the discussion of this chapter.

No attempts were made to synthesise the 1,2-dialkynyl-benzene derivatives, as it was deemed somewhat unwise to incorporate an ene-diyne[9] motif into a system which was to be used for luminescent assay.[10]

5.3 Anion Binding

It was found that the hydrophobic nature of the longer linking units meant that both the free ligands and the metal complexes of all systems were, at best, sparingly soluble in water. It was therefore decided that all the binding studies should be carried out in methanol with a view to exploring the potential selectivity for guests in the most competitive medium compatible with solubility. This had the added advantage of simplifying the solution phase speciation of both host and guest, as well as giving rise to longer luminescent lifetimes due to the presence of fewer proximate quenching oscillators per solvent molecule.

In all the systems described in this chapter, the two macrocyclic domains are separated by long and inflexible linkers, so it was determined to test the binding affinities of similarly large dianions. The three isomers of benzene-dicarboxylate have been used extensively in the group to probe the separation between metal centres in multinuclear complexes containing a *meta*-xylyl bridge.[11, 12] Their photophysics are well understood; furthermore their use allows direct comparison with previously investigated systems. The binding of benzoate was also studied to serve as a mono-dentate control.

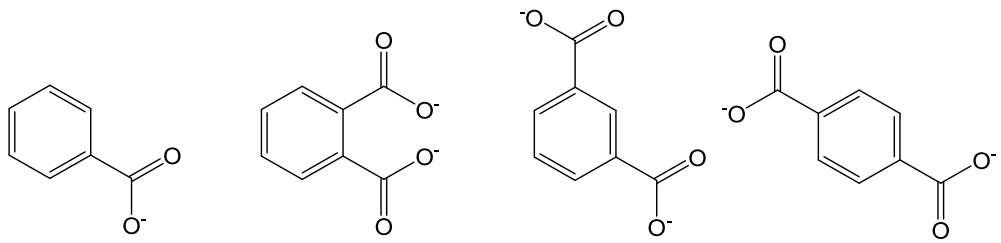

Figure 5-8. Structures of the titrant guests used in this chapter.

To aid in the rationalisation of any associative behaviour later observed, the distances between the carbon atoms of the two carboxylate donor groups of the phthalate isomers were calculated and are tabulated below.

Phthalate Isomer	Inter-carboxylate Separation (pm)
phthalate	275
isophthalate	476
terephthalate	549

Table 5-2. Calculated distances between the carboxylate carbon atoms of the phthalate isomers.

As these titrations were carried out in methanol, the use of a buffer was not appropriate. Instead, to control the speciation of the guest and ensure that it existed solely as the bis-anion, the titrant solutions were made up with one molar equivalent of lithium hydroxide per carboxylate group in the guest. The necessity of this measure was validated by repeating some of the titrations without the base present and in all instances, a marked drop in binding affinity was witnessed, implying that the neutral protonated carboxylic acids are dramatically less effective at donating to the metal cations.

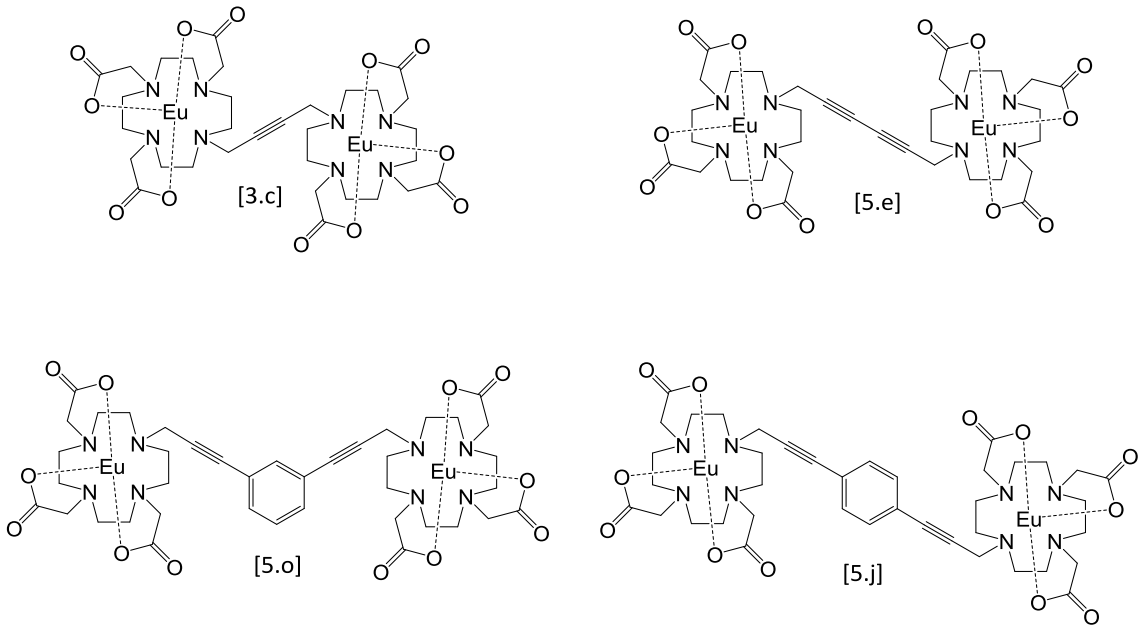

Figure 5-9. Structures of the ditopic europium complexes used in this chapter.

In contrast to the simple aliphatic diacids discussed in earlier chapters, the aryl rings of the phthalate and benzoate guests are more than adequate as antennae for sensitising lanthanide luminescence, provided the solutions were sufficiently dilute to avoid problematic inner-filter effects. It was therefore possible to monitor any binding events by observing changes in the europium-based luminescence following excitation of either the metal, as before, or the aromatic chromophore. In the latter case, if the phthalate is not bound to a metal centre, absorption by the aryl group will not result in emission from the metal. Only if the phthalate were in the inner coordination sphere would it be close enough for sensitisation of the metal to be a possibility. In the systems already containing extended chromophores in the ligand, it is worth noting that these will also absorb light, but that addition of an extra chromophoric motif in the guest would be expected to enhance the overall sensitisation of lanthanide emission.

This hypothesis was probed for the diyne:isophthalate system. UV-analyses of the isophthalate titrant solution found an absorption maximum at 293 nm which arises from the $\pi \rightarrow \pi^*$ transition of the aryl group. Thus parallel titrations were performed, in one case exciting the metal centre directly as usual, and in the other targeting the aryl manifold at 293 nm. In the former, addition of

lithium isophthalate resulted in a sharp but small drop in luminescence intensity, suggesting that LMCT could play a role in reducing the quantum yield for lanthanide emission relative to the host complex in isolation. By contrast, excitation of the isophthalate chromophore resulted in a dramatic increase in luminescence intensity across all bands, indicating that the phthalate chromophore does indeed sensitise the lanthanide emission.

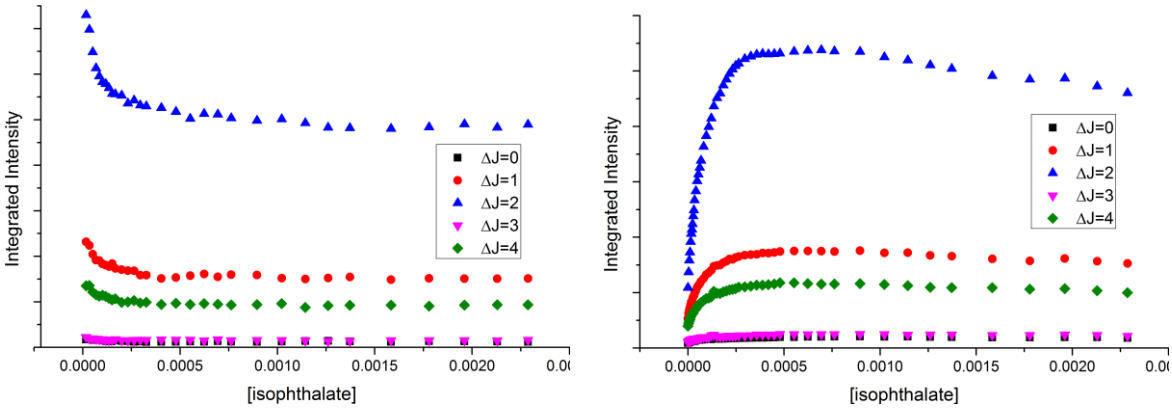

Figure 5-10. The integrated intensities of the component ΔJ peaks of emission from complex [5.e] plotted against concentration of isophthalate. The left plot shows the trend upon direct excitation of the europium at 394 nm. The right plot shows that observed upon irradiation of the isophthalate chromophore at 293 nm.

Binding constants were calculated from both sets of data and were found to be in good agreement with one another. This protocol of parallel titrations was extended to the other host:guest pairings and analogous behaviour was observed universally. In each instance, the wavelength used for the excitation of the aryl group was determined from UV-absorption spectra of the titrant solution.

As expected, changing the separation between the two metal centres altered the guest selectivity of the complex, with the longer spacer units favouring the larger anions. The complex in which the two europium centres were separated by just the single alkyne unit displayed a remarkable selectivity for the 1,2-isomer phthalate. Indeed binding was so strong that the luminescent changes were almost complete after the addition of just one equivalent of the dianion. The binding constant of the 1,3-isomer was over 100 times smaller, with the 1,4-isomer a further order of magnitude weaker than that. This is clearly indicative of a small binding cavity between the metal centres selecting for the ditopic guest with the smallest separation between the donor

groups. In complex [5.e], where the two macrocyclic domains are linked by a longer six-carbon diyne chain, this selectivity was somewhat reversed. Now the affinity for the shorter 1,2-phthalate is much lower than that for the longer 1,3- and 1,4-isomers, indicative of a larger binding cavity between the metals. The binding constants calculated for the various host:guest pairings are shown in table 5-3.

Complex	Titrant	K (M^{-1})	99% Confidence Interval	Calculated ΔG ($kJmol^{-1}$)
[3.c]	Li_2.oxalate	*	*	*
[3.c]	Li.benzoate	1604	1560 - 1650	-18.0
[3.c]	Li_2.phthalate	>6.81 x 10^5 †	†	< -32.7
[3.c]	Li_2.isophthalate	8990	8790 - 9200	-22.2
[3.c]	Li_2.terephthalate	870	863 - 874	-16.5
[5.e]	Li_2.oxalate	*	*	*
[5.e]	Li.benzoate	16907	16300 - 17500	-23.7
[5.e]	Li_2.phthalate	8559	7790 - 9420	-22.1
[5.e]	Li_2.isophthalate	36541	34500 - 38700	-25.6
[5.e]	Li_2.terephthalate	39722	34900 - 45500	-25.8

Table 5-3. The binding constants and confidence intervals calculated for the interactions between complexes [3.c] and [5.e] and different guests. * Titrations were attempted with oxalate to establish a point of comparison with the aqueous systems but the titrant was found to be insoluble in the solvent system. † Binding too strong to be reliably fitted. ΔG values calculated assuming T = 293 K.

For each guest species, the affinity constant observed for binding with the hexadiyne-linked complex [5.e] was significantly higher than that seen for binding to the mono-alkyne species [3.c]. It was thought that this could be a reflection of increased free space around each metal centre due to the other binding domain being further removed. This theory was found to be at odds with the calculated q-values of the metal centres in both complexes. As all the binding studies in this chapter needed to be carried out in methanol for solubility reasons, the q-values were measured also in methanol. This required a further slight modification to the (already) modified Horrocks'

equation (Section **1.4.3**) to allow for each solvent species now only bearing one OH or OD oscillator; in this case, where there are no exchanging NH oscillators, the equation becomes:[13]

$$q = 2.4(1/\tau_{MeOH} - 1//\tau_{MeOD} - 0.125) \quad \textbf{(5.1)}$$

Complex	τ_{MeOH} (ms)	τ_{MeOD} (ms)	q
[3.c]	1.22	1.81	0.34
[5.e]	1.20	1.76	0.34

Table 5-4. Emissive lifetimes and q values for complexes [3.c] and [5.e] in methanolic solution.

Using the lifetimes obtained gives low values of q in these systems, implying there is limited solvation as a consequence of the highly lipophilic nature of the host.

As previously discussed, the formation of the host:guest adduct resulted in a dramatic increase in metal-based luminescence intensity, provided the excitation was of the aryl antenna unit of the guest species. However the extent to which binding sensitised emission from the metal varied from guest to guest and did not correlate with binding strength. By dividing the total integrated emission intensity at the end point of the titration by that at the beginning, it was possible to arrive at a 'sensitisation factor' for each host:guest pairing.

Host Complex	Guest Anion	$I_{final}/I_{initial}$	Binding Constant (M^{-1})
[3.c]	benzoate	6.2	1604
[3.c]	phthalate	27.3	>6.81 x 10^5
[3.c]	isophthalate	19.1	8990
[3.c]	terephthalate	70*	870
[5.e]	benzoate	2.4	16907
[5.e]	phthalate	10.7	8559
[5.e]	isophthalate	3.9	36541
[5.e]	terephthalate	7.8	39722

Table 5-5. 'Sensitisation factors' for the various host:guest pairings discussed so far in this chapter. * In cases where solubility did not permit the titration to reach an end point, estimates were made using the luminescent response of the host:guest adduct as predicted by DynaFit®.

The variation observed could be ascribed to a number of factors, the most mundane of which would be the simple matter of different photon absorption cross-sections of the different aromatic guest species. Absorption spectra of the titrant solutions were not measured in all cases and this combined with the lack of published values made it impossible to discount this possibility. This being said, it would be surprising if there were significant differences between the phthalate isomers in this regard. In an effort to eliminate any other sources of variation between the measurements, the excitation and emission monochromator slits were held constant across the entire series, to ensure that the total intensity of light incident on the sample was as constant as possible.

The other main factor which could contribute to these differences is the efficiency of energy transfer between the guest excited state and the metal ion. This in turn is predominantly determined by two main parameters. First is the spectral and energy overlap between the excited (probably triplet) state of the sensitiser and the lanthanide ion. This is an inherent physical property of the pairing being studied and is thus beyond control. The second component to be considered is that of the distance between the aryl group and the metal ion in the host:guest adduct. Regardless of whether it proceeds via a Förster or Dexter mechanism, energy transfer between the two will display a strong inverse dependence on range and hence the differences observed could arise from different separations of metal and guest in the binding conformer(s).

Comparisons can be drawn to the *m*-xylyl-linked systems studied by Tilney[11] and Hill.[14] As discussed in section **1-9**, they found that *meta*-xylyl-linked bis-DO3A systems of the type shown in figure 5-11 showed a profound selectivity for aryl-1,3-dicarboxylates such as isophthalate.

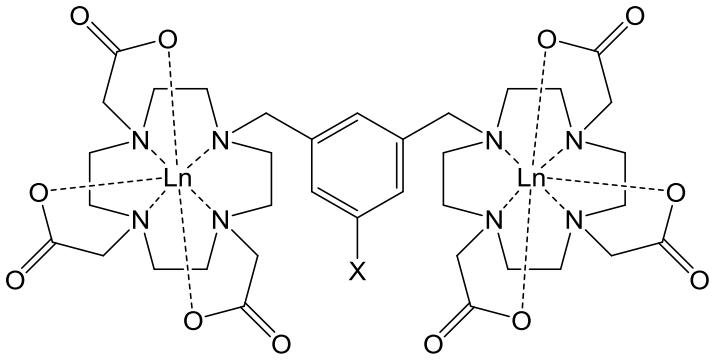

Figure 5-11. General structure of *m*-xylyl-linked class of compounds as described in references 11 & 13.

As their studies were all carried out in a different solvent system, an absolute comparison of binding constants is meaningless, but comparing the relative selectivities of the complexes can be instructive. The intermetallic separation in the *m*-xylyl-linked species is longer than that in complex [3.c] but shorter than that of [5.e]. In light of the results of this chapter it is therefore unsurprising that this class of compounds should bind most strongly with the 1,3-isomer of the phthalate guests.

Obviously increasing the intermetallic separation in the complex makes the binding of longer dianions more favourable, but it is equally clear that this trend is not complete, as the longest complex studied so far, [5.e] displays approximately the same affinities for the 1,3- and 1,4-isomers of the dicarboxylate. In an attempt to determine whether further lengthening the spacer between the metal centres could induce selectivity for the longest guest species alone, binding studies were performed with the europium complexes of both the *meta*- and *para*-dialkynylbenzene-linked ligands. Once again however, the negligible solubilities of these complexes proved a stumbling block as the very low concentrations of the samples meant that the signal recorded was very weak and the signal to noise unacceptably low for reliable determination of binding constants. This lack of solubility is most probably attributable to the hydrophobic nature of the large, rigid linking group separating the two binding domains. It would probably have been possible to perform binding studies in a less polar solvent mixture, such as those used

in the synthesis and study of interlocked supramolecular arrays.[15] However this line of investigation was not pursued.

5.4 Conclusions and Further Work

A family of bimacrocyclic europium complexes was synthesised, in which the metal centres were separated by semi-rigid linking groups of different lengths. Luminescence binding studies were performed to ascertain the affinities of these complexes for different aryl dicarboxylates and it was found that altering the distance between the two metal centres of the host influenced the selectivity for the guest species. The longer the distance between the europium ions in the complex, the greater the selectivity for longer dicarboxylate guests and *vice versa*. Studies on the longest binuclear complexes were thwarted by solubility issues. If such investigations were to be pursued further, efforts would need to be made to increase the hydrophilicity of such complexes, through modification of either the metal-bearing macrocyclic domains or of the spacer unit linking them.

5.5 References

1. I. J. S. Fairlamb, P. S. Bauerlein, L. R. Marrison and J. M. Dickinson, *Chemical Communications*, 2003, 632-633.
2. F. Alonso and M. Yus, *ACS Catalysis*, 2012, **2**, 1441-1451.
3. B. S. Thyagarajan, P. E. Glaspy, E. Baker and P. Brown, *Organic Mass Spectrometry*, 1980, **15**, 224-228.
4. R. C. DeCicco, A. Black, L. Li and N. S. Goroff, *European Journal of Organic Chemistry*, 2012, **2012**, 4699-4704.
5. C. Werner, H. Hopf, I. Dix, P. Bubenitschek and P. G. Jones, *Chemistry – A European Journal*, 2007, **13**, 9462-9477.
6. S. A. Caldarelli, S. El Fangour, S. Wein, C. Tran van Ba, C. Périgaud, A. Pellet, H. J. Vial and S. Peyrottes, *Journal of Medicinal Chemistry*, 2013, **56**, 496-509.
7. T.-J. Hsu, F. W. Fowler and J. W. Lauher, *Journal of the American Chemical Society*, 2011, **134**, 142-145.
8. Y. Yamaguchi, S. Kobayashi, T. Wakamiya, Y. Matsubara and Z.-i. Yoshida, *Journal of the American Chemical Society*, 2000, **122**, 7404-7405.
9. K. C. Nicolaou, W. M. Dai, S. C. Tsay, V. A. Estevez and W. Wrasidlo, *Science*, 1992, **256**, 1172-1178.
10. A. Evenzahav and N. J. Turro, *Journal of the American Chemical Society*, 1998, **120**, 1835-1841.
11. J. A. Tilney, T. J. Sorensen, B. P. Burton-Pye and S. Faulkner, *Dalton Transactions*, 2011, **40**, 12063-12066.
12. T. J. Sørensen, L. R. Hill, J. A. Tilney, O. A. Blackburn, M. W. Jones, M. Tropiano and S. Faulkner, *European Journal of Inorganic Chemistry*, 2014, **2014**, 2520-2528.
13. S. Faulkner and J. L. Matthews, in *Comprehensive Coordination Chemistry II*, Series editors. J. A. McCleverty and J. Meyer, Volume editors. M.D. Ward. Pergamon, Oxford, 2003, pp. 913-944.
14. L. R. Hill, T. J. Sorensen, O. A. Blackburn, A. Brown, P. D. Beer and S. Faulkner, *Dalton Transactions*, 2013, **42**, 67-70.
15. C. Allain, P. D. Beer, S. Faulkner, M. W. Jones, A. M. Kenwright, N. L. Kilah, R. C. Knighton, T. J. Sorensen and M. Tropiano, *Chemical Science*, 2013, **4**, 489-493.

6 Conclusions and Future Work

Different families of related mono- and binuclear lanthanide complexes were synthesised and their properties studied. Their affinities in solution for a wide range of anionic guests were also quantified and the effects of binding on both the host and guest have been shown to be related to the available conformations of the binding site, and to the nature of the system as a whole. As such they provide a good example of the importance of induced fit and solvent effects in defining host-guest chemistry.

6.1 Halide Sensing by Lanthanide luminescence

Chapter 2 saw the introduction of a class of binuclear complexes in which the two metallic domains were linked by a short propyl chain. Having two highly polarising metal cations in close proximity created a highly charged binding cavity which was capable of sequestering small anions including the halides from aqueous solutions. The binding constants calculated for the bis-europium complex [2.d] and the different anions are shown graphically below.

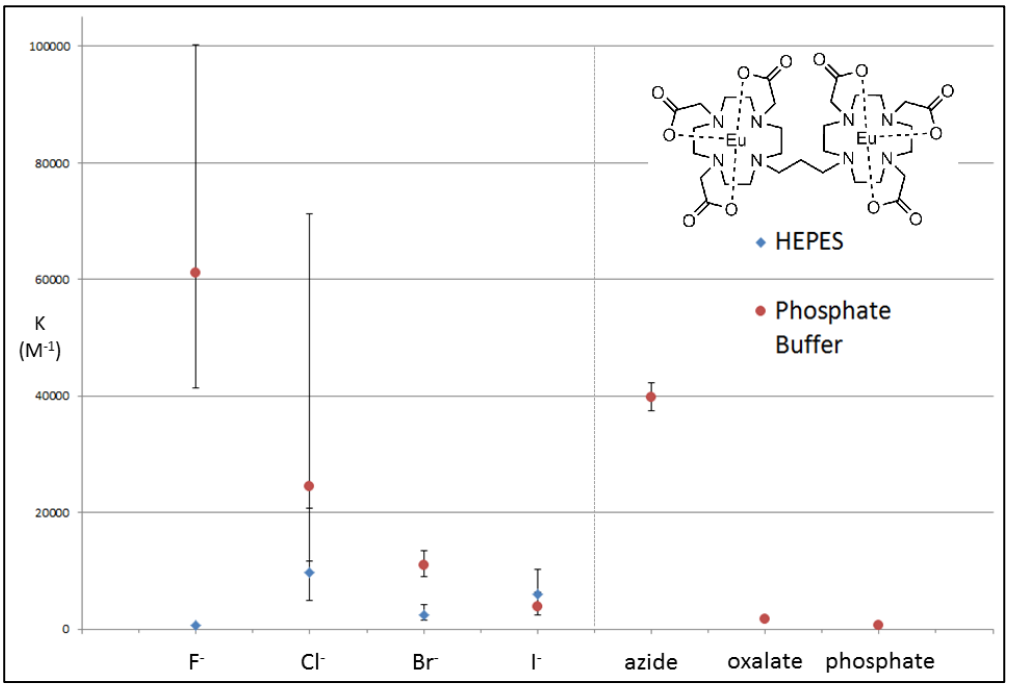

Figure 6-1. The affinities of complex [2.d] for a variety of anionic guests.

The complexes were found to display a strong selectivity for the smaller anionic guests such as fluoride and azide.

In spite of the high binding constants and reasonable selectivities found, the comparatively small magnitude of the modulation of luminescence upon guest binding meant that this class of complexes is most probably not suitable for practical service as an anion sensor. However, the high affinity for chloride ions in water merits further exploration. Simple monometallic systems have previously been observed to bind fluoride in water, but binding of other halide ions is normally negligible. In this case, while affinity for chloride is weaker than fluoride (at least in terms of absolute binding constant, though the uncertainties overlap), it is clear that binding to two lanthanide centres can overcome the problems associated with solvation. When we consider that the complexes discussed in this thesis are all charge neutral, and that binding relies on the residual charge at the lanthanide, it is clear that more can potentially be achieved by using amide donors in lieu of carboxylates (though DO3AM systems will naturally have reduced inertness to metal dissociation).

6.2 Dicarboxylate Recognition

The class of compounds described in Chapter 3 displayed a more rigid geometry with a greater intermetallic separation. These compounds were used to assess the nature of interactions in solution with anionic guest species. Binding studies were performed with a wide range of dicarboxylates to assess ways in which binding was affected by the size, geometry and any other functional groups born by the guest. The binding constants are shown graphically in figure 6-2. It was found that the alkyne-linked bis-europium species [3.c] displayed a remarkable selectivity for the two-carbon dianion oxalate over all other guests. It was also shown that functionalization of the guest backbone with hydroxyl groups, led to an increase in the binding constant for a guest of any given chain length and it was attempted to rationalise this trend.

The induction of chirality at a metal centre via association with a chiral guest species was also investigated and promising preliminary results seen, although the drawing of definitive conclusions was made difficult by a poor signal to noise ratio - in such systems, a more effective sensitiser is clearly desirable.

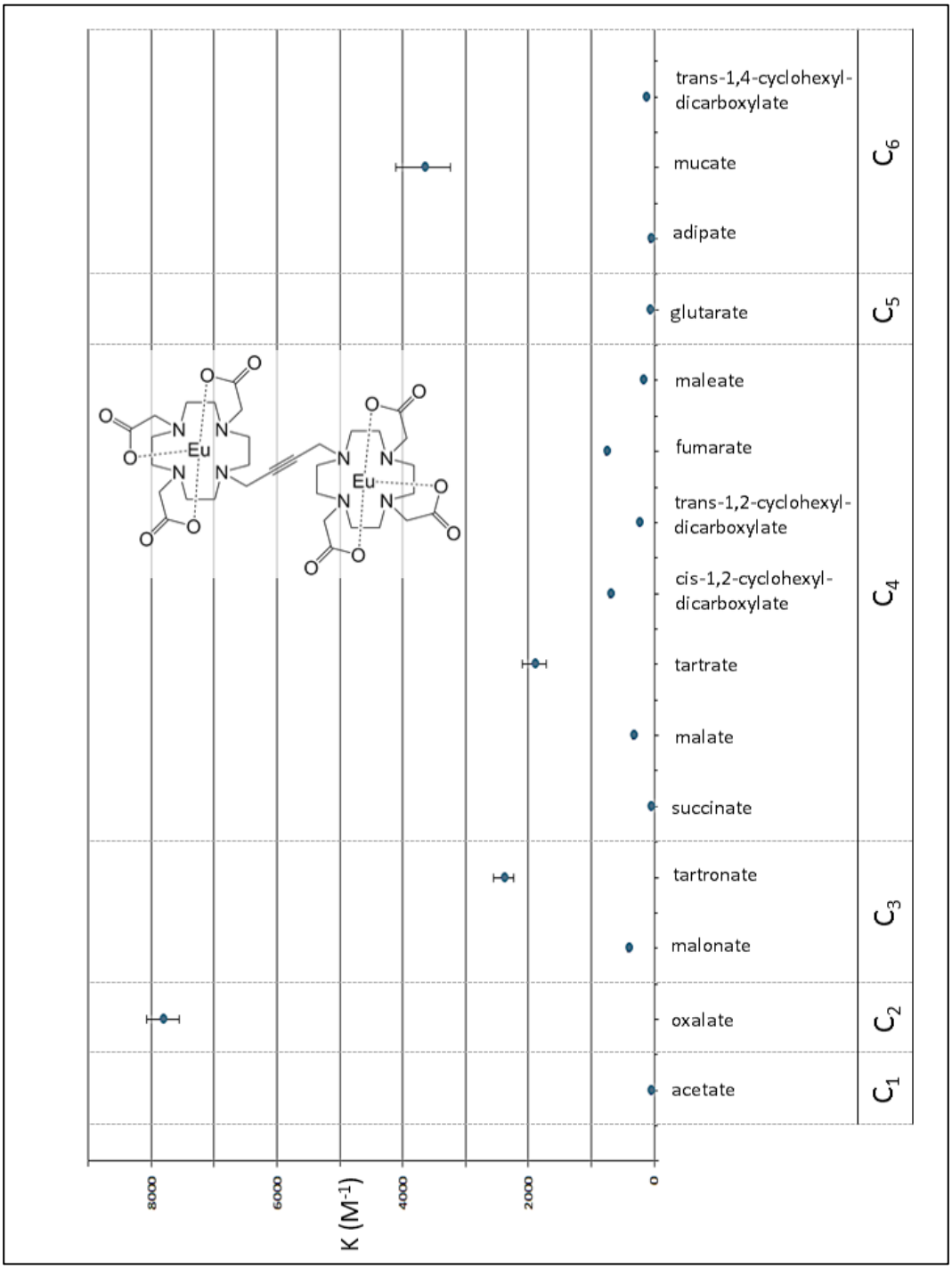

Figure 6-2. The affinities of complex [3.c] for a variety of dicarboxylate guests.

6.3 Binding of biologically relevant phosphates

The alkyne-linked complexes synthesised and studied in Chapter 3 were pressed into further service and it was demonstrated that macrocyclic lanthanide complexes can bind with phosphorylated biomolecules in aqueous solutions and in the presence of competitive endogenous ligands such as phosphate.

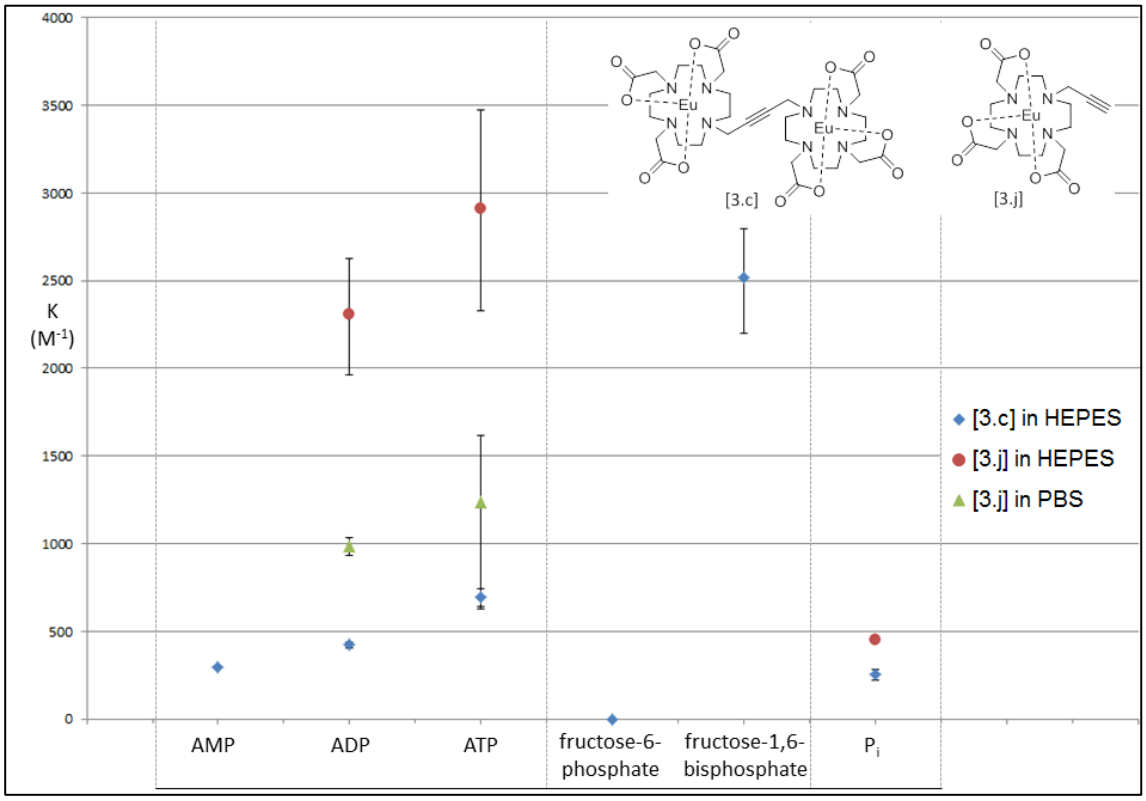

Figure 6-3. The affinities of complex [3.c] for a variety of biologically relevant phosphates.

Perhaps unsurprisingly, the binuclear complexes displayed selectivity for bidentate phosphates such as fructose-1,6-bisphosphate that can chelate to both lanthanide centres. For the pyrophosphate derivatives such as ATP it was noted that binding was probably too weak to be ascribed to a bidentate chelating mode and thus it was suggested that coordination was occurring via the terminal phosphate group of the ester chain.

As noted in section **4.4**, the results described in this thesis have shown that the binding constants of even the most strongly bound phosphate species are relatively low, and that all systems are in exchange with bulk on the timescale of the NMR experiment. One would anticipate that binding

to a metal centre would result in a dramatic reduction in the T_1 relaxation time of the ^{31}P-nuclei and since there is fast exchange with the bulk, this should translate to similar enhancements of T_1 for the same phosphate in bulk solution. This then could open the possibility of ^{31}P contrast media, potentially leading to an imaging technique for the study of endogenous phosphates, essentially analogous in methodology to the ubiquitous proton MRI. Further work carried out in the group has already demonstrated that gadolinium complexes such as those used in this thesis can enhance the ^{31}P relaxation rate of simple inorganic phosphate in solution, although it remains to be established whether complexes that are selective for a single species could play a role in deconvoluting the phosphate speciation involved in complex biological processes.

6.4 Tuning guest affinities by controlling host size

In a pleasant vindication of chemical common sense, it was shown that by using larger ditopic host complexes, it was possible to tune the selectivity for larger bidentate anionic guests.

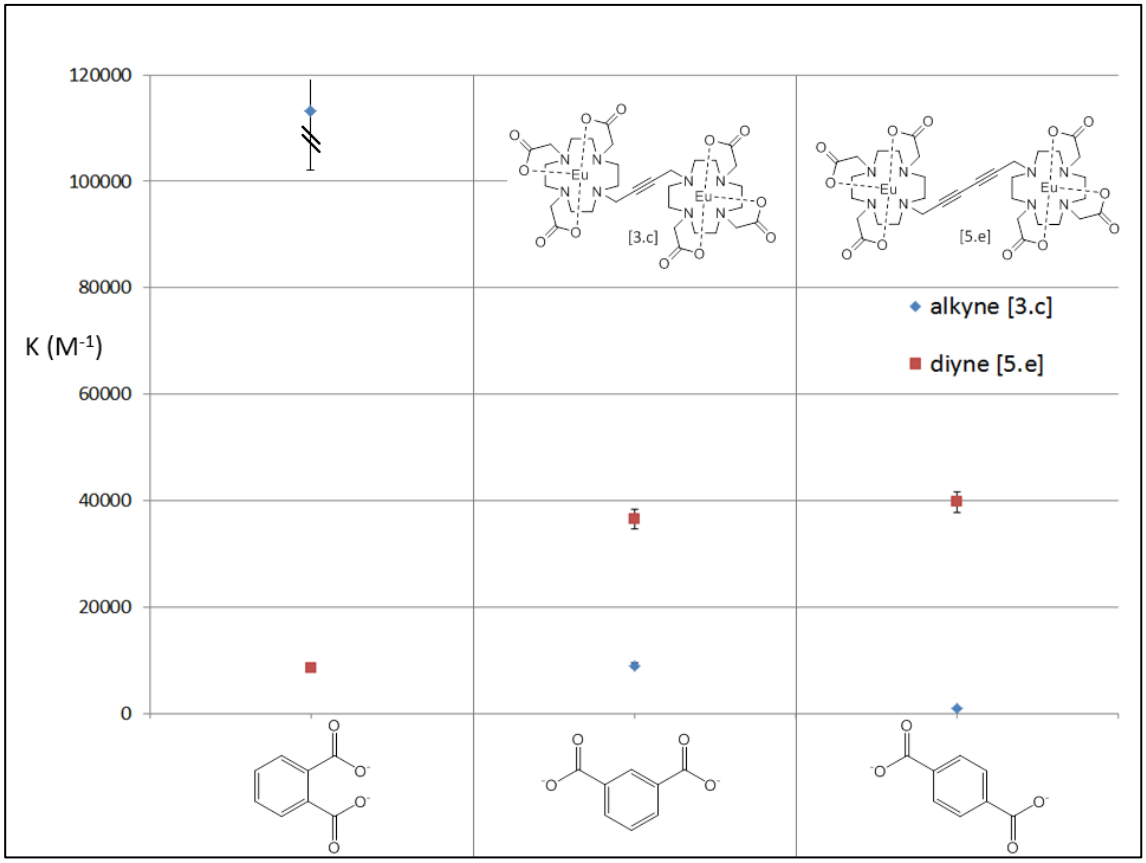

Figure 6-4The affinities of complexes [3.c] and [5.e] for the different isomers of benzene-dicarboxylate.

A more thorough investigation was thwarted by solubility issues on the part of the host complexes. Work is ongoing regarding the design and preparation of ditopic complexes which have similar intermetallic separations and rigidities, but enhanced hydrophilicity and increased solubility in useful solvent systems.

Overall, it is clear that there is great potential for using multinuclear complexes as host molecules for anions in water. These studies represent work at the beginning of what will hopefully be a much longer story. They provide guidelines for the future, and it is hoped that the concepts described here will be explored further to generated ion-specific hosts and responsive sensors.

7 Experimental

7.1 Instrumentation

Commercially available solvents and chemicals were used without further purification unless otherwise stated. Where dry solvents were used, they were degassed with nitrogen, dried by passing through an MBraun MPSP-800 column and then used immediately. Water was deionised and microfiltered using a Milli-Q Millipore machine.

Silica gel for flash column chromatography was purchased from Merck (Geduran 60, 230-400 mesh) and neutral alumina was purchased from Sigma-Aldrich (Merck 90, 70-230 mesh) and soaked in ethyl acetate before use. Silica TLC plates were TLC Silica gel 60 purchased from Merck. Alumina TLC plates were TLC Alumina 60 F254 neutral, purchased from Merck.

Dialysis was performed using a dialysis chamber purchased from Sigma-Aldrich, sealed with a cellulose membrane with a molecular weight cut-off of 500 Da. The sample was dissolved in water and placed in the chamber and the chamber was placed in 3 L beaker filled with deionised water. The water was changed twice per day.

NMR spectra were recorded at 298 K unless otherwise stated. 300 MHz ^{1}H or 76 MHz ^{13}C NMR spectra were recorded on a Varian Mercury 300 spectrometer. 400 MHz ^{1}H or 101 MHz ^{13}C spectra were recorded on a Bruker AVIII400 HD nanobay instrument and 500 MHz ^{1}H or 126 MHz ^{13}C NMR spectra were recorded on a Bruker AVIII 500 spectrometer or a Bruker AVII 500 with ^{13}C cryo-probe. All chemical shift (δ) values are given in parts per million and were referenced to the residual solvent peak. ^{13}C-spectra were recorded where possible. However in most of the macrocyclic structures, the isomeric exchange and conformational fluxionality of the system, combined with the low abundance of the resonant nuclei meant that the ^{13}C-NMR spectra displayed very low signal to noise ratios and very broad resonances, making them unreliable and

incomplete. The introduction of paramagnetic lanthanide centres only exacerbated the line broadening and took the recording of ^{13}C-spectra from exceedingly difficult to all but impossible.

pH values were measured using a Hanna Instruments pH210 Microprocessor pH Meter with a HI 1131B electrode.

Low-resolution mass spectra were recorded on a Micromass LCT Premier XE spectrometer. Accurate masses were determined to four decimal places using Bruker µTOF and Micromass GCT spectrometers. MALDI-TOF mass spectra were recorded on a Waters MALDI Micro MX or recorded by the staff at the National Mass Spectrometry Service Centre facility in Swansea using a Voyager DE-STR MALDITOF system.

Luminescence measurements of europium and terbium complexes were performed either on a Perkin Elmer LS55 or on a Horiba Jobin Yvon FluoroLog-3 equipped with a Hamamatsu R928 PMT detector and a double-grating excitation and emission monochromators. The spectra were corrected to take into account the energy profile of the lamp and the detector sensitivity at each wavelength using the manufacturer's correction file.

Luminescence measurements of ytterbium complexes were conducted using a PTI-3301 pulsed nitrogen laser and an Edinburgh Instruments EI-P germanium photodiode, and were recorded with a Tektronix TDS220 digital oscilloscope. Luminescence lifetimes of these complexes were obtained by iterative reconvolution of the detector response using a Microsoft Excel or Origin Pro spreadsheet.

Solid state infra-red spectra were acquired using a Bio-Rad FTS 6000 Spectrometer.

7.2 General Procedures

7.2.1 General Procedure A for the preparation of homo-metallic complexes.

The free ligand was dissolved in methanol (30 ml/mmol) and the appropriate lanthanide triflate (1.05 equivalents per binding site) added. The reaction mixture was stirred at 323 K for 48 hours. The solvent was removed under reduced pressure and the resulting residue taken up into

deionised water. The solution was adjusted to pH 12 with aqueous sodium hydroxide (1 M) to cause any excess lanthanide metal to precipitate as the hydroxide. This was removed via centrifugation and the supernatant was readjusted to pH 7 with aqueous hydrochloric acid (1.0 M) before being further purified by dialysis. The water was evaporated under reduced pressure to afford the pure product.

7.3 Synthesis

tri-*tert*-butyl 2,2',2''-(1,4,7,10-tetraazacyclododecane-1,4,7-triyl)triacetate [2.a][1]

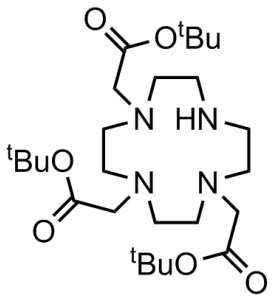

1,4,7,10 tetraazacyclododecane (5.00 g, 29.02 mmol) and sodium hydrogen carbonate (7.80 g, 92.86 mmol) were dissolved in dry acetonitrile (200 mL) and stirred at 273 K. *Tert*-butyl bromoacetate (13.71 mL, 92.86 mmol) was dissolved in acetonitrile (50 mL) and the resulting solution added to the first, drop-wise over two hours. Following addition, the reaction mixture was allowed to return slowly to room temperature and was stirred for 48 hours. The reaction mixture was filtered to remove inorganic salts and the filtrate was then evaporated under reduced pressure to give a beige crude product. The pure product was isolated as a white flocculent solid via successive recrystallisations from hot toluene.

Yield: 8.67 g, (58%).

^{1}H-NMR (400 MHz, $CDCl_3$): δ 10.01 (s, br, 1H), 3.36 (s, 4H), 3.28 (s, 2H), 3.09 (m, 4H), 2.88 (m, br, 12H), 1.45 (s, 18H), 1.44 (s, 9H).

^{13}C NMR (101 MHz, $CDCl_3$): δ 170.5, 169.6, 81.8, 81.7, 58.2, 51.3, 49.2, 47.5, 28.2, 28.2

LR-ES$^+$MS:): *m/z* calc for $[M+H]^+$ 515.38, found 514.37.

1,3-bis-((1,4,7,10-tetraazacyclododecane-1,4,7-triyl)(triacetate-tert-butylester))-propane. [2.b]

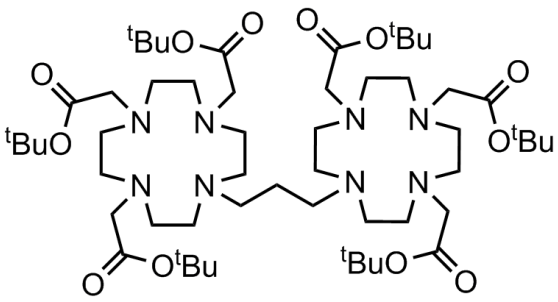

[2.a] (2.50 g, 4.86 mmol) and Cs_2CO_3 (3.77 g, 11.57 mmol) were suspended in anhydrous acetonitrile (150 mL) and stirred under nitrogen. 1,3-dibromopropane (241 µL, 2.37 mmol) was added via syringe. The reaction mixture was refluxed for 44 hours. Inorganic solids were removed by filtration and the filtrate evaporated under reduced pressure to yield a yellow oil. Purification was carried out by alumina column chromatography (dichloromethane/methanol, v/v, 49:1) and the product was isolated as a pale yellow solid.

Yield: 1015 mg, 40.1%

^{1}H-NMR (400 MHz, $CDCl_3$): δ 3.31 (s, br, 4H), 3.27 (s, br, 8H), 2.81 (s, br, 24H), 2.60 (m, br, 8H), 2.38 (m, br, 4H), 1.48 (m, br, 2H), 1.47 (m, br, 54H).

HR-ES$^+$MS (MeOH): *m/z* calc for $[M+2H]^{2+}$ 535.3960, found 535.3962

1,3-bis-((1,4,7,10-tetraazacyclododecane-1,4,7-triyl)(triacetatic acid))-propane. [2.c]

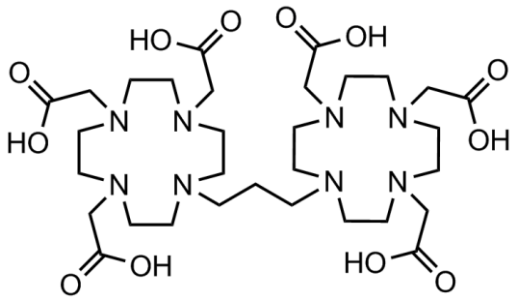

The *tert*-butyl protected pro-ligand [2.b] (806 mg, 0.75 mmol) was dissolved in dichloromethane (3 mL) and trifluoroacetic acid (7 mL) was added. The reaction mixture was stirred at room

temperature for 72 hours. The solution was reduced under vacuum and the product isolated as an off-white powder via repeated trituration with diethyl-ether.

Yield: 486 mg, 88%.

^{1}H-NMR (400 MHz, d_6-DMSO): δ 4.20 (s, br, 4H), 3.70 - 3.38 (m, br, 24H), 3.28 - 2.93 (m, br, 24H), 2.08 (s, br, 2H)

LR-MALDI-MS: *m/z* calc for $[M]^+$ 733.41, found 733.56.

Homometallic complexes of [2.c].

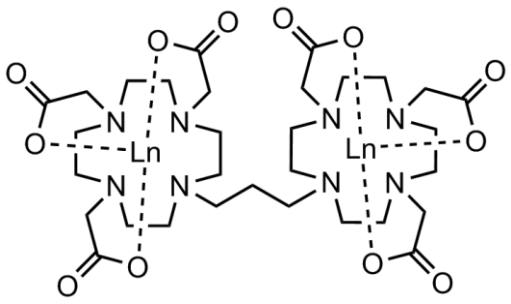

Prepared from [2.c] according to general procedure A.

[2.d] Ln = Eu.

^{1}H-NMR (400 MHz, D_2O): δ 27.45, 24.44, 23.76, 23.12, 20.60, 14.77, 11.87, 11.40, 7.97, 7.24, 2.96, 2.41, 1.18, 0.36, -0.14, -2.52, -3.31, -5.09, -6.32, -7.76, -8.20, -10.25, -11.33, -12.07, -12.68, -13.33, -15.52, -16.75, -17.37, -19.36, -21.56.

MALDI-MS (α-MeOH): *m/z* calc for $[M]^+$ 1031.20, found 1031.40.

[2.e] Ln = Yb

^{1}H-NMR (400 MHz, D_2O): δ 103.25, 100.02, 79.68, 77.12, 74.79, 67.65, 57.62, 52.87, 47.74, 35.19, 29.73, 25.55, 25.14, 21.26, 19.66, 14.21, 12.07, 10.80, 8.34, 3.03, 2.51, -2.26, -3.72, -7.28, -9.26, -11.48, -12.69, -14.56, -16.52, -18.36, -21.16, -23.93, -25.38, -29.73, -30.46, -32.72, -35.41, -40.38, -47.77, -49.85, -51.06, -52.19, -52.98, -53.42, -55.51, -60.48, -63.68, -78.66, -100.08, -113.65.

MALDI-MS (α-MeOH): *m/z* calc for $[M]^+$ 1074.23, found 1074.28.

[2.f] Ln = Lu

^{1}H-NMR (400 MHz, D_2O): δ 3.19 (s, br, 12H), 2.66 (s, br, 16H), 2.59 (m, br, 20H), 1.61 (s, 2H).

MALDI-MS (α-MeOH): *m/z* calc for $[M]^+$ 1076.24, found 1077.30.

[2.g] Ln = Y

^{1}H-NMR (400 MHz, D_2O): δ 3.80 (m, br, 12H), 3.50 - 2.95 (m, br, 32H), 1.95 (s, br, 2H).

MALDI-MS (α-MeOH): *m/z* calc for $[M]^+$ 927.16, found 927.25.

1,4-bis-((1,4,7,10-tetraazacyclododecane-1,4,7-triyl)(triacetate-tert-butylester))-but-2-yne. [3.a]

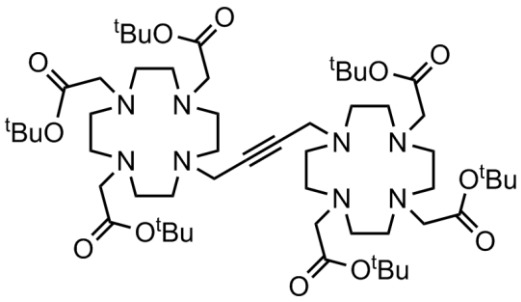

[2.1] (2.50 g, 4.86 mmol) and Cs_2CO_3 (3.77 g, 11.57 mmol) were suspended in anhydrous acetonitrile (150 mL) and stirred under nitrogen. 1,4-dichloro-2-butyne (226 µL, 2.31 mmol) was added via syringe. The reaction mixture was stirred at room temperature for 16 hours. Inorganic solids were removed by filtration and the filtrate evaporated under reduced pressure to yield a yellow-orange oil. Purification was carried out by alumina column chromatography (dichloromethane/methanol, v/v, 49:1) and the product was isolated as a pale yellow powder.

Yield: 1.19 g, 48%

^{1}H-NMR (400 MHz, $CDCl_3$): δ 3.50 (s, br, 4H), 3.40 - 2.10 (m, br, 44H), 1.45 (m, br, 54H)

HR-ES$^+$MS (MeOH): *m/z* calc for $[M+Na]^+$ 1101.7509, found 1101.7524

1,4-bis-((1,4,7,10-tetraazacyclododecane-1,4,7-triyl)(triacetatic acid))-but-2-yne. [3.b]

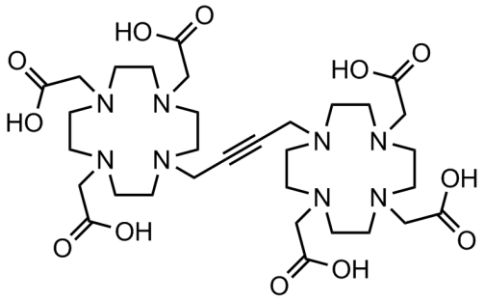

The *tert*-butyl protected pro-ligand [3.a] (1500 mg, 1.39 mmol) was dissolved in dichloromethane (3 mL) and trifluoroacetic acid (9.29 mL, 125.10 mmol) was added. The reaction mixture was stirred at room temperature for 72 hours. The solution was reduced under vacuum and the product isolated as pale beige solid via repeated trituration with diethyl-ether.

Yield: 897 mg, 87%.

^{1}H-NMR (400 MHz,DMSO): δ 4.12 (m, br, 4H), 3.90 (m, br, 12H), 3.39 (m, br, 16H), 3.24 (m, br, 16H)

MALDI-MS: *m/z* calc for $[M]^{+}$ 743.39, found 743.49.

Homometallic complexes of [3.b]

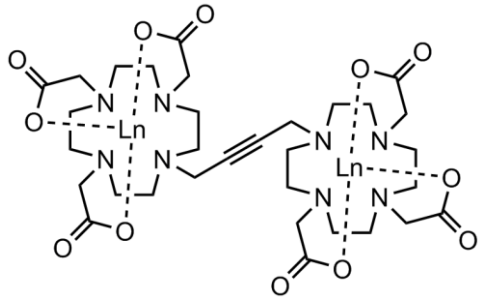

Prepared from [3.b] according to General Procedure A:

[3.c] (Ln = Eu)

^{1}H-NMR (400 MHz,D_2O): δ 23.42, 22.35, 16.87, 15.57, 14.07, 13.50, 11.76, 11.01, 10.29, 9.56, 9.04, 8.10, 6.86, 6.22, 3.93, 3.47, 3.21, 3.10, 2.96, 2.61, 2.46, 2.29, 1.76, 1.58, 1.42, 1.20, 0.26, -0.08, -0.88, -1.57, -2.82, -3.45, -4.55, -5.42, -6.09, -6.29, -6.67, -8.16, -8.71, -9.07, -10.09, -10.78, -10.96, -11.10, -11.94, -12.30, -13.15, -14.06, -14.55, -15.30, -17.15, -17.40, -19.75.

MALDI-MS (α-MeOH): *m/z* calc for $[M+Na]^{+}$ 1065.17, found 1066.22.

[3.d] (Ln = Gd)

MALDI-MS (α-MeOH): *m/z* calc for $[M+H]^+$ 1053.20, found 1054.24.

[3.e] (Ln = Tb)

^{1}H-NMR (400 MHz,D_2O): δ 333.91, 318.34, 273.27, 143.80, 136.43, 88.86, 83.70, 70.36, 67.07, 51.04, 37.48, 24.58, 14.05, 11.14, 3.79, 3.09, 2.94, 2.57, 2.28, 1.41, 1.19, -0.88, -2.10, -2.64, -2.94, -3.17, -3.62, -4.81, -5.58, -7.82, -8.21, -9.57, -10.36, -13.03, -13.38, -16.22, -16.78, -18.67, -19.82, -32.61, -42.97, -47.38, -63.61, -67.23, -68.77, -78.21, -88.99, -92.77, -108.98, -116.22, -152.43, -161.63, -200.19, -228.37, -235.42, -311.76.

MALDI-MS (α-MeOH): *m/z* calc for $[M+Na]^+$ 1077.18, found 1078.22.

[3.f] (Ln = Yb)

^{1}H-NMR (400 MHz,D_2O): δ 87.47, 85.38, 84.85, 64.18, 63.15, 55.09, 53.82, 42.77, 42.11, 39.42, 38.80, 33.03, 29.61, 28.87, 25.83, 24.79, 24.38, 23.23, 13.15, 12.36, 8.39, 3.08, 2.91, 2.58, 2.25, 1.15, 0.34, -2.28, -5.11, -8.67, -10.77, -17.12, -17.79, -19.14, -19.82, -20.63, -25.11, -29.15, -30.48, -51.87, -52.98, -55.38, -56.17, -57.32.

MALDI-MS (α-MeOH): *m/z* calc for $[M+Na]^+$ 1107.21, found 1107.38.

[3.g] (Ln = Lu)

^{1}H-NMR (400 MHz,D_2O): δ 3.46 (s, br, 4H), 3.07 (s, br, 4H), 2.94 (s, br, 8H), 2.57 (m, br, 24H), 2.29 (m, br, 8H).

MALDI-MS (α-MeOH): *m/z* calc for $[M+H]^+$ 1087.23.

tri-tert-butyl 2,2',2''-(10-(prop-2-yn-1-yl)-1,4,7,10-tetraazacyclododecane-1,4,7-triyl)triacetate [3.h][2]

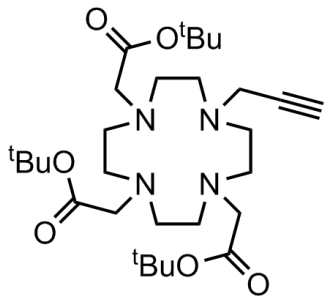

[2.a] (2.00 g, 3.87 mmol) and potassium carbonate (1.61 g, 11.66 mmol) were suspended in dry acetonitrile (75 mL) and stirred. Propargyl bromide (339 µL, 4.26 mmol) was added and the mixture stirred at room temperature, under a nitrogen atmosphere for 16 hours. Inorganic salts were removed via filtration and the solution was concentrated under vacuum. The crude product was taken up in dichloromethane (25 mL) and washed with water, aqueous sodium bicarbonate and brine. The organic layer was dried over magnesium sulphate and the solvent removed under reduced pressure to afford the pure product as a flocculent off-white powder.

Yield: 1.80 g, 84%

^{1}H-NMR (300 MHz, $CDCl_3$): δ 3.40 (d, J = 2.4 Hz, 2H), 3.25 (s, br, 6H), 2.77 (m, br, 8H), 2.63 (m, br, 8H), 2.08 (t, J = 2.4 Hz, 1H), 1.43 (s, 18H), 1.40 (s, 9H).

^{13}C-NMR (76 MHz, $CDCl_3$): δ 171.12, 129.24, 128.35, 125.44, 80.65, 79.18, 72.55, 56.85, 56.78, 53.38, 52.00, 42.97, 28.18.

LR-ES^{+}MS (MeOH): *m/z* calc for $[M+H]^{+}$ 553.40, found 553.39.

2,2',2''-(10-(prop-2-yn-1-yl)-1,4,7,10-tetraazacyclododecane-1,4,7-triyl)triacetic acid [3.i]

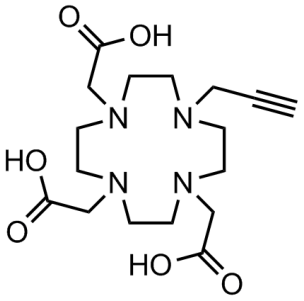

The *tert*-butyl protected pro-ligand [3.h] (1200 mg, 2.17 mmol) was dissolved in dichloromethane (3 mL) and trifluoroacetic acid (7 mL) was added. The reaction mixture was stirred at room temperature for 72 hours. The solution was reduced under vacuum and the product isolated as an off-white solids via repeated trituration with diethyl-ether.

Yield: Quantitative ^{1}H-NMR (400 MHz, $((CD_3)_2SO)$: δ 3.96 (s, br, 2H), 3.77 (s, br, 6H), 3.56 (s, 1H), 3.14 (m, br, 16H)

^{13}C-NMR (100 MHz, $((CD_3)_2SO)$: δ 174.36, 171.99, 77.61, 73.61, 55.95, 53.92, 53.02, 51.73, 48.89, 44.72, 36.86, 31.26.

LR-ES^{+}MS (MeOH): *m/z* calc for $[M+H]^{+}$ 385.21, found 385.23.

Lanthanide complexes of [3.i]

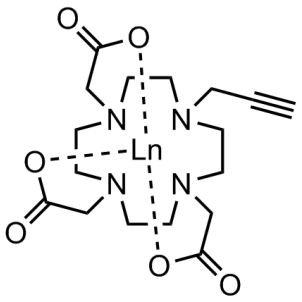

Prepared from [3.i] according to general procedure A.

[3.j] (Ln = Eu)

^{1}H-NMR (400 MHz,D_2O): δ 22.96, 13.73, 11.30, 10.14, 8.31, 6.88, 6.58, 5.54, 3.35, 3.07, 2.94, 2.57, 2.27, -0.73, -1.21, -3.91, -6.09, -6.65, -9.39, -11.19, -11.54, -12.36, -12.70, -12.86, -14.64, -17.62.

MALDI-MS (α-MeOH): *m/z* calc for $[M+Na]^{+}$ 556.36, found 555.44.

[3.k] (Ln = Gd)

MALDI-MS (α-MeOH): *m/z* calc for $[M+Na]^{+}$ 562.09, found 562.17

[3.l] (Ln = Tb):

MALDI-MS (α-MeOH): *m/z* calc for $[M+H]^{+}$ 541.11, found 542.13.

[3.o] (Ln = Tm)

^{1}H-NMR (500 MHz,D_2O): δ 181.06, 132.79, 113.26, 94.47, 58.68, 43.63, 26.10, 20.08, 6.47, -9.61, -16.05, -42.67, -50.40, -52.02, -69.72, -72.18, -73.12, -77.80, -78.31.

[3.m] (Ln = Yb)

^{1}H-NMR (400 MHz,D_2O): δ 85.36, 65.16, 62.36, 53.26, 44.04, 39.43, 33.02, 29.70, 24.95, 24.07, 23.24, 18.91, 12.24, 11.65, 9.34, 3.38, 2.98, 2.57, 2.33, 0.32, -2.54, -4.91, -8.47, -10.98, -11.88, -12.80, -14.92, -17.07, -17.82, -18.13, -19.93, -20.28, -21.14, -21.98, -24.07, -29.72, -30.02, -52.45, -56.37, -56.74, 58.83.

MALDI-MS (α-MeOH): *m/z* calc for $[M+Na]^+$ 578.11, found 578.14.

[3.n] (Ln = Lu)

^{1}H-NMR (400 MHz,D_2O): δ 3.95 (s, br, 1H), 3.39 (m, br, 8H), 3.10 - 2.32 (m, br, 16H)

MALDI-MS (α-MeOH): *m/z* calc for $[M+H]^+$ 557.13, found 577.16.

hexa-2,4-diyne-1,6-diol [5.a][3-6]

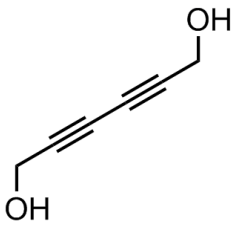

Triphenylphosphine (84 mg, 0.32 mmol), copper (I) iodide (20.5 mg, 0.11 mmol) and bis(triphenylphosphine) palladium (II) dichloride (75 mg, 0.11 mmol) were dissolved in anhydrous triethylamine/acetonitrile (v/v, 5:3, 8 mL) and cooled to 273K. Propargyl alcohol (200 µL, 3.57 mmol) was added. The reaction was stirred in the dark and allowed to warm to room temperature. The mixture was filtered through a celite pad and the solution removed under reduced pressure to yield a pale yellow solid. This was purified via column chromatography (silica, petroleum ether/ethylacetate, v/v, 1:1) to afford the product as a pale yellow solid.

Yield: 27 %.

^{1}H-NMR (400 MHz, $CDCl_3$): δ 4.24 (s, 4H)

^{13}C-NMR (101 MHz, $CDCl_3$): δ 78.3, 70.1, 50.8

1,6-dichloro-hexa-2,4-diyne [5.b]

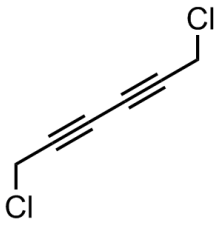

Thionyl chloride (2 mL) and pyridine (1 drop) charged into a flask and cooled to 273K under a nitrogen atmosphere. [5.a] (100 mg, 0.91 mmol) was added in one portion and the mixture stirred at 273K for 3 hours. The reaction was allowed to warm slowly to room temperature and stirred for a further 14 hours, before being poured onto crushed ice. The aqueous mixture was extracted with chloroform. The combined organic layers were washed with sodium hydrogencarbonate aqueous solution and dried over magnesium sulphate and reduced *in vacuo*. The product was used immediately.

Yield: 125 mg, 94%.

^{1}H-NMR (400 MHz, $CDCl_3$): δ 4.16 (s)

^{13}C-NMR (101 MHz, $CDCl_3$): δ 74.0, 68.1, 31.0

Used without further characterisation due to its reactivity and presumed toxicity.

hexa-2,4-diyne-1,6-diylbis-(1,4,7,10-tetraazacyclododecane-1,4,7-triyl)(triacetate-tert-butylester) [5.c]

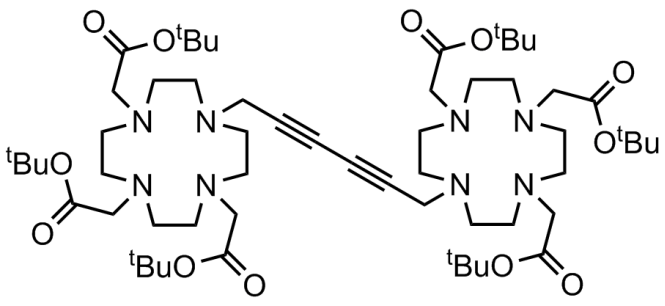

[2.1] (1.00 g, 1.94 mmol) and caesium carbonate (1.51 g, 4.63 mmol) were suspended in anhydrous acetonitrile (50 mL) and stirred. [5.b] (136 mg, 0.93 mmol) was dissolved in anhydrous acetonitrile (10 mL) and added in one portion. The reaction mixture was stirred at room temperature under a nitrogen atmosphere for 16 hours. Solids were removed by filtration and the filtrate concentrated under reduced pressure to afford the crude product as a yellow oil. This was purified by column chromatography (alumina, dichloromethane/methanol, v/v 49:1) and the product isolated as an off-white solid.

Yield: 496 mg, 48%.

^{1}H-NMR (400 MHz, $CDCl_3$): δ 3.55 (s, 4H), 3.25 - 2.00 (m, br, 44H), 1.48 (s, br, 36H), 1.42 (s, br, 18H)

HR-ES^{+}MS (MeOH): *m/z* calc for $[M+Na]^{+}$ 1125.7509, found 1125.7504.

hexa-2,4-diyne-1,6-diylbis-(1,4,7,10-tetraazacyclododecane-1,4,7-triyl)(triacetic acid) [5.d]

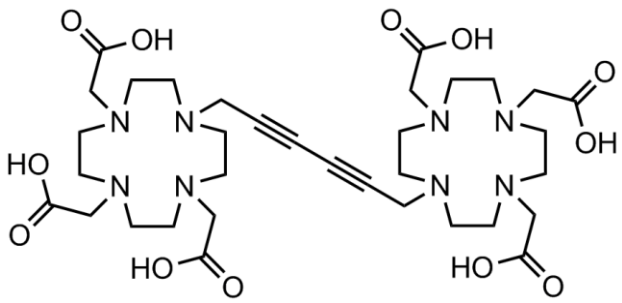

The *tert*-butyl protected pro-ligand [5.c] (375 mg, 0.272 mmol) was dissolved in dichloromethane (3 mL) and trifluoroacetic acid (7 mL) was added. The reaction mixture was stirred at room temperature for 72 hours. The solution was reduced under vacuum and the product isolated as an off-white powder via repeated trituration with diethyl-ether.

Yield: 237 mg, 91%

^{1}H-NMR (400 MHz, D_2O): δ 3.92 (m, br, 8H), 3.84 (m, br, 4H), 3.61 (m, br, 4H), 3.37 (m, br, 8H), 3.15 (m, br, 8H).

LR-ES^{+}MS (MeOH): *m/z* calc for $[M]^{+}$

Eu_2.[5.d] = [5.e]

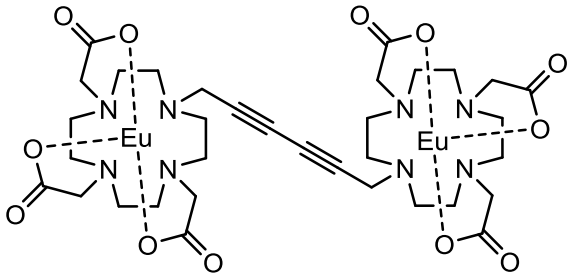

Prepared from [5.d] according to general procedure A.

^{1}H-NMR (400 MHz,D_2O): δ 23.91, 23.27, 16.04, 15.41, 14.23, 13.87, 11.98, 11.52, 10.77, 10.18, 8.97, 8.42, 7.92, 7.06, 6.33, 5.63, 4.16, 3.55, 3.39, 3.14, 2.96, 2.67, 2.53, 2.31, 1.21, 0.25, -0.16, -0.62, -1.03, -2.81, -3.17, -3.98, -4.86, -5.22, -5.57, -5.97, -6.33, -6.58, -8.42, -9.01, -9.43, -10.25, -10.49, -10.96, -11.33, -12.36, -12.67, -12.85, -13.54, -14.26, -14.54, -15.55, -15.73, -17.41, -17.58, -20.19.

3,3'-(1,4-phenylene)bis(prop-2-yn-1-ol) [5.f][7, 8]

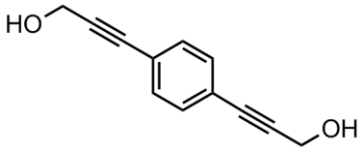

Method 1: 1,4-diethynylbenzene (1.26 g, 10.0 mmol) was dissolved in anhydrous THF (20 mL) and cooled to 195 K. *n*-butyllithium (1.6 M solution in hexanes, 15 mL, 24.0 mmol) was added dropwise and the solution allowed to warm to 260 K. The mixture turned blue/grey and was then cooled again to 195 K Paraformaldehyde (0.841 g, 28.0 mmol) was suspended in anhydrous THF (20 mL) and added via cannula. The mixture was stirred at 195 K for 3 hours, allowed to warm slowly to room temperature and stirred for 16 hours. Saturated ammonium chloride aqueous solution (50 mL) was added and the aqueous layer extracted with diethylether. The combined organic layers were washed with brine, dried over magnesium sulphate and concentrated under reduced pressure to give the crude product. This was purified by column chromatography (petroleum ether/ethylacetate, 1:1 on silica). Petroleum ether was removed via repeated

washings with dichloromethane and the pure product was isolated as a very pale yellow solid. Yield: 220 mg, 12%.

Method 2: 1,4-dibromobenzene (1.00 g, 4.24 mmol) was dissolved in an anhydrous mixture of dichloromethane and triethylamine (v/v, 1/3, 10 mL/mmol) and the solution degassed. Copper (I) iodide (32 mg, 0.17 mmol), propargyl alcohol (616 µL, 10.60 mmol) and tetrakis (triphenylphosphine) palladium (98 mg, 0.085 mmol) were added and the reaction mixture refluxed under nitrogen overnight. The solvent was removed under reduced pressure and the resulting residue was taken up in ethylacetate and washed successively with saturated ammonium chloride aqueous solution, brine and finally distilled water. The organic layer was dried over magnesium sulphate and the solvent removed *in vaccuo* to give the crude product as a beige solid. This was purified by column chromatography (petroleum ether/ethylacetate, 1:1 on silica). Petroleum ether was removed via repeated washings with dichloromethane and the pure product was isolated as a very pale yellow solid. Yield: 726 mg, 92%.

^{1}H-NMR (400 MHz, $CDCl_3$): δ 7.39 (s, 4H), 4.51 (d, J = 6.2 Hz, 4H), 1.66 (t, J=6.2 Hz, 2H).

^{13}C-NMR (101 MHz, $CDCl_3$): δ 134.5, 120.2, 91.5, 86.6, 53.5.

LR-ES^{+}MS (MeOH): *m/z* calc for $[M]^{+}$ 186.07, found 187.09.

1,4-bis(3-bromoprop-1-yn-1-yl)benzene [5.g][9]

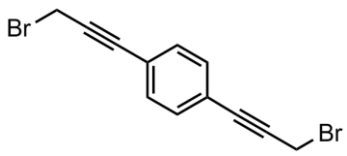

The bis-propargyl alcohol [5.f] (210 mg, 1.13 mmol) was dissolved in anhydrous diethylether (22 mL) and cooled to 273 K. Phosphorus tribromide (265 µL, 2.82 mmol) was dissolved in dry diethylether (10 mL) and was added via cannula. The reaction mixture was stirred at 273 K for 6 hours, before slowly being allowed to warm to room temperature and then stirred for a further 18 hours. The reaction mixture was poured onto crushed ice and extracted with diethylether. The combined organic layers were washed with a saturated sodium bicarbonate aqueous solution and

deionised water, before being dried over magnesium sulphate. The solvent was removed under reduced pressure to yield the product as an off-white solid.

Yield: 144 mg, 41%.

^{1}H-NMR (400 MHz, $CDCl_3$): δ 7.40 (s, 4H), 4.17 (s, 4H).

^{13}C-NMR (101 MHz, $CDCl_3$): δ 132.2, 123.1, 87.0, 81.1, 14.

Used immediately without further characterisation due to its reactivity and presumed toxicity.

1,4-phenylenebis(prop-2-yne-3,1-diyl)bis-(1,4,7,10-tetraazacyclododecane-1,4,7-triyl)(triacetate-tert-butylester) [5.h]

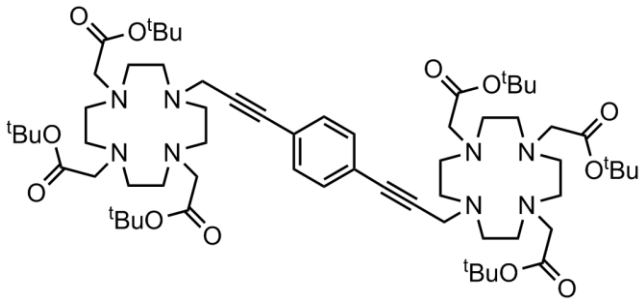

[2.1] (500 mg, 0.97 mmol) and caesium carbonate (750 mg, 2.30 mmol) were suspended in anhydrous acetonitrile (30 mL) and [5.g] (144 mg, 0.46 mmol) was added. The reaction mixture was stirred under a nitrogen atmosphere for 16 hours. Inorganic solids were removed by filtration and the solvent evaporated under reduced pressure to yield a pale green oil. The residue was taken up into dichloromethane (30 mL) and washed with brine. The crude product was concentrated under reduced pressure and purified by column chromatography on neutral alumina, eluting with dichloromethane/methanol (v/v, 49:1) to afford the pure product as a pale green solid.

Yield: 148 mg, 27 %.

^{1}H-NMR (400 MHz, $CDCl_3$): δ 7.29 (s, br, 4H), 3.58 (s, br, 4H), 3.25 - 2.20 (m, br, 44H), 1.42 (s, br, 54H).

HR-ESMS: *m/z* calc for $[M+Na]^+$ 1201.7822, found 1201.7864.

1,4-phenylenebis(prop-2-yne-3,1-diyl)bis-(1,4,7,10-tetraazacyclododecane-1,4,7-triyl)(triacetic acid) [5.i]

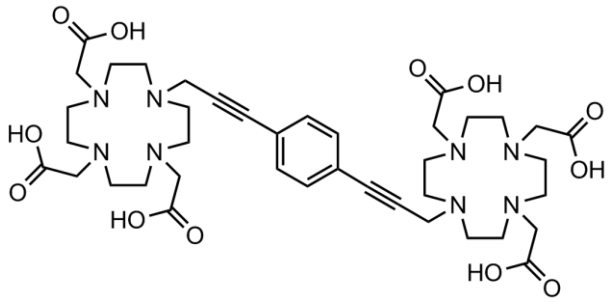

The *tert*-butyl protected pro-ligand [5.h] (100 mg, 0.85 mmol) was dissolved in dichloromethane (3 mL) and trifluoroacetic acid (7 mL) was added. The reaction mixture was stirred at room temperature for 72 hours. The solution was reduced under vacuum and the product isolated via repeated trituration with diethyl-ether. The product was obtained as a very pale yellow powder.

Yield: 94%.

^{1}H-NMR (400 MHz, D_2O): δ 7.48 (s, 4H), 4.09 (s, br, 4H), 3.81 (s, br, 8H), 3.62 (s, br, 4H), 3.47 - 3.04 (m, br, 32H)

HR-ESMS: *m/z* calc for $[M+H]^+$ 843.4252, found 843.4268

Eu_2[5.i] = [5.j]

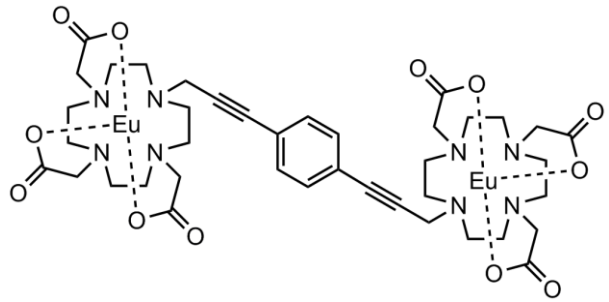

[5.i] (50 mg, 0.0593 mmol) was suspended in methanol (10 ml) and europium triflate (74.6 mg, 0.125 mmol) added. The turbid suspension was heated to 328 K and stirred. After 10 days the mixture was observed to have dissolved and the reaction was assumed complete. The methanol was removed under reduced pressure and the residue suspended in deionised water. The suspension was agitated and then allowed to settle.

^{1}H-NMR (400 MHz, D_2O): δ 26.47, 7.78, 7.69, 7.55, 4.02, 3.65, 3.37, 3.06, 2.82, 2.56, 1.09, 0.19, -5.85, -7.29, -9.17, -10.38, -15.32, -16.52, -19.59.

3,3'-(1,3-phenylene)bis(prop-2-yn-1-ol) [5.k][7, 8]

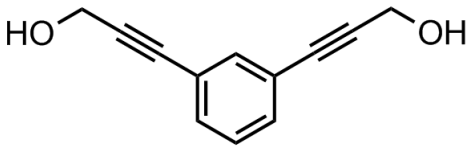

1,3-dibromobenzene (1.00 mL, 1.95 g, 8.27 mmol) was dissolved in an anhydrous mixture of dichloromethane and triethylamine (v/v, 1/3, 10 mL/mmol) and the solution degassed. Copper (I) iodide (94.5 mg, 0.50 mmol), propargyl alcohol (2.89 mL, 49.64 mmol) and tetrakis (triphenylphosphine) palladium (287 mg, 0.248 mmol) were added and the reaction mixture refluxed under nitrogen for 72 hours. The solvent was removed under reduced pressure and the resulting residue was taken up in ethylacetate and washed successively with saturated ammonium chloride aqueous solution, brine and finally distilled water. The organic layer was dried over magnesium sulphate and the solvent removed *in vacuo* to give the crude product as a dark orange oil. This was purified by column chromatography (petroleum ether/ethylacetate, 2:3 on silica) to afford the pure product as a pale yellow oil.

Yield: 68 %.

^{1}H-NMR (400 MHz, $CDCl_3$): δ 7.50 (m, br, 1H), 7.39 (dd, J = 7.6 Hz, J = 1.5 Hz, 2H), 7.26 (t, J = 7.6 Hz, 1H), 4.50 (s, 4H), 1.88 (s, br, 2H).

^{13}C-NMR (101 MHz, $CDCl_3$): δ 134.7, 131.6, 128.4, 122.9, 87.9, 84.7, 51.6.

LR-ES^{+}MS (MeOH): *m/z* calc for $[M]^{+}$ 186.07, found 187.10.

1,3-bis(3-bromoprop-1-yn-1-yl)benzene [5.l][9]

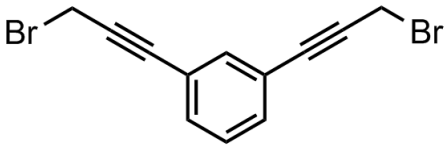

The bis-propargyl alcohol [5.k] (500 mg, 2.69 mmol) was dissolved in anhydrous diethylether (55 mL) and cooled to 273 K. Phosphorus tribromide (2.52 mL, 26.9 mmol) was dissolved in dry diethylether (10 mL) and was added via cannula. The reaction mixture was stirred at 273 K for 6 hours, before slowly being allowed to warm to room temperature and then stirred for a further 18 hours. The reaction mixture was poured onto crushed ice and extracted with diethylether. The combined organic layers were washed with a saturated sodium bicarbonate aqueous solution and deionised water, before being dried over magnesium sulphate. The solvent was removed under reduced pressure to yield the product as an off-white solid.

Yield: 88 %.

^{1}H-NMR (400 MHz, $CDCl_3$): δ 7.53 (s, br, 1H), 7.41 (d, br, J = 7.5 Hz, 2H), 7.29 (t, J = 7.6 Hz, 1H), 4.15 (s, br, 4H).

^{13}C-NMR (101 MHz, $CDCl_3$): δ 133.9, 130.2, 127.9, 122.5, 86.7, 80.5, 14.1

Used without further characterisation due to its reactivity and presumed toxicity.

1,3-phenylenebis(prop-2-yne-3,1-diyl)bis-(1,4,7,10-tetraazacyclododecane-1,4,7-triyl)(triacetate-tert-butylester) [5.m]

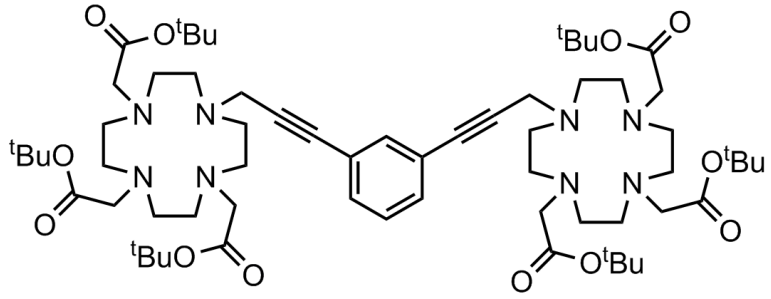

[2.a] (300 mg, 0.59 mmol) and caesium carbonate (454 mg, 1.39 mmol) were suspended in anhydrous acetonitrile (25 mL) and [5.l] (87 mg, 0.28 mmol) was added. The reaction mixture was

stirred under a nitrogen atmosphere for 16 hours. Inorganic solids were removed by filtration and the solvent evaporated under reduced pressure to yield a viscous yellow oil. The residue was taken up into dichloromethane (25ml) and washed with brine. The crude product was concentrated under reduced pressure and purified by column chromatography on neutral alumina, eluting with dichloromethane/methanol (v/v, 49:1) to afford the pure product as a beige solid.

Yield: 115 mg, 34%

^{1}H-NMR (400 MHz, $((CD_3)_2SO)$: δ 7.46 (s, 1H), 7.41 (m, 2H), 7.35 (m, 1H), 3.69 (s, br, 4H), 3.09 - 2.55 (m, br, 32H), 2.43 - 2.20 (m, br, 12H), 1.44 (m, 54H).

HR-ESMS: *m/z* calc for $[M+Na]^+$ 1201.7822, found 1201.7855.

1,3-phenylenebis(prop-2-yne-3,1-diyl)bis-(1,4,7,10-tetraazacyclododecane-1,4,7-triyl)(triacetic acid) [5.n]

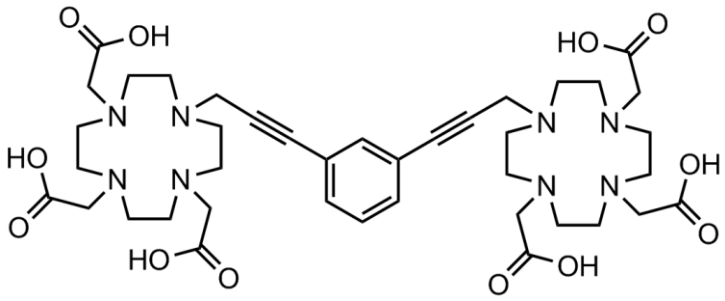

The *tert*-butyl protected pro-ligand [5.m](100 mg, 0.085 mmol) was dissolved in dichloromethane (3 ml) and trifluoroacetic acid (7 ml) was added. The reaction mixture was stirred at room temperature for 72 hours. The solution was reduced under vacuum and the product isolated as a pale yellow solid via repeated trituration with diethyl-ether.

Yield: 85%

^{1}H-NMR (400 MHz, $((CD_3)_2SO)$: δ 7.53 (s, 1H), 7.48 (m, 2H), 7.41 (m, 1H), 3.69 (s, br, 4H), 3.14 - 2.66 (m, br, 32H), 2.49 - 2.25 (m, br, 12H).

HR-ESMS: *m/z* calc for $[M+H]^+$ 843.4252, found 843.4258

Atempted synthesis of Eu_2[5.n] = [5.o].

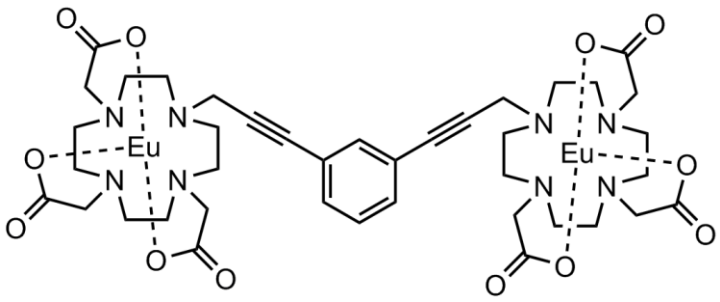

[5.n] (50 mg, 0.0593 mmol) was suspended in methanol (10 mL) and europium trifluoromethanesulfonate (75.2 mg, 0.126 mmol) added. The turbid suspension was heated to 328 K and stirred. After 10 days the mixture had not dissolved and the reaction was halted. The reaction mixture was filtered and the methanol removed under reduced pressure. Nothing was recovered and so it was assumed that the product was insoluble. Paramagnetic ^{1}H-NMR of the solid removed by filtration showed only starting material, with no proton resonances shifted by europium. The reaction was thus deemed to have failed.

7.4 Luminescence Titrations

A stock solution of the host complex was made by dissolving the complex in water with the relevant buffer. The solution was adjusted to approximately pH 7.6 using 1.0 M aqueous HCl or NaOH as appropriate. The volume was then increased with more buffered solution to adjust the final complex concentration to approximately 1.0 x 10^{-4} mol^1dm^{-3}. To ensure that the luminescence intensity was not altered by dilution, the titrant solutions were made using the complex stock solution as the solvent, thereby holding the concentration of the complex constant throughout the experiment. Titrant solutions were typically one hundred times more concentrated than the stock solution (c. 1 x 10^{-2} mol^1dm^{-3}) and the pH adjusted to match that of the parent stock solution. To begin, 2.00 ml of the stock solution was transferred to a lidded quartz cuvette and an emission spectrum recorded. Successive emission spectra were then taken as the concentration of the guest being studied was increased via repeated addition of aliquots of

the titrant solution. In each instance, the optimal excitation wavelength was determined by measuring the excitation spectrum whilst observing one of the well-defined emission maxima associated with lanthanide-centred emission.

7.5 Fitting Methodology

The titrations were monitored by following changes in the emission spectrum of the lanthanide complexes. Each lanthanide centre emitted from a single excited state by radiative transition to a series of states lower in the excited state manifold. Each transition gave rise to a band in the emission spectrum. The separable bands were integrated and these values tied with the concentration of the titrant. The procedure was repeated for each spectrum and gave rise to a number of datasets equal to the number of separable bands. Each lanthanide could be addressed directly by excitation into the lanthanide excited state manifold. Alternatively, in cases where the guest species bears an organic chromophore, lanthanide emission can be induced by sensitisation by the light-harvesting group. In this way more datasets can be generated: from excitation of organic chromophore and each of the lanthanide centres. Note that the intensity of direct excitation was significantly lower than when exciting into the organic chromophore.

7.6 DynaFit[10] Software

DynaFit software was used to fit the datasets generated from the integrated luminescence intensities. DynaFit is based on a stripped-down version of the program EQUIL and uses a multidimensional Newton-Raphson method to solve multiple simultaneous equilibria. Both DynaFit® 3 and DynaFit® 4 programs were used to fit the luminescence data. Examples of typical input scripts for each program are shown below; the programs then calculated the desired parameters automatically.

Typical DynaFit®3 script:

```
[task]
task = fit
data = equilibria

[mechanism]
Eu + Cl <==> complex1 : K1 assoc
Cl + complex1 <==> complex2 : K2 assoc

[constants]
K1 = 1e6 ??, K2 = 1e2 ?

[concentrations]
Eu= 5.81635E-4


[equilibria]
variable Cl
file C:\Users\James\Desktop\Dynafit_Txt_Files\349-1-Cl-1-dJ0.txt | response Eu = 4.788e8 , complex1 = 2e10 ? , complex2 = 1e8 ?
file C:\Users\James\Desktop\Dynafit_Txt_Files\349-1-Cl-1-dJ1.txt | response Eu = 2.702e9 , complex1 = 2e10 ? , complex2 = 1e8 ?
file C:\Users\James\Desktop\Dynafit_Txt_Files\349-1-Cl-1-dJ2.txt | response Eu = 4.776e9 , complex1 = 2e10 ? , complex2 = 1e8 ?
file C:\Users\James\Desktop\Dynafit_Txt_Files\349-1-Cl-1-dJ3.txt | response Eu = 1.925e8 , complex1 = 2e10 ? , complex2 = 1e8 ?
file C:\Users\James\Desktop\Dynafit_Txt_Files\349-1-Cl-1-dJ4.txt | response Eu = 1.235e9 , complex1 = 2e10 ? , complex2 = 1e8 ?



[output]
directory C:\Users\James\Desktop\Dynafit_Txt_Files\Results

[end]
```

Typical DynaFit®4 script.

```
[task]

task = fit
data = equil

[mechanism]

EuBMM + tartronate <==> complex1 : K1 assoc
tartronate + complex1 <==> complex2 : K2 assoc

[constants]

K1 = 1e3 ?? , K2 = 1?

[concentrations]

EuBMM= 5.035E-4

[equil]
```

variable tartronate

file C:\Users\James\Desktop\Dynafit_Txt_Files\JT329-D-HEPES-EuBMM-tartronate-J0.txt | response EuBMM = 6.1569e8 ?, complex1 = 9e9 ? , complex2 = 0 ?
file C:\Users\James\Desktop\Dynafit_Txt_Files\JT329-D-HEPES-EuBMM-tartronate-J1.txt | response EuBMM = 4.0071e9 ?, complex1 = 6e9 ? , complex2 = 0 ?
file C:\Users\James\Desktop\Dynafit_Txt_Files\JT329-D-HEPES-EuBMM-tartronate-J2.txt | response EuBMM = 8.6292e9 ?, complex1 = 1e10? , complex2 = 0 ?
file C:\Users\James\Desktop\Dynafit_Txt_Files\JT329-D-HEPES-EuBMM-tartronate-J3.txt | response EuBMM = 4.0596e8 ?, complex1 = 9e8 ? , complex2 = 0 ?
file C:\Users\James\Desktop\Dynafit_Txt_Files\JT329-D-HEPES-EuBMM-tartronate-J4.txt | response EuBMM = 2.4604e9 ?, complex1 = 4e9 ? , complex2 = 0 ?

;file C:\Users\James\Desktop\Dynafit_Txt_Files\JT329-D-HEPES-EuBMM-tartronate-R10.txt | response EuBMM = 33995 , complex1 = 30000 ? ;, complex2 = 0?
;file C:\Users\James\Desktop\Dynafit_Txt_Files\JT329-D-HEPES-EuBMM-tartronate-R20.txt | response EuBMM = 68818 , complex1 = 60000 ? ;, complex2 = 0?
;file C:\Users\James\Desktop\Dynafit_Txt_Files\JT329-D-HEPES-EuBMM-tartronate-R21.txt | response EuBMM = 8879 , complex1 = 6500 ? ;, complex2 = 0?

[output]

directory C:\Users\James\Desktop\Dynafit_Txt_Files\Results

[end]

7.7 References

1. A. Dadabhoy, S. Faulkner and P. G. Sammes, *Journal of the Chemical Society, Perkin Transactions 2*, 2000, 2359-2360.
2. M. Jauregui, W. S. Perry, C. Allain, L. R. Vidler, M. C. Willis, A. M. Kenwright, J. S. Snaith, G. J. Stasiuk, M. P. Lowe and S. Faulkner, *Dalton Transactions*, 2009, 6283-6285.
3. I. J. S. Fairlamb, P. S. Bauerlein, L. R. Marrison and J. M. Dickinson, *Chemical Communications*, 2003, 632-633.
4. F. Alonso and M. Yus, *ACS Catalysis*, 2012, **2**, 1441-1451.
5. B. S. Thyagarajan, P. E. Glaspy, E. Baker and P. Brown, *Organic Mass Spectrometry*, 1980, **15**, 224-228.
6. R. C. DeCicco, A. Black, L. Li and N. S. Goroff, *European Journal of Organic Chemistry*, 2012, **2012**, 4699-4704.
7. S. A. Caldarelli, S. El Fangour, S. Wein, C. Tran van Ba, C. Périgaud, A. Pellet, H. J. Vial and S. Peyrottes, *Journal of Medicinal Chemistry*, 2013, **56**, 496-509.
8. T.-J. Hsu, F. W. Fowler and J. W. Lauher, *Journal of the American Chemical Society*, 2011, **134**, 142-145.
9. Y. Yamaguchi, S. Kobayashi, T. Wakamiya, Y. Matsubara and Z.-i. Yoshida, *Journal of the American Chemical Society*, 2000, **122**, 7404-7405.
10. P. Kuzmič, *Analytical Biochemistry*, 1996, **237**, 260-273.

8 Appendix A - Fitted Luminescence Data

Complex

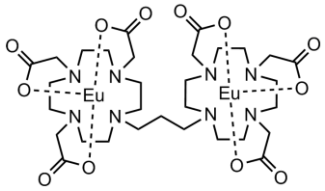

Titrant

NaCl

Solvent: H_2O

Buffer: PB

pH: 7.70

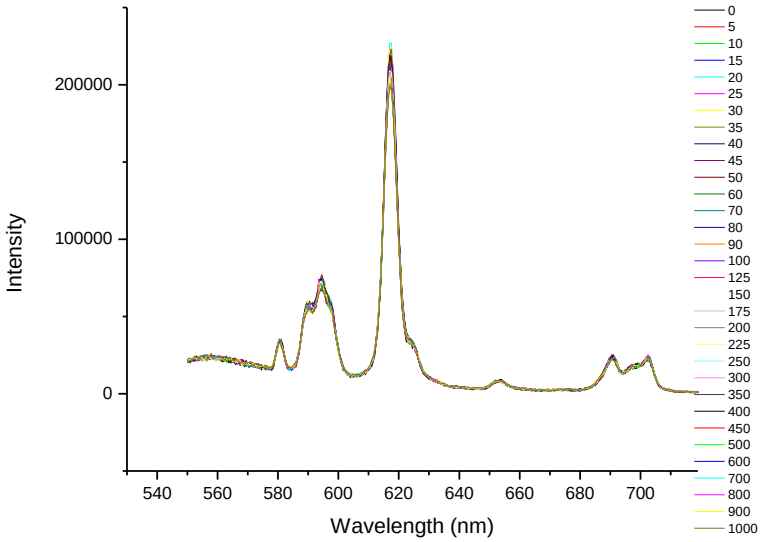

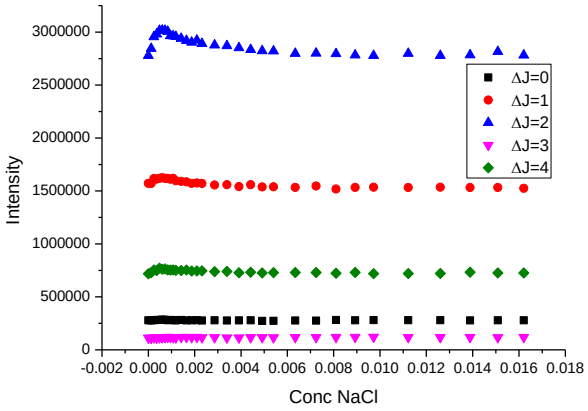

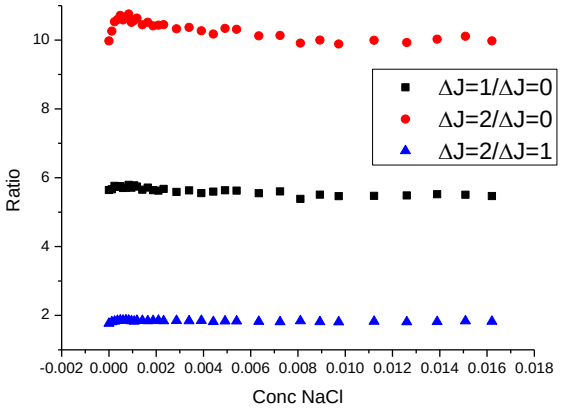

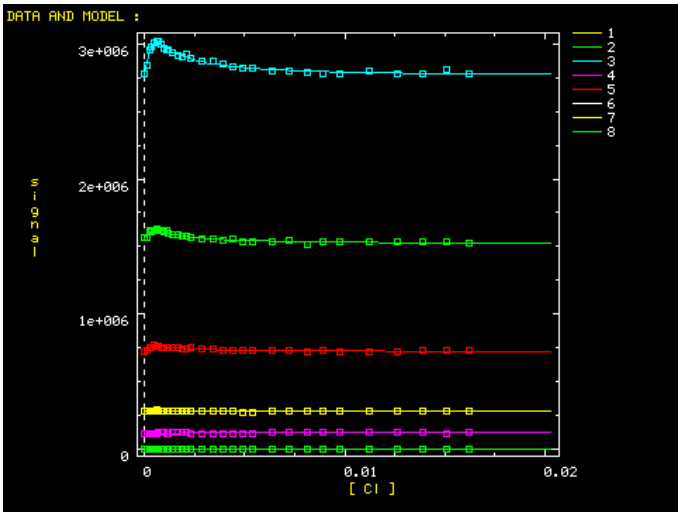

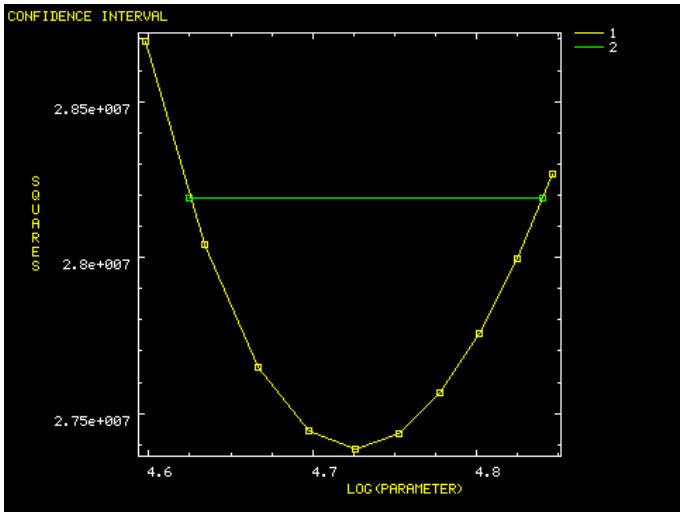

K_1 = 53210 (36260 - 70170)
K_2 = 849

Complex

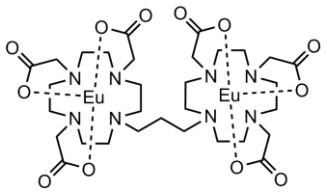

Titrant

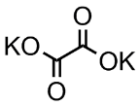

Solvent: H_2O

Buffer: PB

pH: 7.76

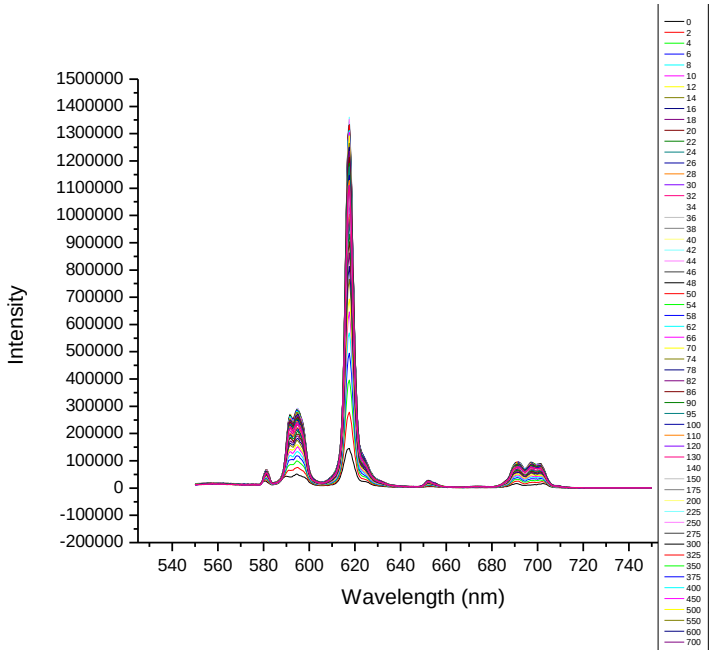

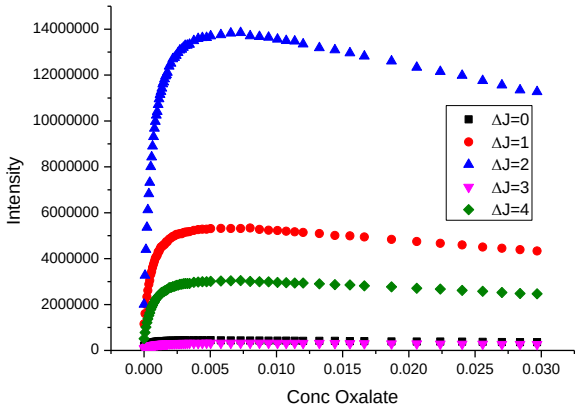

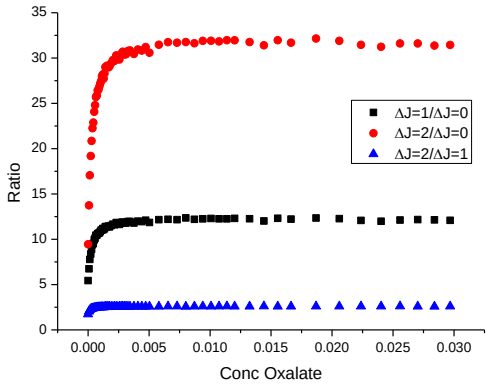

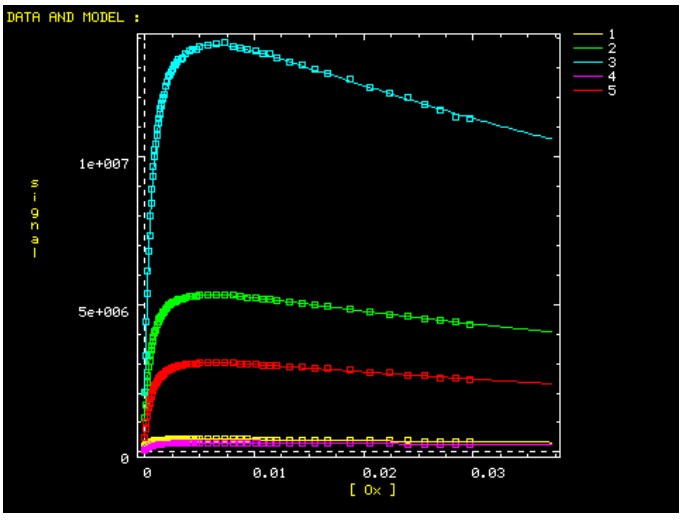

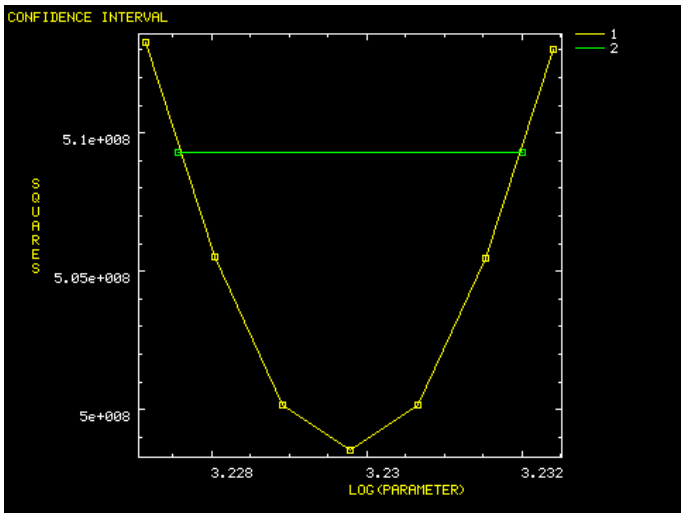

K_1 = 1697 (1689 - 1706)
K_2 = 13

Complex

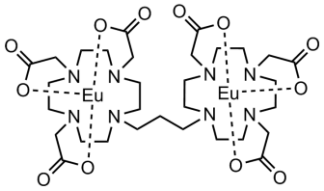

Titrant

NaN_3

Solvent: H_2O

Buffer: PB

pH: 7.76

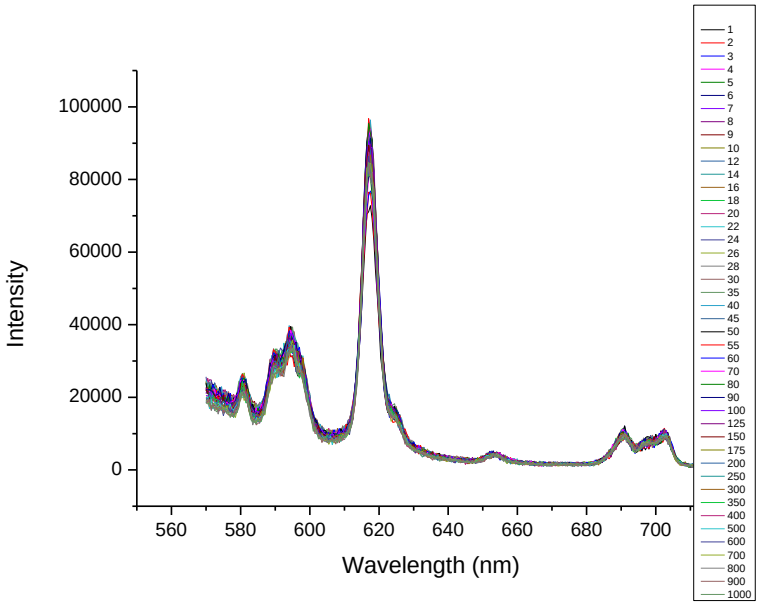

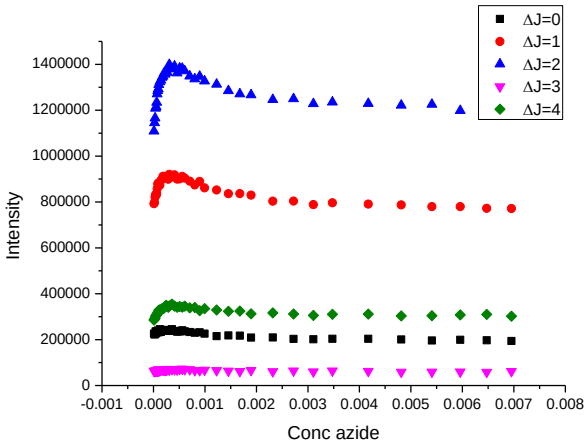

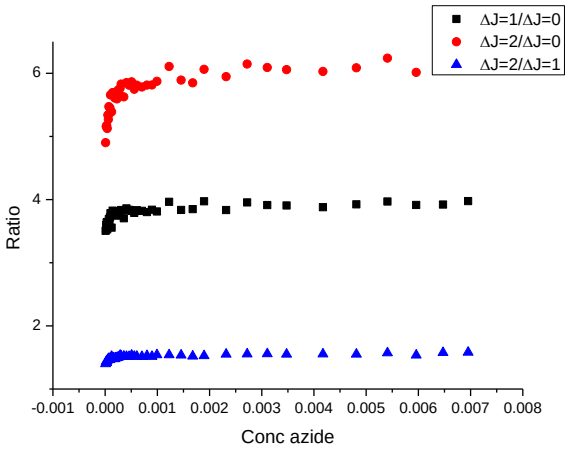

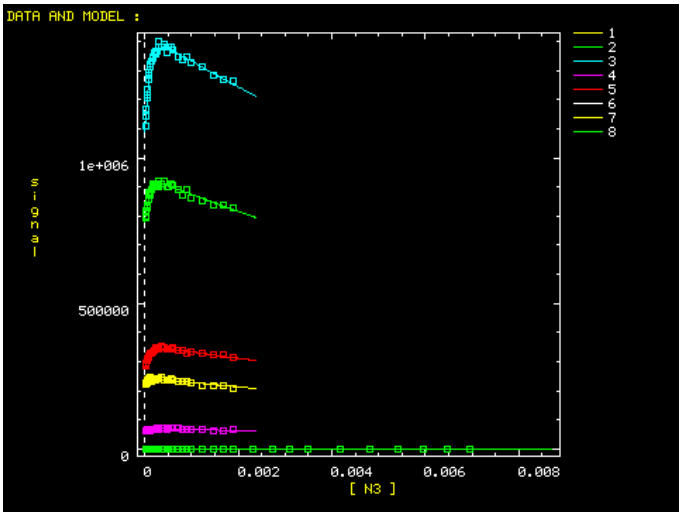

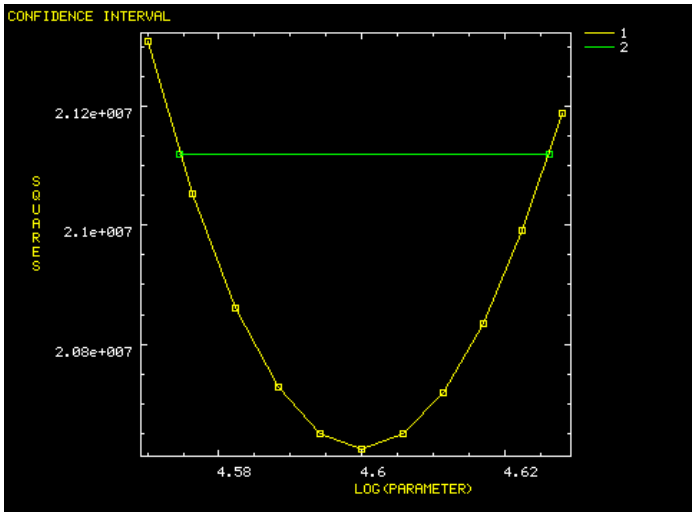

K_1 = 39814 (37546 - 42287)
K_2 = 80

Complex

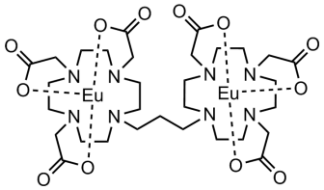

Titrant

KBr

Solvent: H_2O

Buffer: PB

pH: 7.39

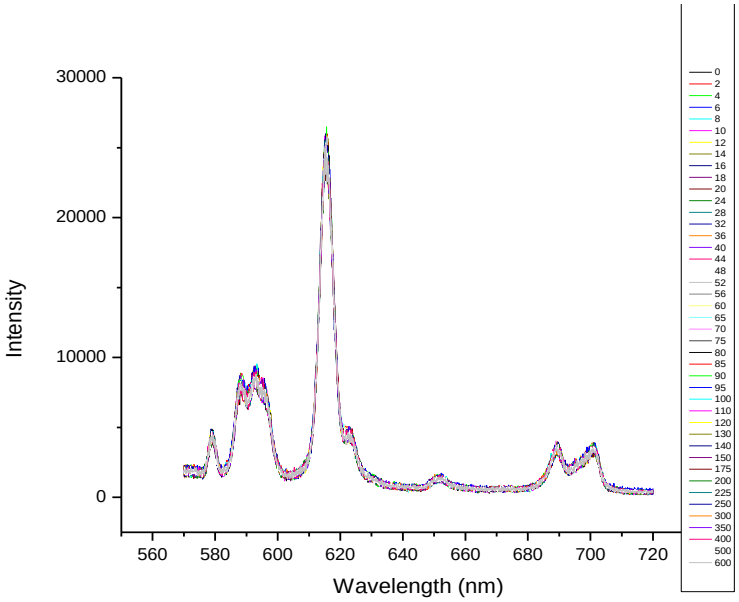

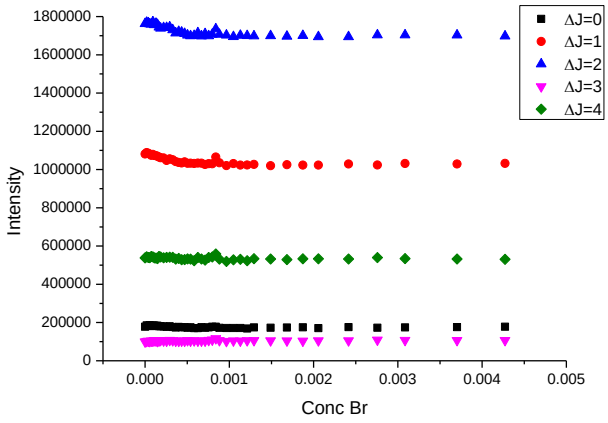

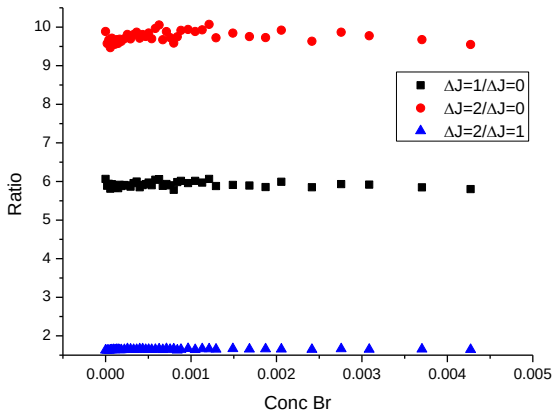

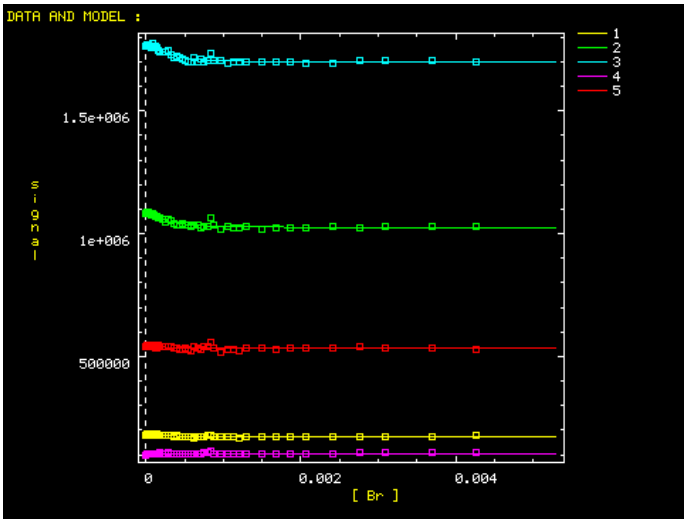

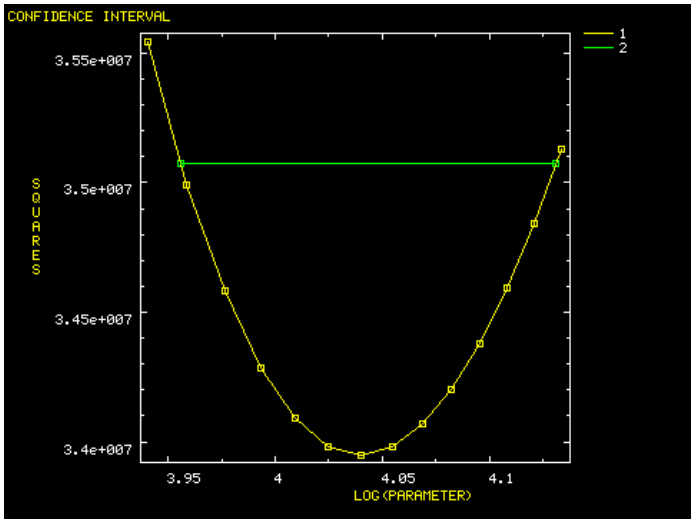

K_1 = 10960 (9036 - 13530)

Complex

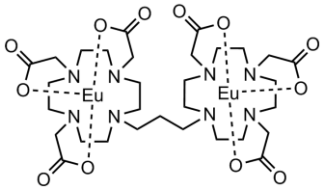

Titrant

KCl

Solvent: H_2O

Buffer: PB

pH: 7.39

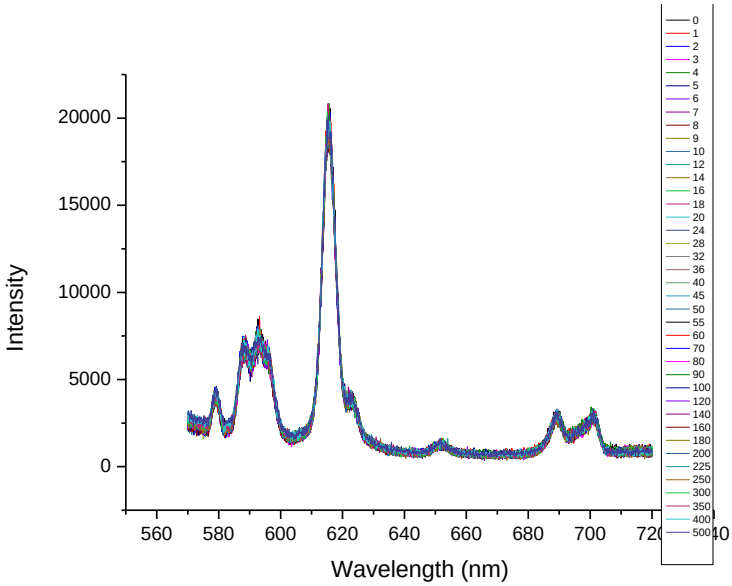

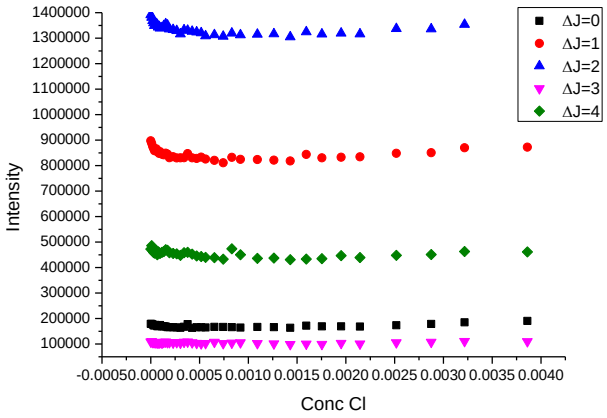

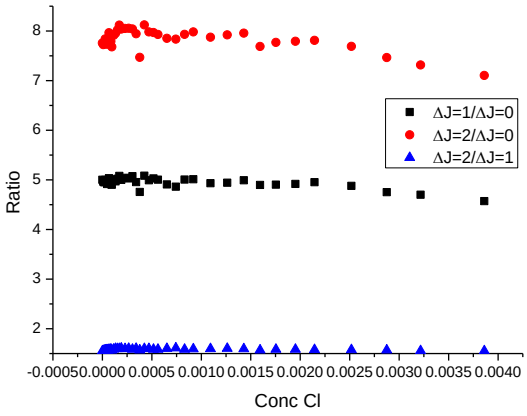

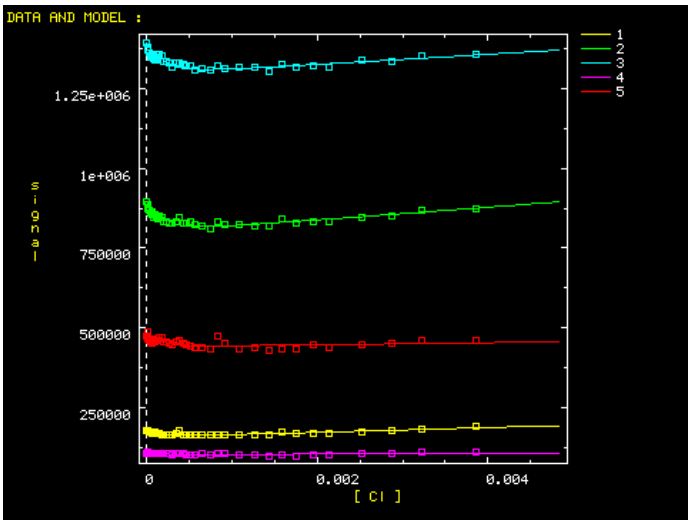

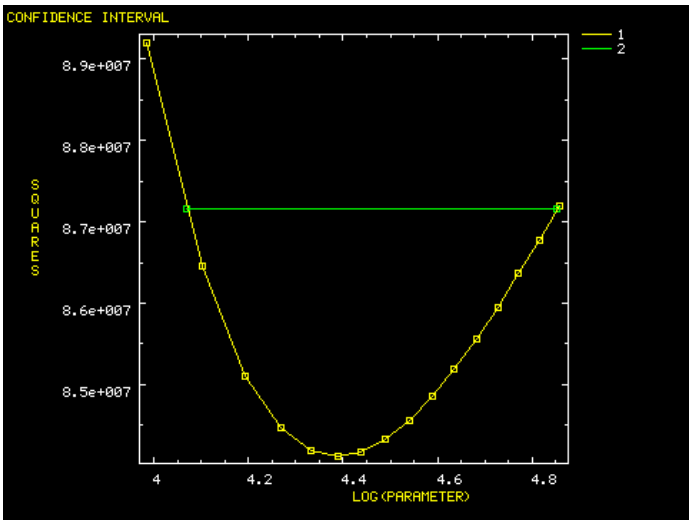

K_1 = 24440 (11760 - 71310)

K_2 = 0.1072

Complex

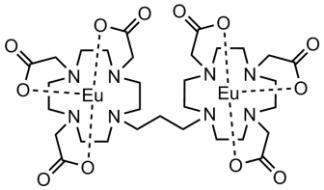

Titrant

KF

Solvent: H_2O

Buffer: PB

pH: 7.39

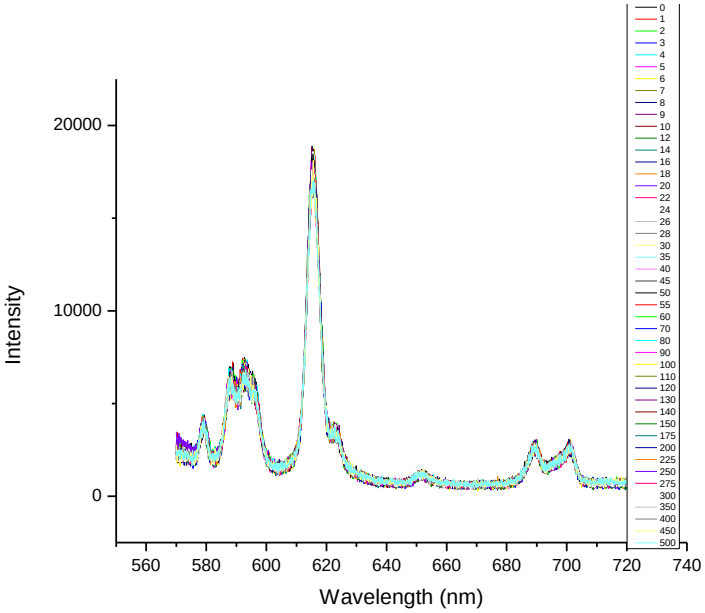

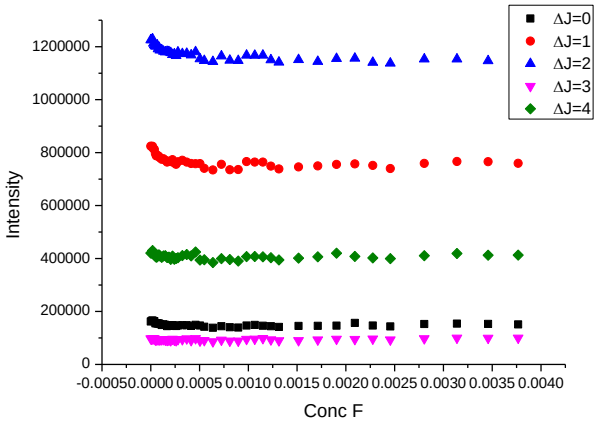

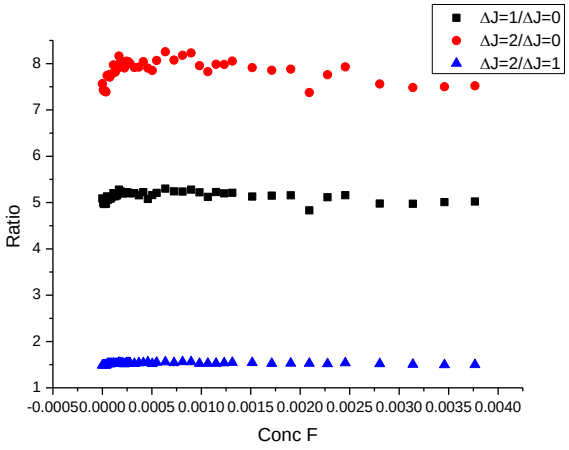

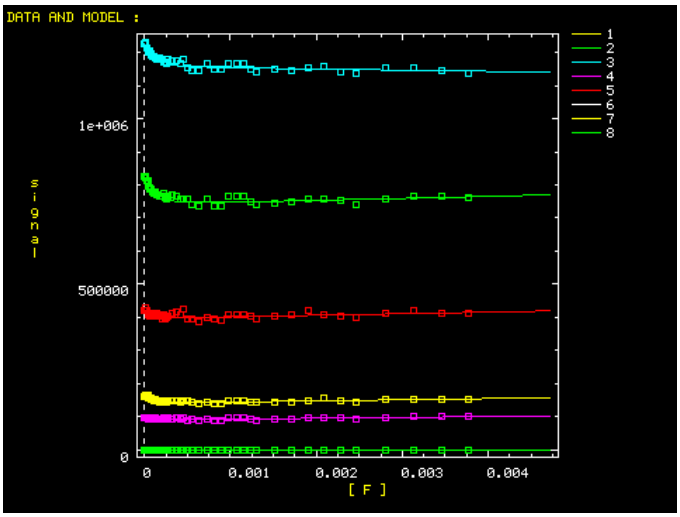

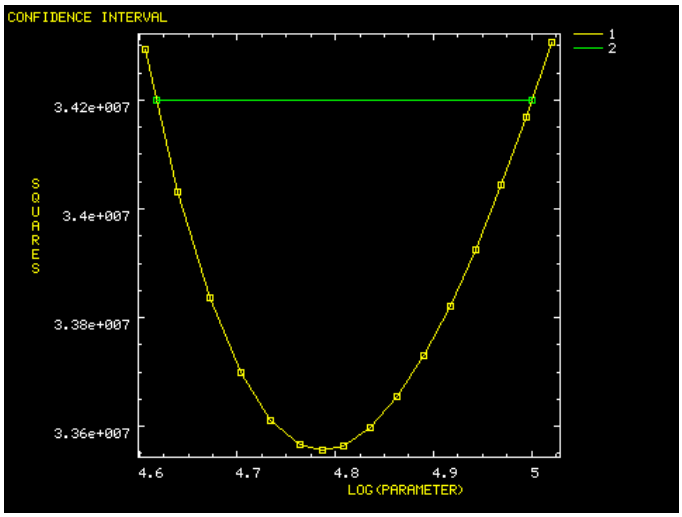

K_1 = 61190 (41460 - 100200)

K_2 = 0.0001

Complex

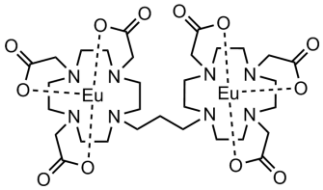

Titrant

KI

Solvent: H_2O

Buffer: PB

pH: 7.58

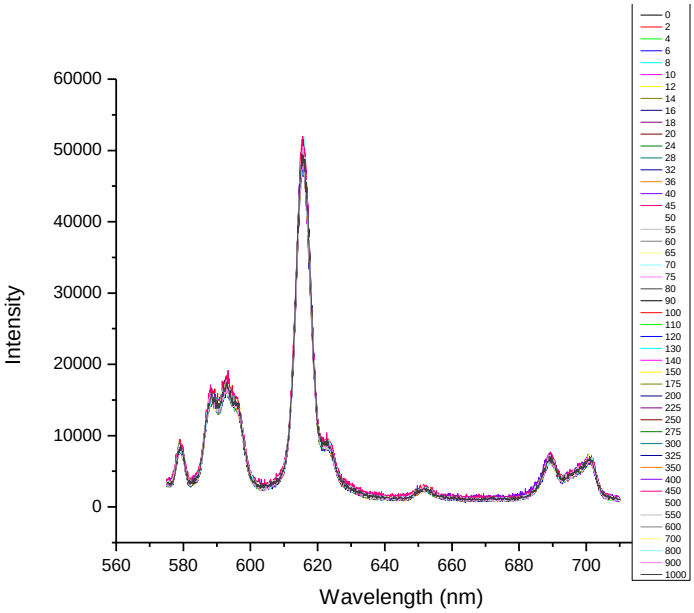

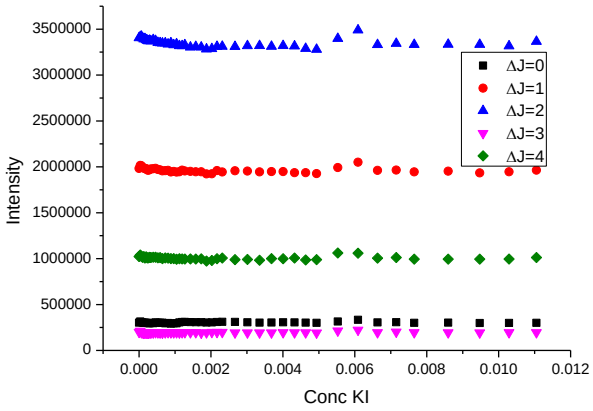

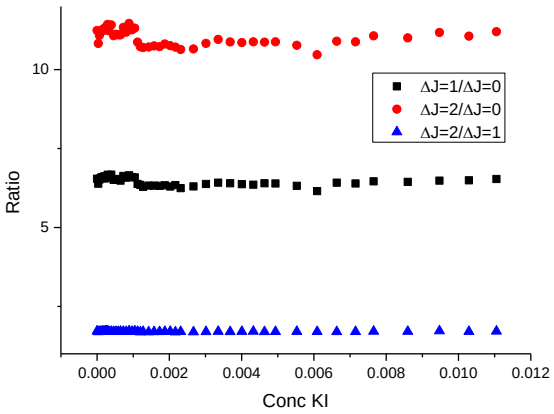

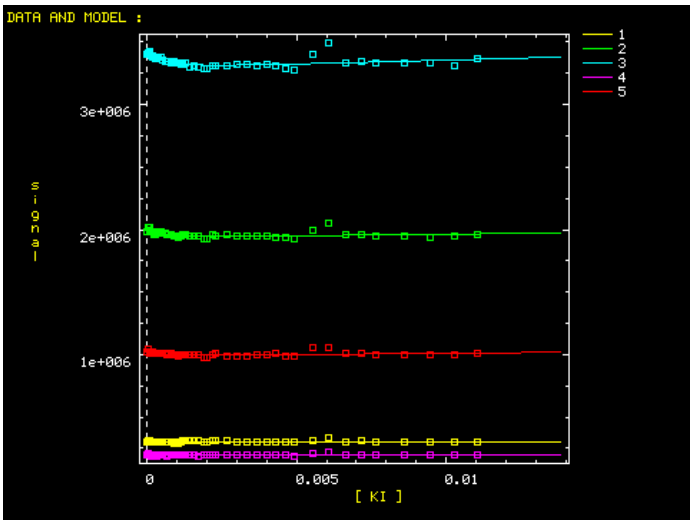

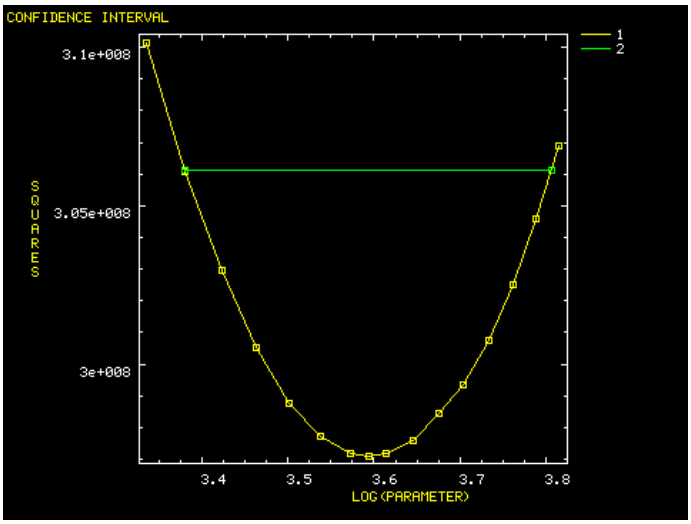

K_1 = 3926 (2401 - 6395)
K_2 = 0.000011

Complex

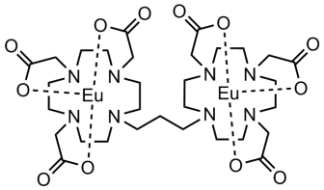

Titrant

KF

Solvent: H_2O

Buffer: HEPES

pH: 7.54

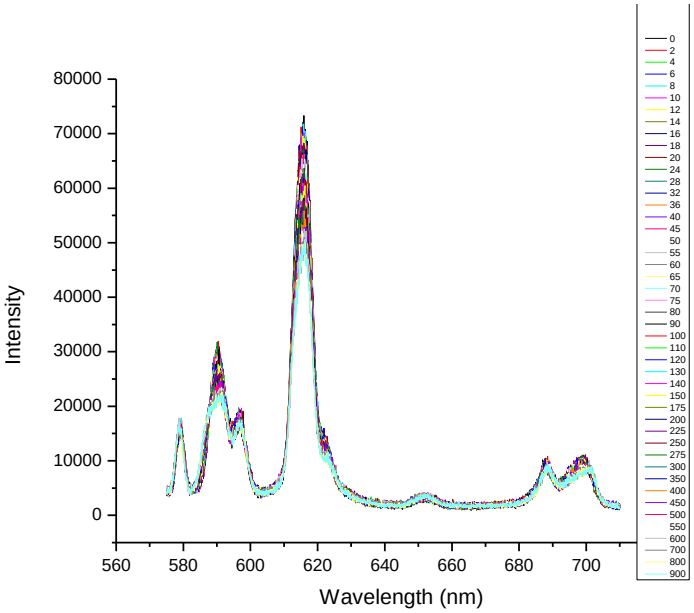

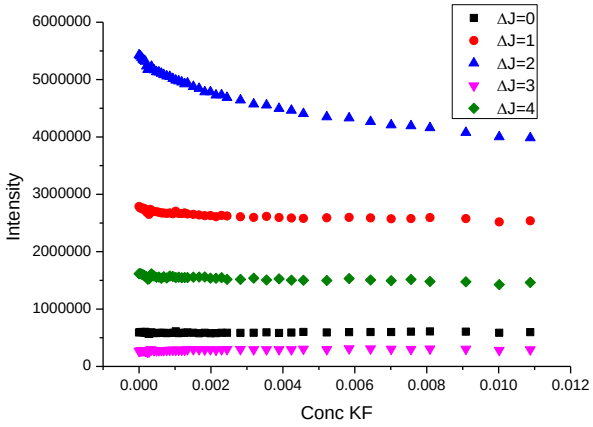

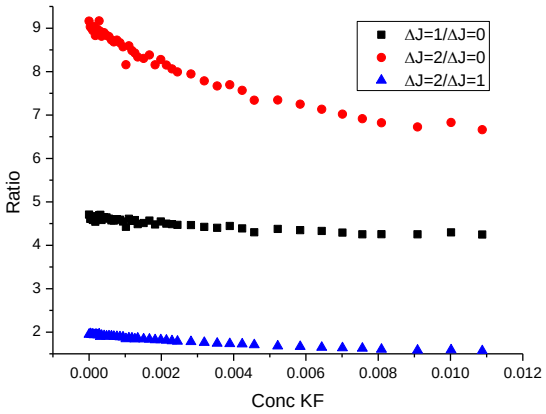

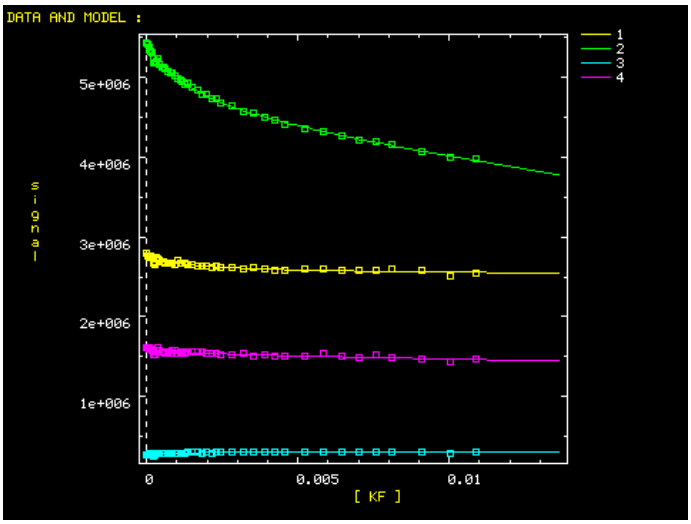

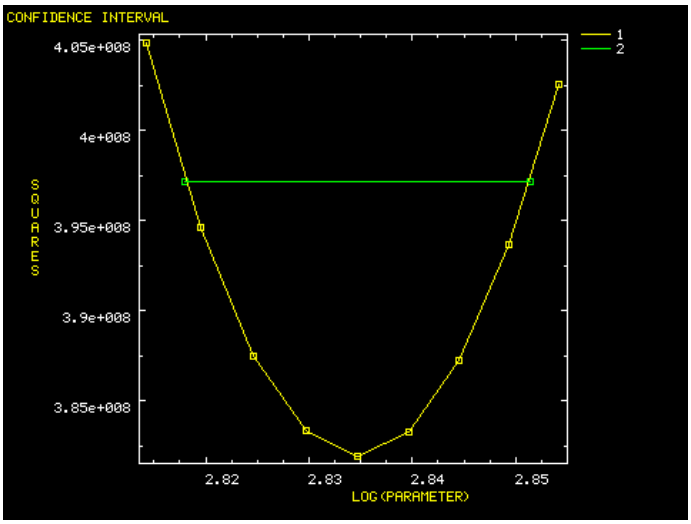

K_1 = 684 (658 - 710)
K_2 = 0.0000126

Complex

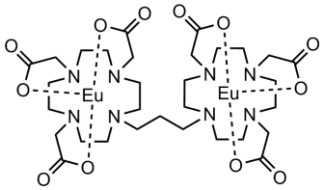

Titrant

KCl

Solvent: H_2O

Buffer: HEPES

pH: 7.48

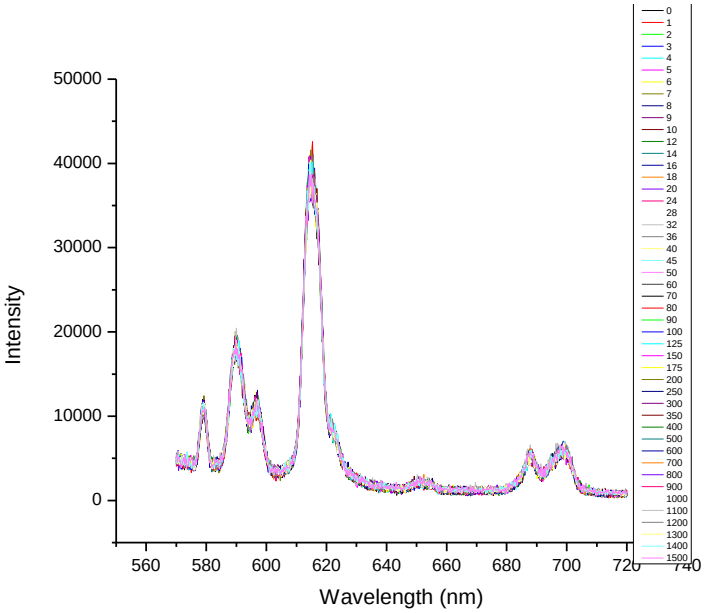

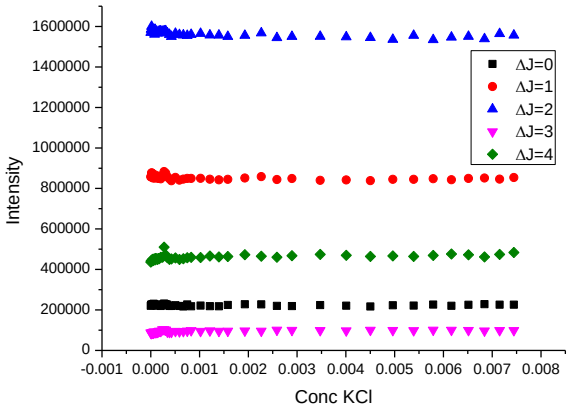

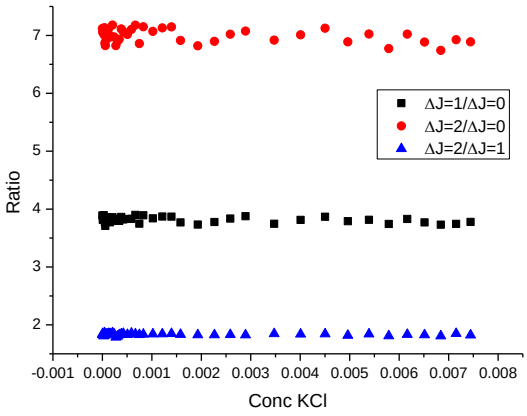

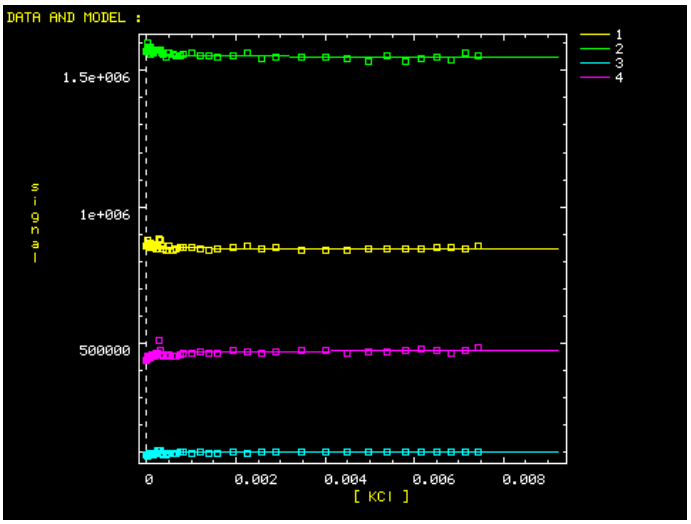

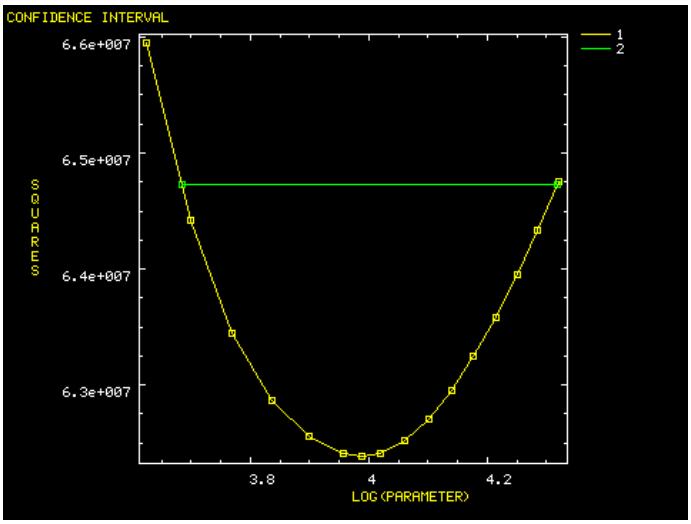

K_1 = 9761 (4830 - 20800)

K_2 = 0

Complex

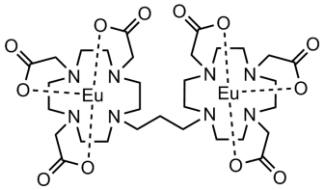

Titrant

KBr

Solvent: H_2O

Buffer: HEPES

pH: 7.48

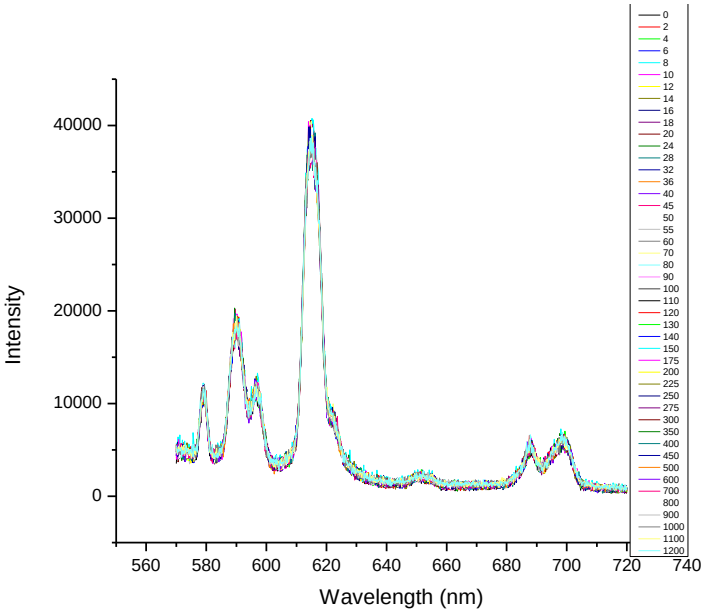

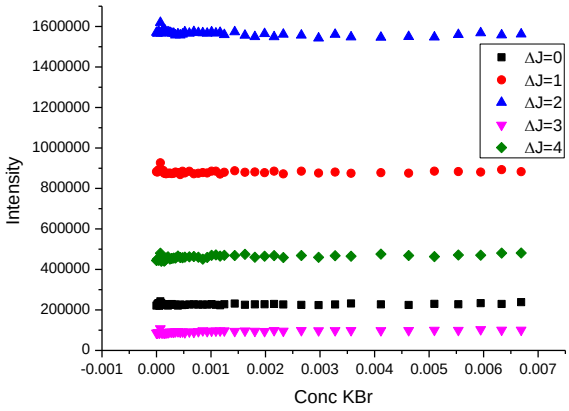

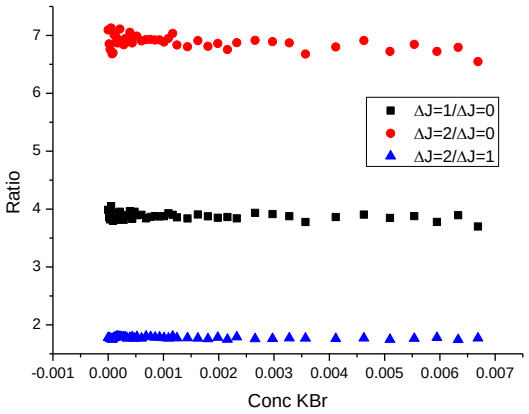

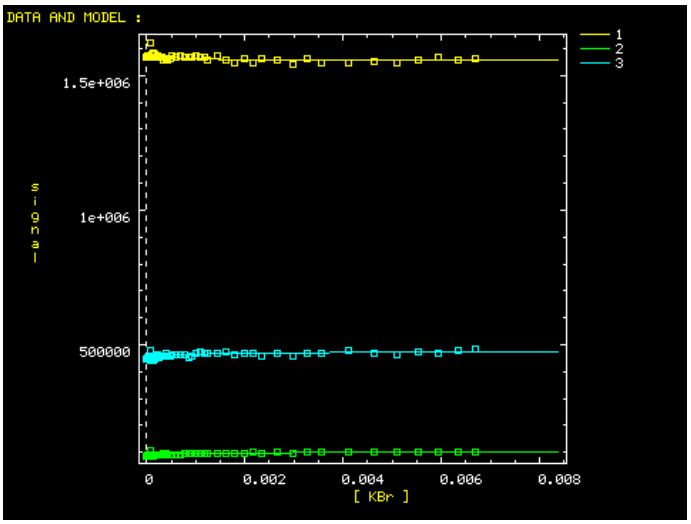

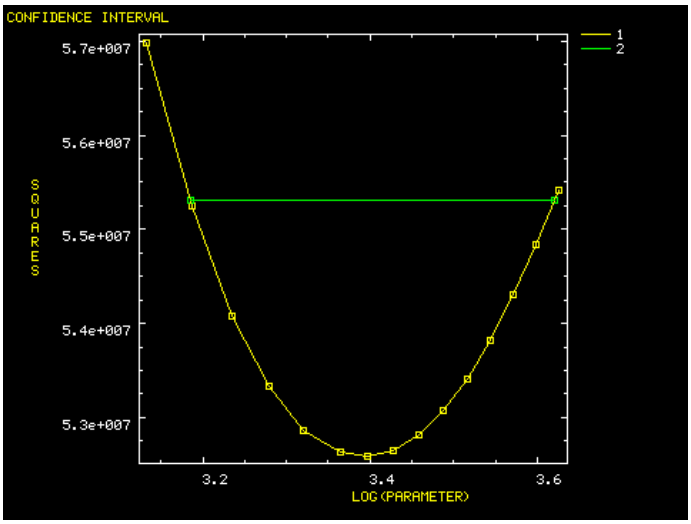

K_1 = 2495 (1530 - 4178)

K_2 = 0

Complex

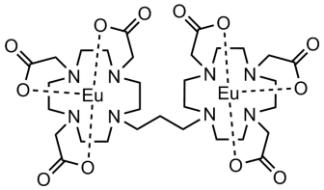

Titrant

KI

Solvent: H_2O

Buffer: HEPES

pH: 7.48

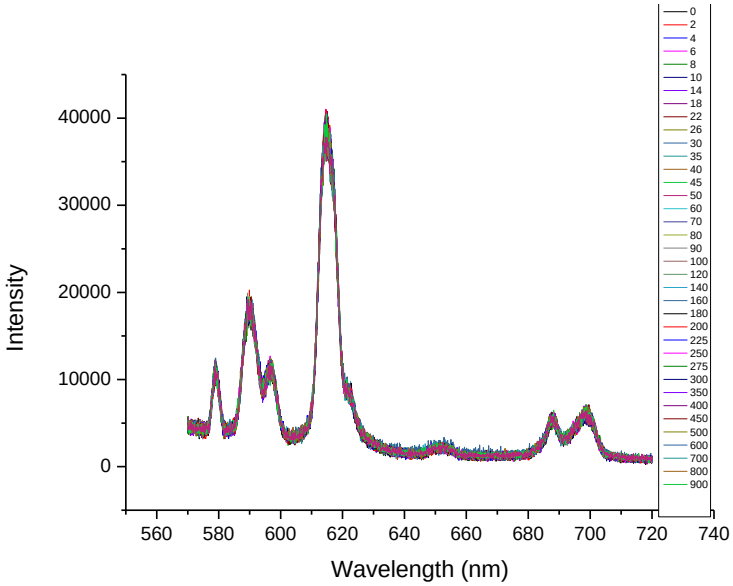

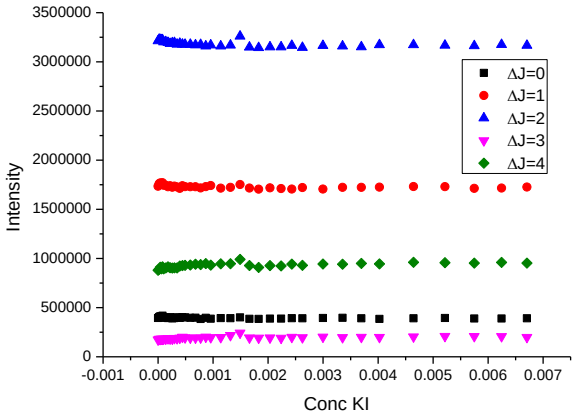

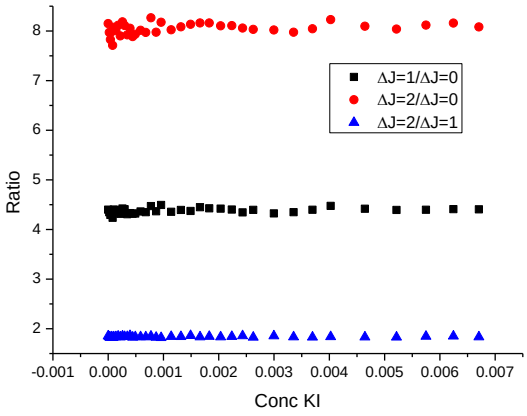

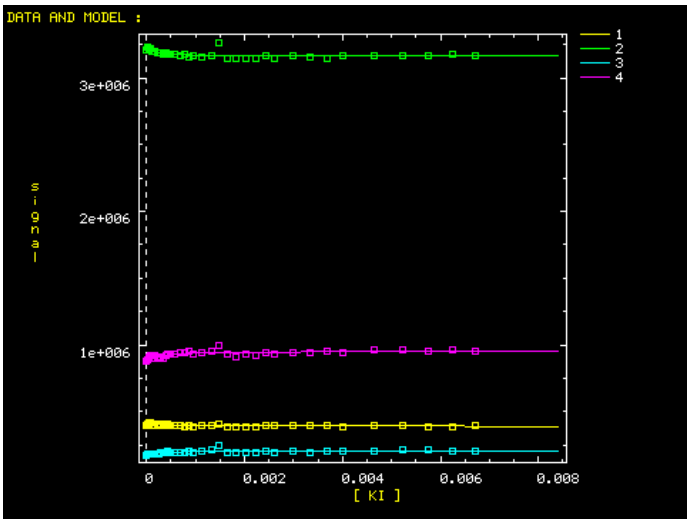

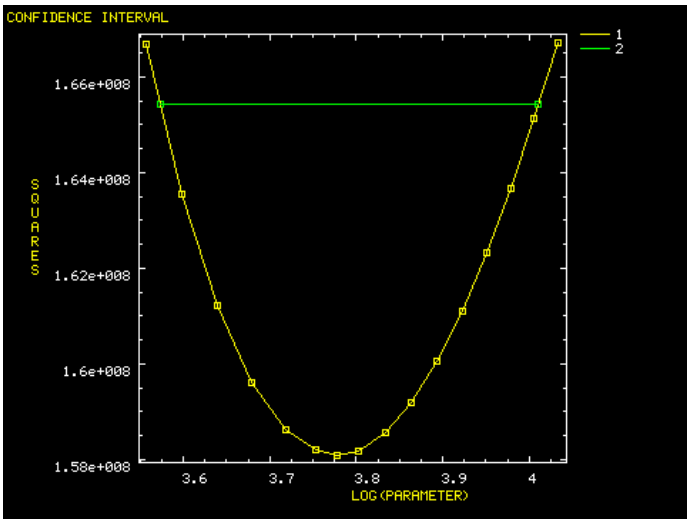

K_1 = 6005 (3746 - 10260)
K_2 = 0.0001

Complex

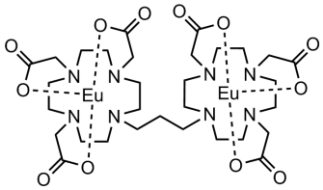

Titrant

Na_3PO_4

Solvent: H_2O

Buffer: HEPES

pH: 7.55

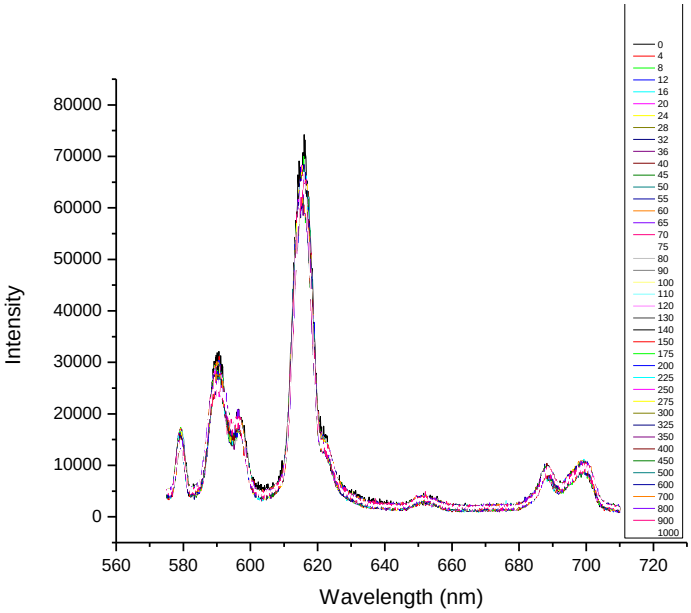

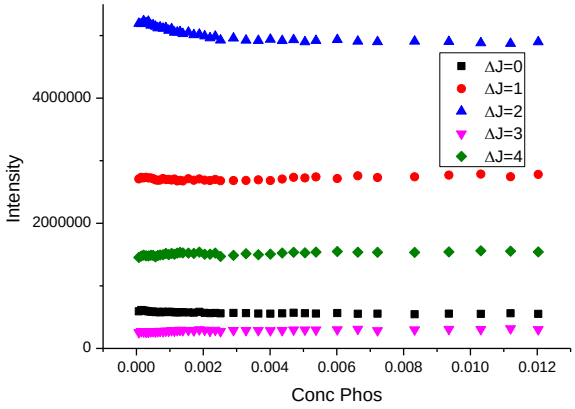

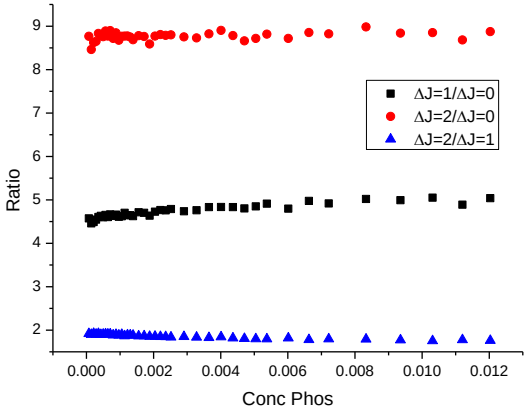

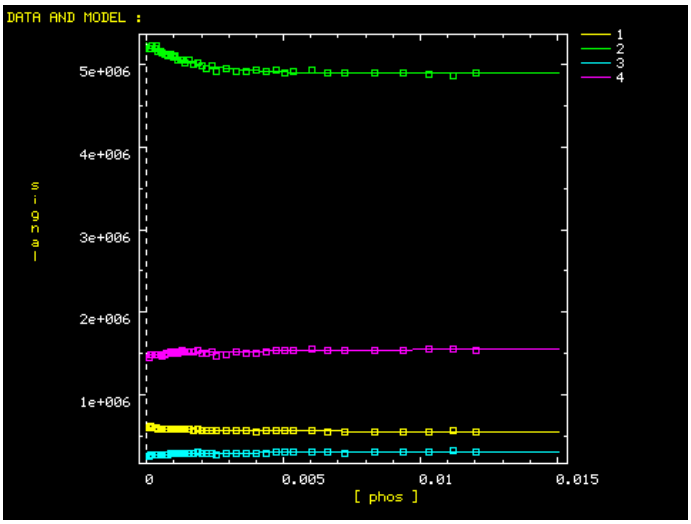

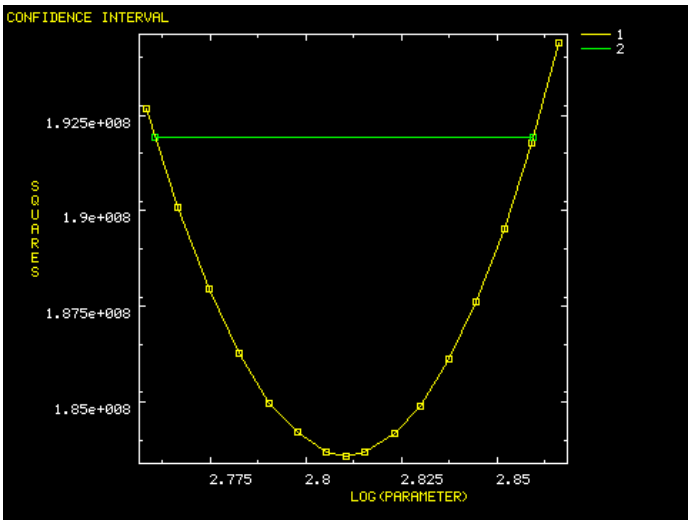

K_1 = 646 (576 - 723)
K_2 = 0.0000776

Complex

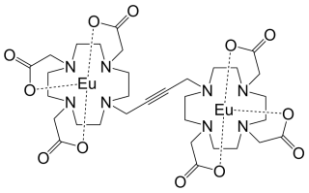

Titrant

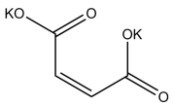

Solvent: H_2O

Buffer: PBS

pH: 7.70

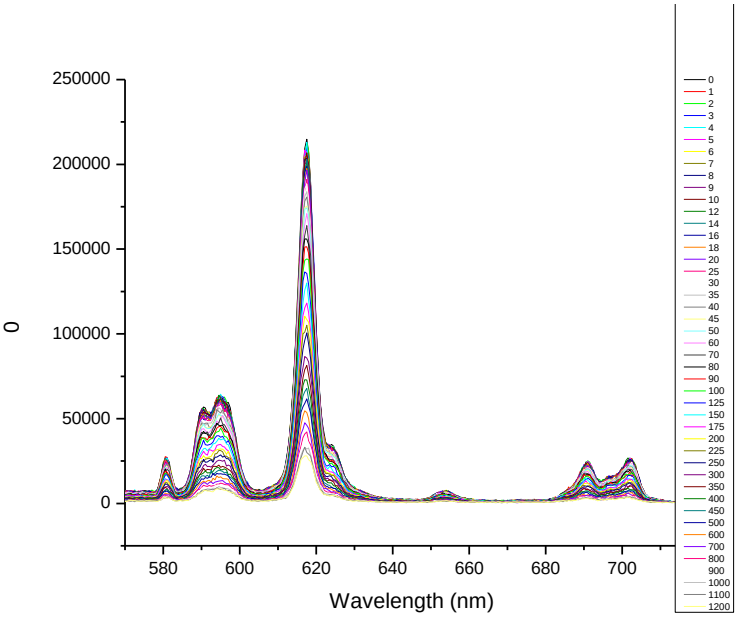

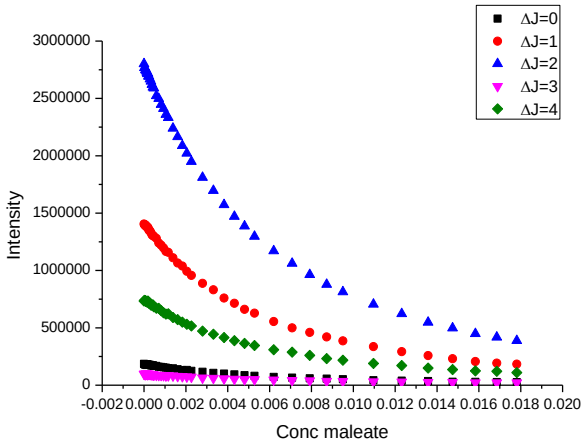

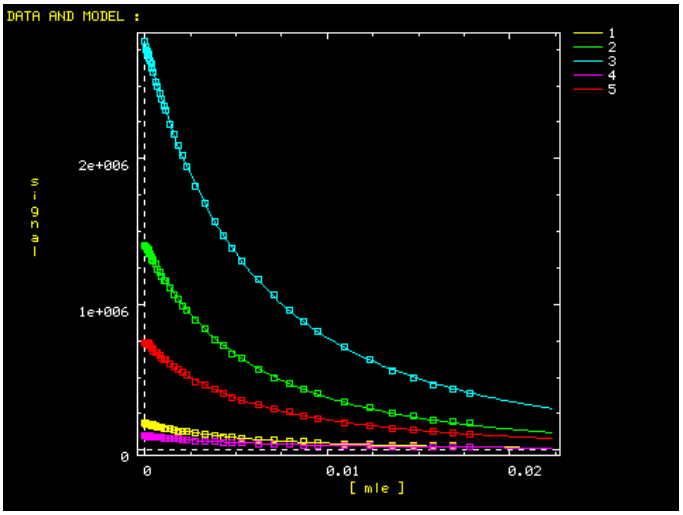

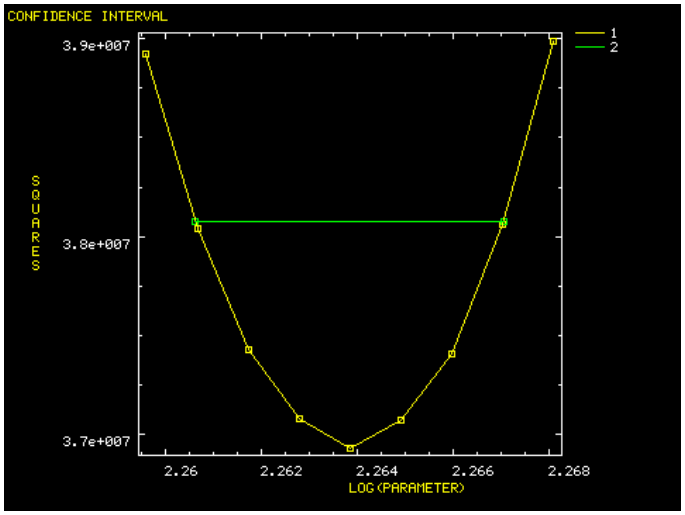

K_1 = 184 (182 - 185)

K_2 = 44

Complex

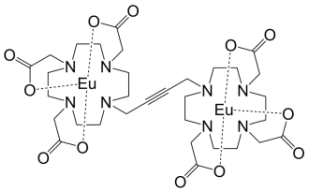

Titrant

K.Ox

Solvent: H_2O

Buffer: PBS

pH: 7.70

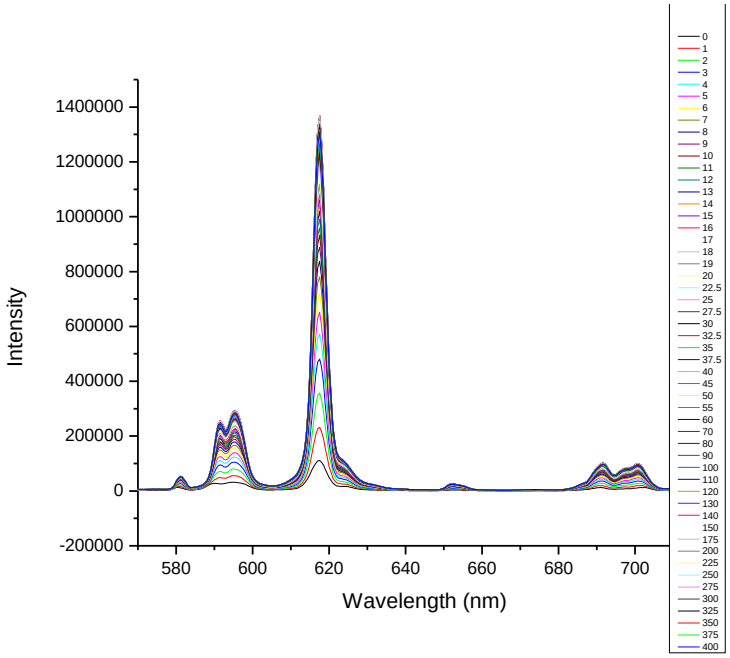

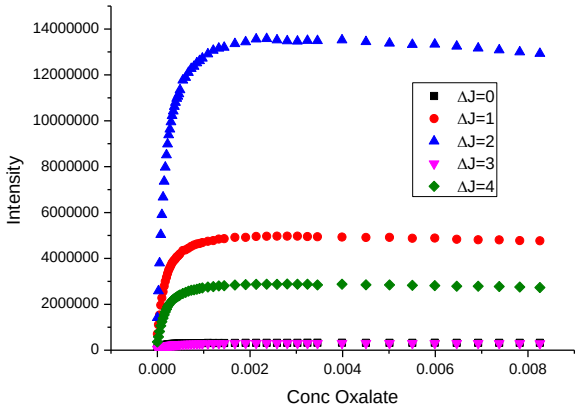

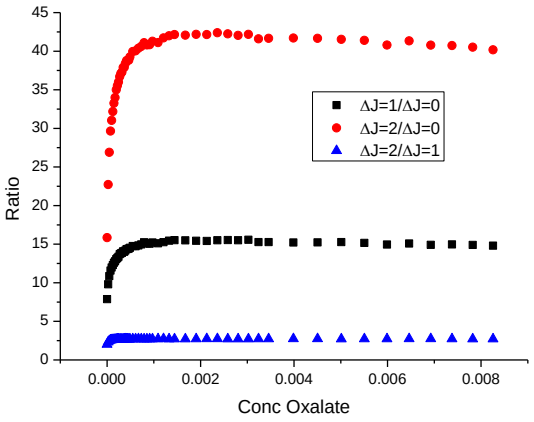

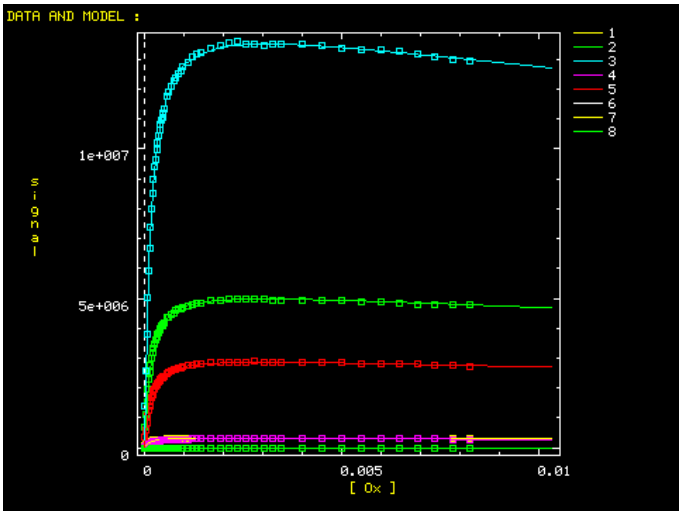

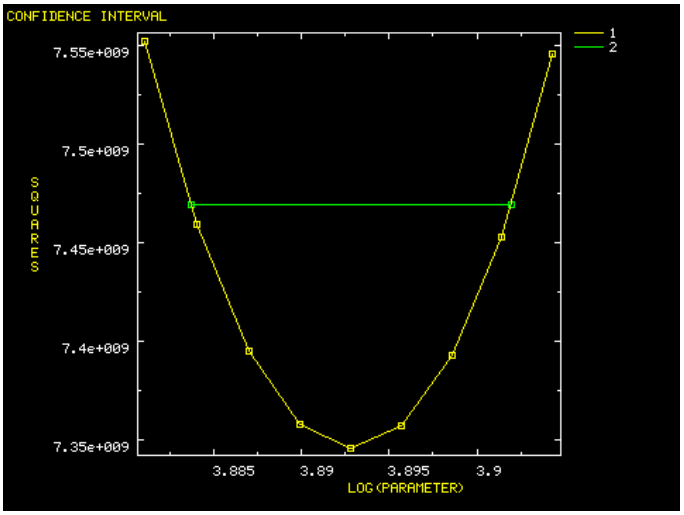

K_1 = 7813 (7553 - 8074)
K_2 = 13

Complex

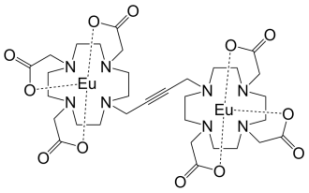

Titrant

Na_2.ADP

Solvent: H_2O

Buffer: HEPES

pH: 7.58

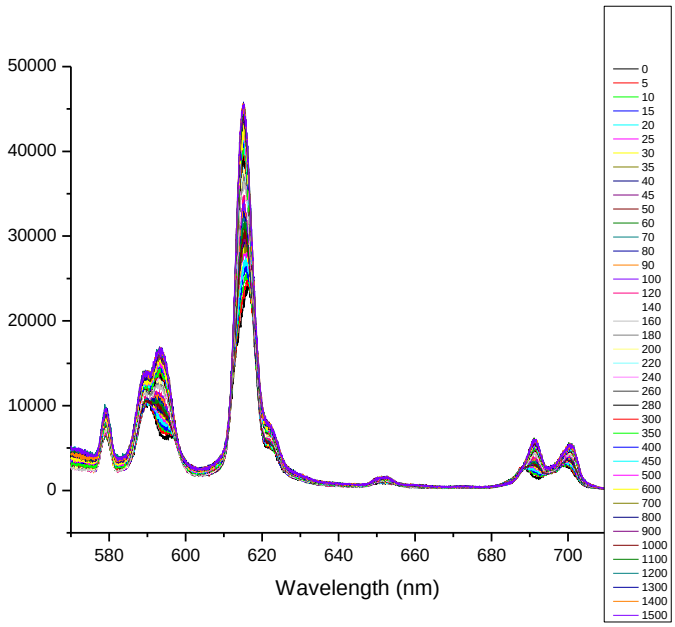

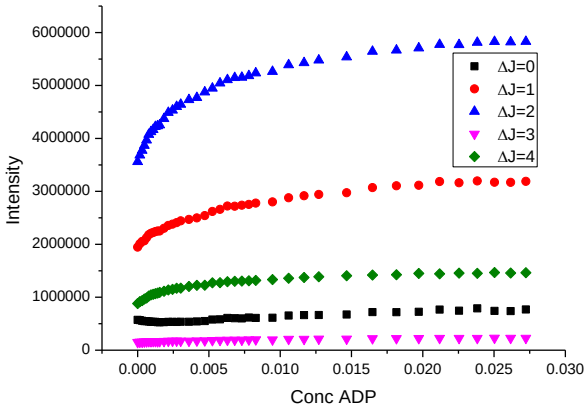

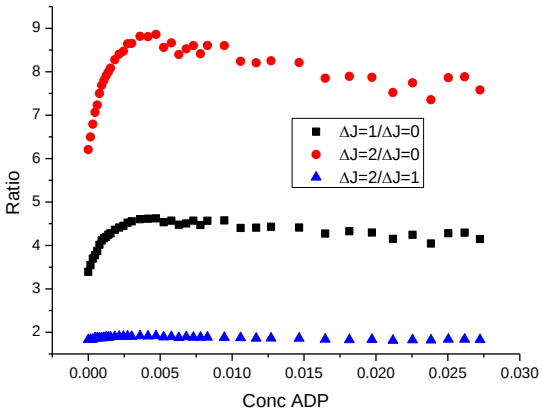

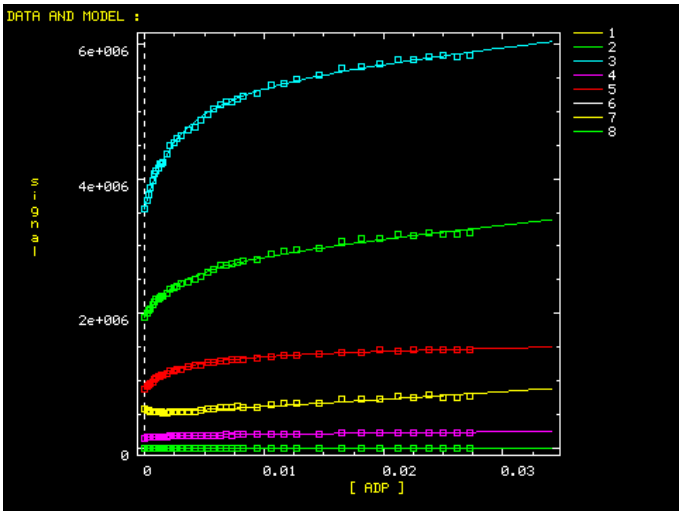

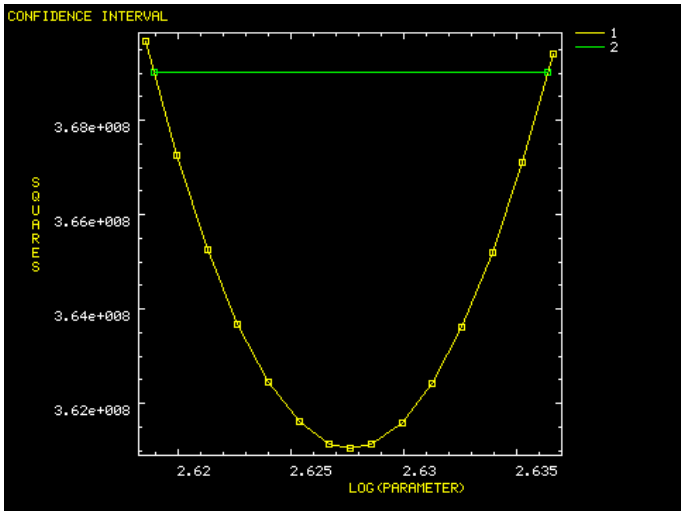

K_1 = 424 (416 - 433)
K_2 = 0.012

Complex

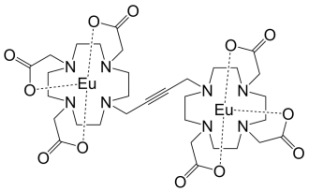

Titrant

Na_3.ATP

Solvent: H_2O

Buffer: HEPES

pH: 7.64

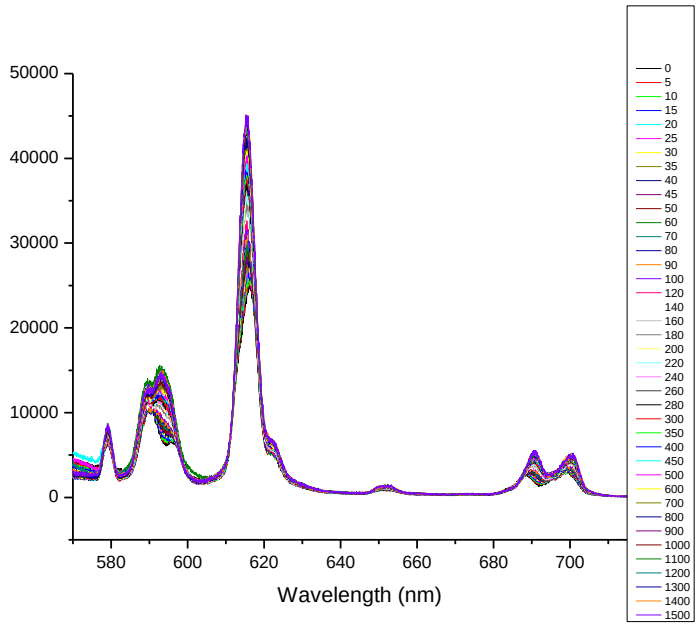

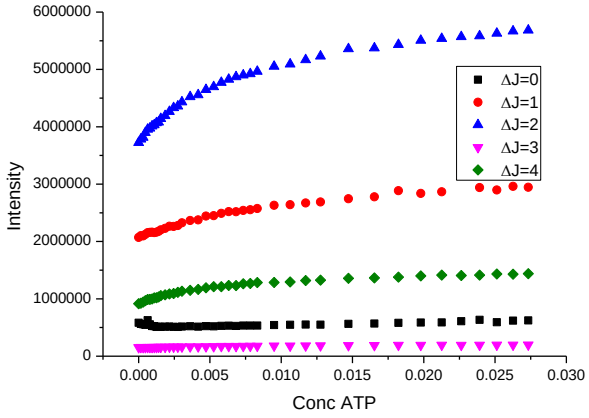

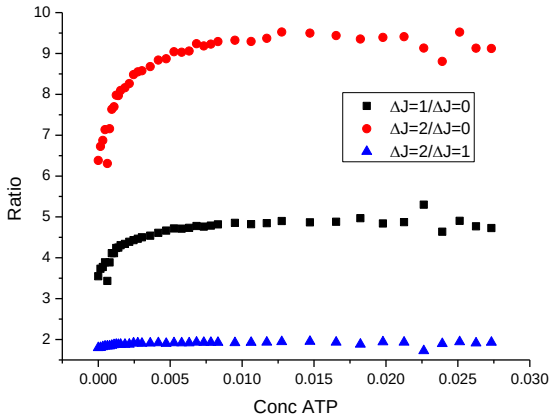

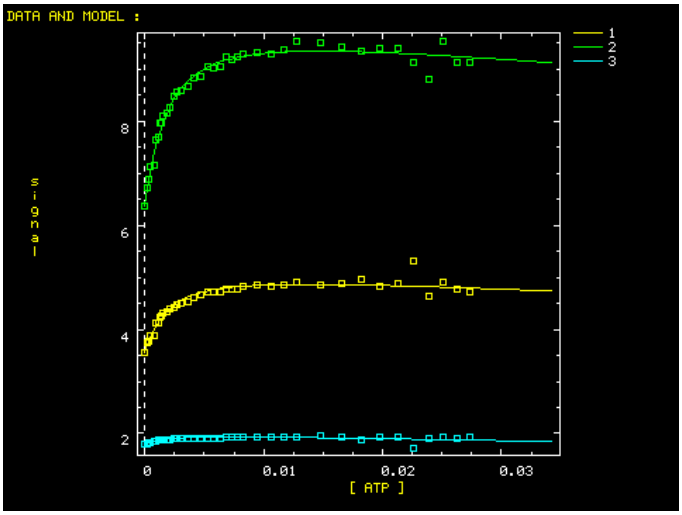

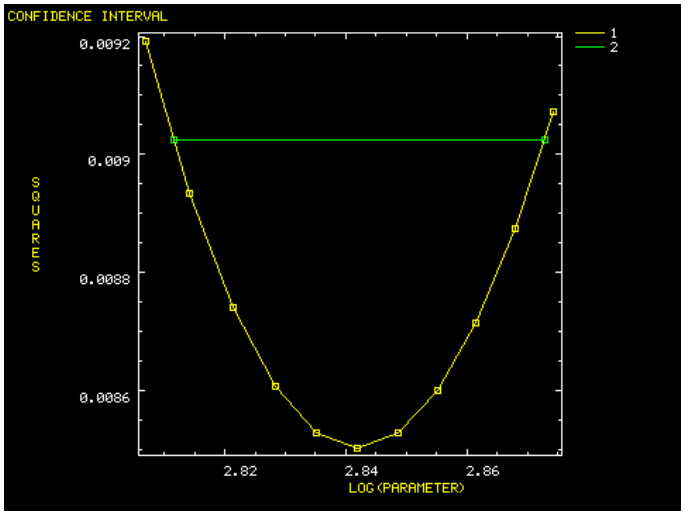

K_1 = 695 (648 - 746)
K_2 = 2.35

Complex

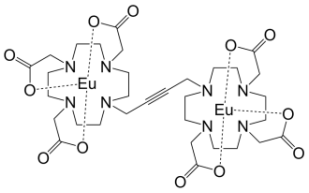

Titrant

fructose-1,6-bisphosphate

Solvent: H_2O

Buffer: HEPES

pH: 7.66

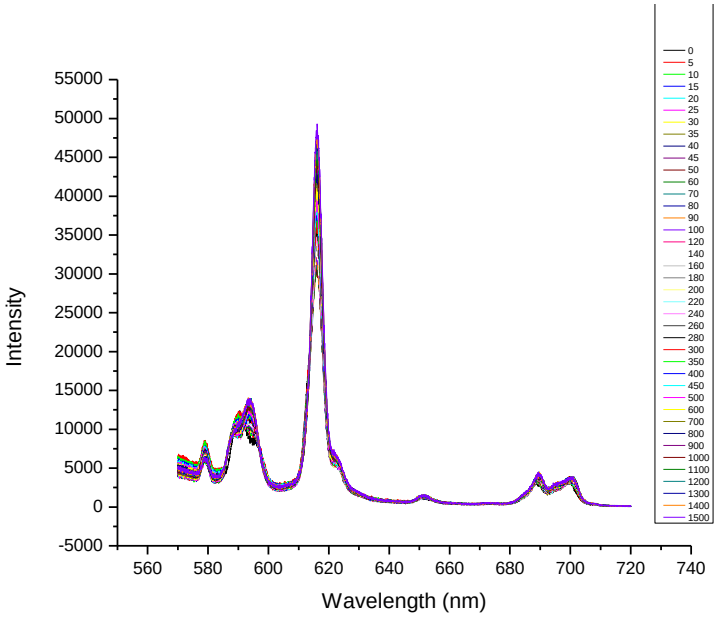

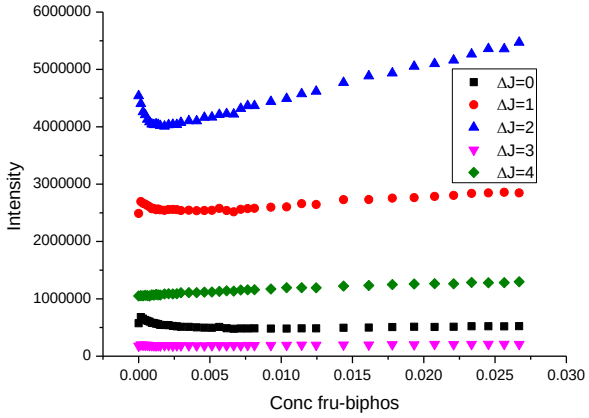

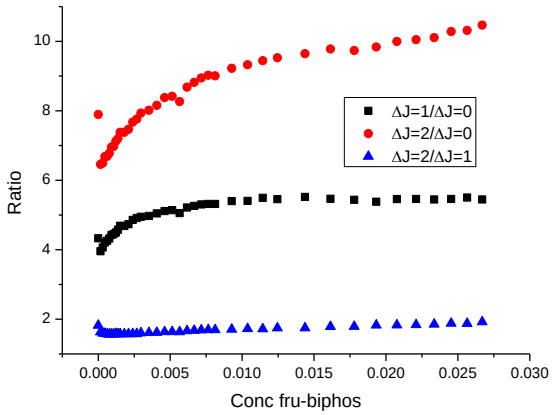

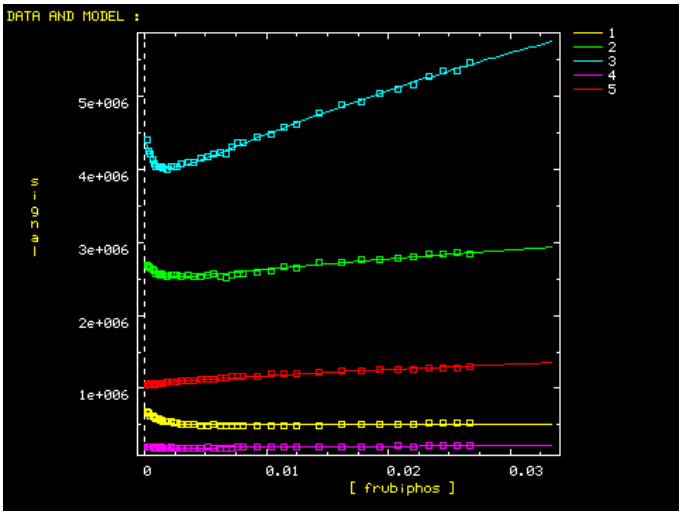

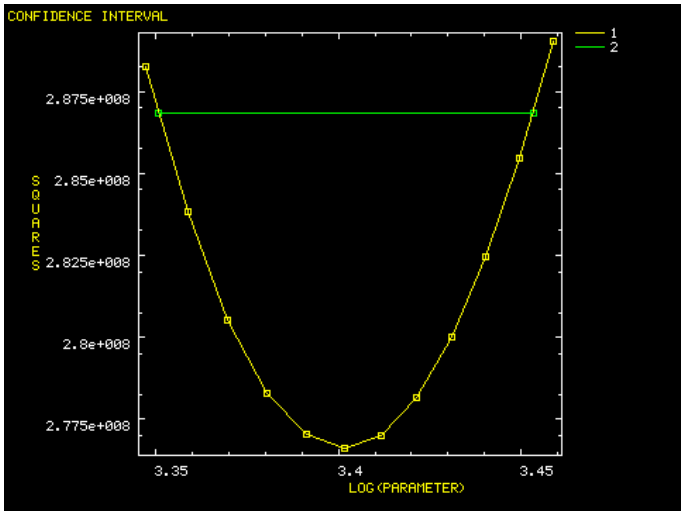

K_1 = 2521 (2243 - 2840)
K_2 = 10.80

Complex

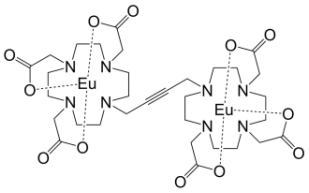

Titrant

fructose-1,6-bisphosphate

Solvent: H_2O

Buffer: PBS

pH: 7.77

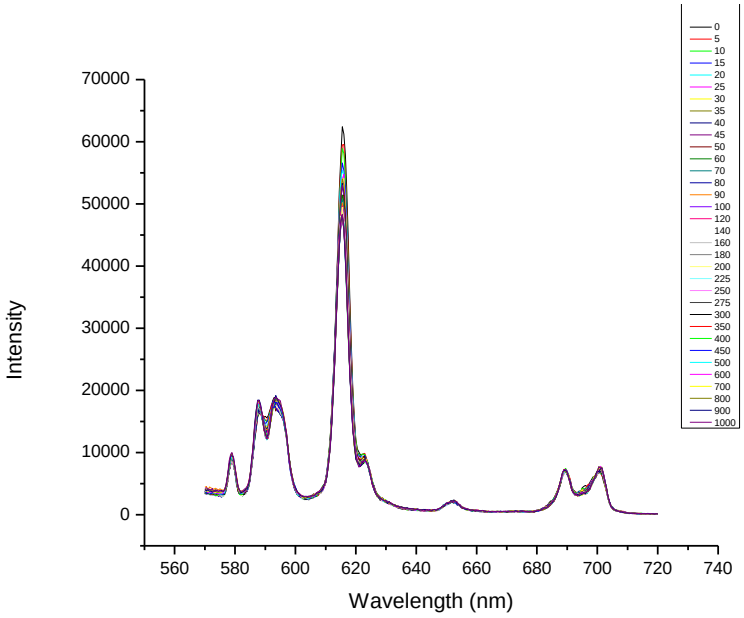

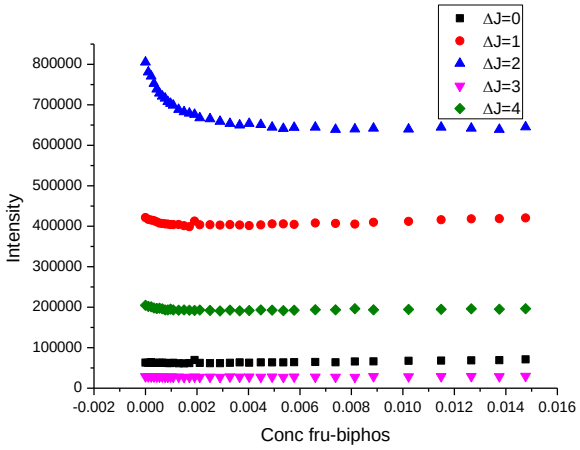

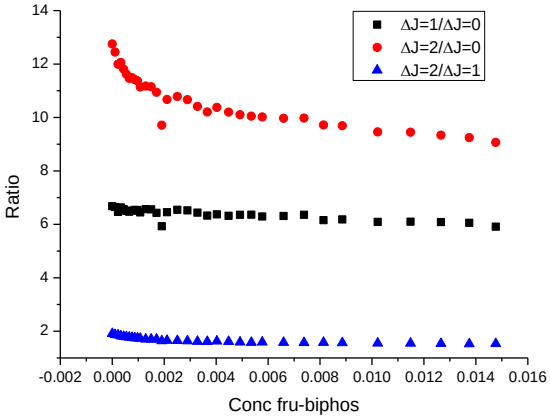

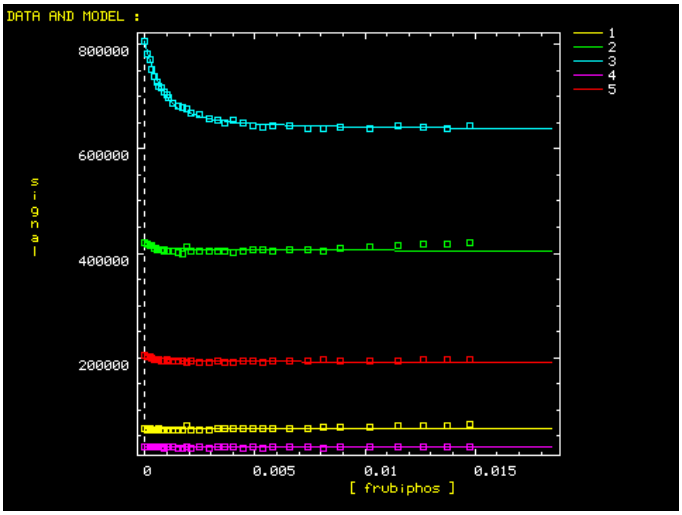

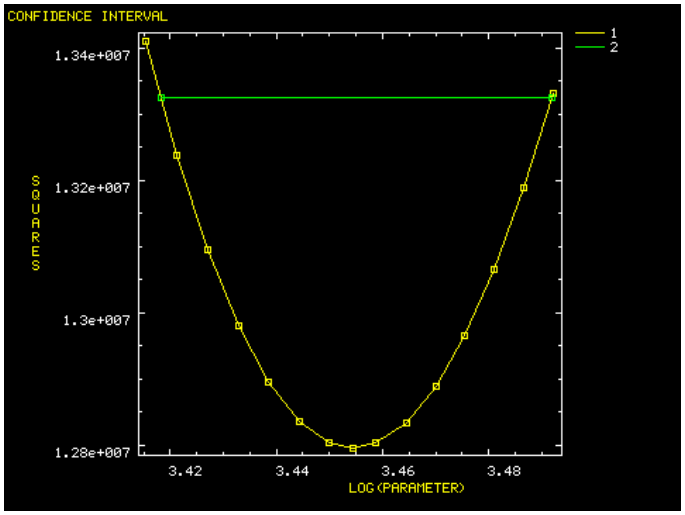

K_1 = 2848 (2619 - 3104)

K_2 = 3

Complex

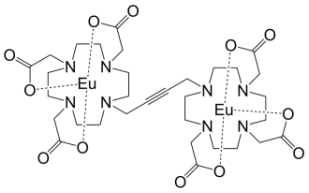

Titrant

Na.AMP

Solvent: H_2O

Buffer: HEPES

pH: 7.77

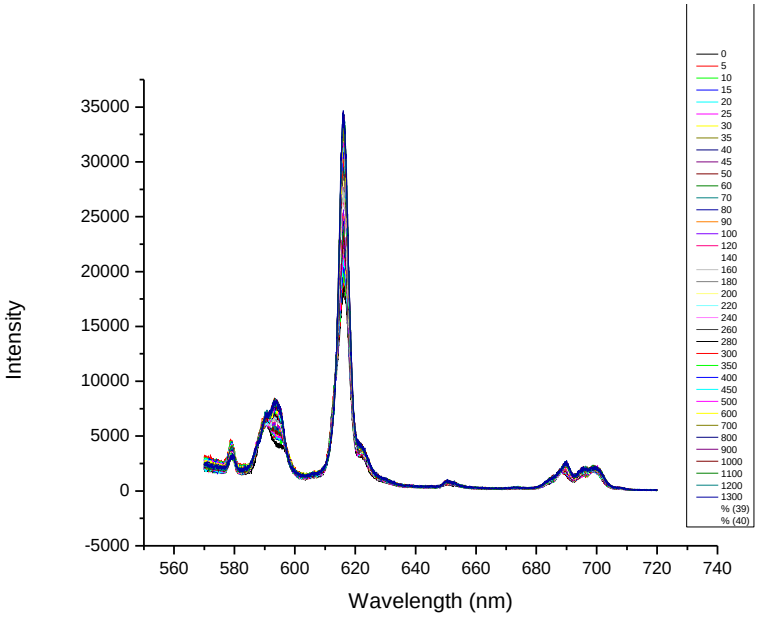

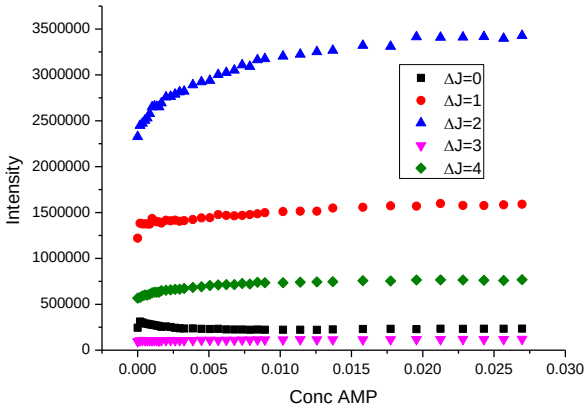

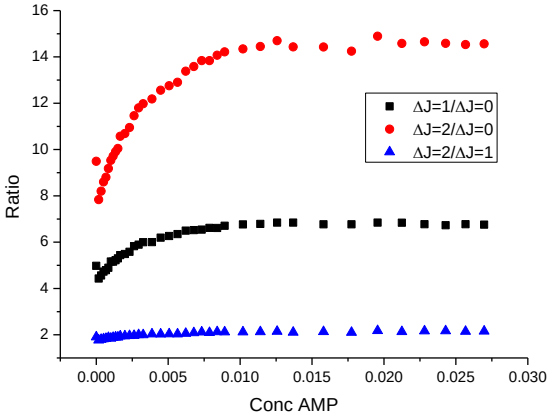

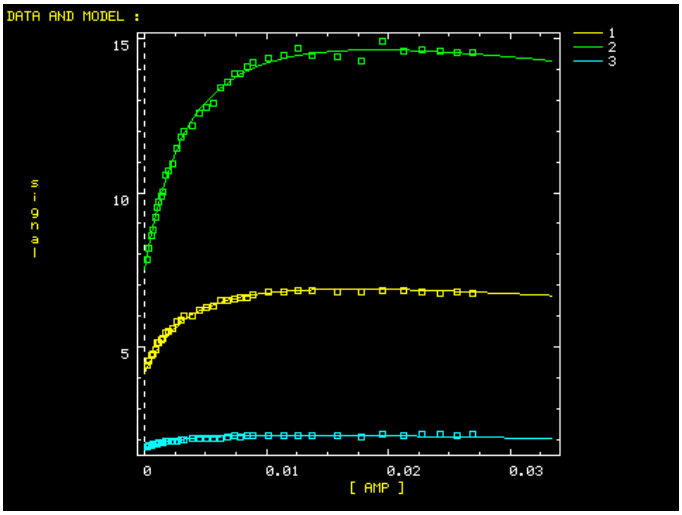

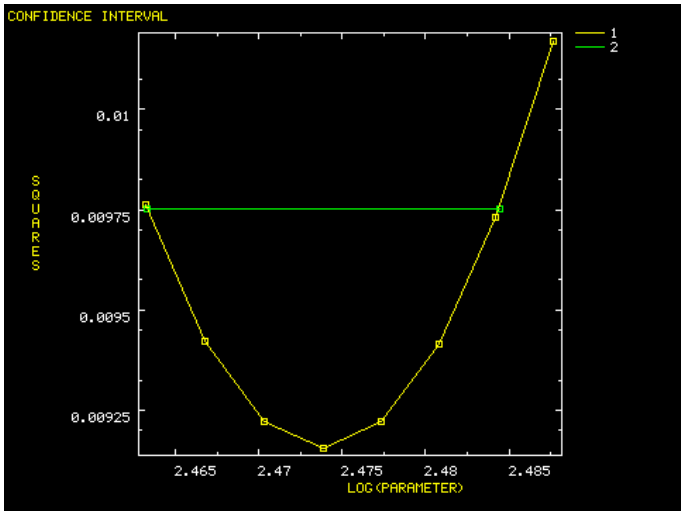

K_1 = 298 (291 - 305)
K_2 = 4.9

Complex

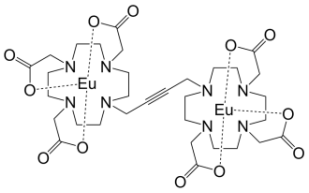

Titrant

Na.pyruvate

Solvent: H_2O

Buffer: HEPES

pH: 7.72

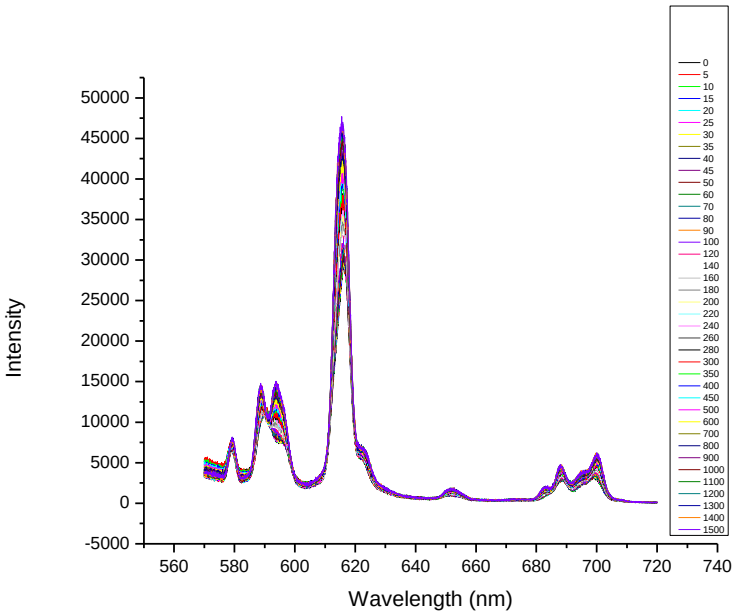

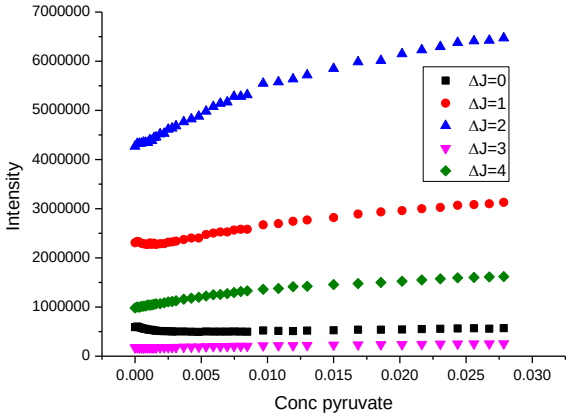

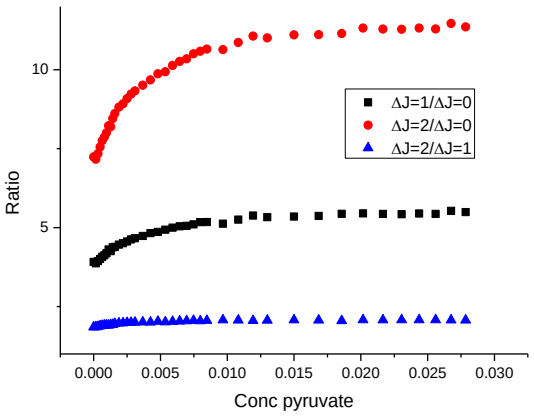

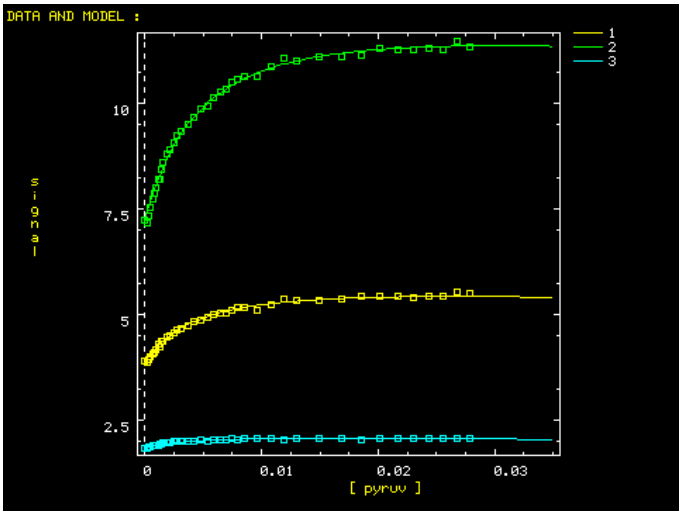

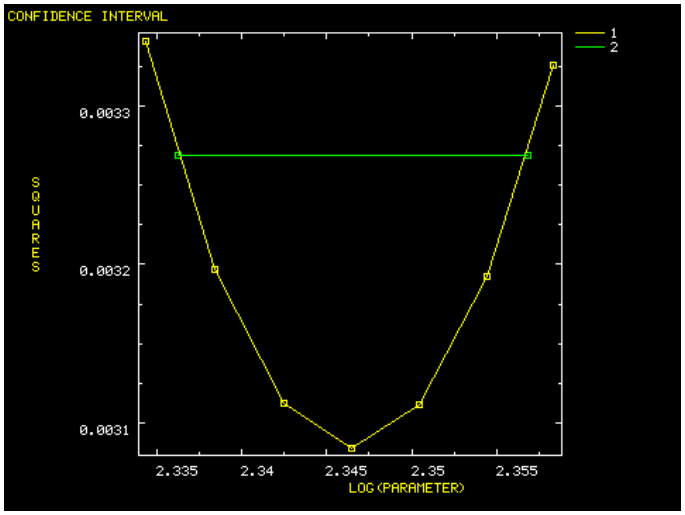

K_1 = 222 (212 - 232)
K_2 = 1.9

Complex

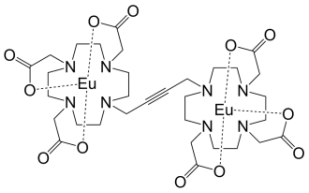

Titrant

Na_3PO_4

Solvent: H_2O

Buffer: HEPES

pH: 7.75

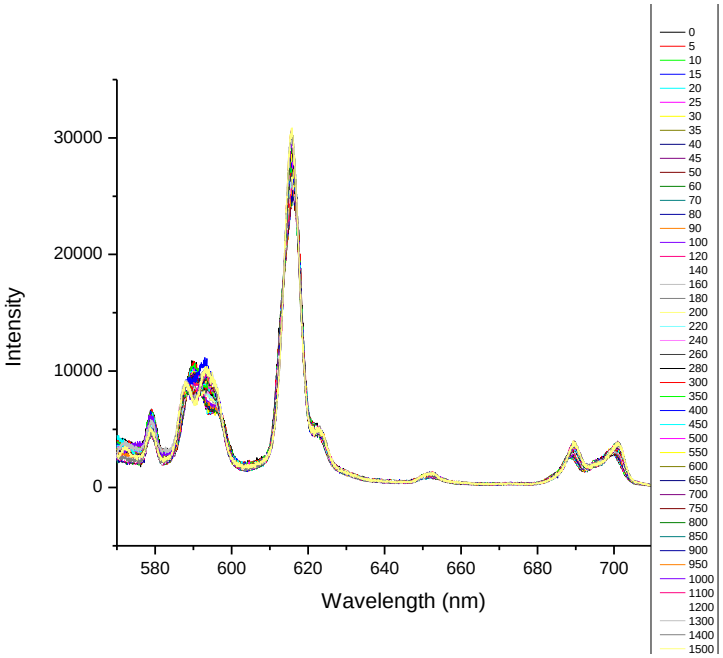

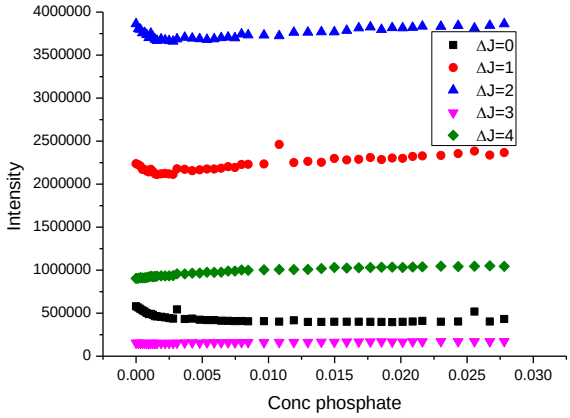

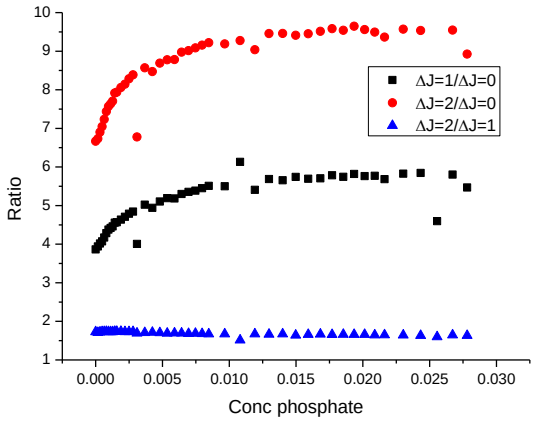

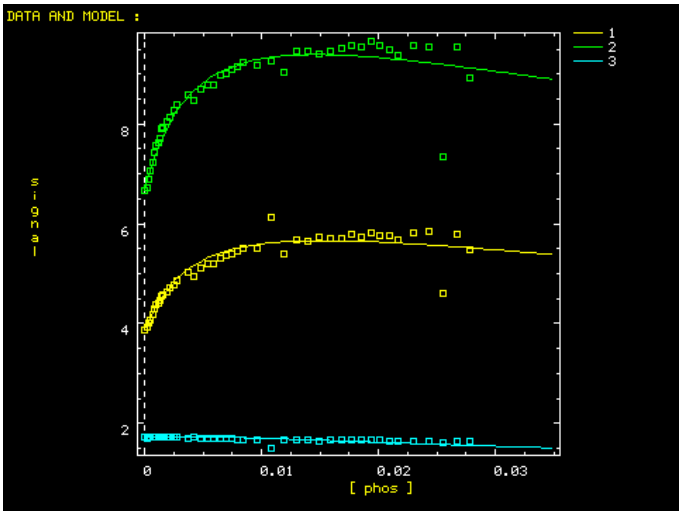

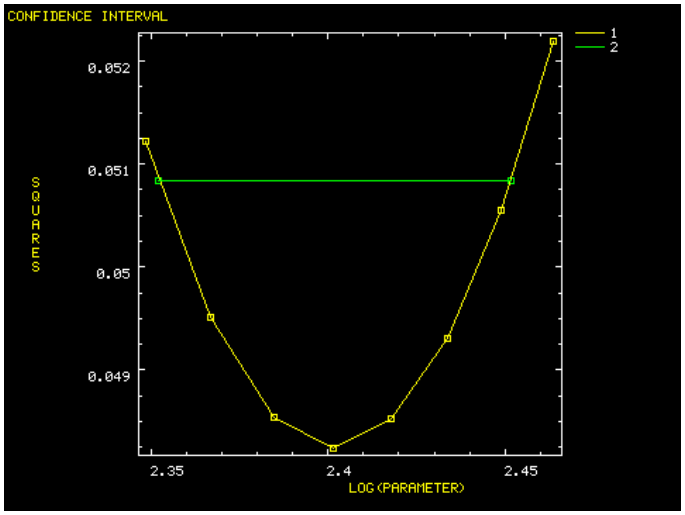

K_1 = 252 (225 - 283)
K_2 = 5.9

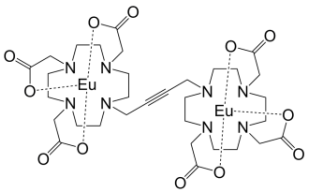

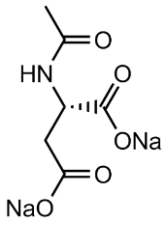

N-acetyl-aspartate

Solvent: H_2O

Buffer: HEPES

pH: 7.70

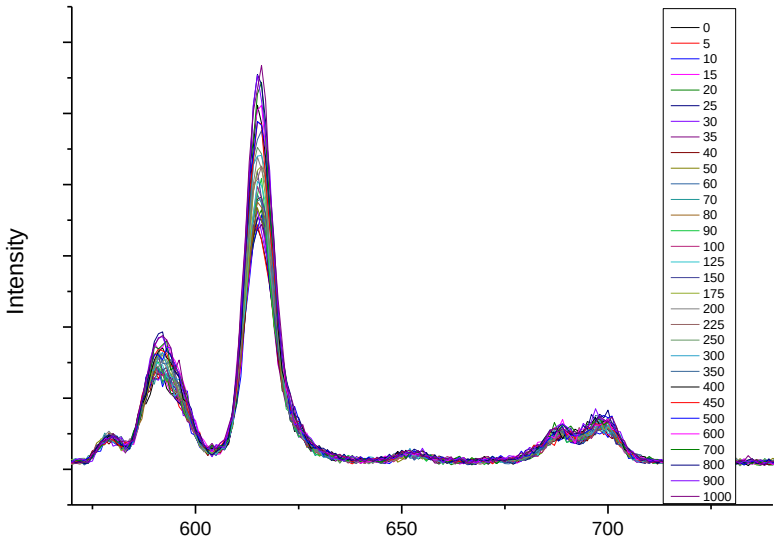

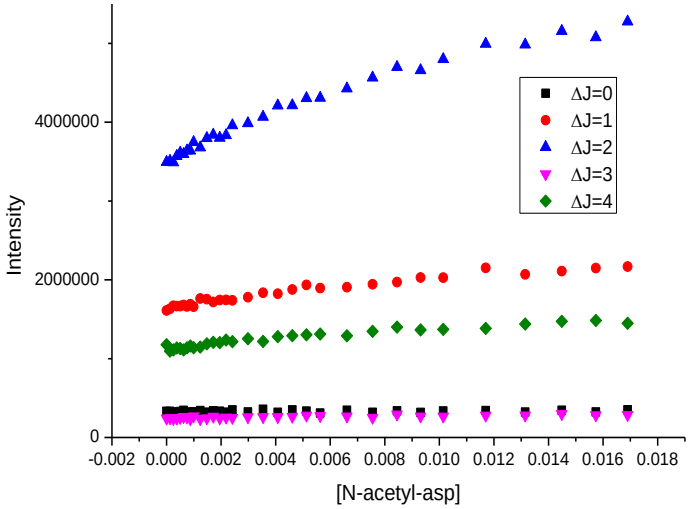

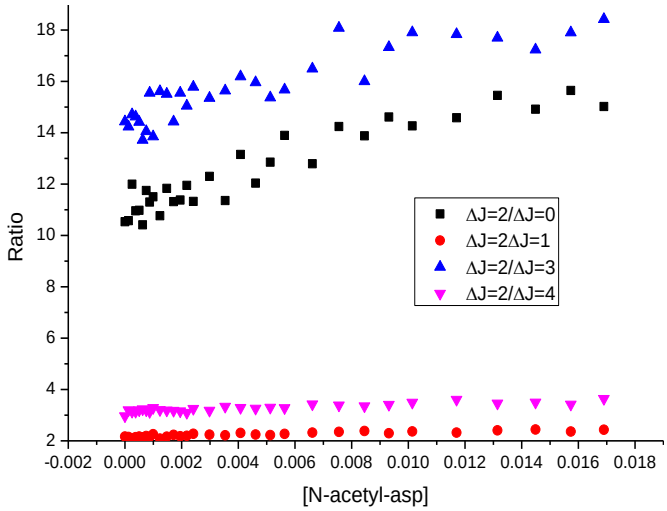

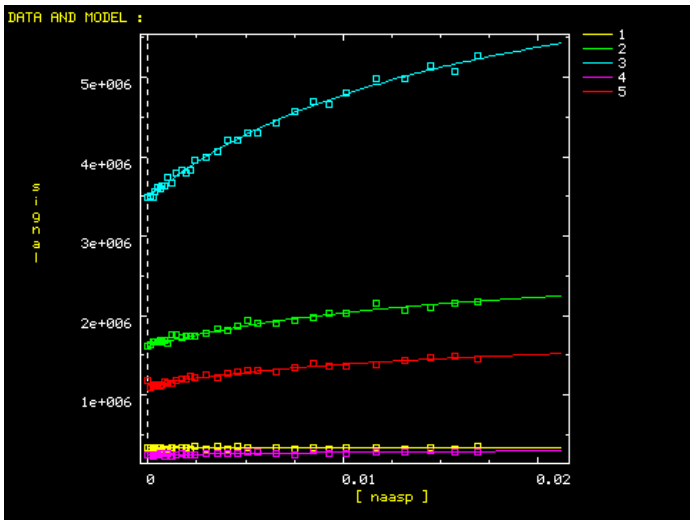

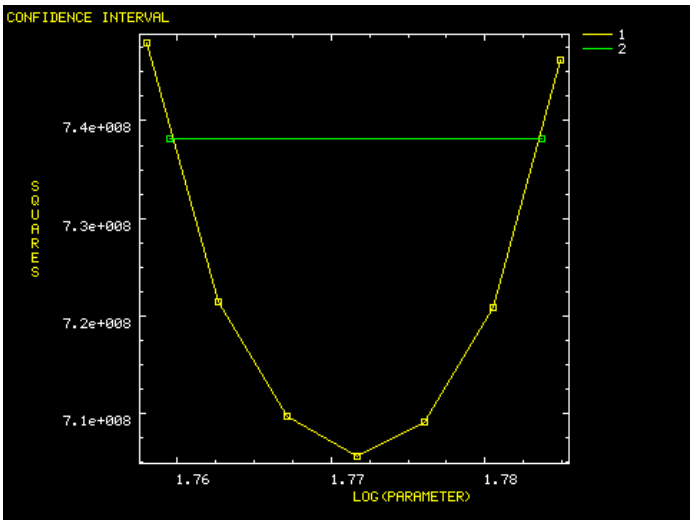

K_1 = 59.111 (57.484 - 60.767)

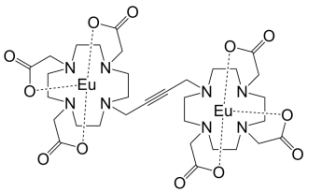

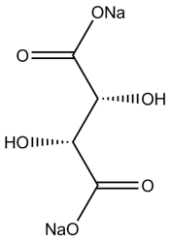

L-tartrate

Solvent: H_2O

Buffer: HEPES

pH: 7.70

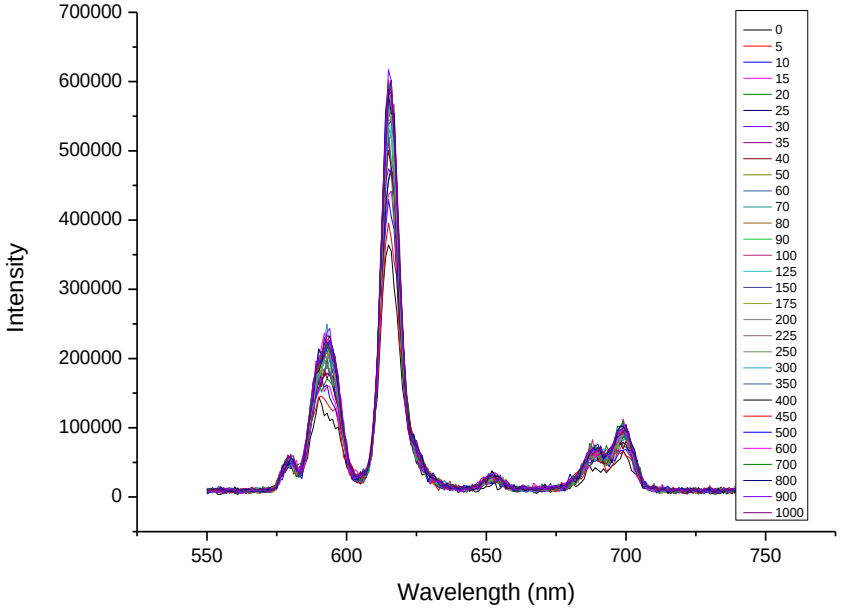

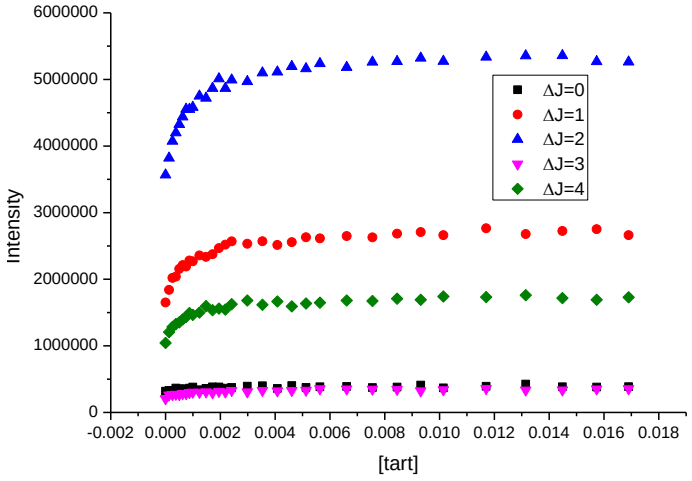

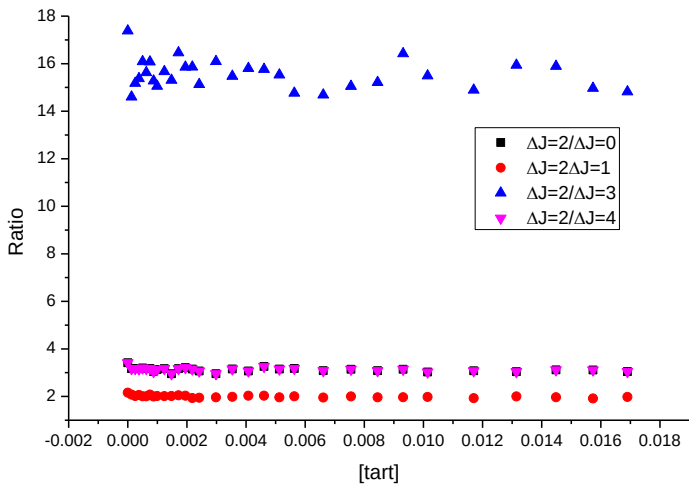

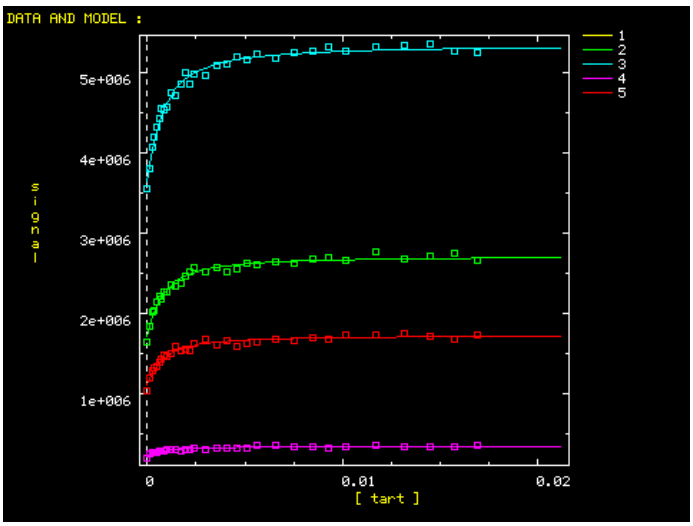

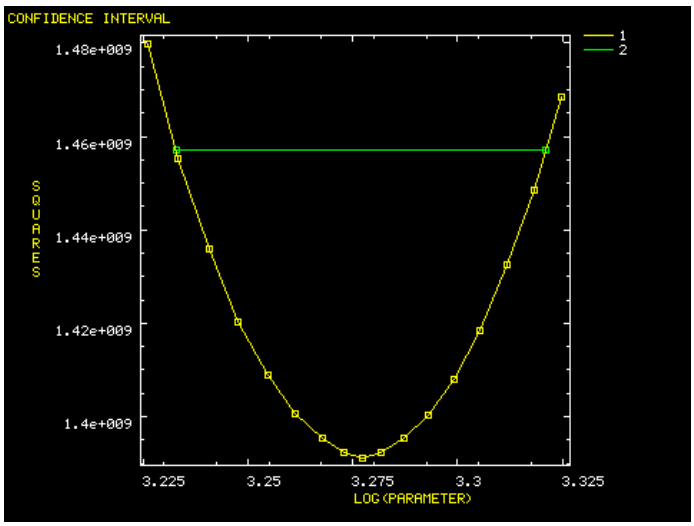

K_1 = 1894.3 (1709.8 - 2094.6)

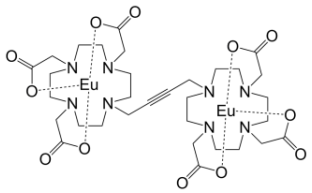

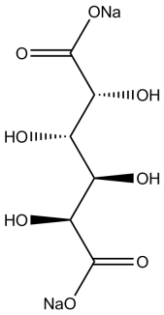

mucate

Solvent: H_2O

Buffer: HEPES

pH: 7.70

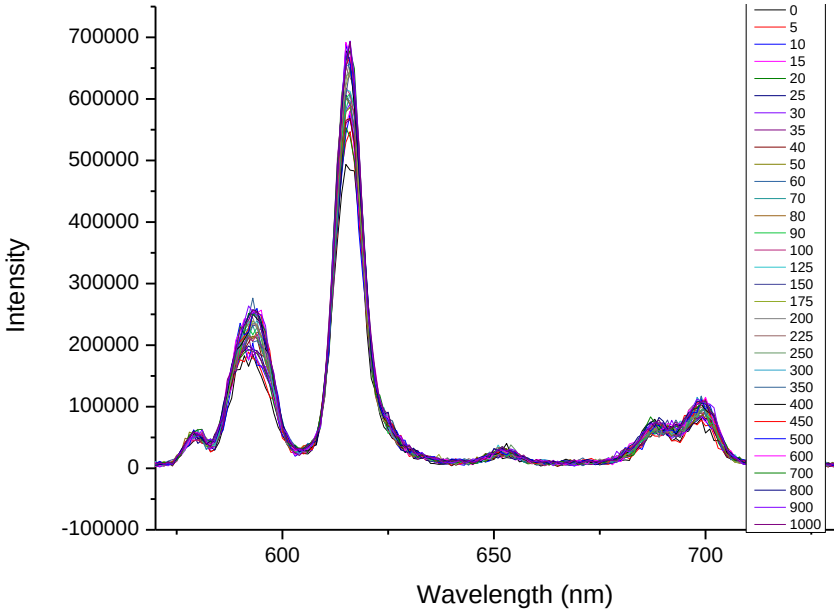

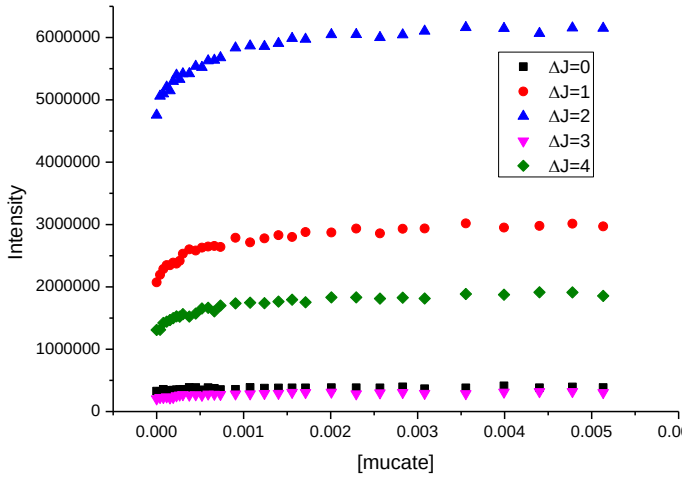

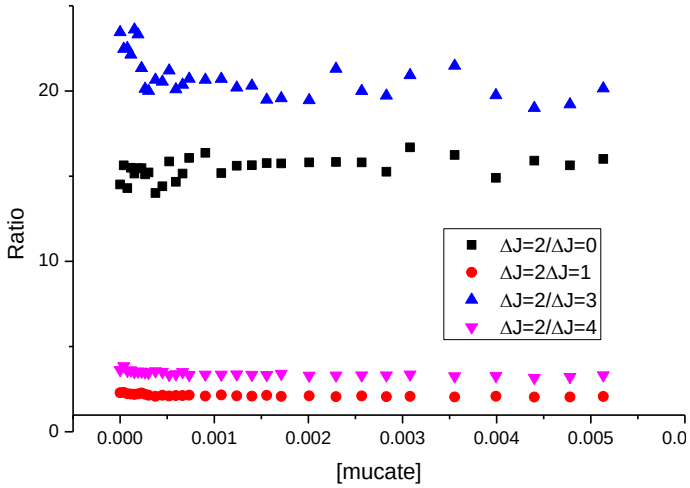

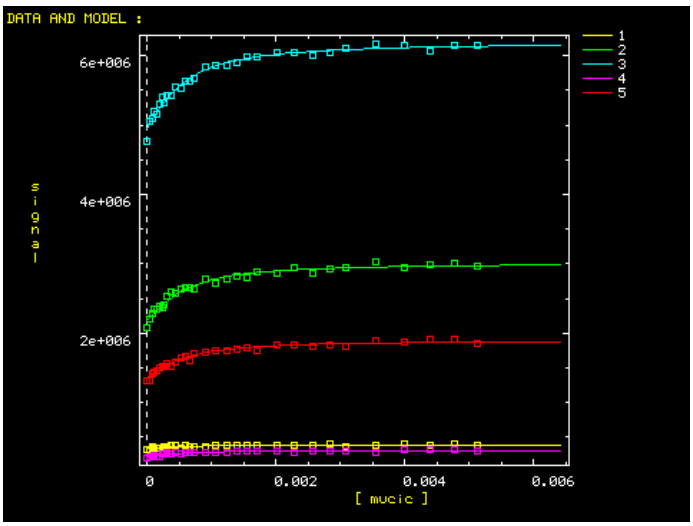

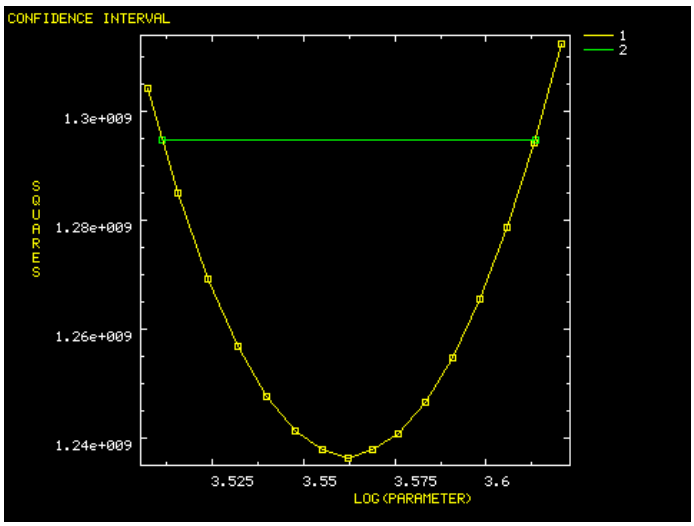

K_1 = 3647.8 (3246 - 4106)

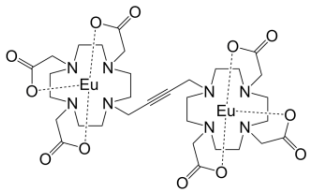

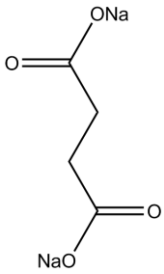

Solvent: H_2O

Buffer: HEPES

pH: 7.70

succinate

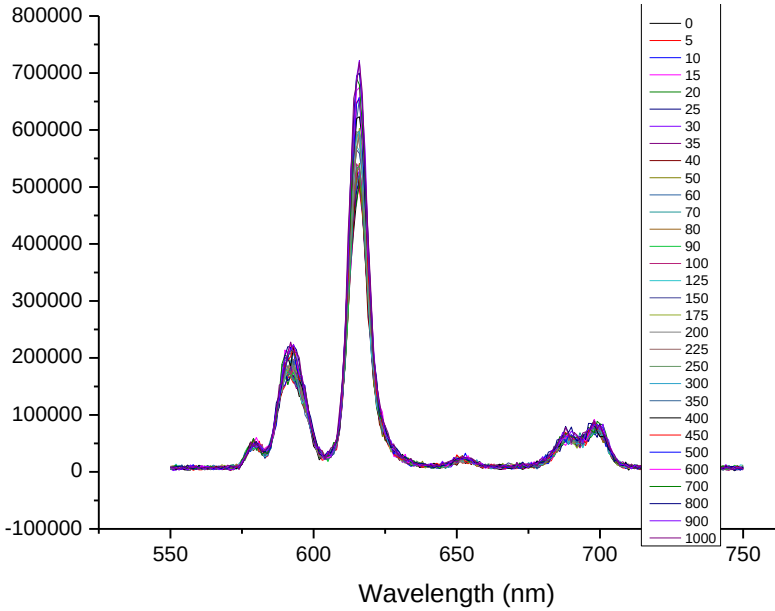

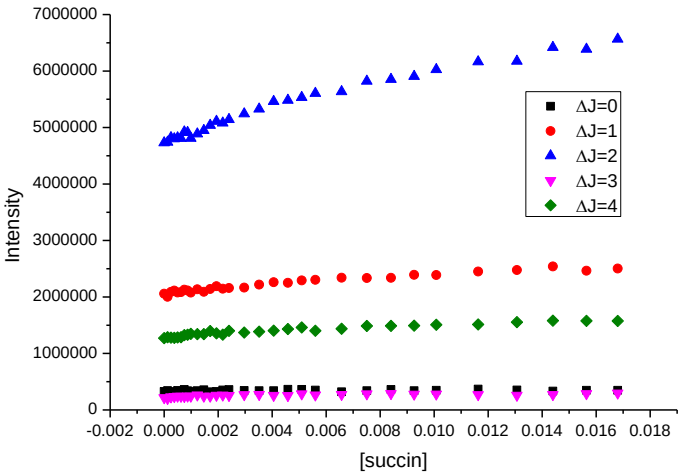

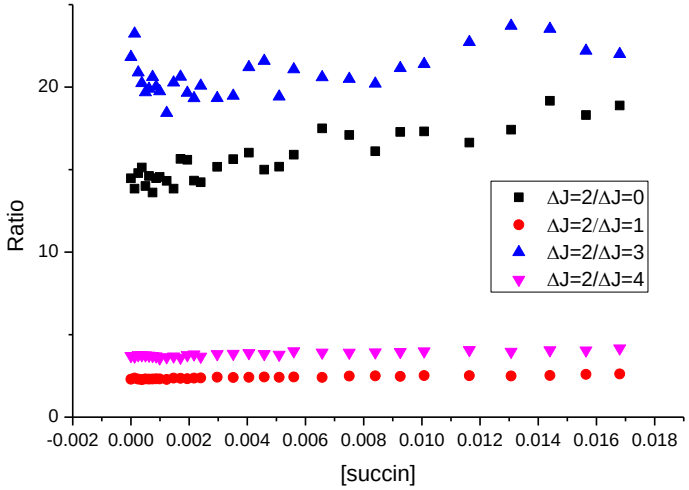

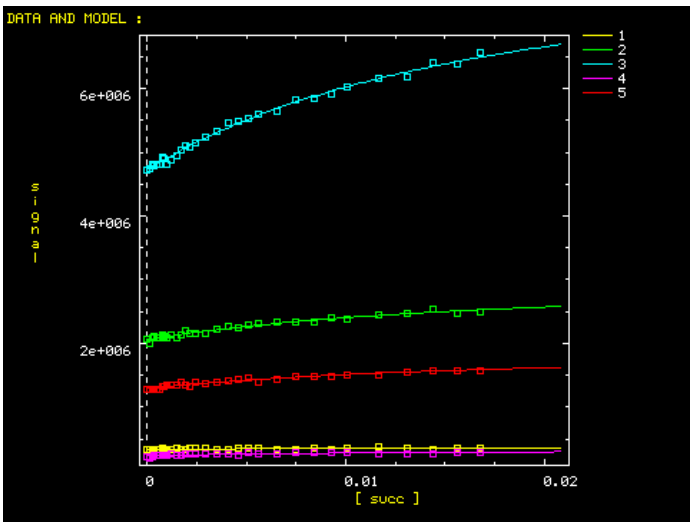

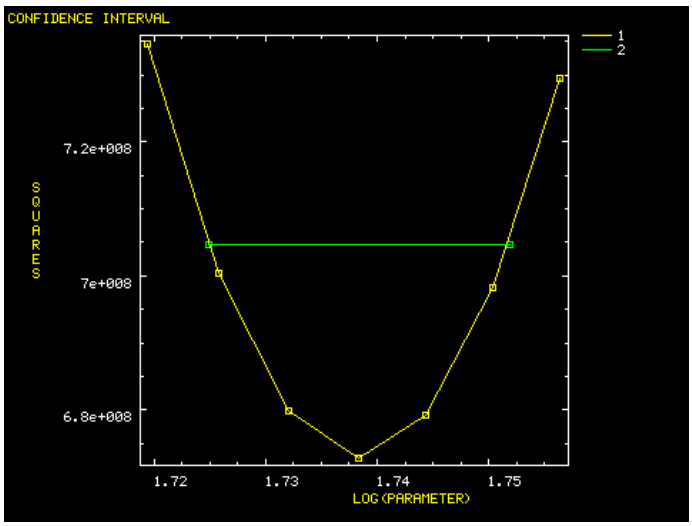

K_1 = 54.737 (53.070 - 56.473)

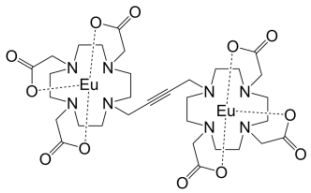

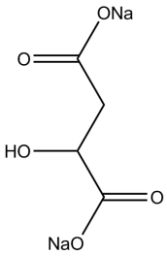

malate

Solvent: H_2O

Buffer: HEPES

pH: 7.70

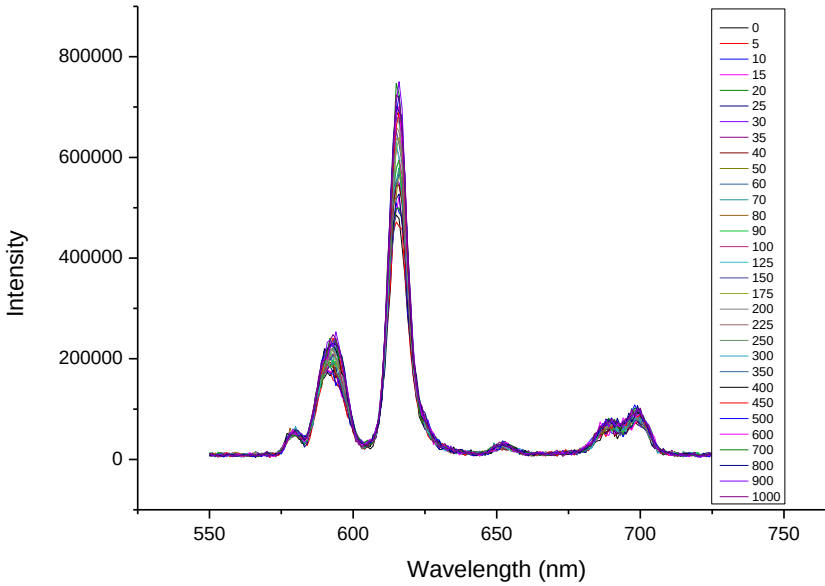

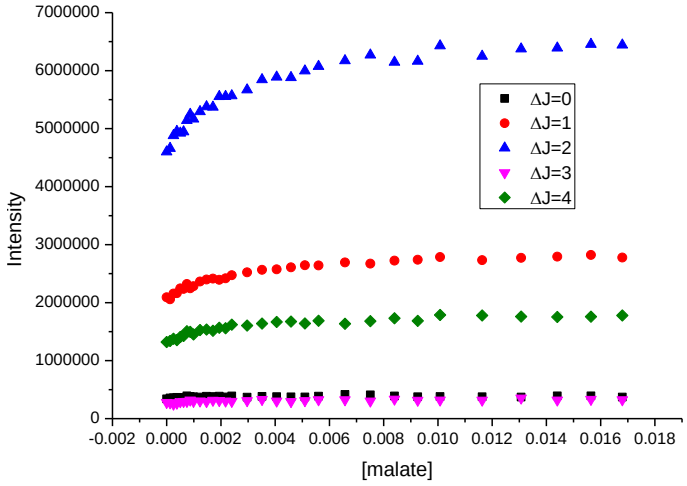

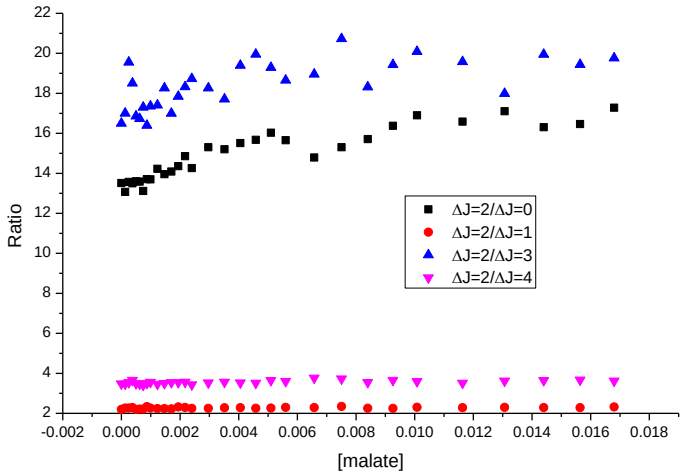

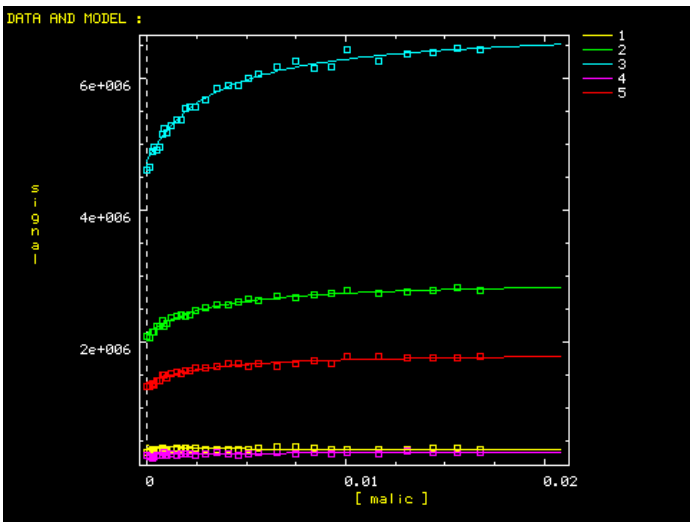

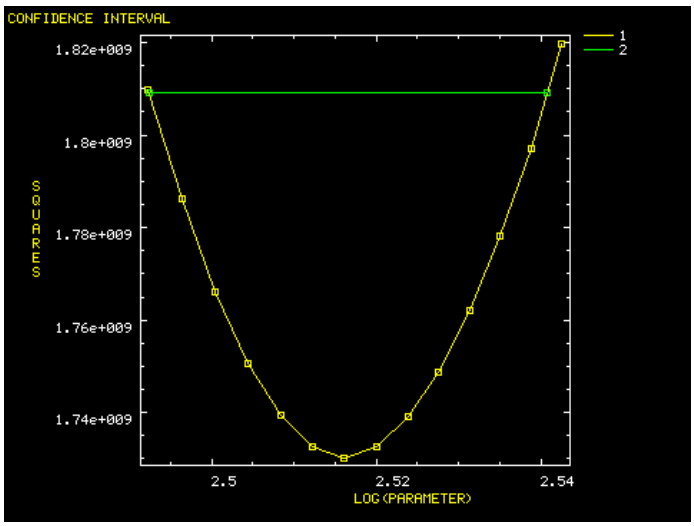

K_1 = 328.21 (310.72 - 347.39)

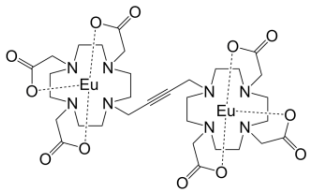

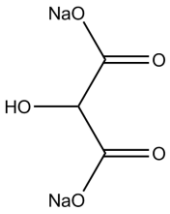

tartronate

Solvent: H_2O

Buffer: HEPES

pH: 7.70

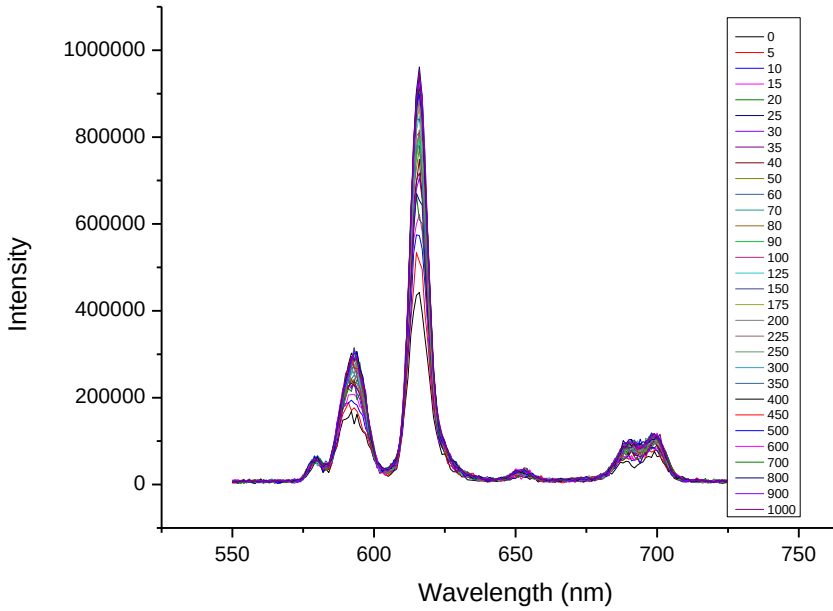

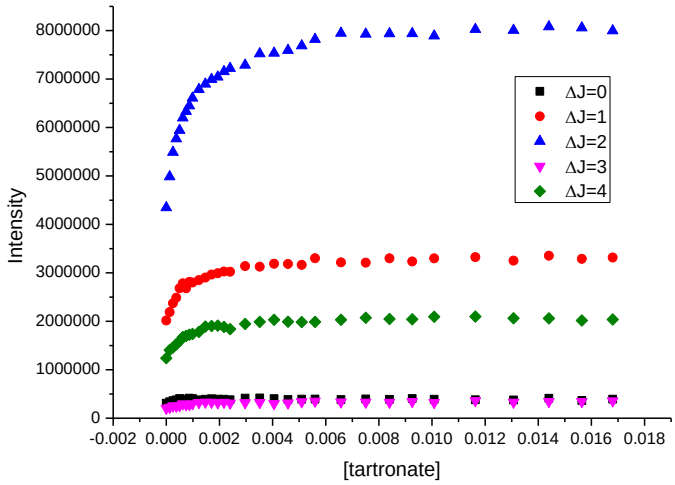

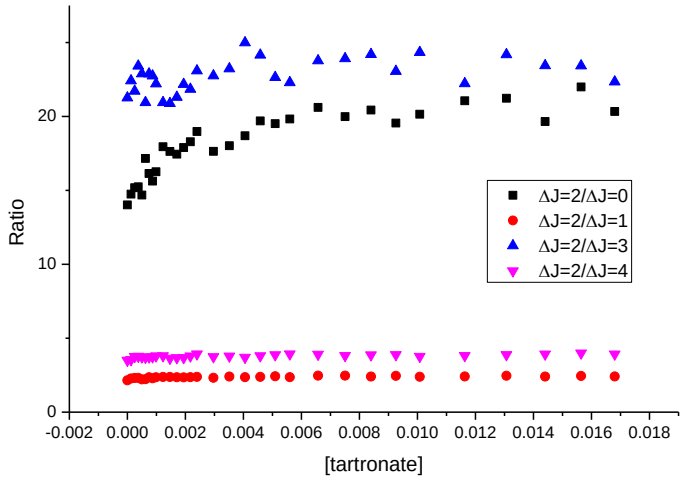

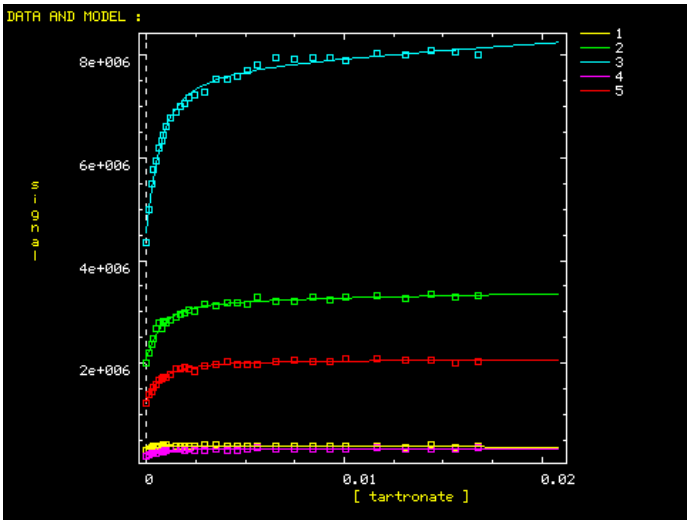

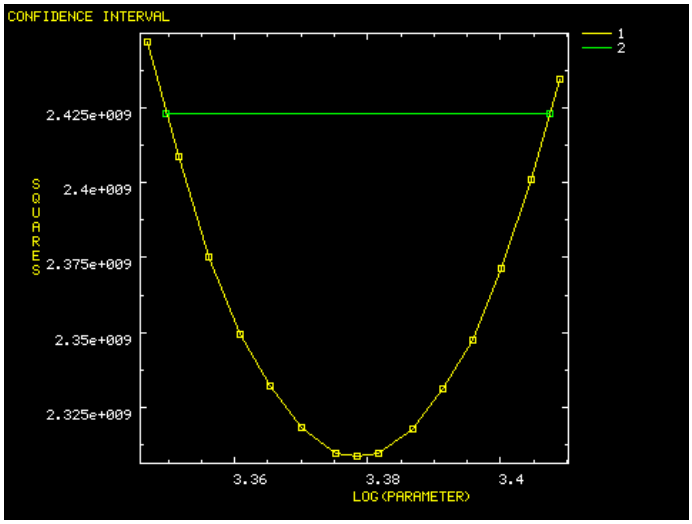

K_1 = 2390.6 (2237.3 - 2555.3)

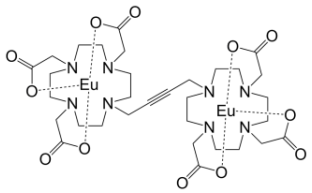

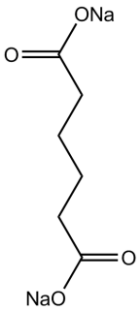

adipate

Solvent: H_2O

Buffer: HEPES

pH: 7.70

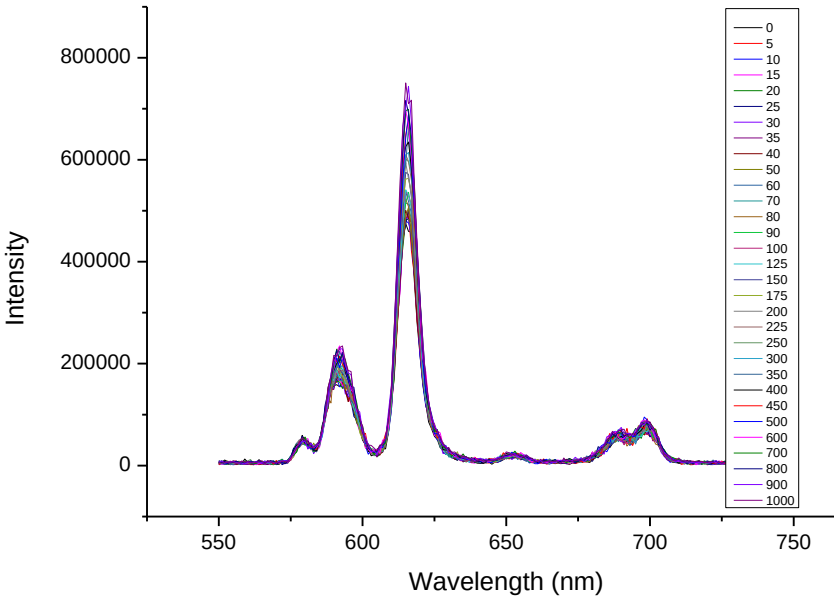

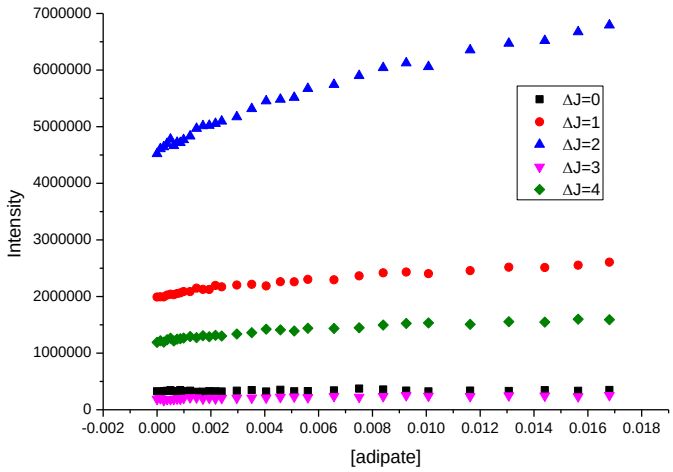

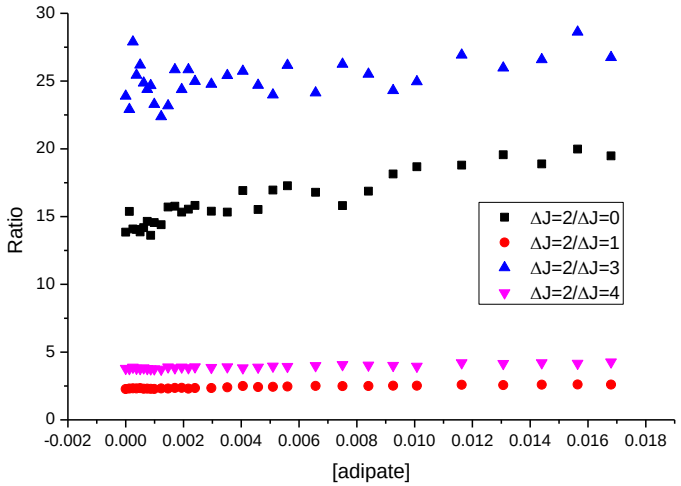

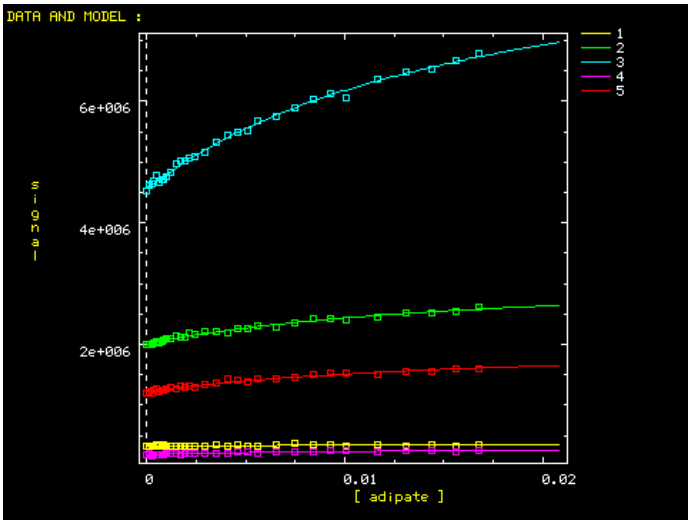

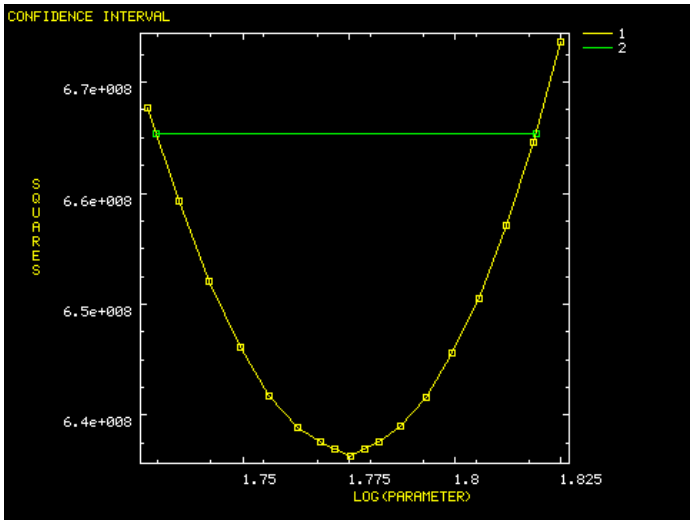

K_1 = 59.604 (53.649 - 65.939)

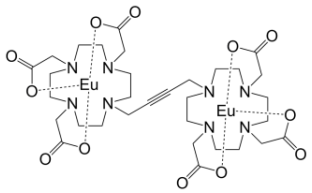

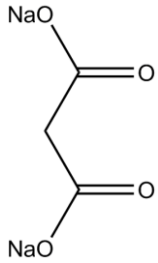

malonate

Solvent: H_2O

Buffer: HEPES

pH: 7.70

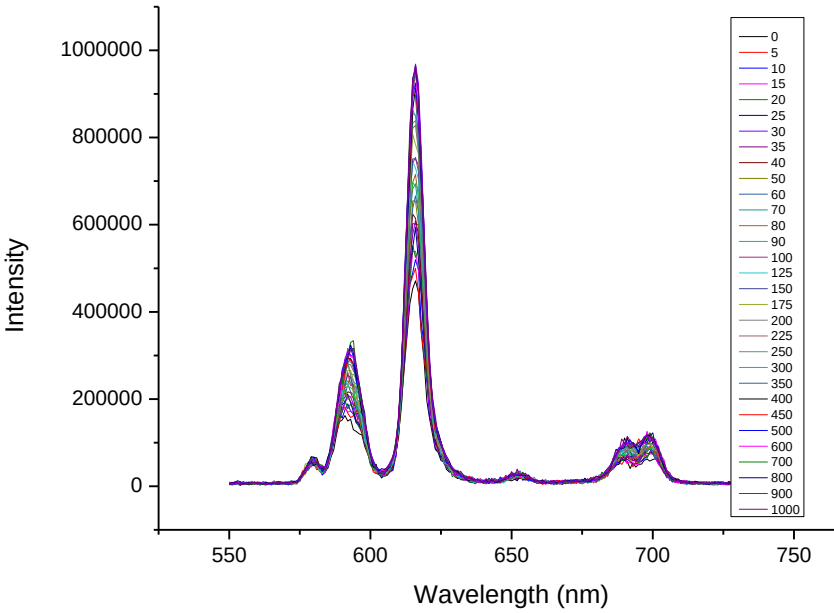

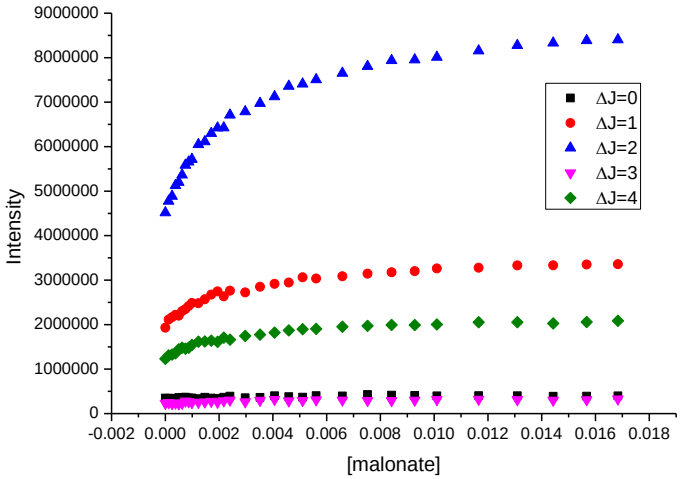

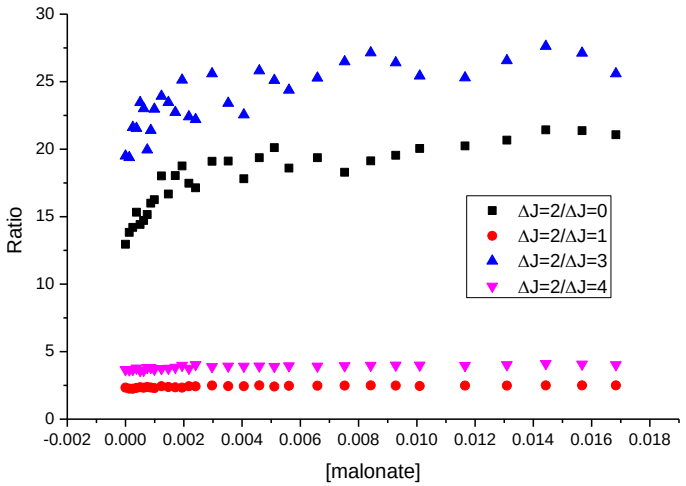

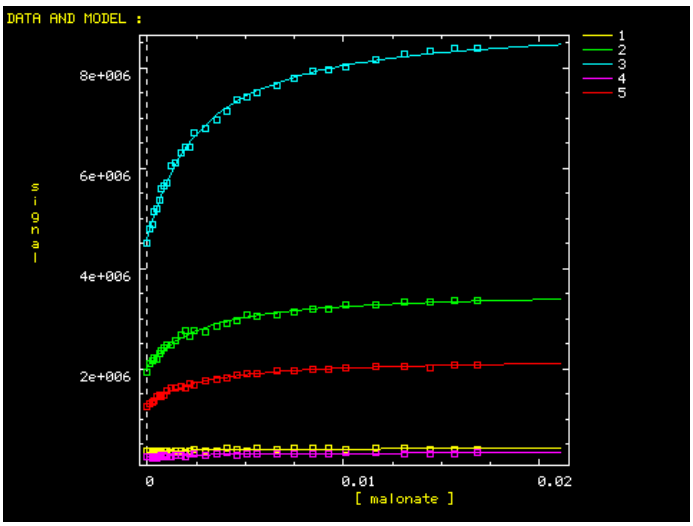

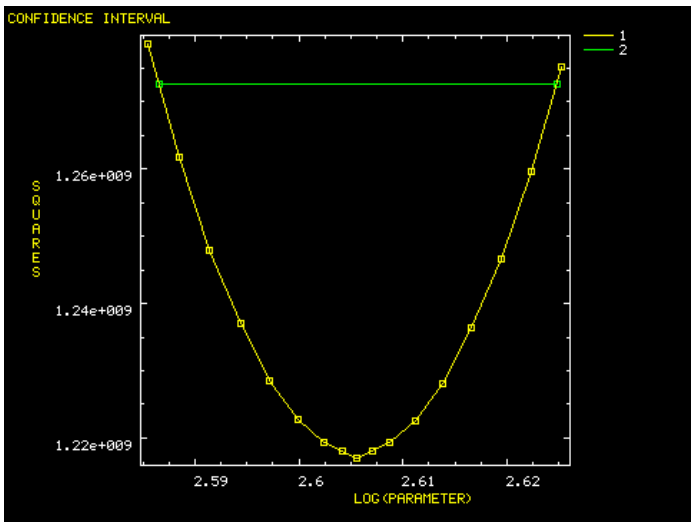

K_1 = 403.25 (385.92 - 421.47)

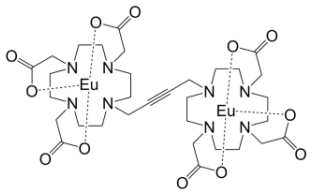

glutarate

Solvent: H_2O

Buffer: HEPES

pH: 7.70

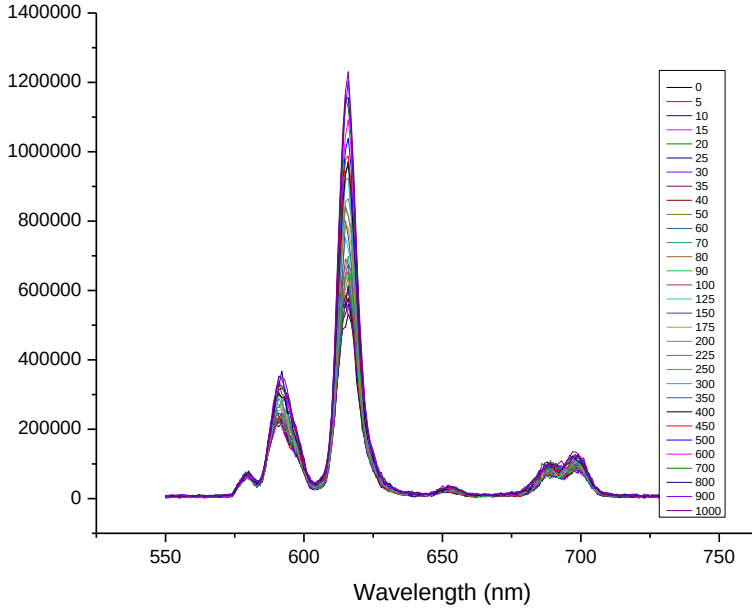

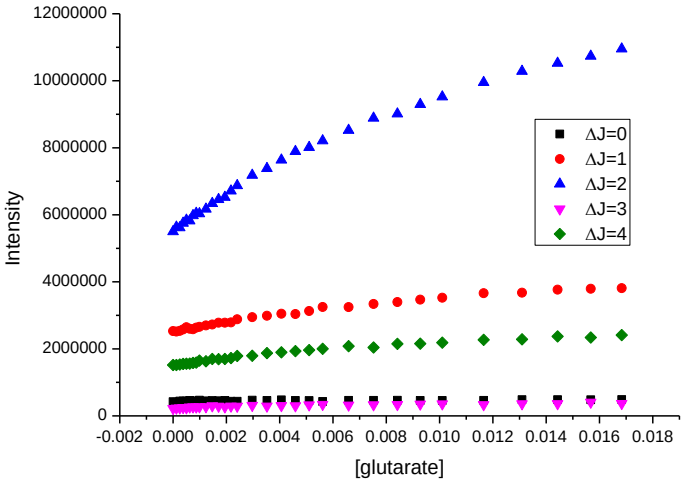

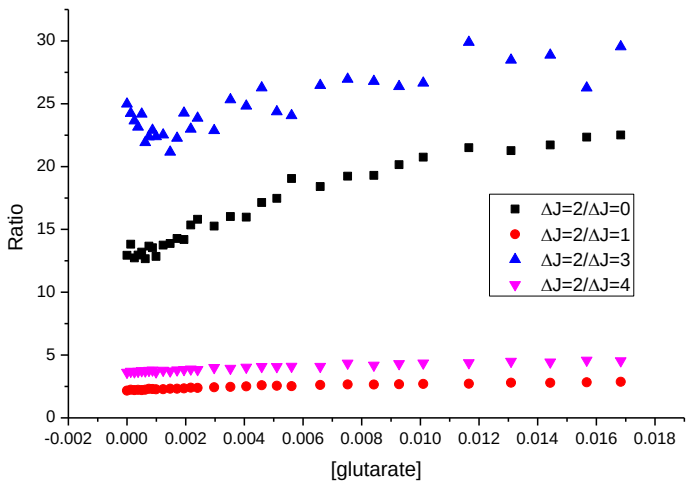

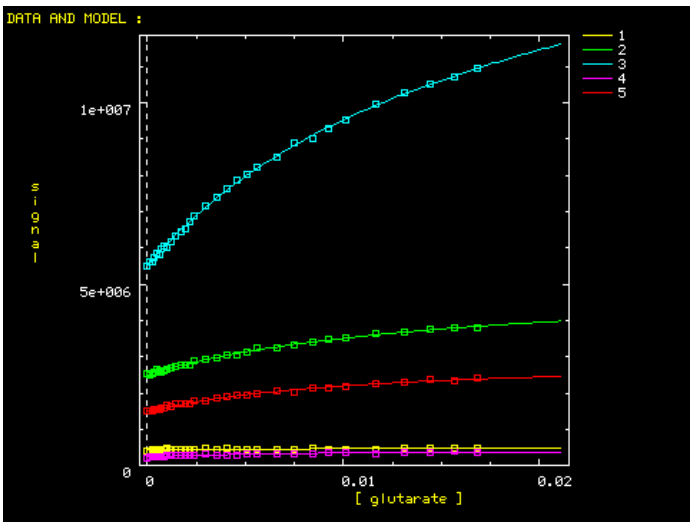

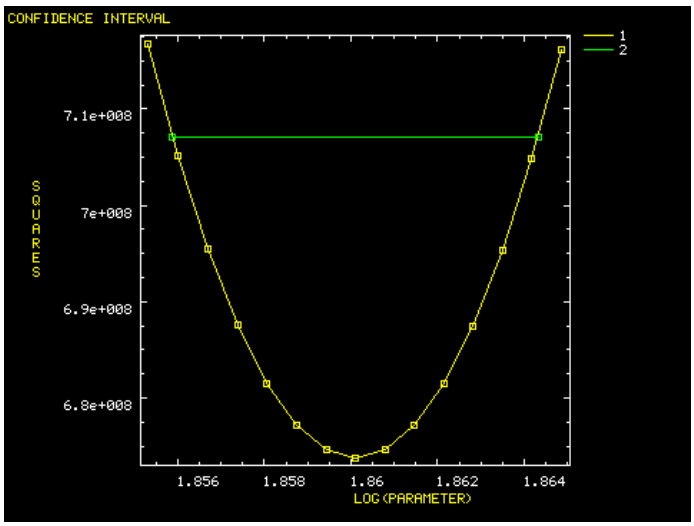

K_1 = 72.4616 (71.7596 - 73.1676)

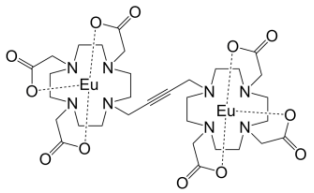

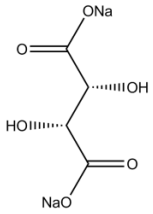

tartrate

Solvent: H_2O

Buffer: PBS

pH: 7.70

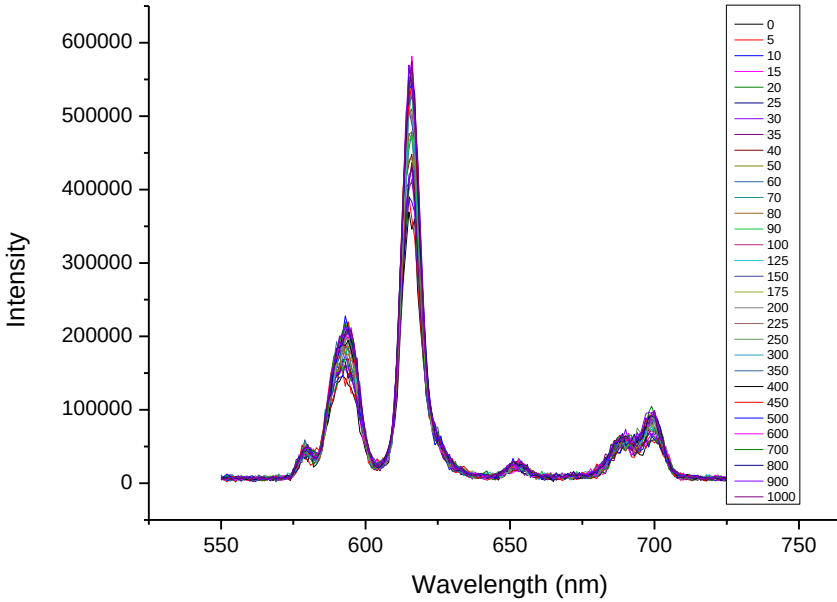

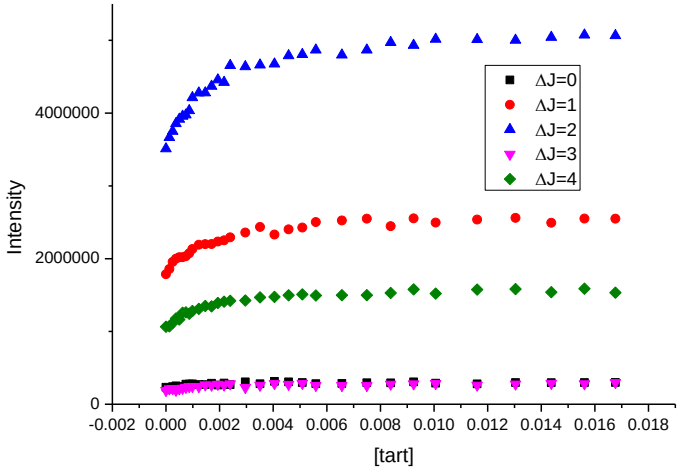

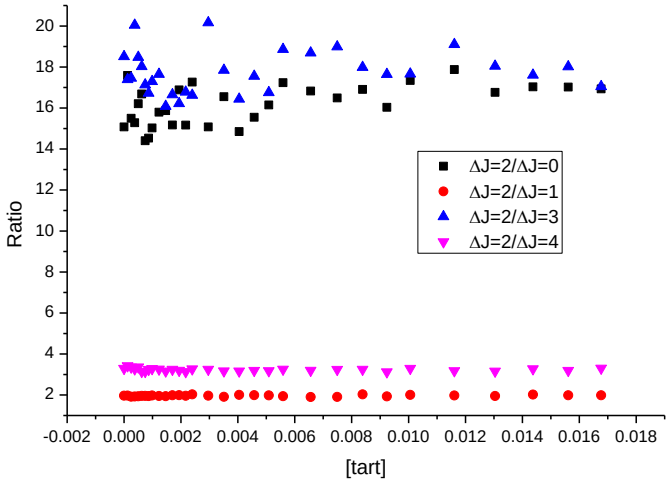

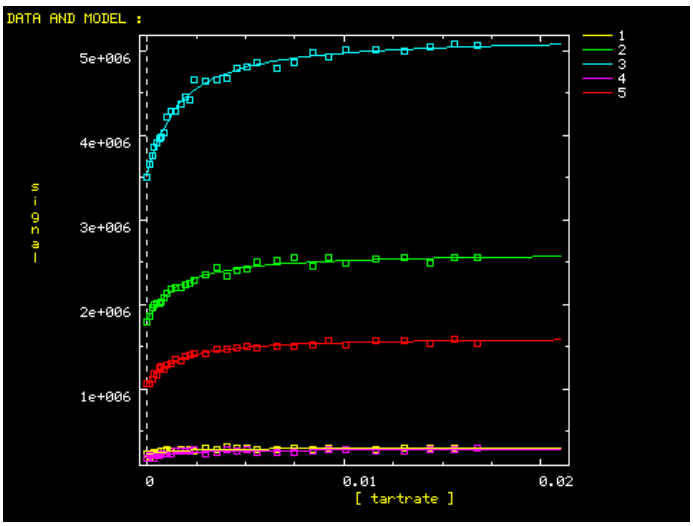

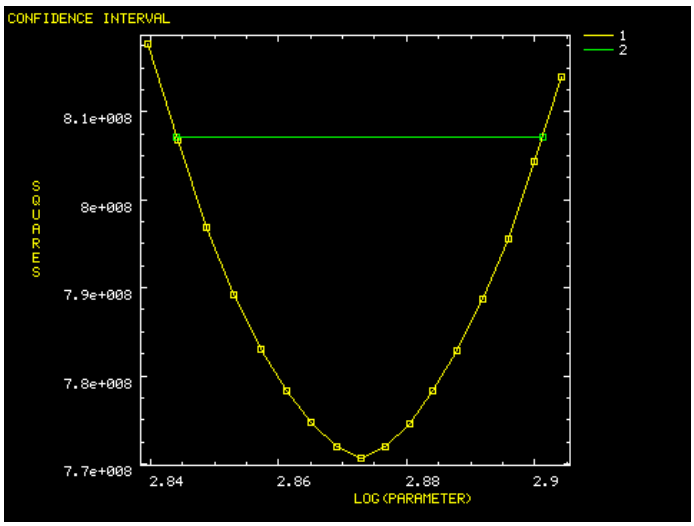

K_1 = 746.16 (698.36 - 796.49)

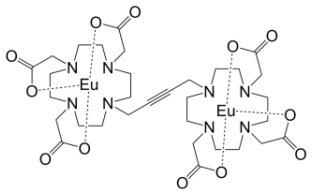

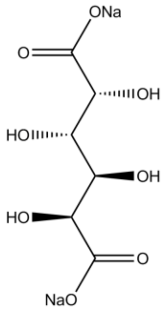

Solvent: H_2O

Buffer: PBS

pH: 7.70

mucate

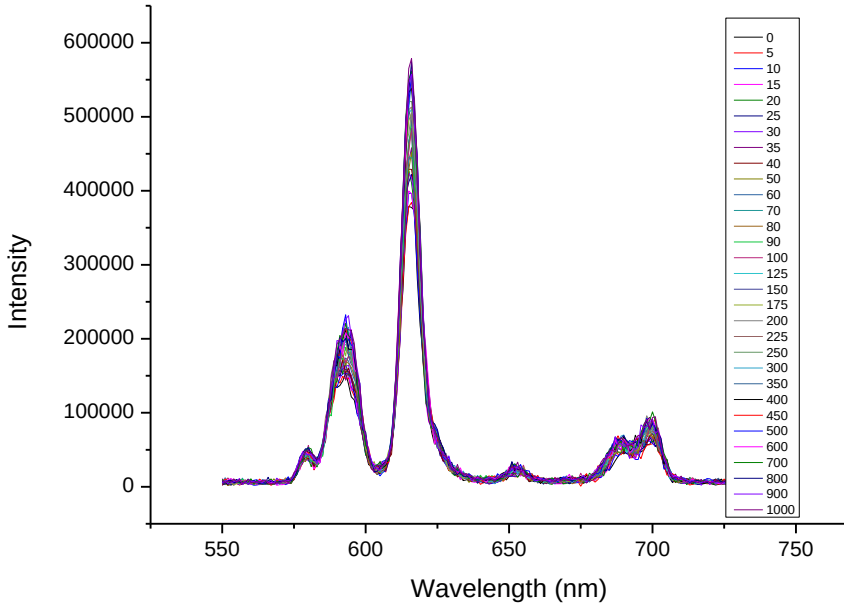

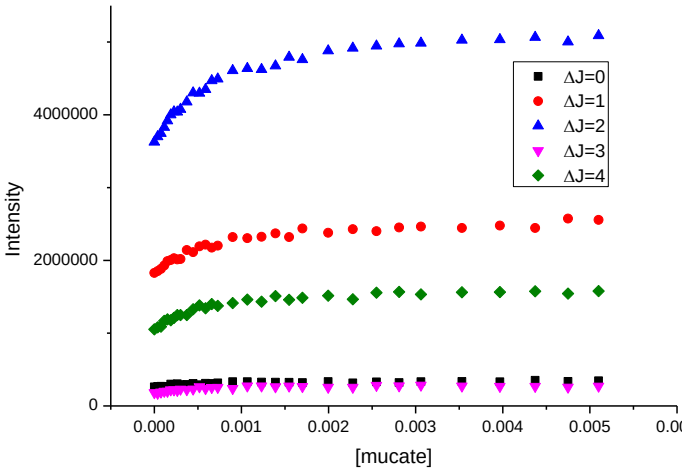

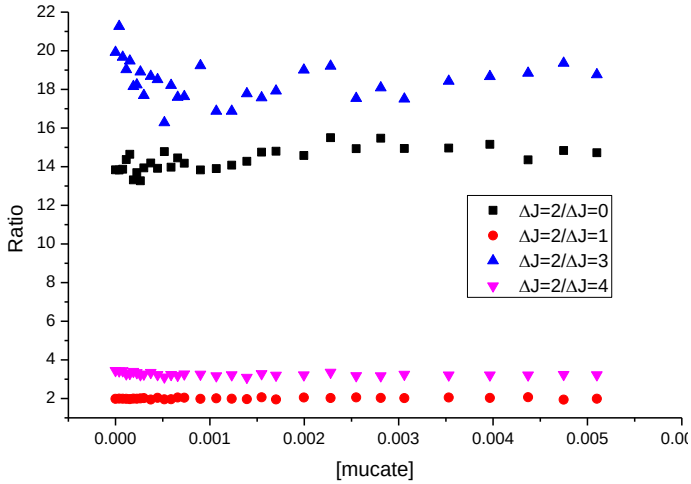

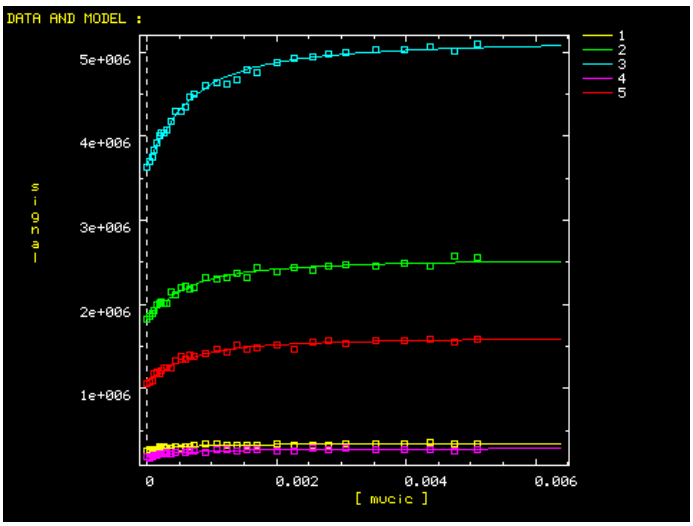

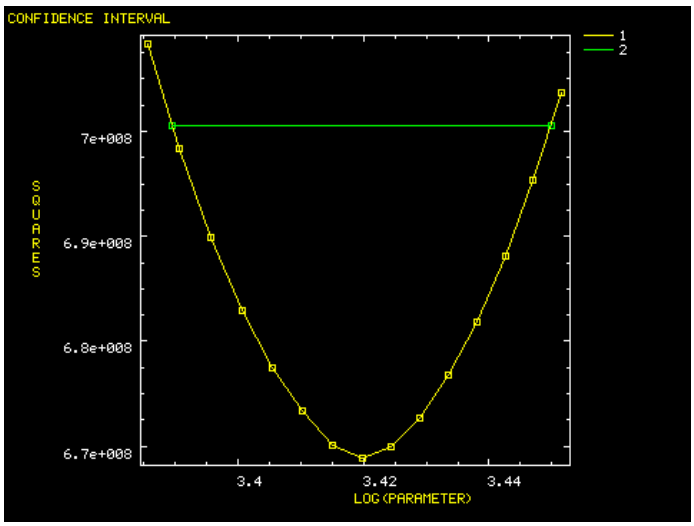

K_1 = 2629.2 (2452.6 - 2817.3)

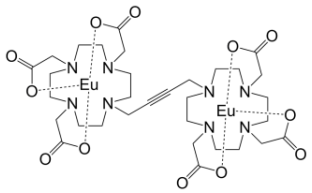

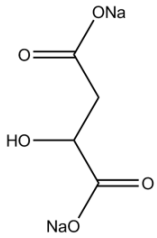

malate

Solvent: H_2O

Buffer: PBS

pH: 7.70

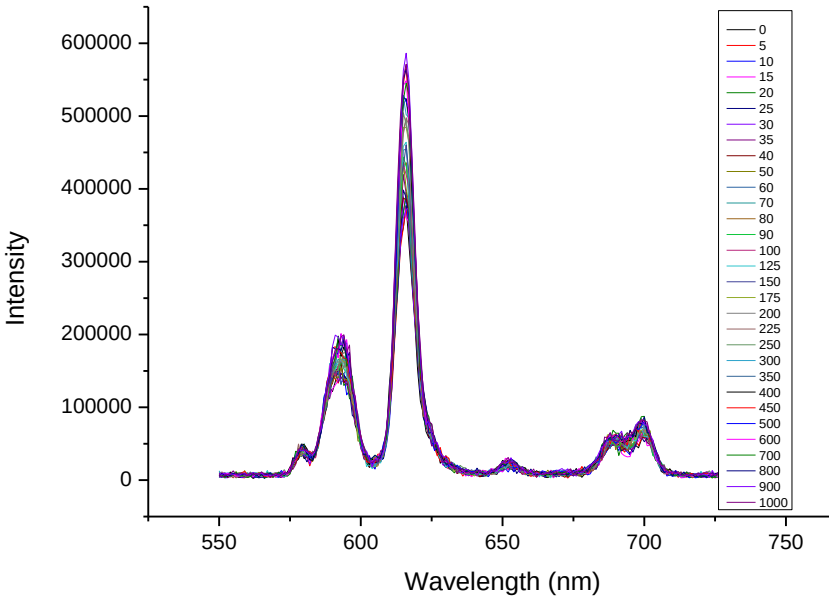

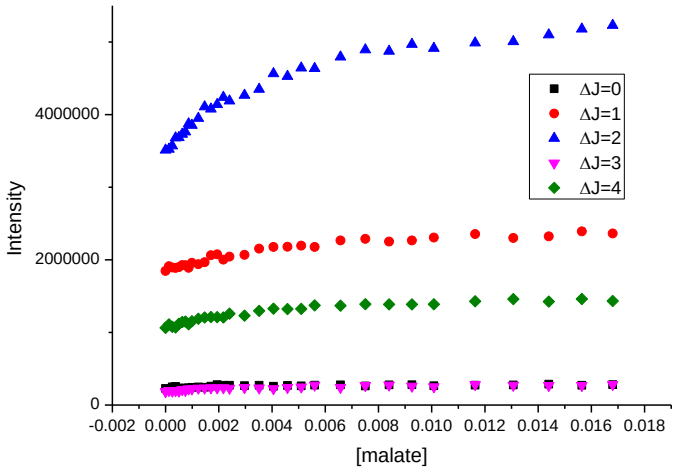

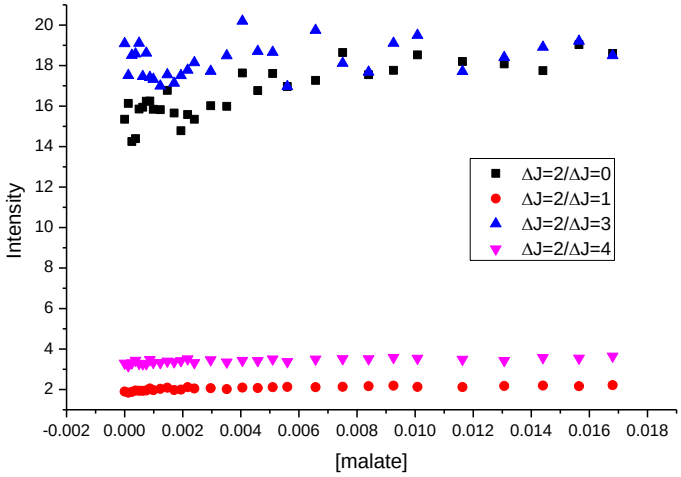

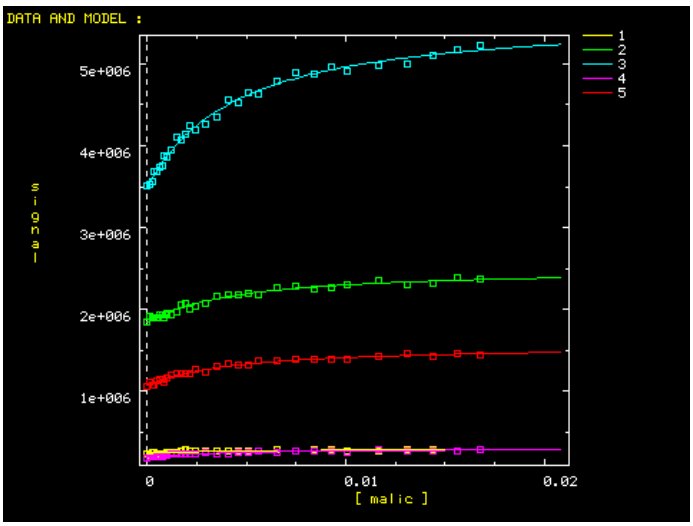

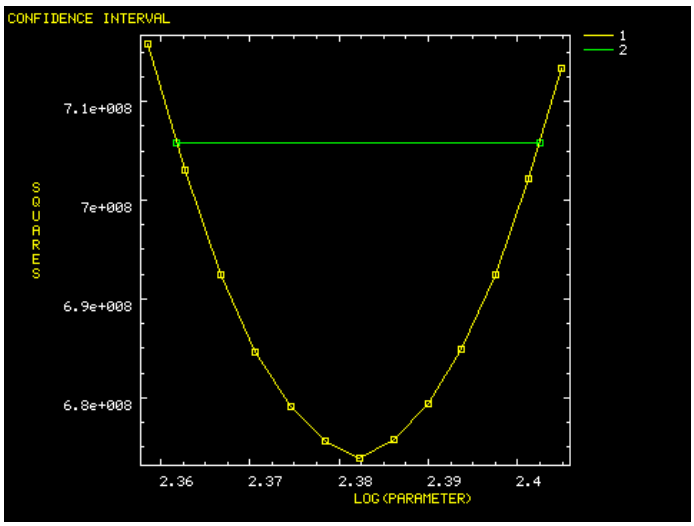

K_1 = 241.18 (229.99 - 252.61)

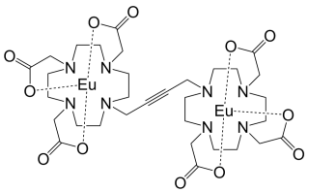

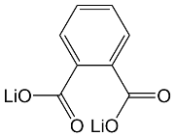

Solvent: MeOH

Buffer: N/A

pH: N/A

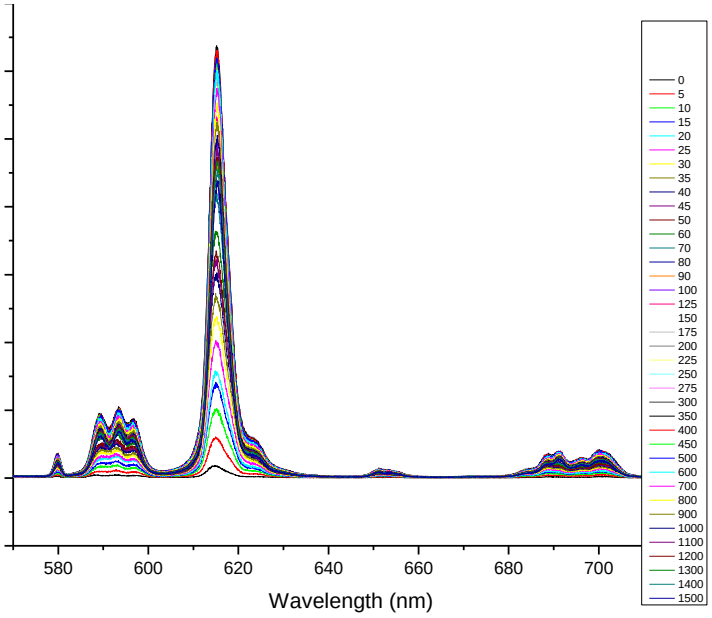

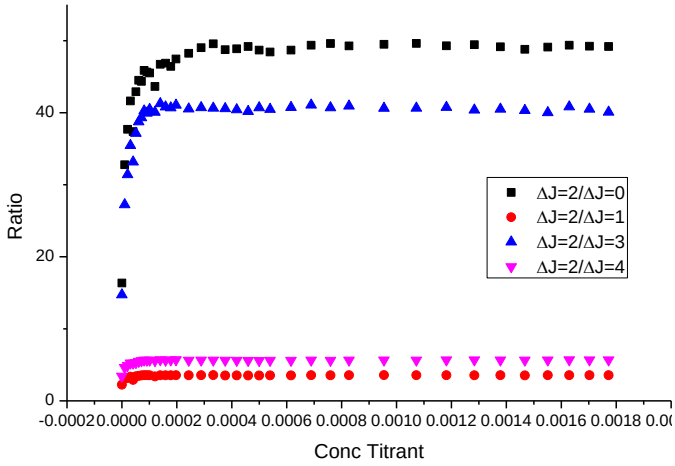

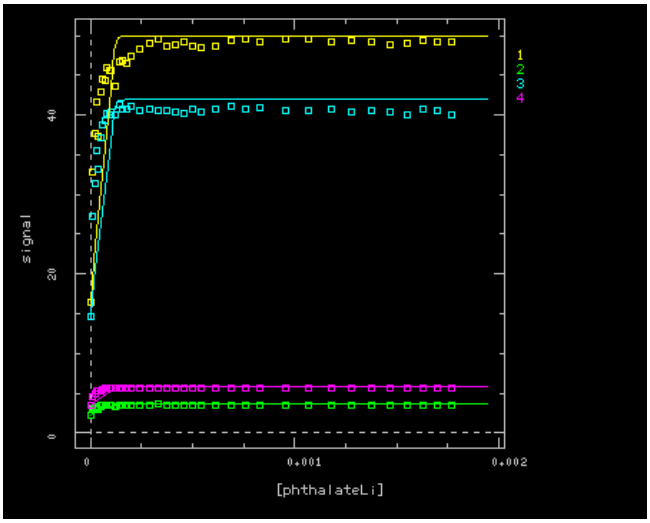

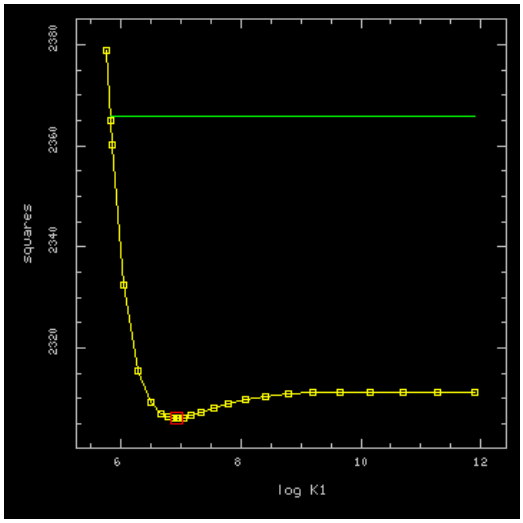

K_1 > 680767 (95%)

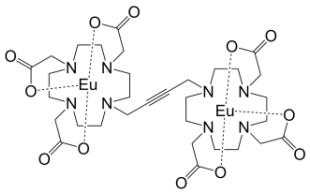

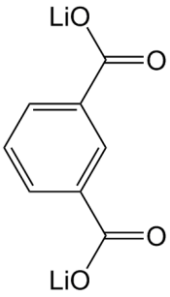

Solvent: MeOH

Buffer: N/A

pH: N/A

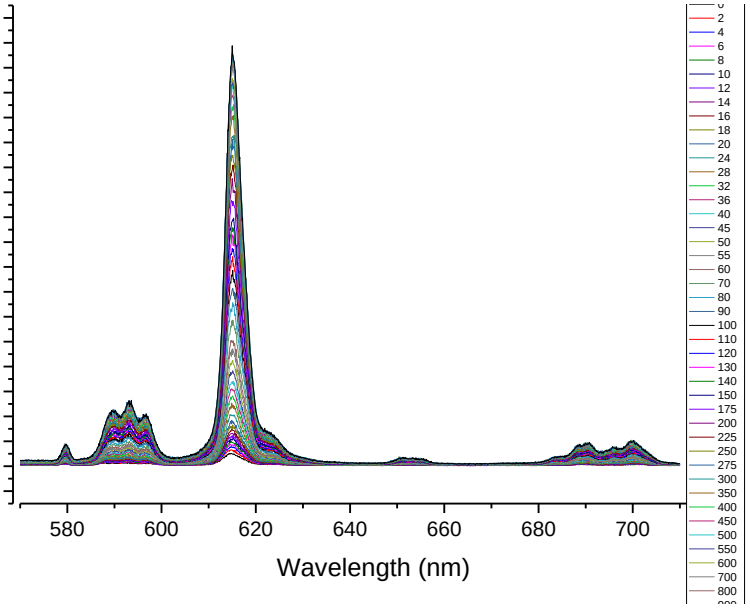

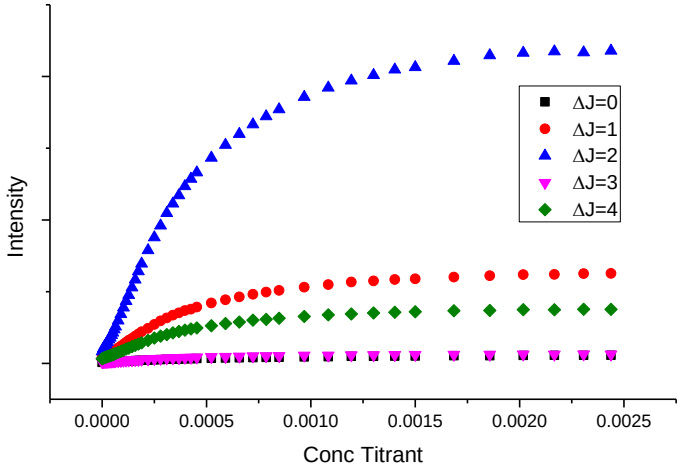

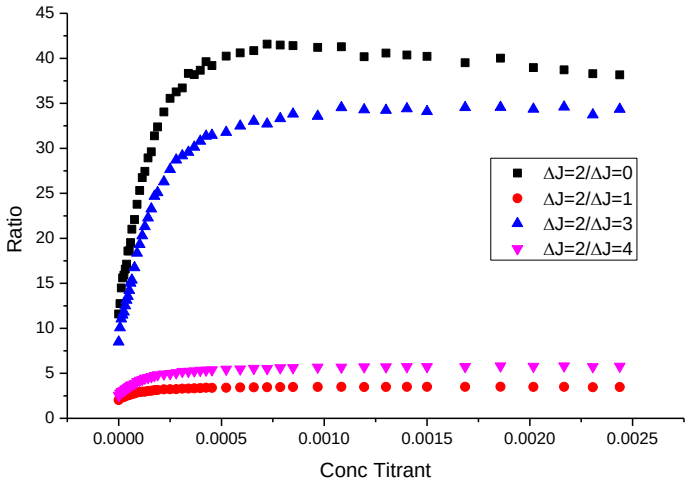

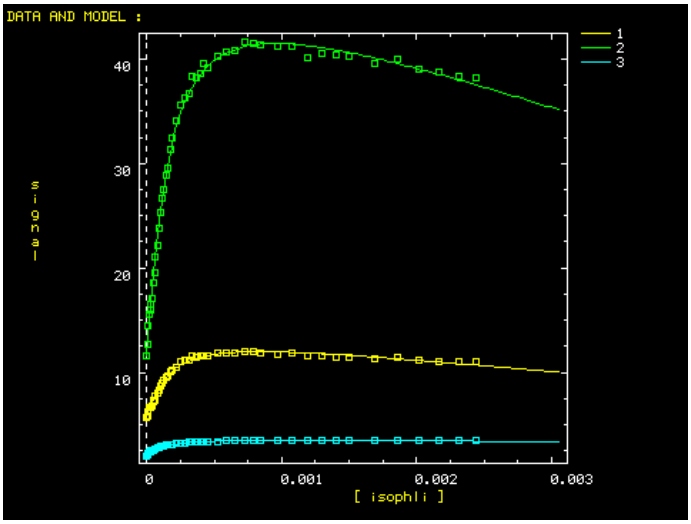

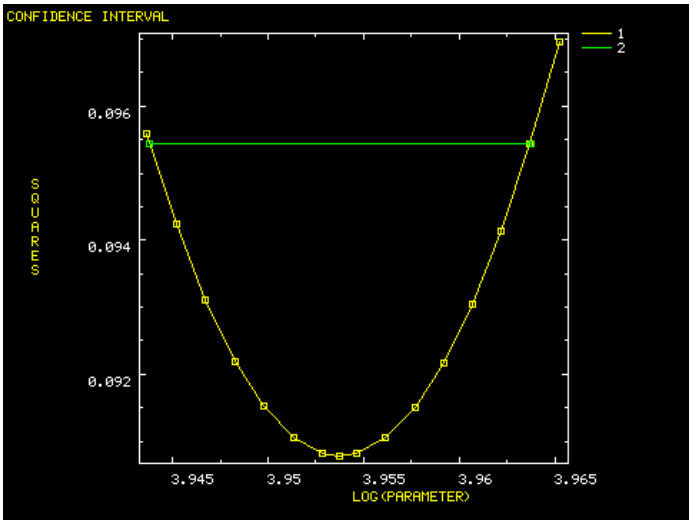

K_1 = 8989.7 (8786.7 - 9198.4)

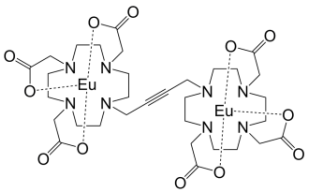

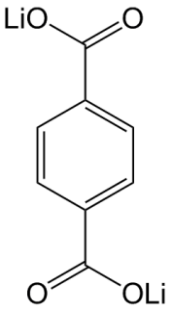

Solvent: MeOH

Buffer: N/A

pH: N/A

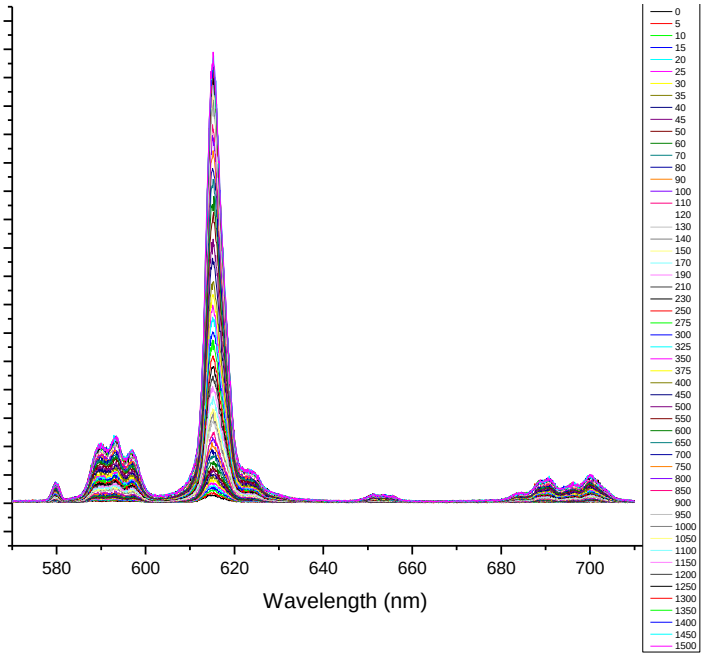

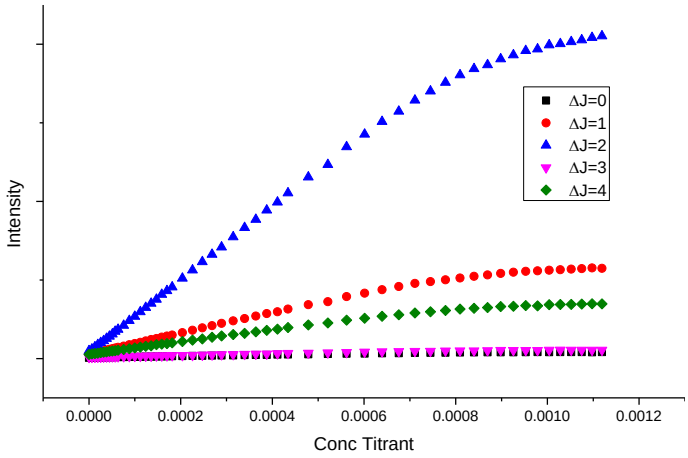

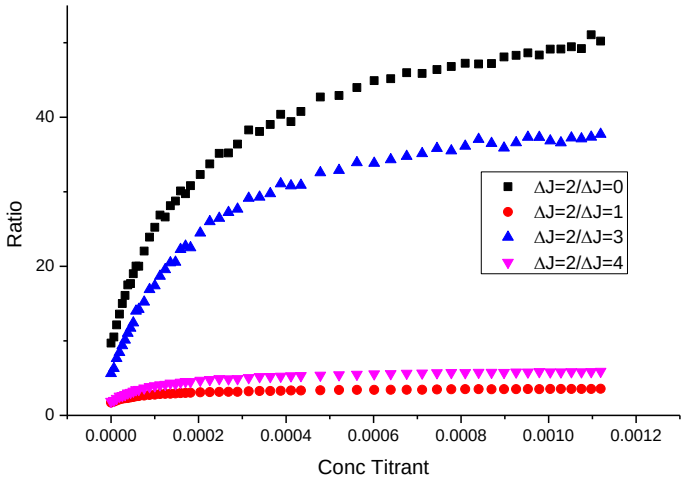

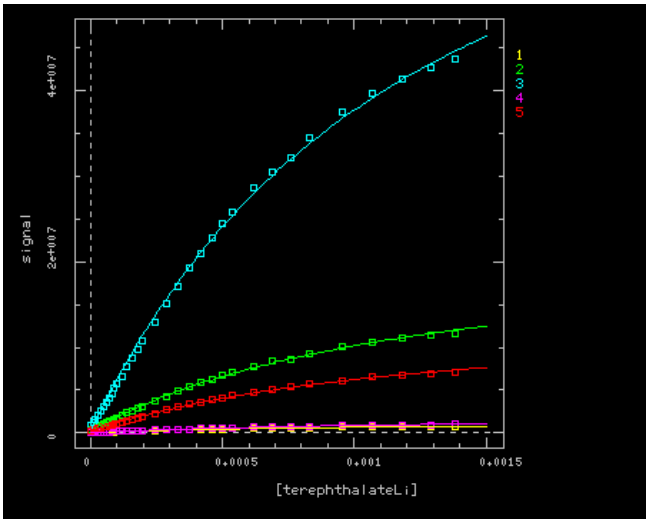

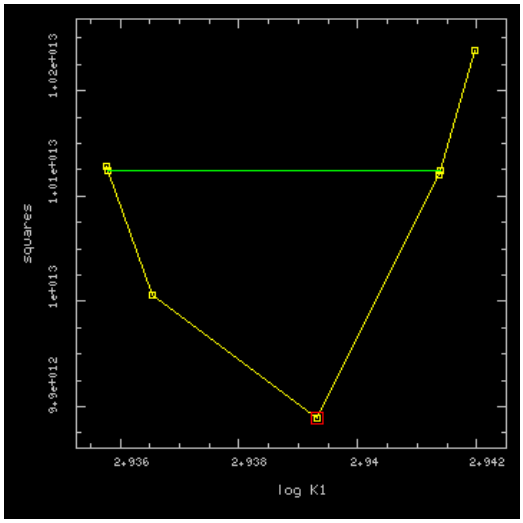

K_1 = 870 (862.55 - 873.77)

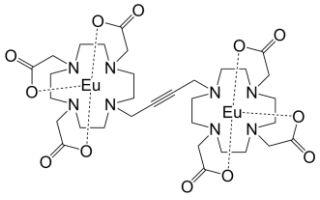

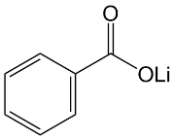

Solvent: MeOH

Buffer: N/A

pH: N/A

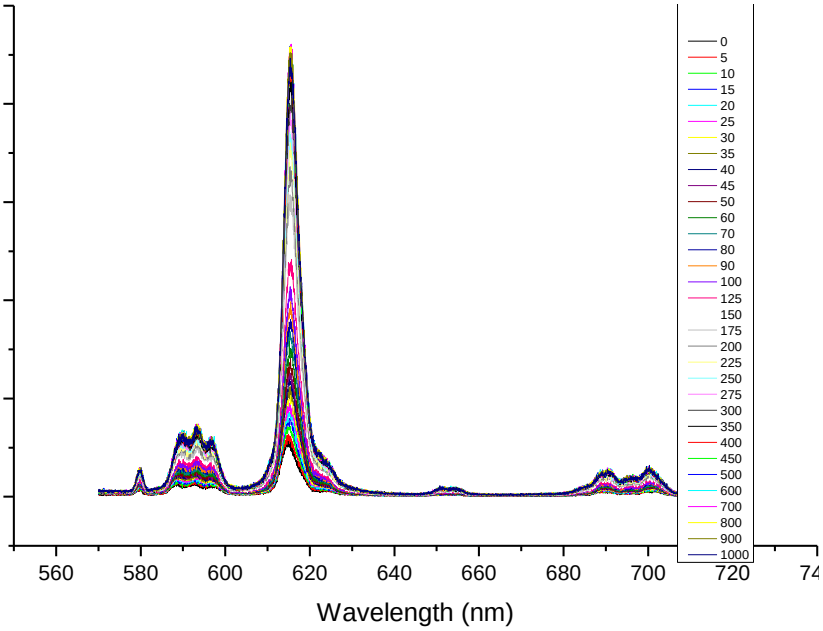

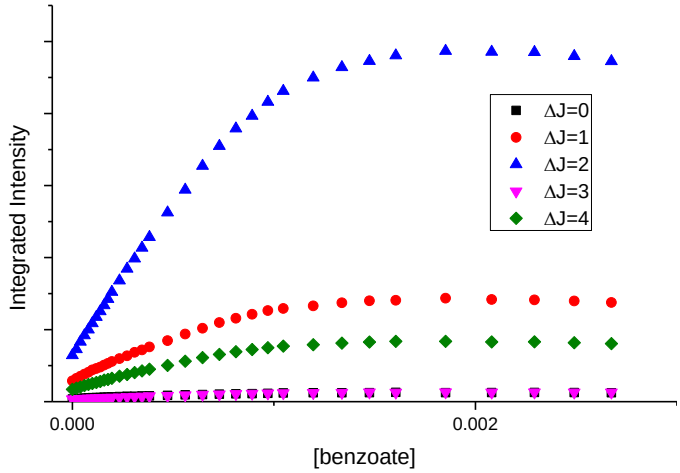

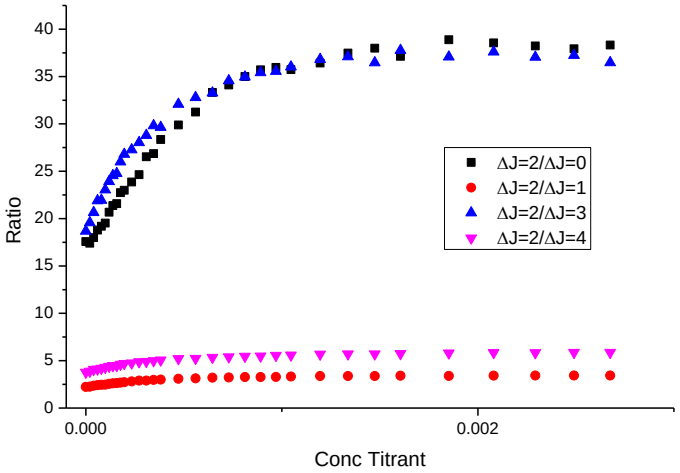

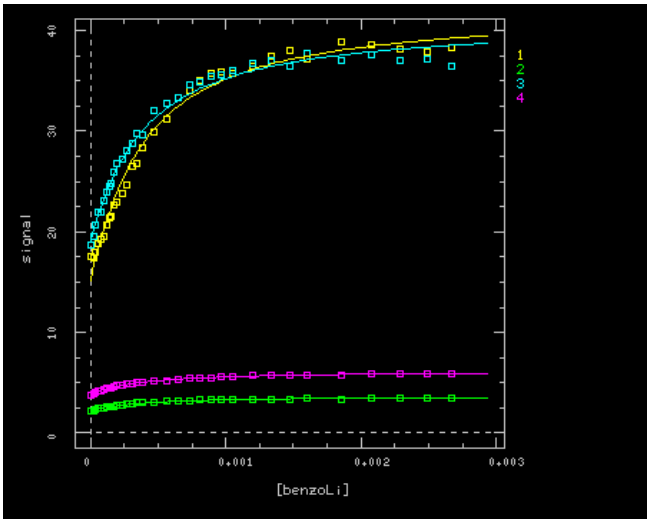

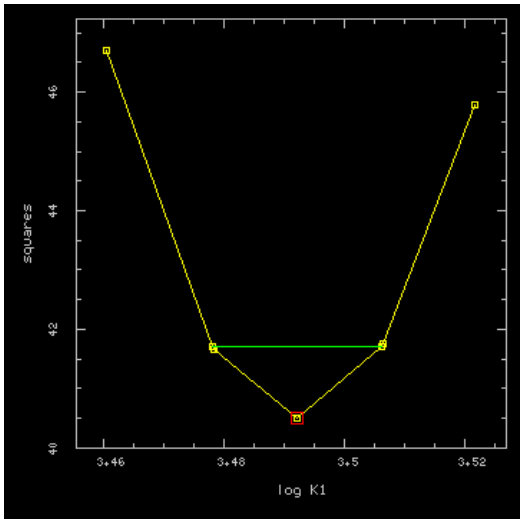

K_1 = 1604 (1559.65 - 1648.94)

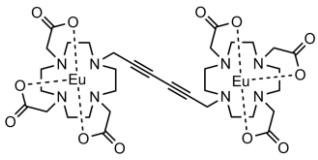

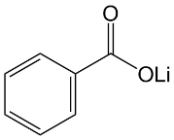

Solvent: MeOH

Buffer: N/A

pH: N/A

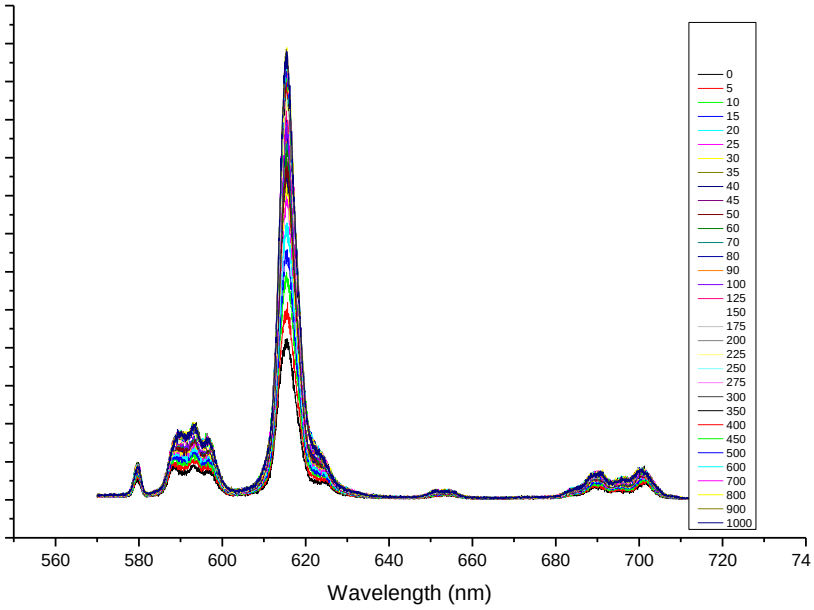

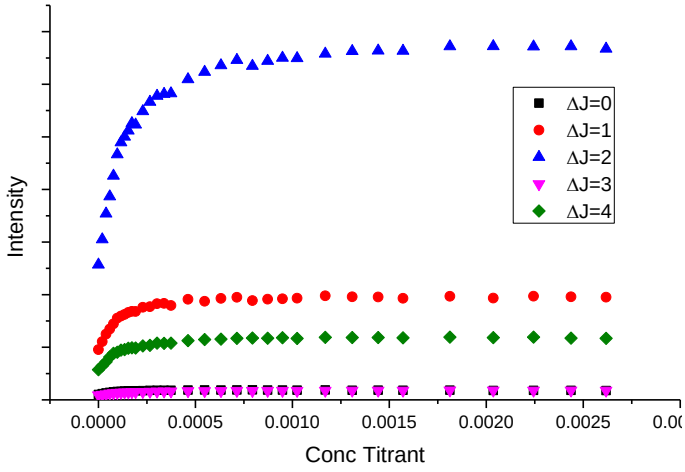

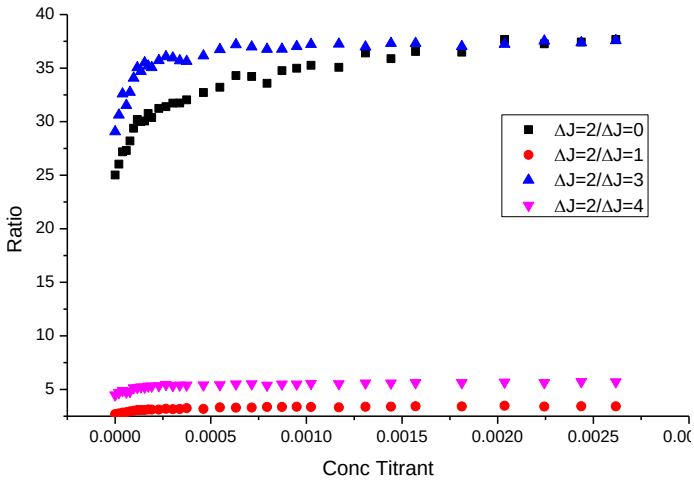

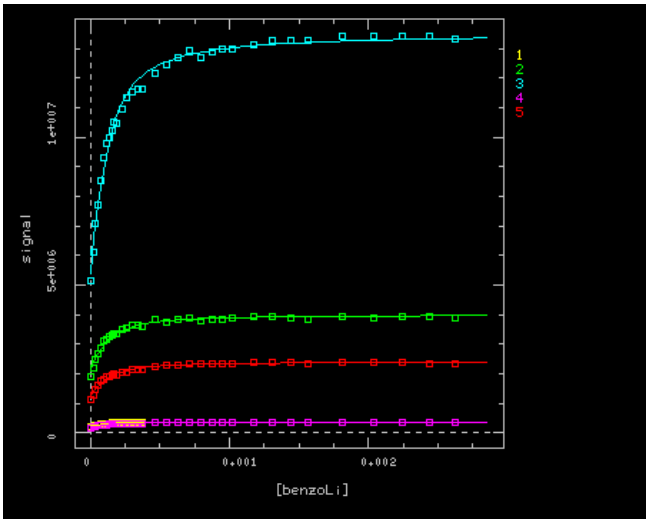

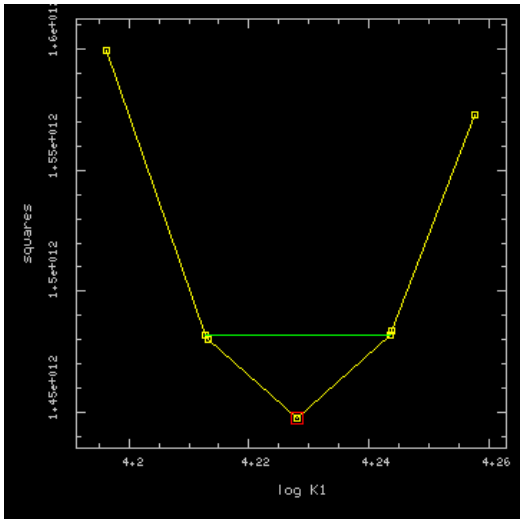

K_1 = 16907 (16324.3 - 17518.4)

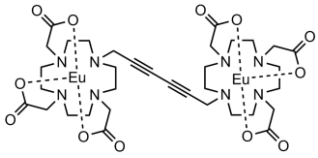

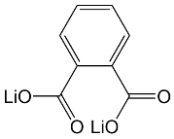

Solvent: MeOH

Buffer: N/A

pH: N/A

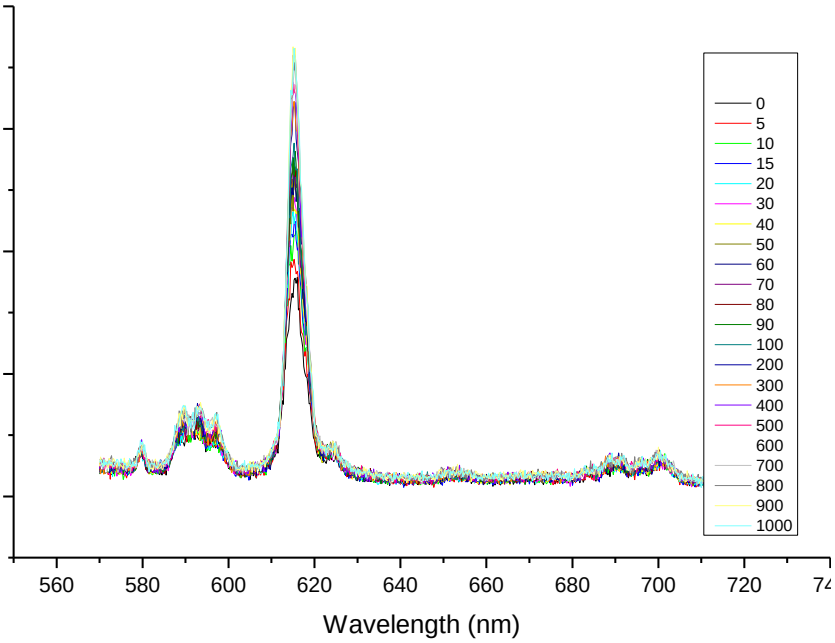

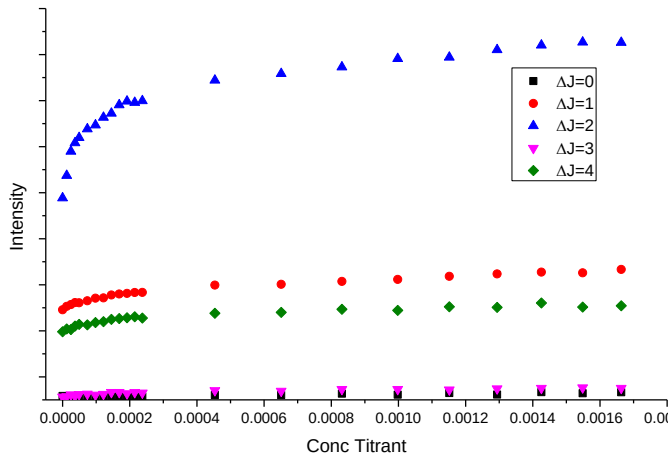

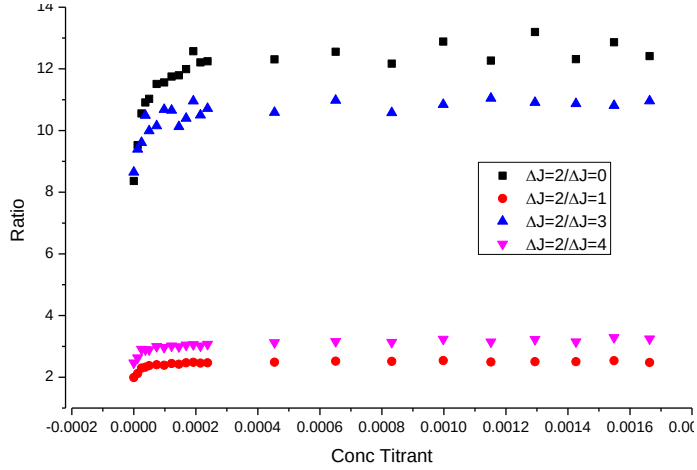

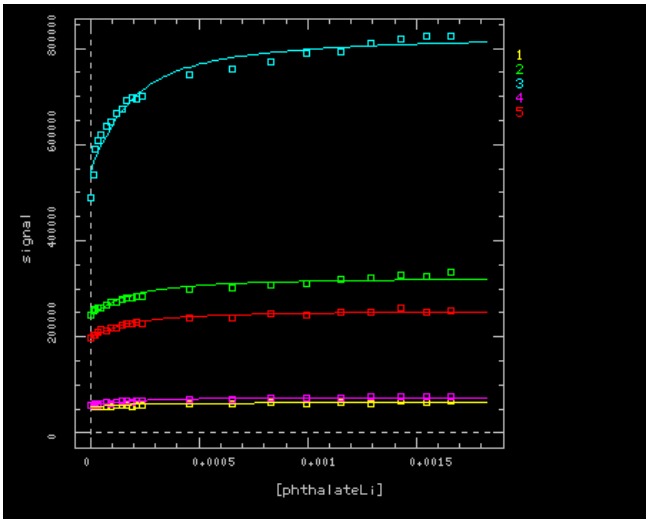

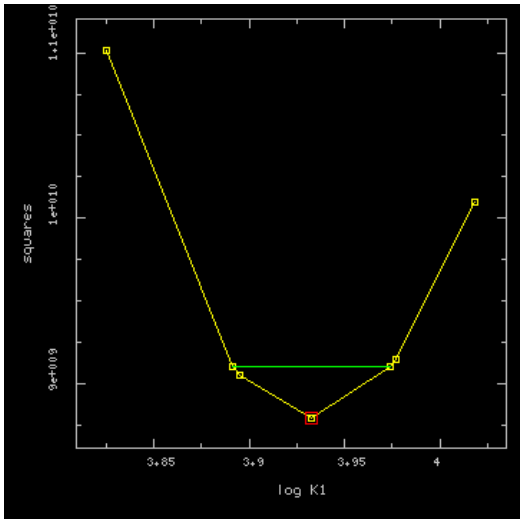

K_1 = 8559.25 (7786.56 - 9422.6

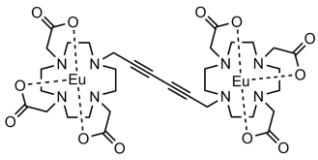

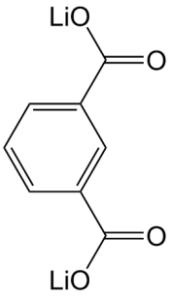

Solvent: MeOH

Buffer: N/A

pH: N/A

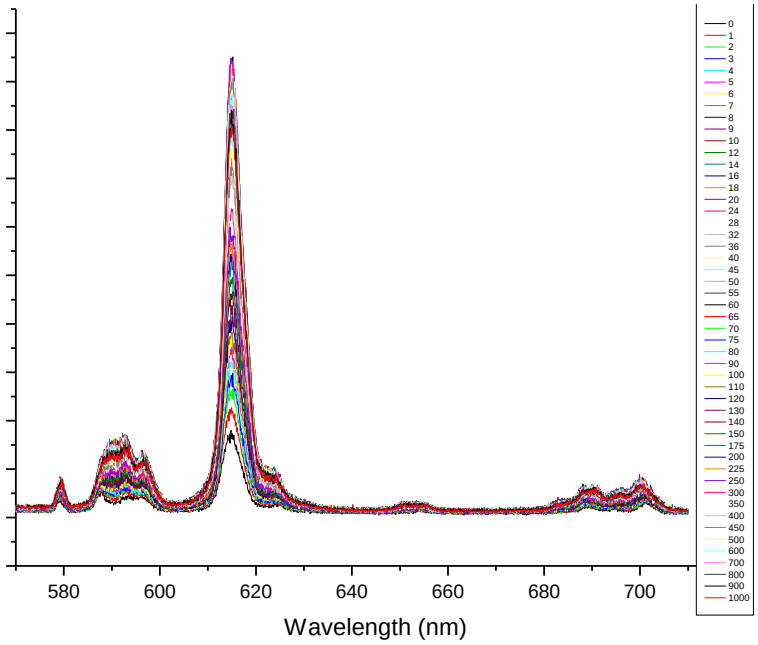

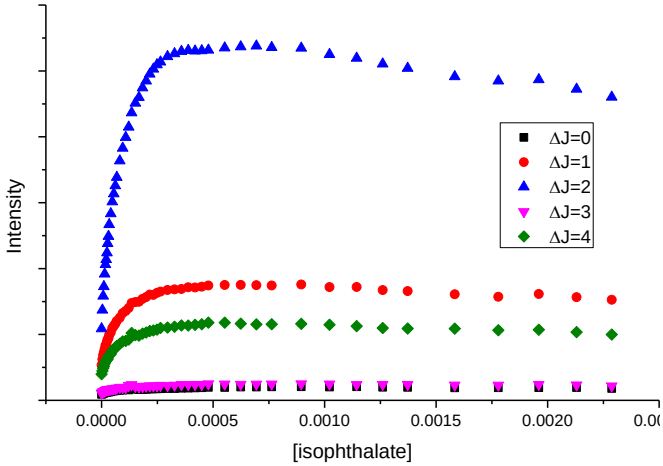

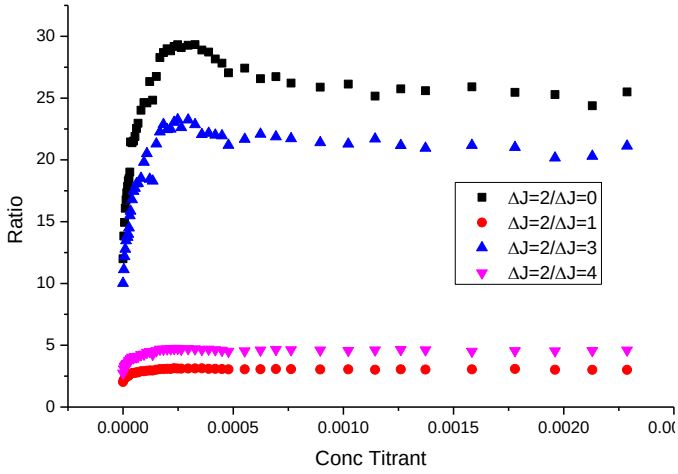

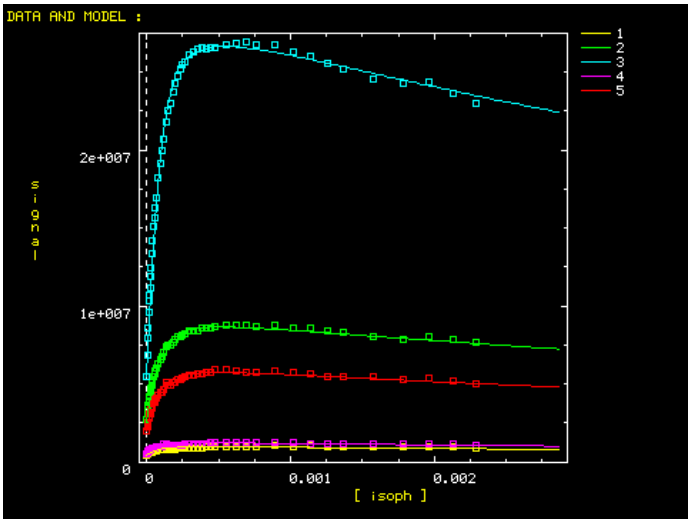

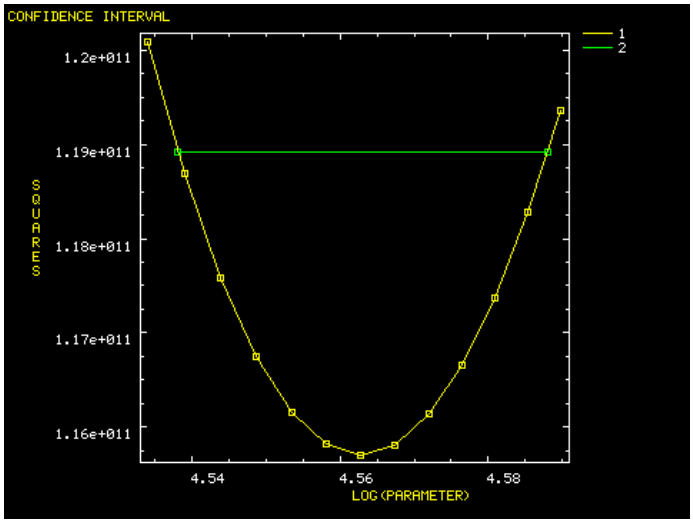

K_1 = 36541 (34528 - 38724

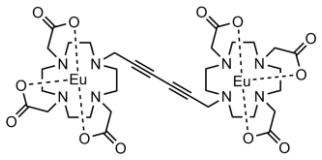

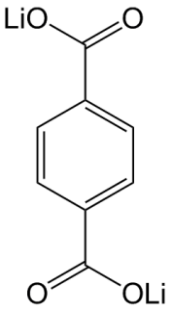

Solvent: MeOH

Buffer: N/A

pH: N/A

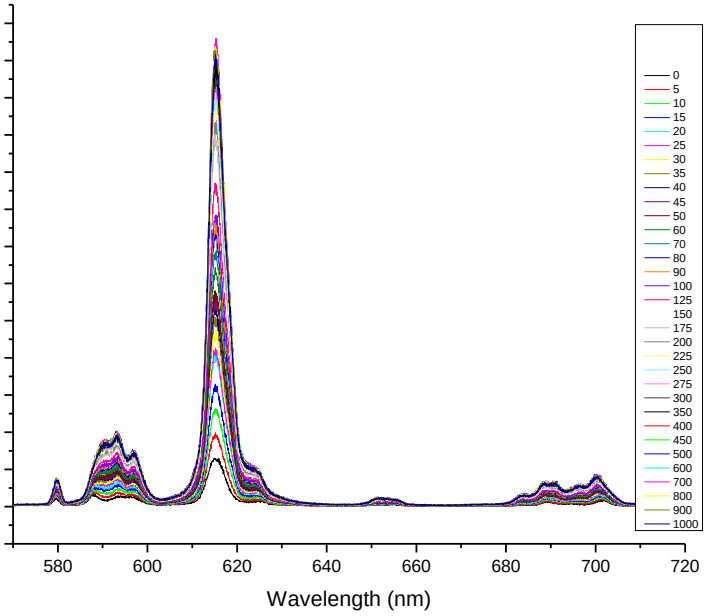

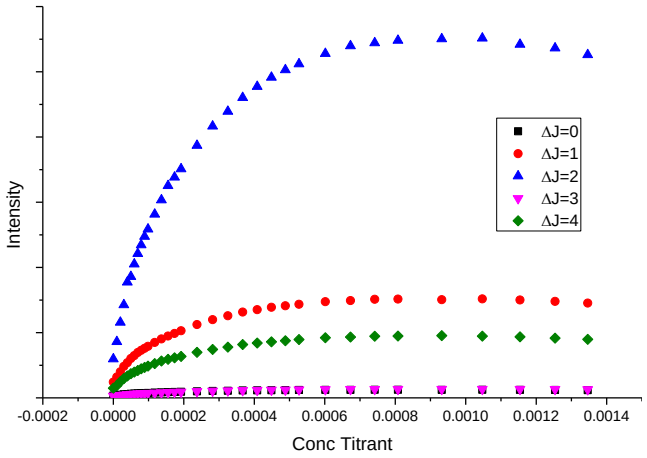

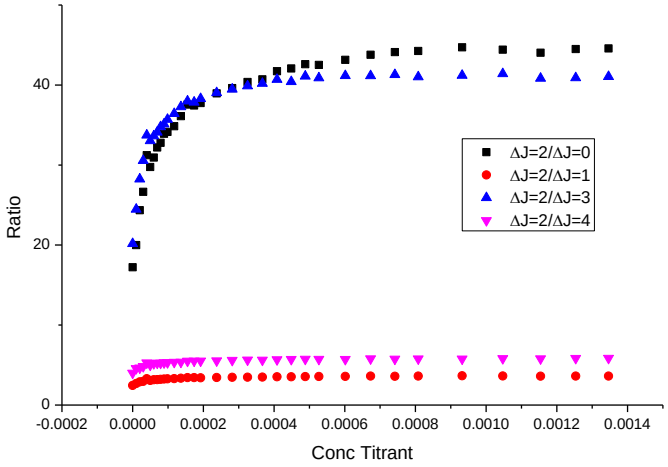

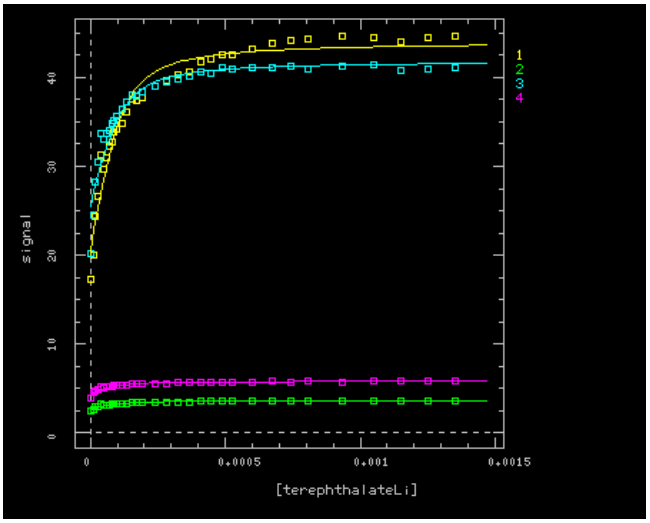

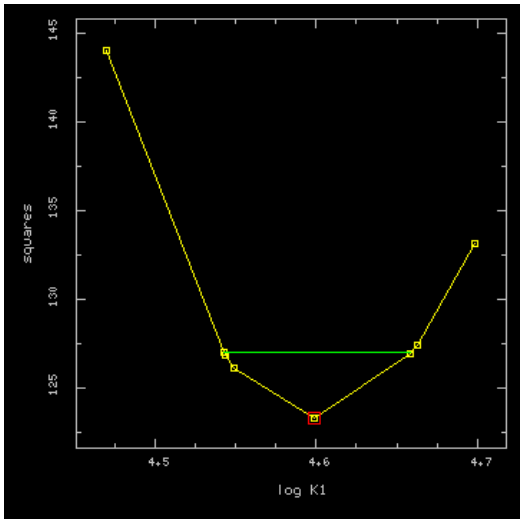

K_1 = 39722.8 (34886.8 - 45545.3)